HIGH TEMPERATURE SULFIDATION AND REDUCTION OF ZINC TITANATE AND ZINC OXIDE SORBENTS

by

Susan Lew

Bachelor of Science
Columbia University (1985)

Master of Science
Massachusetts Institute of Technology (1987)

Submitted to the Department of Chemical Engineering
in Partial Fulfillment of the Requirements
for the Degree of

DOCTOR OF PHILOSOPHY

at the

MASSACHUSETTS INSTITUTE OF TECHNOLOGY

October, 1990

Signature of Author:

Department of Chemical Engineering
October, 1990

Certified by:

Maria Flytzani-Stephanopoulos
Thesis Supervisor

Certified by:

Adel F. Sarofim
Thesis Supervisor

Accepted by:

William C. Deen
Chairman, Departmental Committee for Graduate Students

HIGH TEMPERATURE SULFIDATION AND REDUCTION OF ZINC TITANATE AND ZINC OXIDE SORBENTS

by

Susan Lew

Submitted to the Department of Chemical Engineering on October 1, 1990 in partial fulfillment of the requirements for the degree of Doctor of Philosophy in Chemical Engineering.

ABSTRACT:

A comparative study of the reduction and sulfidation of zinc titanate and zinc oxide solids was performed in order to determine the potential benefits of using zinc titanates over zinc oxides for coal gas desulfurization. Precursors of bulk zinc titanate mixed oxides and zinc oxides were prepared by a complexation method using citric acid. The formation of macroporous solids by this method eliminated gas-phase pore diffusion. Thus, the reaction rate measured was controlled by intrinsic kinetic and/or product layer diffusion.

Zinc titanates were reduced more slowly to volatile elemental zinc than single zinc oxide. Based on the inhibitory effect of water vapor and the effect of Zn/Ti ratio, a two-sites mechanism was proposed for reduction. In the absence of water vapor, solids with Zn:Ti atomic ratio of 3:1 had significantly lower reduction rate than ZnO. Higher relative concentrations of titanium did not significantly change the reduction rate. No effect was observed by the presence of different zinc titanate phases (i.e. Zn_2TiO_4, $ZnTiO_3$, and $Zn_2Ti_3O_8$). Water vapor suppressed the rate of reduction of ZnO and zinc titanate solids. In this situation, increasing the relative concentration of titanium was accompanied by decreasing reduction rates.

The initial sulfidation rate of zinc titanates was only half that of ZnO. No change in the initial sulfidation rate was observed when either the Zn:Ti atomic ratio was varied between 3:1 to 2:3 or the zinc titanate phase was varied. Similar activation energies (7-9 kcal/mol) indicate that the reaction mechanisms are the same for ZnO and zinc titanate solids. Increasing the relative concentration of titanium, however, led to a corresponding drop in the product layer diffusion coefficient. Because diffusion in TiO_2 was at least ten times slower than in ZnS, the product layer diffusion in zinc titanate solids was dominated by diffusion through ZnS. Consequently, similar activation energies (26.6 kcal/mol) for the product layer diffusion coefficient were obtained for the sulfidation of ZnO and Zn-Ti oxide sorbents.

Thesis Supervisors: Dr. M. Flytzani-Stephanopoulos

Professor A.F Sarofim

Acknowledgements

I would like to thank both my advisors, Dr. Miretta Stephanopoulos and Professor Sarofim, who supported me through this long and tortuous path towards completing this thesis. Without their help and words of encouragement, this research would not have reached its successful conclusion. The many hours I have spent with my advisors in discussions about the direction of the research have been something I have come to look forward to with anticipation.

Without the financial support of the U.S. Department of Energy, this work would not have been possible. Although some people speak about government waste, here I think is one example of money well spent.

I would like to thank all the post-doctoral associates who have worked in my laboratory for their support and friendship: Dr. Jothimurugesan (a.k.a. Jothi), Dr. Richard Shao (whose strange sense of humor was always great to liven up the lab), and Dr. Zhi-Cheng Hu. I shall always remember your friendship.

I wish to thank my parents for their support. Although they still do not know exactly what a chemical engineer does, they are happy I am finally graduating. To a friend of mine down in the wasteland of Indiana, thanks for calling me every week and never forgetting me.

Finally I wish to thank all the support staff (i.e. secretaries, technicians, mailmen, etc.) at MIT. Whereas all the faculty members get the fame and the graduate students...well...eventually graduate, you (the support staff) go underpaid and underappreciated. Although I cannot offer any monetary compensation, with these last words I like to say THANK YOU.

TABLE OF CONTENT

LIST OF TABLES

LIST OF FIGURES

CHAPTER 1

INTRODUCTION

1.1 COAL GASIFICATION FOR POWER GENERATION

Coal gasification integrated with combined-cycle power generation (IGCC) and coal gasification followed by oxidation in a molten carbonate fuel cell are emerging as viable methods for more efficient and cleaner power generation. Cost analyses of integrated gasifier utilizing conventional gas cleanup (i.e. water scrubbing) show that the capital cost for construction of an oxygen-based Texaco IGCC plant and the associated operating cost for electricity generation are competitive with conventional coal-fired steam plants (Gluckman and Louks, 1982). Increasingly more stringent emission control requirements are expected to dramatically increase the cost advantage of both IGCC and coal gasification-molten carbonate fuel cells. With the emergence of these technologies as promising routes for power generation, an emphasis has been placed on

improving the efficiencies and decreasing the costs of these processes. One focus has been fuel gas cleanup. This is important both for environmental reasons as well as equipment protection (e.g. from fouling). The other focus has been on increasing the value of the fuel gas temperature that the gas turbine and fuel cell can accept. Higher temperature increases the efficiency of the process.

Coal gasification involves the high temperature chemical conversion of carbon and hydrogen in coal to produce a fuel gas containing mainly carbon monoxide and hydrogen. The partial combustion of coal generates the heat needed for the chemical conversion reactions. Because of the presence of ash, sulfur, nitrogen, akali metals, and trace contaminants in coal, the gas produced from coal is similarly contaminated. Ash, sulfur, and nitrogen will cause environmental problems. Ash and alkali metal can erode and deposit on the gas turbine blades.

The fuel gas produced can be used either in a combined cycle plant or a fuel cell. The fuel cell offers the advantage of higher efficiencies over the combined cycle plant. The combined cycle consists of a gas turbine in series with a steam turbine. The maximum efficiency for this type of process is limited by the Carnot cycle limitation. The fuel cell, on the other hand, can directly convert chemical energy to electrical energy. Thus, higher efficiencies are possible. However, this technology is at a more early stage of development than the combined-cycle process.

This research has focused on high-temperature regenerative sulfur removal from coal-derived fuel gas streams. In the gasifier, the sulfur in the coal is released primarily as hydrogen sulfide. The level of H_2S removal for the coal-derived fuel gas depends on the method of power generation. For a combined-cycle power plant, the H_2S level of the coal gas must be $\leq$ 100 ppm in order to meet current environmental regulations. The

fuel gas must be purified to less than 1 ppm of H_2S for use in a molten carbonate fuel cell to prevent the poisoning of the nickel-based electrode to nickel sulfide.

1.2 H_2S REMOVAL

Several commercial methods exist for the removal of hydrogen sulfide. These processes are based on the reversible physical absorption of H_2S by a solvent such as methanol (Rectisol process) or dimethyl ether of polyethylene glycol (Selexol process). However, the disadvantage of these commercial methods for the purification of fuel gas used in power generation facilities is that the hot fuel gas must be cooled down to near ambient temperatures and then reheated prior to its final combustion.

Direct removal of H_2S from the hot fuel gas can significantly improve the process thermal efficiency (Marqueen et al., 1986). A high inlet gas temperature to the gas turbine and fuel cell is essential for high efficiency. Hot gas cleanup will eliminate the costs of heat exchangers to cool down the fuel gas, reheating equipment, and expensive wastewater cleanup process. Figure 1.1 shows a diagram of a proposed integrated combined-cycle power plant in which hot gas cleanup is utilized is incorporated.

Metal oxides have been proposed to remove H_2S by using a sulfidation-regeneration scheme with the following general reactions:

$$MO_x(s) + x\ H_2S(g) \text{ --> } MS_x(s) + x\ H_2O(g) \qquad (1.1)$$

$$MS_x(s) + 3x/2\ O_2(g) \text{ --> } MO_x(s) + x\ SO_2(g) \qquad (1.2)$$

In addition, there is the possibility of solid reduction by H_2 and CO:

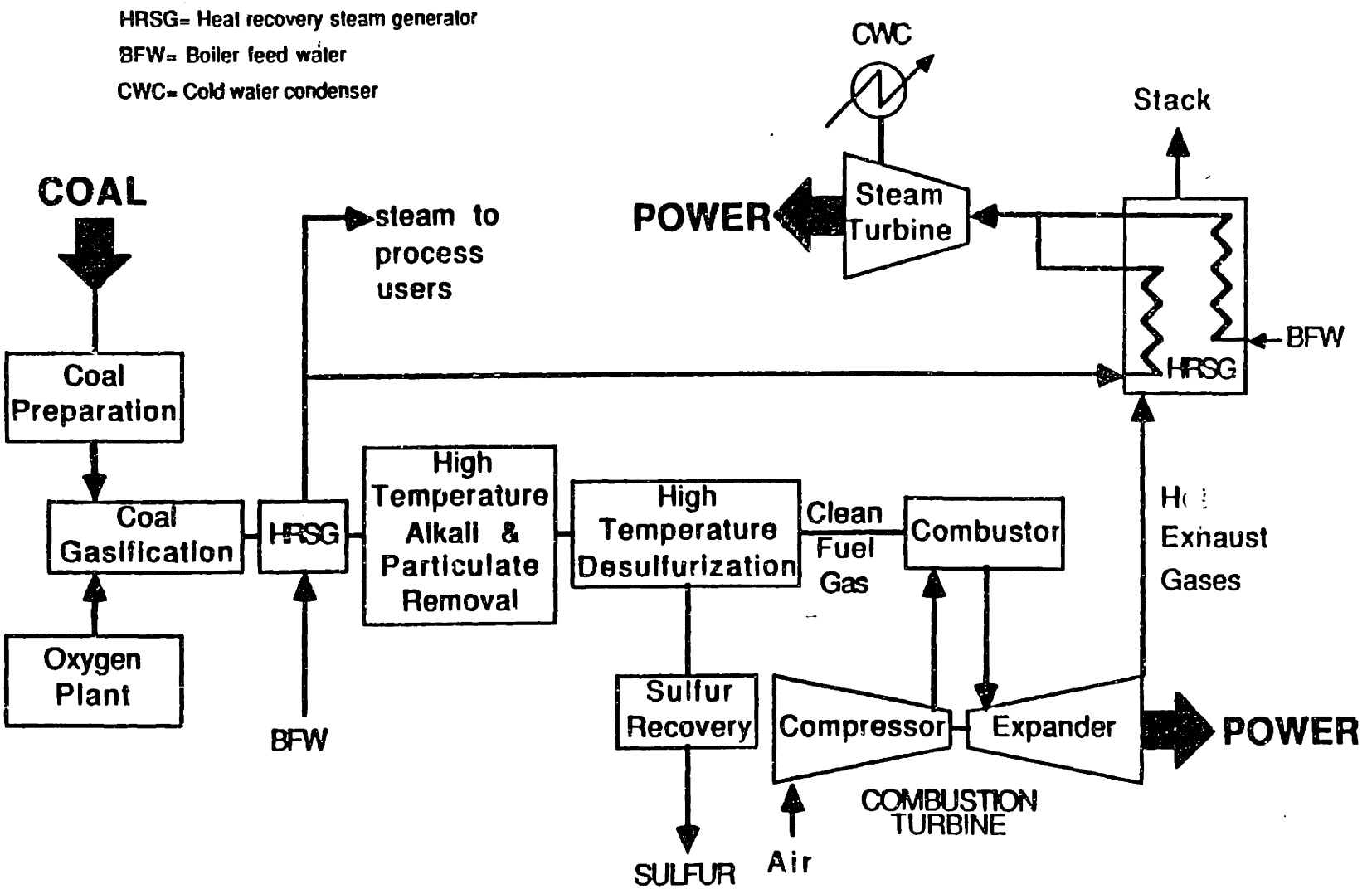

Figure 1.1 A proposed integrated combined-cycle power plant utilizing hot gas cleanup (Marqueen et al., 1986).

$$MO_x \xrightarrow{H_2,\ CO} MO_y \qquad (y < x) \tag{1.3}$$

Reactions 1.1 and 1.2 can ideally be repeated many times. The sulfur product, sulfur dioxide (SO_2), produced during regeneration is in a much more concentrated stream than hydrogen sulfide is in the untreated fuel gas. It can be sent to a sulfur recovery unit to produce elemental sulfur. To remove H_2S at high temperature, various metal oxide sorbents have been considered such as iron, zinc, calcium, and copper oxides. However, each of these oxides has it own distinct set of advantages and disadvantages. Calcium oxide is very inexpensive. It can meet the environmental regulation regarding H_2S level ($\leq$ 100 ppm). However, it cannot remove H_2S to the level required by a fuel cell. Sulfided calcium oxide is not regenerable. This leads to the additional cost of solid waste removal. The sulfidation rate with iron oxide is very rapid. Sulfided iron oxide is regenerable. However, iron oxide, Fe_2O_3, is reduced to Fe_3O_4 by H_2 and CO which are found in coal gases. Fe_3O_4 has low thermodynamic efficiency (equilibrium H_2S level > 100 ppm). Copper oxide is similarly reduced to Cu which has much worse H_2S removal efficiency than CuO. ZnO can remove H_2S to 1-10 ppm at 500-800°C based on the thermodynamic equilibrium. Subequilibrium H_2S level (< 1 ppm) can be attained with ZnO due to additional chemisorption of H_2S (Flytzani-Stephanopoulos et al., 1985). However, at temperatures above 600°C, zinc loss is observed due to the reaction:

$$ZnO\ (s) + H_2(g) \rightarrow Zn(g) + H_2O(g) \tag{1.4}$$

The resulting sorbent loss with repeated cycling (sulfidation-regeneration) represents a major problem with zinc oxide sorbents.

1.3 THESIS OBJECTIVES

The overall objective of this thesis is to investigate the properties of and evaluate mixed oxides of zinc and titanium for hot fuel gas desulfurization. Uncombined ZnO is also investigated as a base case. Zinc oxide can remove H_2S to the level required, has a high sulfidation rate (Westmoreland et al., 1977), and can be completely regenerated if sufficiently high temperatures or low oxygen concentrations are used to avoid zinc sulfate formation ($ZnSO_4$). However, zinc loss during sulfidation, loss of surface area and incomplete regeneration limit the application of ZnO to temperatures below 600°C. To address these problems, mixed oxides of zinc and titanium are proposed. In previous studies in this laboratory using a packed-bed reactor in sulfidation-regeneration cycles (Flytzani-Stephanopoulos, 1987; Lew, 1987; Lew et al., 1989), Zn-Ti-O sorbents were found to be more resistive to reduction than pure zinc oxide. In addition, the sulfidation performance of the mixed oxides was not adversely affected.

In this thesis, detailed investigation of the reduction and sulfidation reactions of Zn-Ti-O sorbents was performed. The intrinsic kinetics and the product layer diffusion rates in reduction and sulfidation were determined. Kinetic experiments with sorbents containing various Zn/Ti atomic ratios were performed. Chemical phase and structural transformations were followed by various methods. The results were compared to similar experiments performed with ZnO. The purpose of these experiments were to determine mechanistically how the presence of titanium dioxide affects the reduction and sulfidation of ZnO. This information will be used to propose the type of sorbents in terms of preparation method, (Zn/Ti) ratio and chemical phases which will give the best combination of low reduction rate and acceptable sulfidation performance at temperatues exceeding 600°C.

In Chapter 2, the preparation of various bulk Zn-Ti-O solids using a complexation method with citric acid is discussed. Various zinc titanate phases, formed as a function of temperature and Zn/Ti ratio, were determined by X-ray diffraction. Physical properties (i.e. surface areas and pore volumes) of Zn-Ti-O solids were compared to ZnO. High surface area is desirable because it enhances reaction rates. High pore volume ensures that pore diffusion is not limiting and prevents pore plugging from occurring.

In Chapter 3, the reduction characteristics of various Zn-Ti-O solids are compared to ZnO. The intrinsic reduction kinetics of Zn-Ti-O solids as a function of Zn/Ti ratio and crystalline phases were investigated to determine the mechanism of reduction and how titanium dioxide interacts to inhibit reduction. The effect of H_2O was examined because not only is it a major component (10-50%) in the coal gases, but also because of its inhibitory effects on ZnO reduction (Hegedus and Kiss, 1966; Flytzani-Stephanopoulos et al., 1987). Comparisons of the reactivity of bulk Zn-Ti-O sorbents with a ZnO single crystal coated with a thin film of TiO_2 were performed. The purpose of these experiments was to determine whether similar inhibition in reduction could be obtained by this method of preparation. The reduction experiments were compared with similar sulfidation experiments of the TiO_2-coated single crystal of ZnO to determine if any inhibition in reduction rate was at the cost of similar inhibition in sulfidation.

Sulfidation of various Zn-Ti-O and ZnO solids is the topic of Chapter 4. The effects of Zn/Ti ratios and zinc titanate phases on sulfidation were determined. Parametric studies were performed examining the effects of temperature and hydrogen sulfide, hydrogen and water vapor concentrations Structural changes (i.e. surface morphology and surface area) and chemical phase changes were followed with the extent of sulfidation.

In Chapter 5, modeling of the sulfidation conversion profiles of ZnO and Zn-Ti oxides is presented. Different gas-solid models (e.g. the grain model) were investigated to calculate the product layer diffusion coefficients. The effects of titanium dioxide on the product layer diffusion coefficient are discussed. Finally, Chapter 6 summarizes the major conclusions of this thesis with recommendations for future work.

CHAPTER 2

PREPARATION OF ZN-TI-O MATERIALS

2.1 INTRODUCTION

Mixed metal oxides have demonstrated potential advantages over single component oxides for the regenerative removal of hydrogen sulfide from coal-derived gases at high temperatures in conjunction with power generation from combined cycle power plants or molten carbonate fuel cells. Mixed oxides containing Cu-Al, Cu-Fe-Al, Zn-Fe, and Zn-Ti have been studied in this laboratory (Flytzani-Stephanopoulos et al., 1987; Lew et al., 1989) as well as by others (Tamhankar et al., 1986; Focht et al., 1988; Patrick et al., 1989; Sa et al., 1989; Ayala et al., 1989).

Zinc oxide has been considered as a sorbent for hydrogen sulfide removal (MERC, 1978; Giner, 1981; Grindley and Steinfeld, 1981) because its sulfidation equilibrium

constant is high enough (Barin and Knacke, 1973; Barin et al., 1976) to adequately remove hydrogen sulfide. However, because of the reducing atmosphere of coal gases, zinc oxide is reduced to metallic zinc which at high temperatures is volatile. Consequently, sorbent loss is observed at temperatures above 600°C. Based on work performed in this laboratory, zinc oxide in association with titanium dioxide is reduced more slowly to volatile zinc than zinc oxide alone (Chapter 3). Also, the desulfurization properties of ZnO were not comparably compromised by the presence of titanium dioxide (Chapter 4). This chapter examines the interaction of zinc oxide and titanium dioxide in terms of chemical phase formations and physical properties as a function of preparation conditions and Zn-Ti atomic compositions.

Phase formation in the Zn-Ti-O system has been of considerable interest because of the importance of zinc titanate as white pigments and as fusion cast thermistors. In most of the early literature (Cole and Nelson, 1938; Dulin and Rase, 1960; Bartram and Slepetys, 1961; Shienkman et al., 1977), specific zinc titanate phases were prepared by mixing slurries of ZnO and TiO_2, drying the mixture, and calcining the mixture for an extended period of time. For example, Cole and Nelson (1938) required calcination at 1000°C for 20 h to completely react $2ZnO + TiO_2$. The extended calcination period was required in order to obtain sufficient compositional homogeneity. Because the diffusional paths between reactants are quite large (~ 10^6 Å), long calcination times are required to ensure complete mixing of the reactants on an atomic scale. The final product from this preparation is often of low surface area, highly crystalline, and may possess poor homogeneity.

In more recent studies (Reddy et al., 1984; Lercher et al., 1984; Yamaguchi et al., 1987), zinc titanates have been prepared by a hydrolysis-pyrolysis technique. Because

of the smaller reactant diffusion length, better compositional homogeneity can be achieved with this method. Thus, lower calcination temperatures and shorter calcination times are possible. However, in this method, the composition is restricted by the stoichiometric requirement of the precipitate. Also, due to the change in the composition of the liquid medium as the precipitate is formed, there may be some problems with maintaining the homogeneity of the product.

Synthesis of mixed oxides by complexation with citric acid can yield homogeneous and highly dispersed mixed oxides. This technique (Marcilly et al., 1970; Courty et al., 1973), produces an amorphous completely homogeneous solid obtained by evaporating a solution of metallic ions and a complexing polyfunctional hydroxyacid. Because of the intimate mixing of the metal ions, lower calcination temperatures than for the hydrolysis-pyrolysis technique can be used to achieve desired chemical phases. Since any initial stoichiometry of metal ions can be used, this method can potentially produce new multi-component mixed oxides. Villa et al. (1987) prepared zinc titanates by the complexation technique as catalysts for the synthesis of alcohols from carbon monoxide and hydrogen. They found that zinc titanates prepared by this method were more homogeneous with a moderately high surface area than zinc titanates prepared by a hydrolysis-pyrolysis technique.

In this chapter, Zn-Ti mixed oxides were prepared by complexation with citric acid. Various compositions of Zn-Ti and calcination temperatures were used to determine their effects on the formation of various chemical phases and physical properties. These results will be compared with those found in the literature.

2.2 EXPERIMENTAL

2.2.1 Zn-Ti-O Preparation

The mixed metal oxides were prepared by the complexation method with citric acid. Preparation was performed by dissolving citric acid monohydrate and $Zn(CH_3CO_2)_2 \cdot 2H_2O$ (zinc acetate dihydrate) in water. One mole of citric acid was used for each gram-equivalent of metal ions (Zn+Ti). Acetic acid was added to $Ti[OCH(CH_3)_2]_4$ (titanium (IV) isopropoxide, TTIP) in a 3:1 volumetric ratio to prevent the precipitation of titanium when it is added to the aqueous solution. The TTIP-acetic acid solution was slowly added to the aqueous solution. The product of partial hydrolysis of TTIP formed was dissolved by stirring the solution. The relative amounts of TTIP and zinc precursor were varied according to the desired Zn/Ti ratio of the product.

Evaporation of the liquid was performed in a rotary evaporator at 65-75°C under vacuum (26-29 in. Hg). It was stopped when the viscosity increased to the point where discharge of the liquid became difficult. Evaporation was completed in a vacuum oven (29 in. Hg) for 4-6 h at 70-80°C. A white amorphous foam was formed. The foam was calcined in a furnace at the desired temperature under a stream of air to produce the final mixed oxide product.

2.2.2 Chemical Analyses

To quantitatively determined the amount of zinc and titanium in the solid, atomic absorption analyses were performed with a Perkin Elmer 360 Atomic Absorption (AA) Spectrophotometer. The Zn-Ti-O solids were dissolved in a hot solution of $HF:HCl:H_2O$. To completely dissolve the solid, it was necessary to heat the solution

containing the solid to 80-90°C for several hours. The relative concentrations of zinc and titanium ions in the solution were measured with the AA. Zinc concentrations were determined at a wavelength of 213.9 nm using an air-acetylene flame for ionization. Titanium concentrations were determined at 365 nm with a nitrous oxide-acetylene flame.

The crystalline phase compositions were determined with a Rigaku RU300 X-ray diffractometer using Cu (Kα) radiation. The X-ray tube was operated at 200 mA and 50 kV. A diverging slit of 1°, scattering slit of 1°, and receiving slit 0.3° were used. Solid samples were finely crushed (<325 mesh) and slurried in a polymeric solution. Grinding the solids to a fine size reduces preferred orientation and microabsorption effects. Preferred orientation is a major source of intensity error. Microabsorption is the effect of the solid particles geometry on the X-ray intensities diffracted by the solid. Microabsorption is affected by the surface roughness and bulk porosity of the solid. The slurry was spread on a glass slide and heated in an oven to evaporate the liquid. X-ray diffraction patterns in the range 10° to 100° were obtained. For powders containing multi-components, it is possible to estimate the relative concentration of each component by measuring the intensity of the diffraction pattern. The relationship (from Klug and Alexander, 1954) between the intensity (I_i) and weight fraction (x_i) of the ith component is:

$$I_i = \frac{K_i x_i / \rho_i}{\sum_{i=1}^{n} \mu^*_i x_i} \qquad (2.1)$$

where K_i depends on the nature of component i and the geometry of the apparatus, x_i is the weight fraction, ρ_i is the density, and μ^*_i is the mass absorption coefficient of the *i*th component. The weight fraction (x_i) is related to the intensity (I_i) of a chosen peak in the sample containing n crystalline phases and the intensity of the same peak in the pure phase (I_{io}) by:

$$x_i = \frac{I_i \mu^*_s}{I_{io} \mu^*_i} \tag{2.2}$$

where

$$\mu^*_s = \sum_{i=1}^{n} \mu^*_i x_i \tag{2.3}$$

Many papers have been written on the Reference Intensity Ratio (RIR) and its use for semi-quantitative phase analysis (e.g. Hubbard and Snyder, 1988; de Woolf and Visser, 1988; Davis et al., 1990). Values for the RIR for many crystalline phases using corundum (α-Al_2O_3) as the reference standard are available in the Powder Diffraction File. The RIR using corundum as the reference standard (also called I/I_c) is the ratio of the strongest line intensity of the chemical phase of interest divided by the strongest (113) corundum line intensity. These values were measured from a physical mixture, 1:1 by weight, of the crystalline phase and α-Al_2O_3. Thus, the ratio is

$$RIR_{i,c} = \left(\frac{I_i}{I_c}\right)_{x_c = x_i} = \frac{I_{io} \mu^*_i}{I_{co} \mu^*_c} \tag{2.4}$$

where subscript c is the corundum phase. To calculate the weight fraction of different phases in a crystalline solid, equations for a two-phase system are given:

$$\frac{x_1}{x_2} = \frac{I_1}{I_2} \frac{I_2^{rel} \, RIR_{2,c}}{I_1^{rel} \, RIR_{1,c}} \qquad (2.5)$$

$$x_1 + x_2 = 1 \qquad (2.6)$$

I_1^{rel} and I_2^{rel} are relative intensity values which are tabulated for each diffraction line of a crystalline phase in the Powder Diffraction File. Similar types of equations can be obtained for an n-phase system. To reduce preferred orientation effects, the intensities of several diffraction lines of each phase are measured. In this study, the value of I_i is the sum of three different diffraction lines. Correspondingly, I_i^{rel} is the corresponding sum of the tabulated intensities of these lines. When possible, the largest non-overlapping line, next largest non-overlapping line, and so on were chosen. Unless the peaks were broad, in which case the integrated intensities were used, the peak heights were used. The values calculated by this method are at best semi-quantitative due to the unspecified errors in tabulated I_i^{rel} and RIR_i, microabsorption, and preferred orientation. Gross changes can be identified. However, smaller changes can only be interpreted with caution.

2.2.3 Physical Analyses

The surface areas of the solids were determined with a Micromeritics Flow Sorb II 2300 BET apparatus. The solids were degassed at 220°C to remove any adsorbed H_2O. The surface areas were determined by the BET method developed by Brunauer, Emmet, and Teller (1938) using a 30% N_2-70% He gas. A single point method technique was used to determine the surface area. This is equivalent to assuming that a plot of P/P_o vs. $P/[V(P_o-P)]$ has a zero intercept (where P is the partial pressure of nitrogen, P_o is the saturation pressure of nitrogen at the experimental temperature, and V is the volume of nitrogen adsorbed at pressure P).

The pore volume and corresponding pore size distribution of the solids were measured by mercury porosimetry using a Micromeritics Autopore 9200. The pore size distribution was determined by measuring the pressure needed to fill the pores with a nonwetting liquid such as mercury, according to the equation:

$$r = \frac{-2\sigma \cos\theta}{P} \qquad (2.7)$$

where r is the pore radius, σ is the surface tension, θ is the contact angle between liquid and solid, and P is the applied pressure. Pressure as high as 60000 psia can be applied. This is equivalent to a pore radius of 0.0015 μm. All the measurements were performed from 5 to 60000 psia (18-0.0015 μm).

The surface morphologies of the solids were observed using a Cambridge Scientific Instruments Stereoscan 250. Solid sample was adhered to a standard SEM specimen mount coated with graphite paint. The sample was then coated with a thin layer of gold by vapor phase deposition to provide the necessary electric conductivity and to prevent charge buildup on the sample. (For samples which contained sulfur, coating must be performed with palladium because of the overlap of the gold and sulfur X-ray floruescence peaks). The SEM has an additional Tracor Northern TN-5400 X-ray analyzer for quantitative energy dispersive X-ray spectrometry (EDS).

2.3 PRESENTATION AND DISCUSSION OF SOLID PREPARATION

2.3.1 Chemical Phase Formation

Zinc titanate phase formation was investigated as a function of Zn/Ti ratio and calcination temperature. Solids with Zn/Ti atomic ratios ranging from 2/3 to 1/0 were

calcined at temperatures from 500 to 1000°C. In Table 2.1, the crystalline phases formed as a function of temperature (500-800°C) are listed for Z2T3 (2 Zn:3 Ti), ZT (1 Zn:1 Ti), and Z2T (2 Zn:1 Ti). Figures 2.1 and 2.2 show examples of the typical XRD diffraction patterns obtained for Z2T and Z2T3 from 500-800°C for 4 h. The increasing intensity as the diffraction angle decreased was due to the contribution of air scattering to the background intensity. At very low 2θ angles, the background intensity increased due to the grazing incident beam. The phase transformations observed with increasing temperature are:

Z2T3

500°C: amorphous ($Zn_2Ti_3O_8$ and/or α-Zn_2TiO_4) --> 600°C: $ZnTiO_3$, TiO_2(rutile), small amounts of $Zn_2Ti_3O_8$ and/or α-Zn_2TiO_4 --> 700°C: $ZnTiO_3$, TiO_2(rutile), α-Zn_2TiO_4, $Zn_2Ti_3O_8$, small amounts of ZnO --> 800°C: $ZnTiO_3$, TiO_2(rutile), α-Zn_2TiO_4, ZnO

ZT

500°C: amorphous ($Zn_2Ti_3O_8$ and/or α-Zn_2TiO_4) --> 600°C: $ZnTiO_3$, $Zn_2Ti_3O_8$ and α-Zn_2TiO_4 --> 700°C: α-Zn_2TiO_4, $ZnTiO_3$, ZnO, TiO_2(rutile) --> 800°C: α-Zn_2TiO_4, ZnO, TiO_2(rutile)

Z2T

500°C: $Zn_2Ti_3O_8$ and/or α-Zn_2TiO_4, ZnO --> 600°C: $Zn_2Ti_3O_8$, α-Zn_2TiO_4, ZnO --> 700°C: α-Zn_2TiO_4, $ZnTiO_3$, ZnO --> 800°C: α-Zn_2TiO_4, $ZnTiO_3$, ZnO

At 500 and 600°C, the peaks of all solids are very broad which indicates the presence of amorphous material. In contrast, a fully crystalline material would be characterized by peaks whose shape approaches that of a delta function. At these temperatures, it was

Table 2.1 Crystalline Phases Formed at Various Temperatures.

Sample[1]	Temperature (°C)	Crystalline Phase (wt %)				
		ZnO	α-Zn_2TiO_4	$Zn_2Ti_3O_8$	$ZnTiO_3$	TiO_2(rutile)
Z2T	500[2]	30	70-x	x	0	0
	600	25	75-x	x	0	0
	700	20	57	0	23	0
	800	10	70	0	20	0
ZT	500[3]	0	0	0	0	0
	600	0	54-x	x	46	0
	700	20	23	0	40	17
	800	23	43	0	0	34
Z2T3	500[2]	0	0	0	0	0
	600	0	0	0	67	17
	700	0	7	8	64	21
	800	9	16	0	43	32

[1] Prepared by the amorphous citrate technique with Ti (IV) isopropoxide and zinc acetate as precursors. Calcined for 4 h.

[2] Very broad peaks.

[3] Amorphous, Zn_2TiO_4 or $Zn_2Ti_3O_8$ might be present.

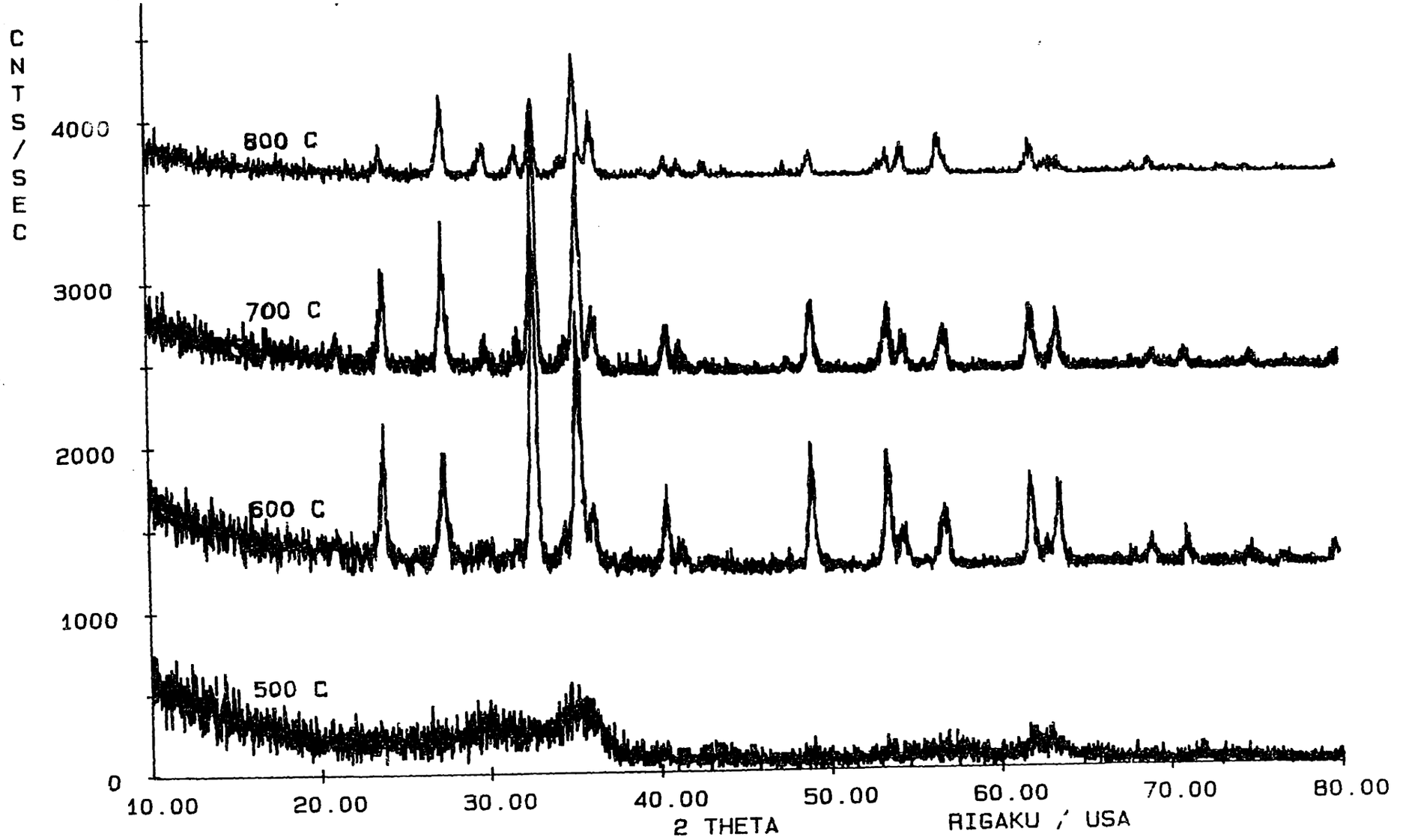

Figure 2.1 XRD patterns of Z2T3 (2 Zn : 3 Ti) calcined at 500-800 C for 4 h.

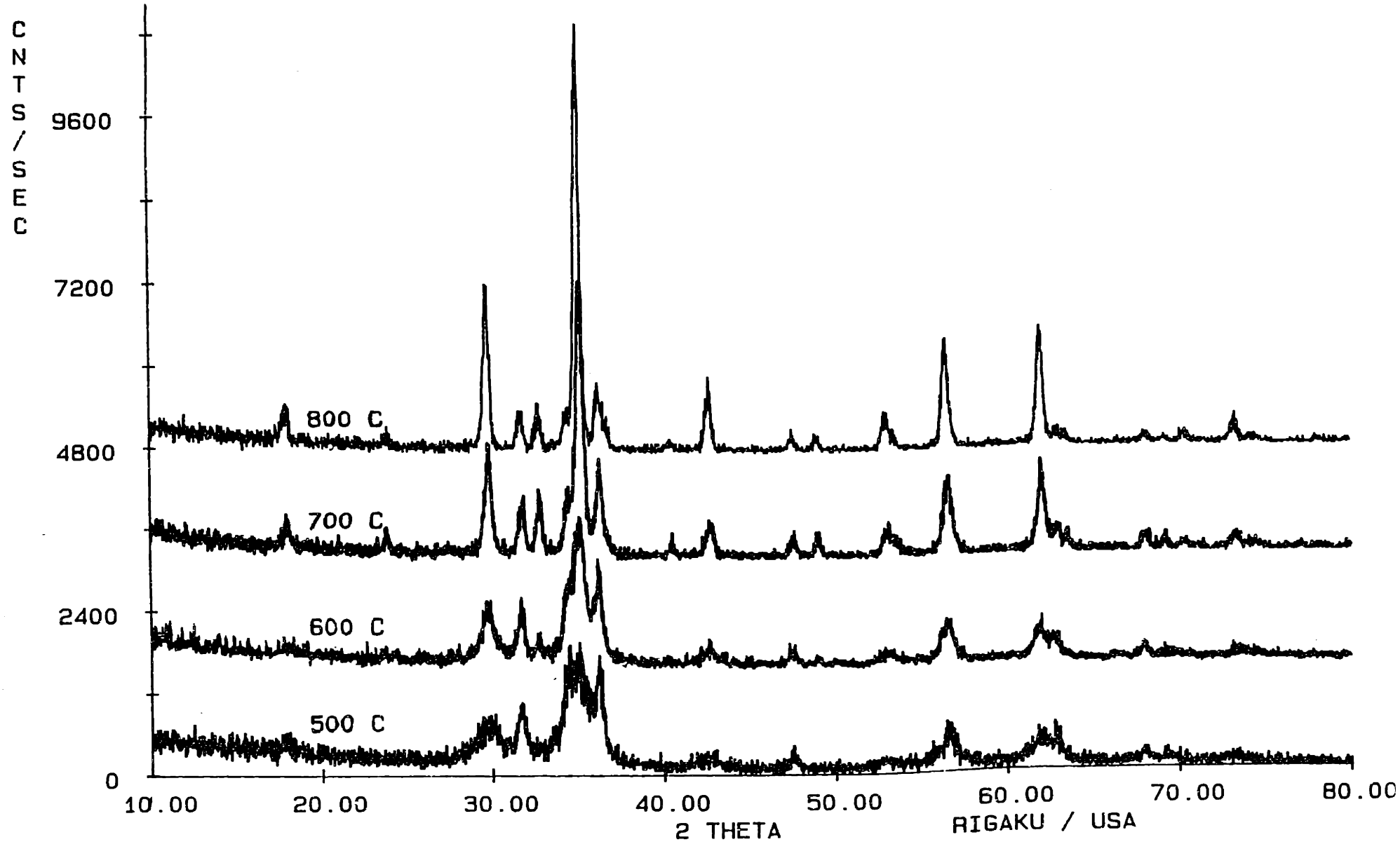

Figure 2.2 XRD patterns of Z2T (2 Zn : 1 Ti) calcined at 500-800 C for 4 h.

difficult to distinguish between α-Zn_2TiO_4 and $Zn_2Ti_3O_8$ because of the broadness of the peaks. The diffraction lines of these two phases are quite close, and the experimentally measured patterns were not well-resolved. The formation of ZnO at temperatures between 700-800°C is probably due to reduction by residual carbon followed by oxidation to form ZnO. This is discussed further in Section 2.3.2. A phase diagram showing the chemical phase formation as a function of Zn/Ti is shown in Figure 2.3. The solids were calcined at 720°C for 12 h with Zn/Ti ratio ranging from 2/3 to 1/0. These solids are completely crystalline. Figure 2.4 shows the XRD pattern of Z2T calcined at 720°C for 12 h. The higher crystallinity in this case made it easier to resolve the peaks of $Zn_2Ti_3O_8$ and α-Zn_2TiO_4. With increasing relative concentration of titanium, the phase transformation follows ZnO --> Zn_2TiO_4 --> $ZnTiO_3$, $Zn_2Ti_3O_8$ --> TiO_2. All solids with Zn/Ti $\geq$ 2, form Zn_2TiO_4 and/or ZnO. With higher concentration of titanium, all three zinc titanate phases (Zn_2TiO_4, $ZnTiO_3$ and $Zn_2Ti_3O_8$) are viable. At 1000°C, Zn_2TiO_4 is stable. Solids containing either $ZnTiO_3$ or $Zn_2Ti_3O_8$ form Zn_2TiO_4 and TiO_2 at 1000°C.

There are some differences between the results of this work and the work of others. All previous investigators (Cole and Nelson, 1938; Dulin and Rase, 1960; Bartram and Slepetys, 1961; Reddy et al., 1984; Yamaguchi et al., 1987) agree that the phase Zn_2TiO_4 is formed when either Zn/Ti $\geq$ 2 or the calcination temperature is $\geq$ 1000°C. Dulin and Rase (1960) found that $ZnTiO_3$ is stable up to 925 $\pm$ 25°C while Yamaguchi et al. (1987) found a slightly higher temperature (965°C). Above these temperatures, $ZnTiO_3$ decomposes into Zn_2TiO_4 and rutile TiO_2. However, for lower Zn/Ti ratios and lower calcination temperatures, substantial disagreement in the zinc titanate phase formation exists. Table 2.2 summarizes these findings. The major difference is that some investigators reported the formation of $ZnTiO_3$ and Zn_2TiO_4 or $Zn_2Ti_3O_8$ and

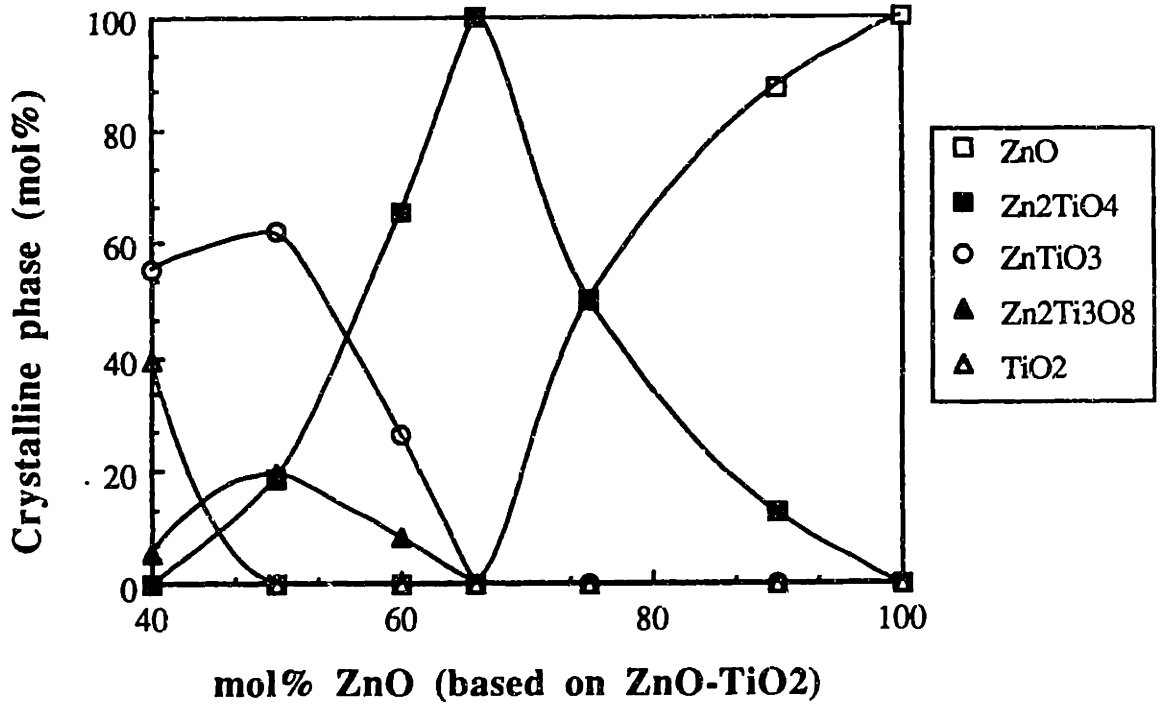

Figure 2.3 Chemical phase formation as a function of Zn-Ti composition of solids calcined at 720°C for 12 h.

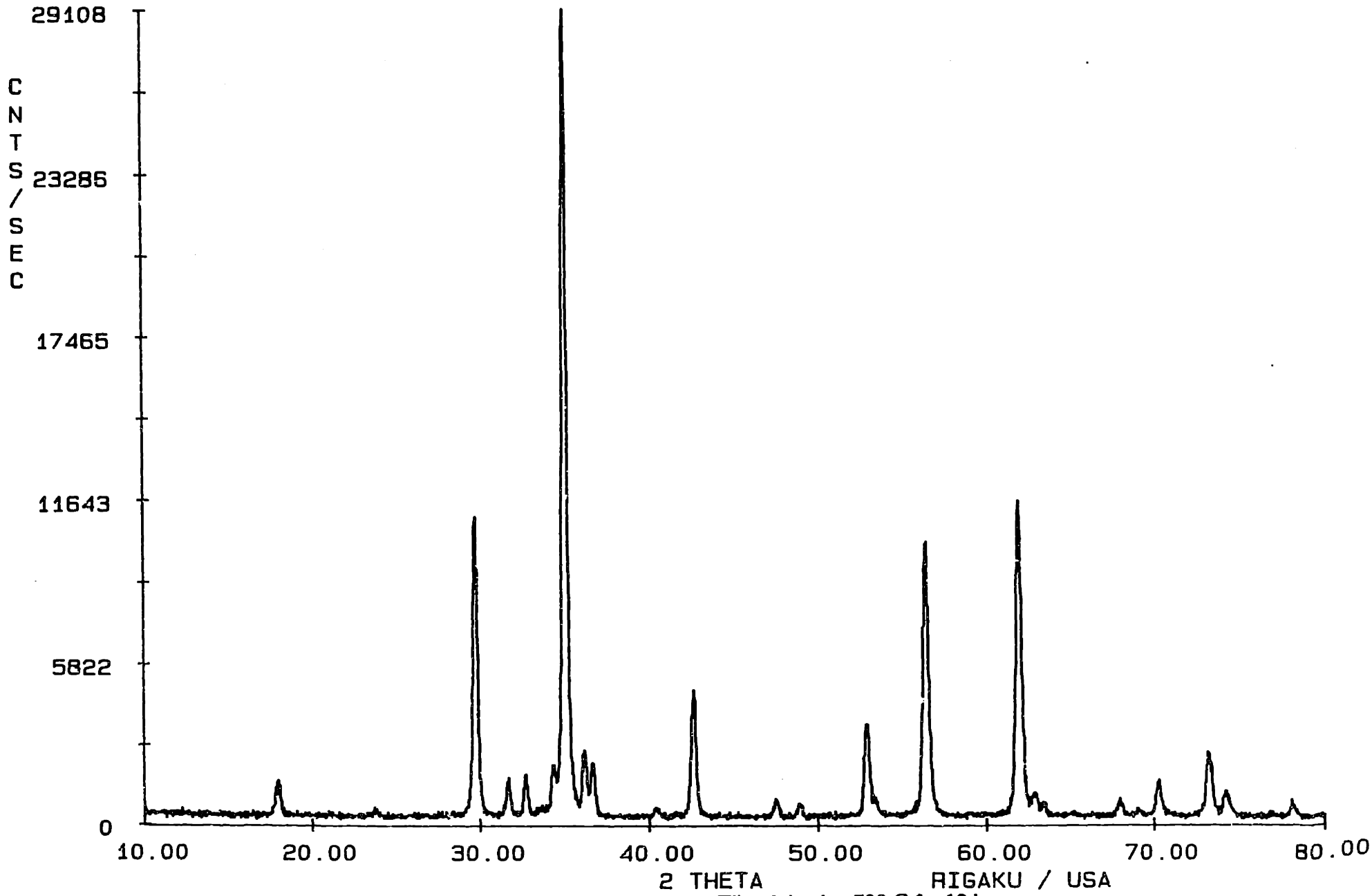

Figure 2.4 XRD patterns of Z2T (2 Zn : 1 Ti) calcined at 720 C for 12 h.

Table 2.2 Stable zinc titanate phases for Zn/Ti < 2 and temperatures below 1000°C.

Literature Source	Preparation Method	Zinc Titanate Phase
Cole and Nelson (1938)	ZnO-TiO_2 solid reaction (600-1000°C)	Zn_2TiO_4-TiO_2 solid solutions
Dulin and Rase (1961)	ZnO-TiO_2(anatase) solid reaction (750-925°C)	Zn_2TiO_4 and $ZnTiO_3$
Bartram and Slepetys (1961)	ZnO-TiO_2(hydrous anatase) solid reaction	Zn_2TiO_4 and $Zn_2Ti_3O_8$
	ZnO-TiO_2(hydrous rutile) solid reaction (600-900°C)	$ZnTiO_3$
Sheinkman et al. (1977)	ZnO-TiO_2(anatase) solid reaction (800°C)	Zn_2TiO_4 and $Zn_2Ti_3O_8$
	ZnO-TiO_2(rutile) solid reaction (800°C)	Zn_2TiO_4 and $ZnTiO_3$
Reddy et al. (1984)	Hydrolysis-pyrolysis of $TiCl_4$ and $ZnCl_2$ (700-900°C)	Zn_2TiO_4 and $Zn_2Ti_3O_8$

Table 2.2 Stable zinc titanate phases for Zn/Ti < 2 and temperatures below 1000°C (cont'd.).

Literature Source	Preparation	Zinc Titanate Phase
Lercher et al. (1984)	Hydrolysis-pyrolysis of $TiCl_4$ and $ZnCl_2$ (500°C)	$ZnTiO_3$
Yamaguchi et al. (1987)	Hydrolysis-pyrolysis of $Ti(OC_3H_7)_4$ and $Zn(C_5H_7O_2)_2$	$Zn_2Ti_3O_8$ (600-765°C) $Zn_2Ti_3O_8$ --> $ZnTiO_3$ (820-965°C) $ZnTiO_3$ --> Zn_2TiO_4 (965-1010°C)
This work	Complexation with citric acid (600-720°C) $Ti(OC_3H_7)_4$ and$Zn(CH_3CO_2)\cdot 2H_2O$	Zn_2TiO_4, $ZnTiO_3$ and $Zn_2Ti_3O_8$

Zn_2TiO_4. Cole and Nelson (1938) observed the formation of Zn_2TiO_4-TiO_2 solid solutions. However, these solid solutions are believed to be the results of poorly resolved Zn_2TiO_4 or $Zn_2Ti_3O_8$ reflections (Bartram and Slepetys, 1961). Bartam and Slepetys (1961) and Sheinkman et al. (1977) found that the type of zinc titanate phase formed depends on the titanium dioxide starting material. Combination of ZnO with anatase forms $Zn_2Ti_3O_8$ as well as Zn_2TiO_4, while with rutile, $ZnTiO_3$ and Zn_2TiO_4 are formed. From their results, Sheinkman et al. (1977) proposed the following reactions:

$$2\,ZnO + TiO_2 \text{ --> } Zn_2TiO_4 \qquad (2.8)$$

$$Zn_2TiO_4 + 2\,TiO_2(\text{anatase}) \text{ --> } Zn_2Ti_3O_8 \qquad (2.9)$$

$$Zn_2TiO_4 + TiO_2(\text{rutile}) \text{ --> } 2\,ZnTiO_3 \qquad (2.10)$$

In contrast, Dulin and Rase (1961) found that $ZnTiO_3$ and Zn_2TiO_4 are formed from the anatase phase of TiO_2. Yamaguchi et al. (1987) proposed an alternate reaction scheme. Upon heating the hydrolysis products at a rate of 10°C/min of $Ti(OC_3H_7)_4$ and $Zn(C_5H_7O_2)_2$, they observed the following reactions:

$$600\text{-}765°C: \quad \text{hydrolysis product} \text{ --> } Zn_2Ti_3O_8 + ZnO \qquad (2.11)$$

$$820°C: \quad Zn_2Ti_3O_8 + ZnO \text{ --> } ZnTiO_3 \qquad (2.12)$$

$$965°C: \quad ZnTiO_3 \text{ --> } 1/2\,Zn_2TiO_4 + 1/2\,TiO_2(\text{rutile}) \qquad (2.13)$$

This reaction scheme is in better agreement with the experimental results obtained in this study. At 1000°C, both $ZnTiO_3$ and $Zn_2Ti_3O_8$ were found to form break into Zn_2TiO_4 and rutile TiO_2. However, in this work, $ZnTiO_3$ was formed at temperatures below 820°C. Whether $ZnTiO_3$ or $Zn_2Ti_3O_8$ is formed depends to a large degree on the preparation conditions and titanium precursor. In most of the previous studies, either rutile or anatase TiO_2 was used. In those cases, either $ZnTiO_3$ or $Zn_2Ti_3O_8$ was formed

exclusively. However, in this study, titanium (IV) i-prepoxide was used which can yield both $ZnTiO_3$ and $Zn_2Ti_3O_8$. $ZnTiO_3$ is present at lower temperatures than 820°C because a complexation technique with citric acid was used. As discussed previously, because of the smaller diffusion length of the reactants, lower temperatures (than the hydrolysis-pyrolysis technique) can be used to form different phases. In this study, at 500°C, the solids were very microcrystalline with the formation of either $Zn_2Ti_3O_8$ and/or Zn_2TiO_4. At 600°C, $ZnTiO_3$ is formed. The transformations observed here ($Zn_2Ti_3O_8$ and/or Zn_2TiO_4 --> $ZnTiO_3$ --> Zn_2TiO_4+TiO_2) would be in agreement with Yamaguchi et al. (1987) if the low temperature (500°C) zinc titanate phase was $Zn_2Ti_3O_8$.

2.3.2 Physical Properties

The effects of mixed oxide compositions and calcination temperatures on the solid physical properties were determined. SEM micrographs of ZT (1 Zn:1 Ti) calcined from 500-800°C are shown in Figures 2.5-2.8. The surface area variations with temperature are shown in Figure 2.9 for ZT in addition to Z2T3, Z2T and ZnO. ZT calcined at 500°C is very microcrystalline (Figure 2.5). The average crystal size is between 0.01-0.08 μm with a corresponding surface area of 51.3 m^2/g. At 600 and 700°C, there is no large change in the surface morphologies of the solids (Figure 2.6 and 2.7). The surface of these solids has higher zinc concentration than the bulks. Zn/Ti ratios of 1.5 were detected by EDS. The crystallinity of the solids increases with increasing calcination temperature with a corresponding drop in surface area (to 2.4 m^2/g at 700°C). The largest change is observed in ZT calcined at 800°C (Figure 2.8). Large rod-shaped crystals are found on the surface. EDS analyses of these crystals find

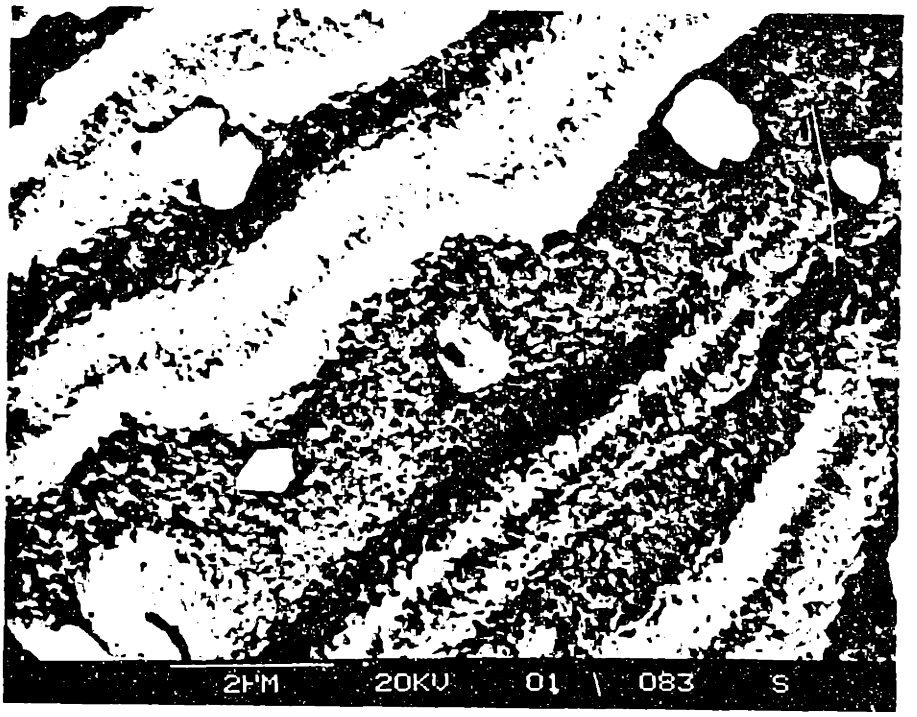

a)

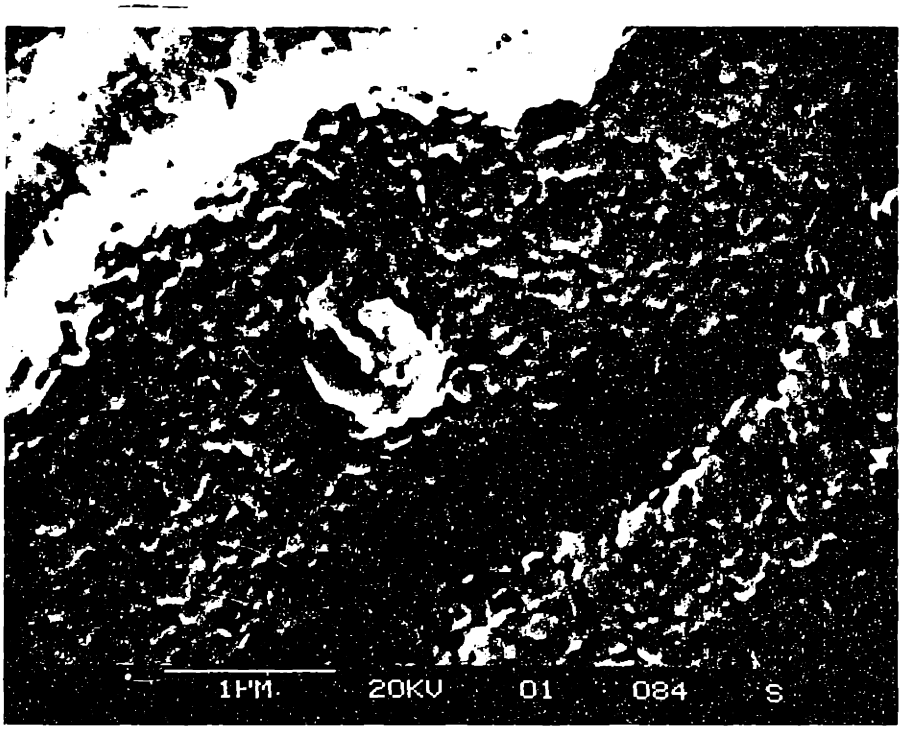

b)

Figure 2.5 SEM micrographs of ZT (1 Zn : 1 Ti) calcined at 500°C for 4 h a) 10000x and b) 20000x.

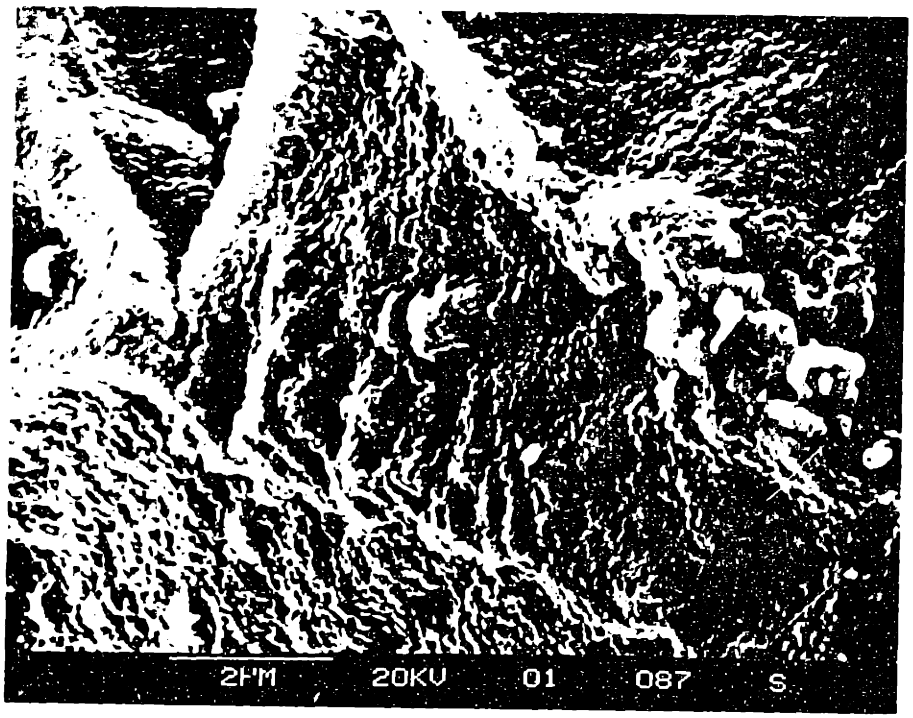

a)

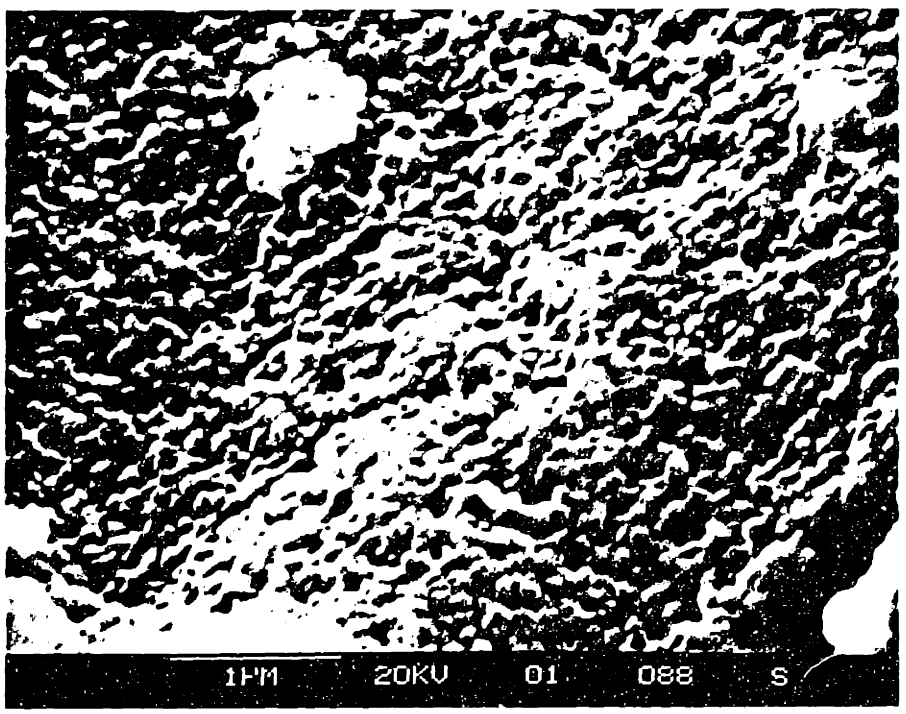

b)

Figure 2.6 SEM micrographs of ZT (1 Zn : 1 Ti) calcined at 600°C for 4 h a) 10000x and b) 20000x.

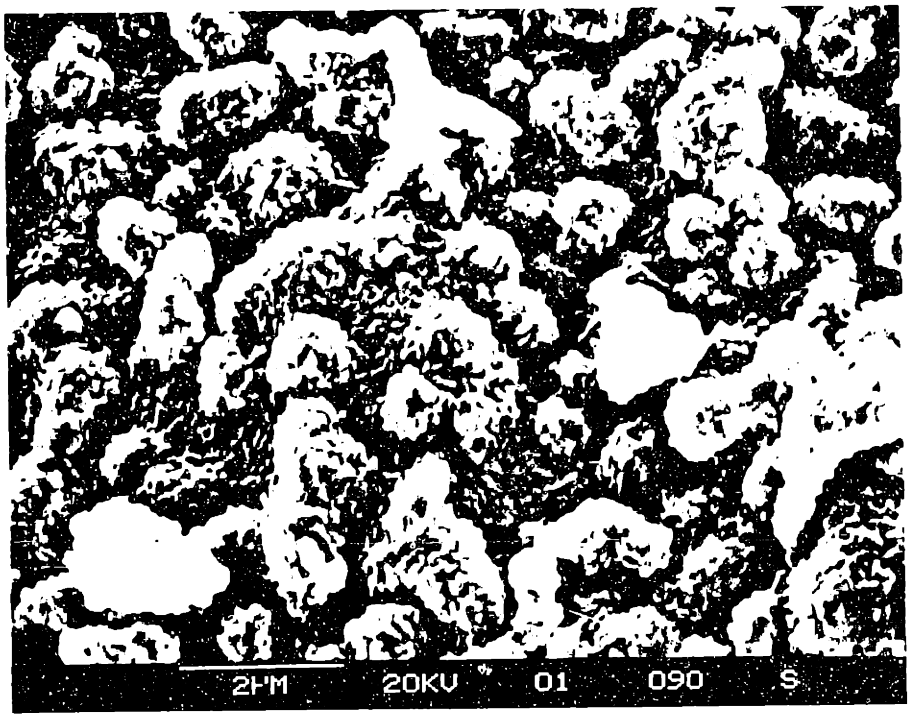

a)

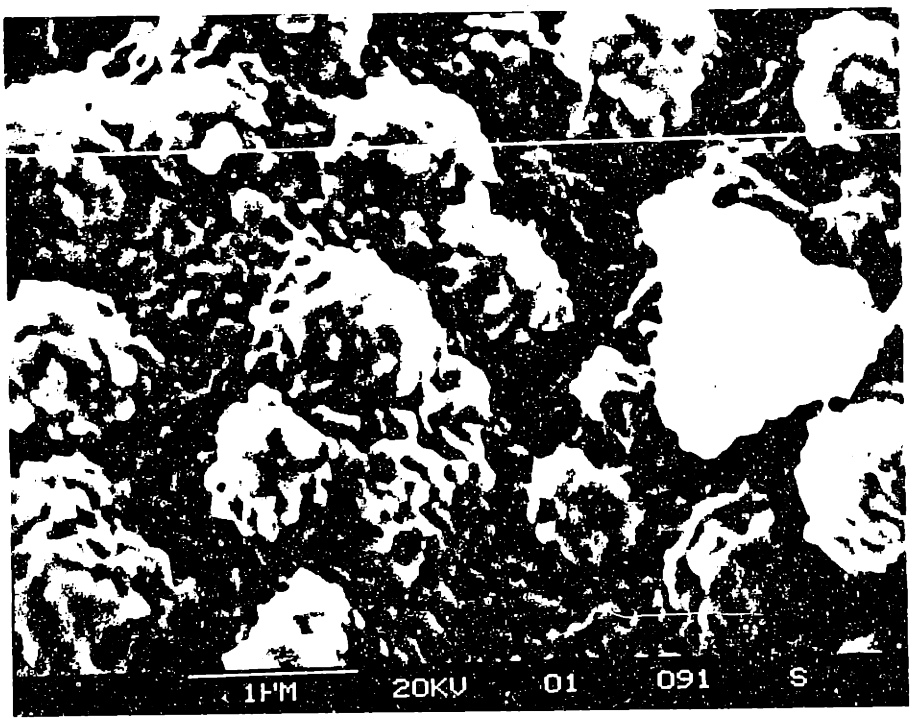

b)

Figure 2.7 SEM micrographs of ZT (1 Zn : 1 Ti) calcined at 700°C for 4 h a) 10000x and b) 20000x.

a)

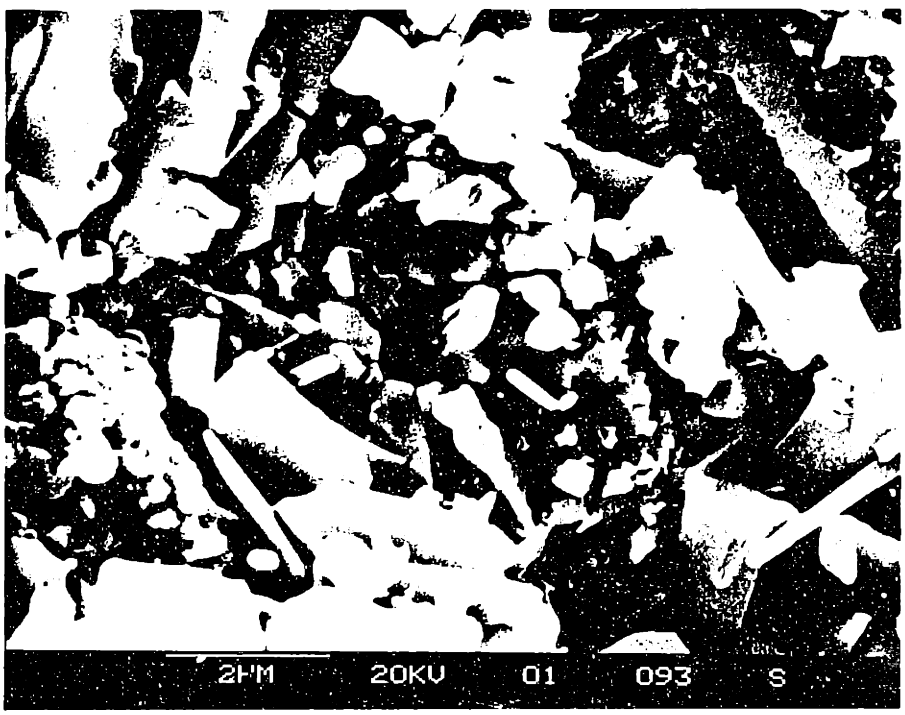

b)

Figure 2.8 SEM micrographs of ZT (1 Zn : 1 Ti) calcined at 800°C for 4 h a) 5000x and b) 10000x.

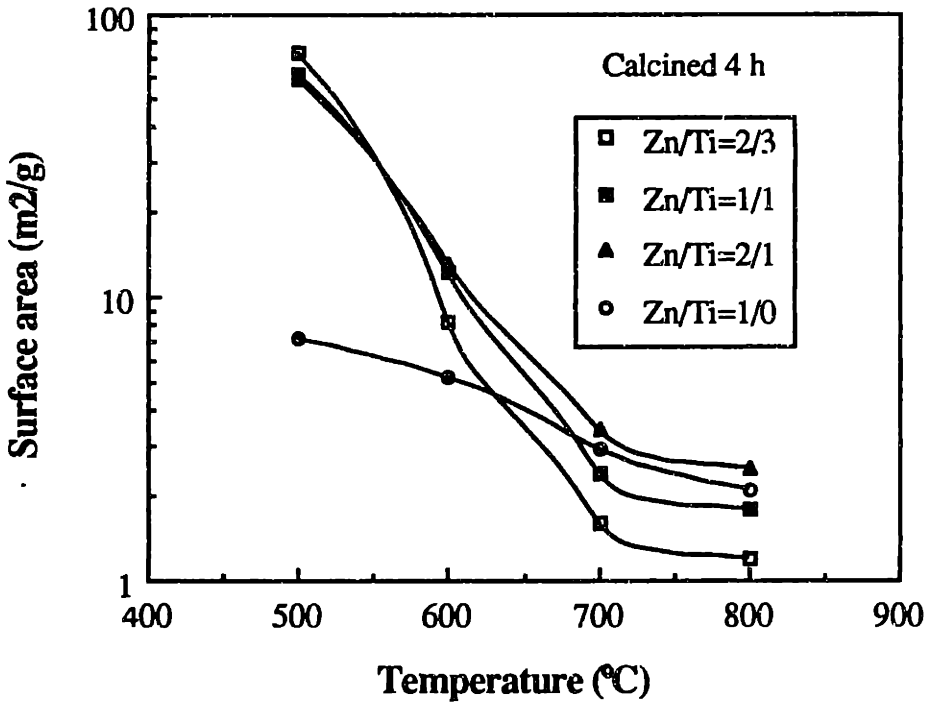

Figure 2.9 Effect of calcination temperature on the Zn-Ti-O surface area.

Zn/Ti=8.9. These crystals are believed to result from the reduction of zinc titanate and zinc oxide by carbon in the bulk of the solid to form Zn(g), according to the reactions:

$$Zn_xTi_yO_{x+2y}(s) + x\ C(s) \rightarrow x\ Zn(g) + x\ CO(g) + y\ TiO_2(s) \qquad (2.14)$$

$$Zn_xTi_yO_{x+2y}(s) + x\ CO(g) \rightarrow x\ Zn(g) + x\ CO_2(g) + y\ TiO_2(s) \qquad (2.15)$$

Whereupon Zn(g) diffuses out and reacts with O_2 to form ZnO crystals by:

$$Zn(g) + 1/2\ O_2(g) \rightarrow ZnO(s) \qquad (2.16)$$

Zinc titanates prepared by the amorphous citrate technique form a "skin" (or "crust") of low porosity. Figure 2.10 shows SEM micrographs of the solid Z3T calcined at 720°C for 12 h. In comparison to this "skin" (Figure 2.10a), the bulk of the solid (Figure 2.10b) is much more porous. The zinc titanate "skin" formation causes lower solid reactivity in sulfidation (Chapter 4). Since sulfidation is accompanied by the formation of a solid product of higher molar volume than the reactant, the reactivity decreases as the "skin" porosity goes to zero. This effect can be lessened by crushing the solid to a small size. Another way to diminish the effect of the "skin" formation is by preparing a solid with a higher amount of citric acid. The evolution of large amounts of CO_2 and H_2O causes the formation of a more porous "skin". ZnO also formed a "skin". In contrast, however, this "skin" is very porous (Figure 2.11).

Typical pore size distributions are shown in Figure 2.12 for solid Z3T and ZnO calcined at 720°C for 12 h with particle size, 90-125 μm. Solids prepared by the amorphous citrate technique have characteristically large pores formed by the evolution of CO_2 and H_2O during the heating process. For Z3T, a bimodal pore size distribution is present. The pores are predominantly 12 μm (radius). There is also a smaller peak (approximately 10% to the total pore volume) with pores approximately 0.028 μm

a)

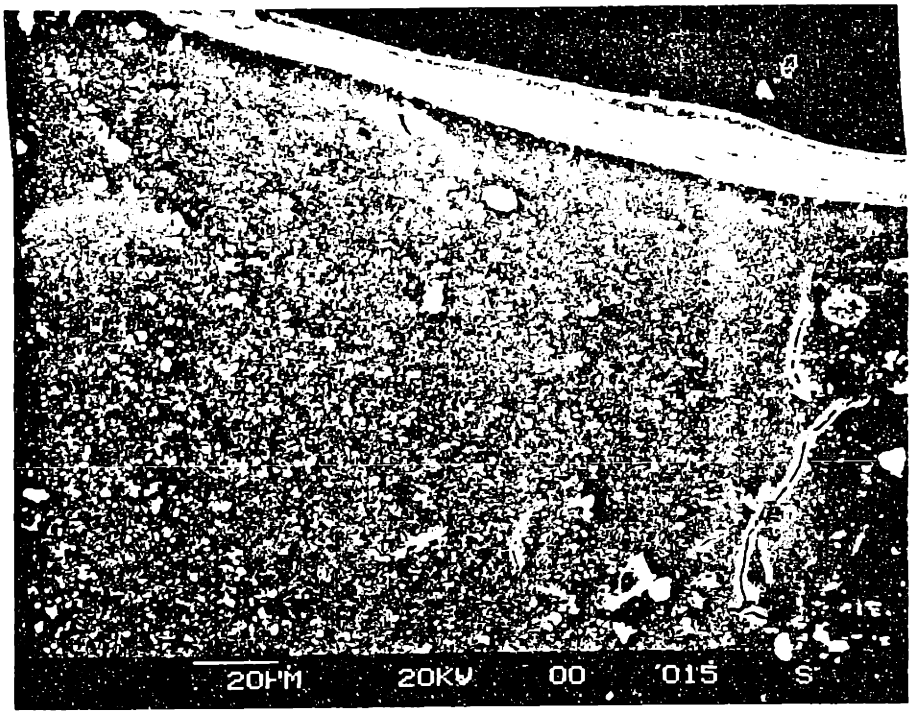

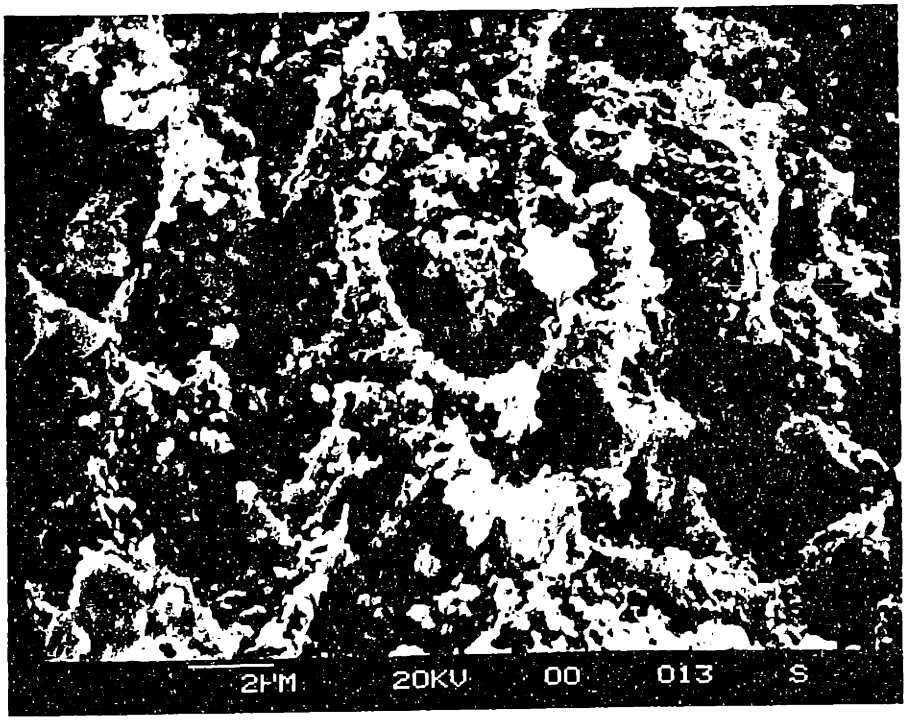

b)

Figure 2.10 SEM micrographs of Z3T (3 Zn : 1 Ti) calcined at 720°C for 12 h a) surface "skin" and b) porous bulk.

a)

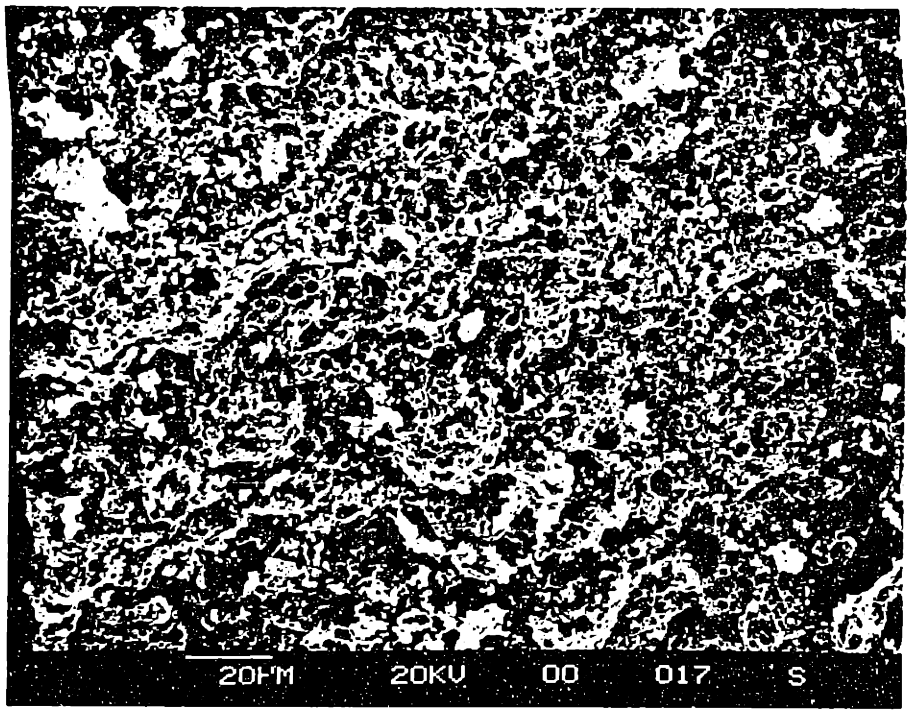

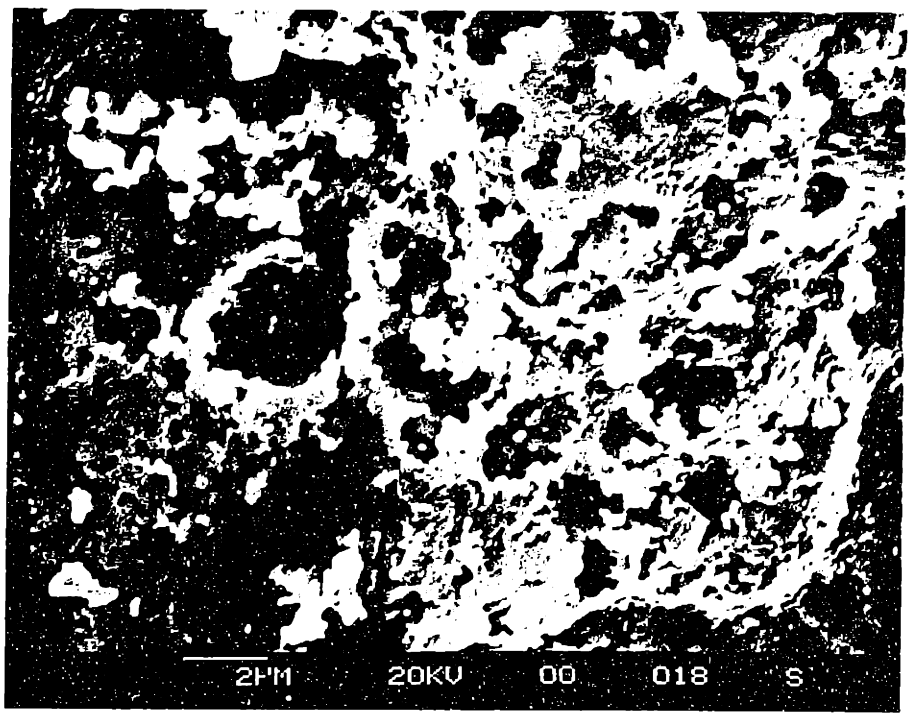

b)

Figure 2.11 SEM micrographs of ZnO calcined at 720°C for 12 h.

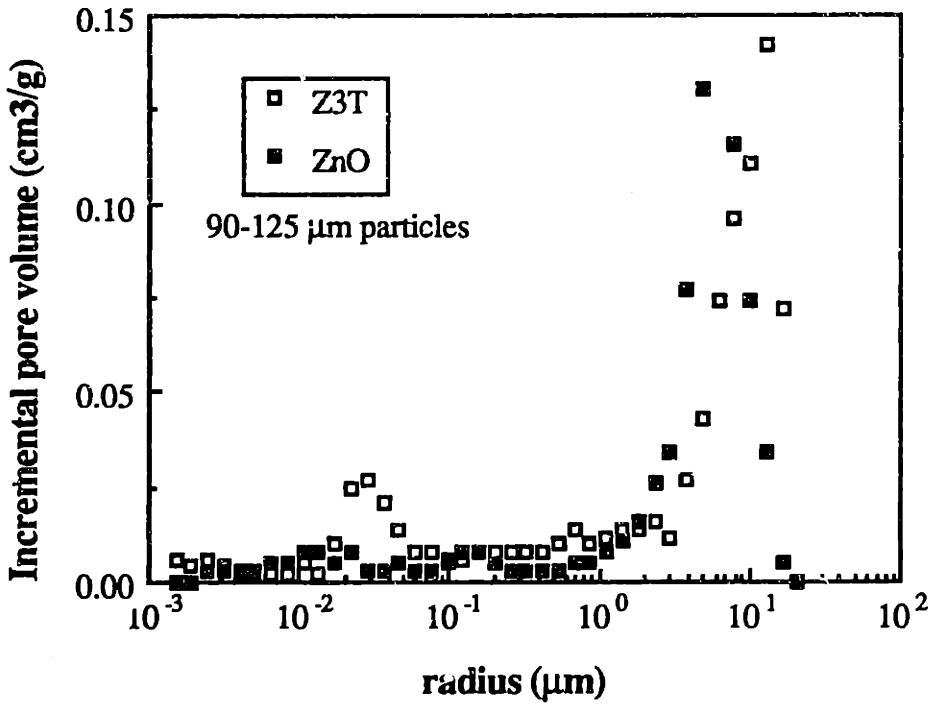

Figure 2.12 Pore size distributions of Z3T (3 Zn:1 Ti) and ZnO calcined at 720°C for 12 h.

(radius). ZnO, however, is characterized by a unimodal pore size distribution. The center of the peak in the ZnO pore size distribution plot is approximately 6 μm (radius). The lower percentage (< 1%) of smaller pores (~0.028 μm) in ZnO is consistent with the lower surface area of ZnO (1.3 m^2/g) compared to Z3T (7.6 m^2/g).

The effect of Zn/Ti ratio on the solid surface area and pore volume is shown in Figures 2.13 and 2.14, respectively. These solids were calcined at 720°C for 12 h. The presence of titanium in the solids can yield higher surface area than pure ZnO. Maxima in the surface area and pore volume profiles are found at Zn/Ti ≈ 9. Figure 2.9 also shows similarly high surface for Zn-Ti mixed oxides at various temperatures. At 500°C, the surface area of Zn-Ti mixed oxides with Zn/Ti ratio ranging from 2/3 to 2/1 is in the range of 73-54 m^2/g, while for ZnO it is only 7 m^2/g. Thus, TiO_2 addition into ZnO suppresses the grain growth of the latter. Inhibition of grain growth by second solid phase inclusion has been observed by others. Weyl (1952) observed that lithium oxide can decrease the rate of ZnO sintering while aluminum oxide increases it. Gupta (1971) found that potassium oxide can decrease the rate of ZnO sintering.

2.4 CONCLUSIONS

1. Three zinc titanate phases (Zn_2TiO_4, $ZnTiO_3$, $Zn_2Ti_3O_8$) can be formed through solids preparation by the complexation method with citric acid using zinc acetate and titanium (IV) iso-propoxide precursors followed by pyrolysis at different time-temperature conditions.

2. The observed phase transformation with increasing temperature is: $Zn_2Ti_3O_8$ --> $ZnTiO_3$ --> Zn_2TiO_4.

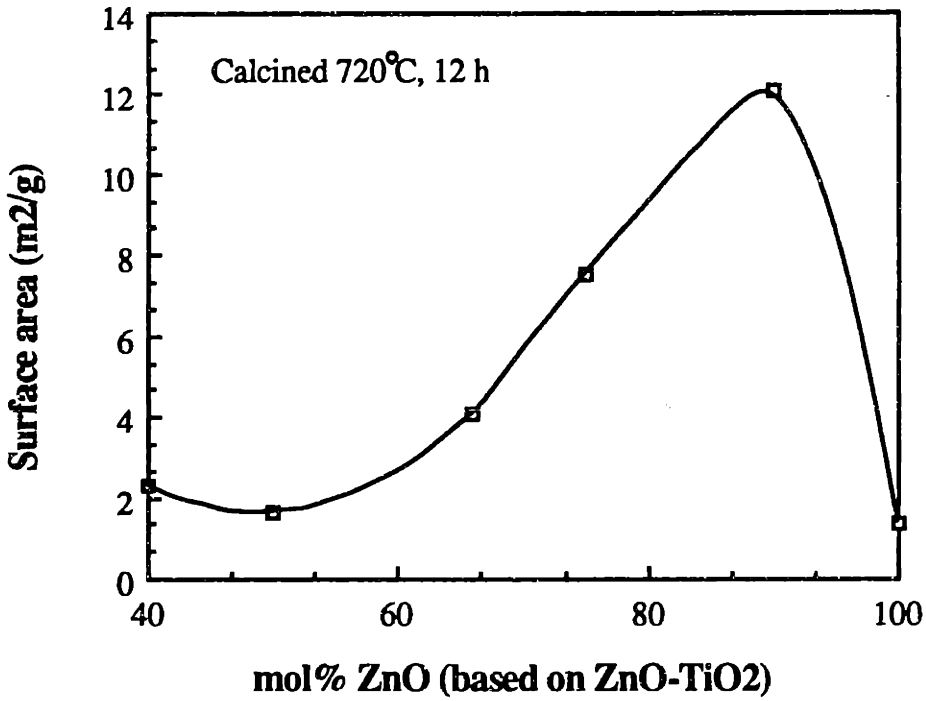

Figure 2.13 Effect of Zn-Ti composition on the surface area.

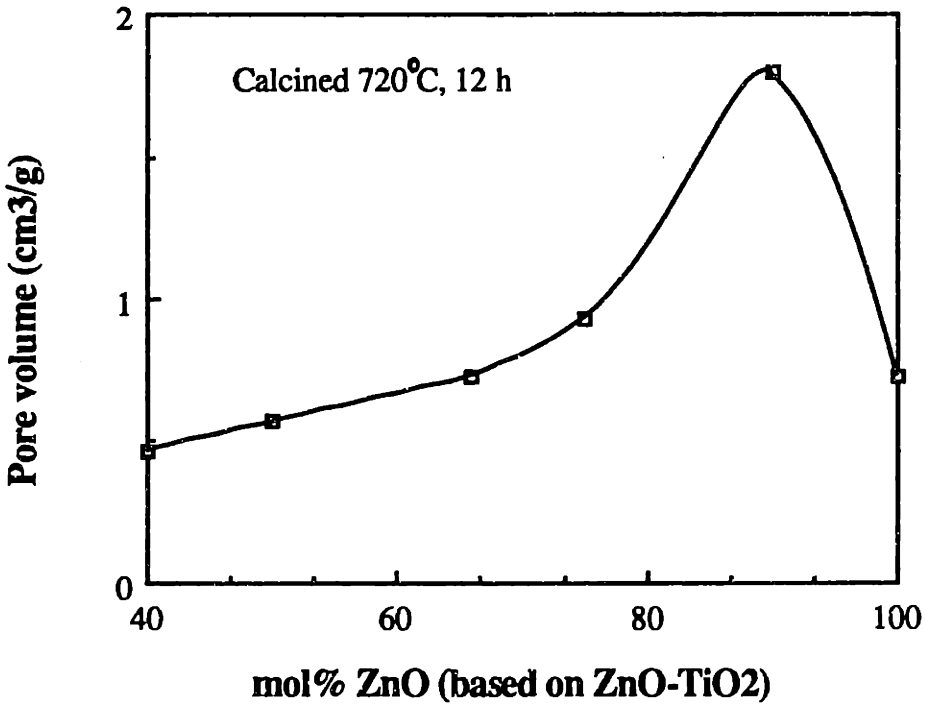

Figure 2.14 Effect of Zn-Ti composition on the pore volume.

3. Zn_2TiO_4 is the stable phase for all Zn-Ti-O solids calcined at temperatures $\geq$ 1000°C or for solids with Zn/Ti $\geq$ 2 calcined at temperatures $\geq$ 700°C and for long period of time ($\geq$ 12 h). At temperatures below 800°C, all three phases ($Zn_2Ti_3O_8$, $ZnTiO_3$, Zn_2TiO_4) may be present.

4. Higher surface area and pore volume (than for pure ZnO) can be attained with Zn-Ti mixed oxides.

CHAPTER 3

REDUCTION OF ZN-TI-O MATERIALS

3.1 INTRODUCTION

The removal of H_2S to sufficiently low levels from coal-derived gas streams at elevated temperatures is crucial for the efficient and economic coal utilization in emerging advanced power generating systems such as the integrated gasification-combined cycle and the gasification-molten carbonate fuel cell. Previous studies (Jalan and Wu, 1980; Grindley and Steinfeld, 1981) have investigated zinc oxide as a regenerable sorbent. The thermodynamic equilibrium for ZnO sulfidation is quite favorable, yielding desulfurization down to a few parts per million (ppm) H_2S at typical hot gas cleanup temperatures (500-700°C). However, a difficulty with all sorbents containing zinc oxide is some reduction to volatile elemental zinc at temperatures above 600°C. Typically, coal gases contain a mixture of CO (7-42%), H_2 (18-29%), H_2O (10-50%), and CH_4 (0.1-4.3%). The relative composition depends on the type of gasifier used (e.g. fluidized-bed KRW gasifier) and the extent of quenching the gas with water. In addition to these gases, minor compounds, most of them undesirable or deleterious, such as H_2S and alkali, exit the coal gasifier. The amounts of these components depend

on the type of coal and the type of gasifier used. The instability of zinc oxide in a reducing atmosphere limits its operating temperature to approximately 600°C. Mixed Zn-Ti-O materials were examined in this thesis as possible alternative, regenerable sulfur sorbents for H_2S capture which may be more resistive towards reduction to volatile elemental zinc.

The reduction of ZnO by carbon monoxide and hydrogen gas has been the subject of many studies over the years. Some of the earlier investigators (Bodenstein, 1927; Maier and Ralston, 1928) were mainly interested in the extraction of zinc from ores in a retort furnace by the reaction:

$$ZnO(s) + C(s) = Zn(g) + CO(g) \qquad (3.1)$$

Subsequently, the carbon monoxide formed can itself reduce ZnO by:

$$ZnO(s) + CO(g) = Zn(g) + CO_2(g) \qquad (3.2)$$

$$CO_2(g) + C(s) = 2CO(g) \qquad (3.3)$$

These early studies, however, were performed at near equilibrium conditions.

More recent investigations (discussed in the next paragraph) examined the reaction of ZnO with H_2 as well as CO under non-equilibrium conditions to determine kinetic parameters of the reaction. Because the reduction reaction is highly reversible, various methods were used to ensure that gas diffusion was not rate determining and the reaction was not at equilibrium. The equilibrium constants at various temperatures for the reduction of ZnO and Zn_2TiO_4 with H_2 are shown in Figure 3.1 (Barin and Knacke, 1973; Barin et al., 1976). Typically, the equilibrium constants are small ($\sim 10^{-2}$) with $\Delta G > 0$.

Several studies (Truesdale and Waring, 1944; Guger and Manning, 1971; Gioia et al., 1977) used sintered ZnO pellets to investigate the reaction. Hegedus and Kiss (1966) used ZnO powders in their studies. Grunze and Hirschwald (1974; 1975) studied the reaction of powders, sintered samples, and single crystals at low pressure (0.01-10 Torr). The low pressure served to eliminate as much as possible any diffusional effects. Table 3.1 lists the experimental conditions and activation energies reported in the literature for the reduction of ZnO with H_2 and CO. These experiments were performed in the temperature range of 350-1500°C. ZnO reduction by H_2 has been detected at temperature as low as 160°C (Bonasewicz et al., 1981). From the similarity in the activation energies for both reduction in H_2 and CO, it was concluded that the same reduction mechansim is present in reaction with both gases (Grunze and Hirschwald, 1975). However, the frequency factor of the rate constant for reduction of ZnO with H_2 is approximately twice as large as that with CO. At higher pressures, Grunze and Hirschwald (1974; 1975) observed increasing activation energies. As the temperature increased and the pressure decreased, the reaction order increased from 0.25 to 1. Interesting results were obtained with different types of samples. Reduction of zinc oxide single crystals gave lower activation energies than with powders. Grunze and Hirschwald (1975) hypothesized that in porous powders, removal of the products is hindered. Part of the enthalpy of reaction is included in the experimental activation energies. Consequently, higher activation energies are observed.

The presence of water vapor significantly affected the reduction of ZnO. Through thermogravimetric studies, Hegedus and Kiss (1966) observed that as the water vapor content in a flowing stream of hydrogen increased from 7.0×10^{-3}% (0.053 Torr) to 5.9×10^{-2}% (0.45 Torr), the activation energy for reduction increased from 27.4 kcal/mol to 52 kcal/mmol. Correspondingly, as the amount of water vapor was

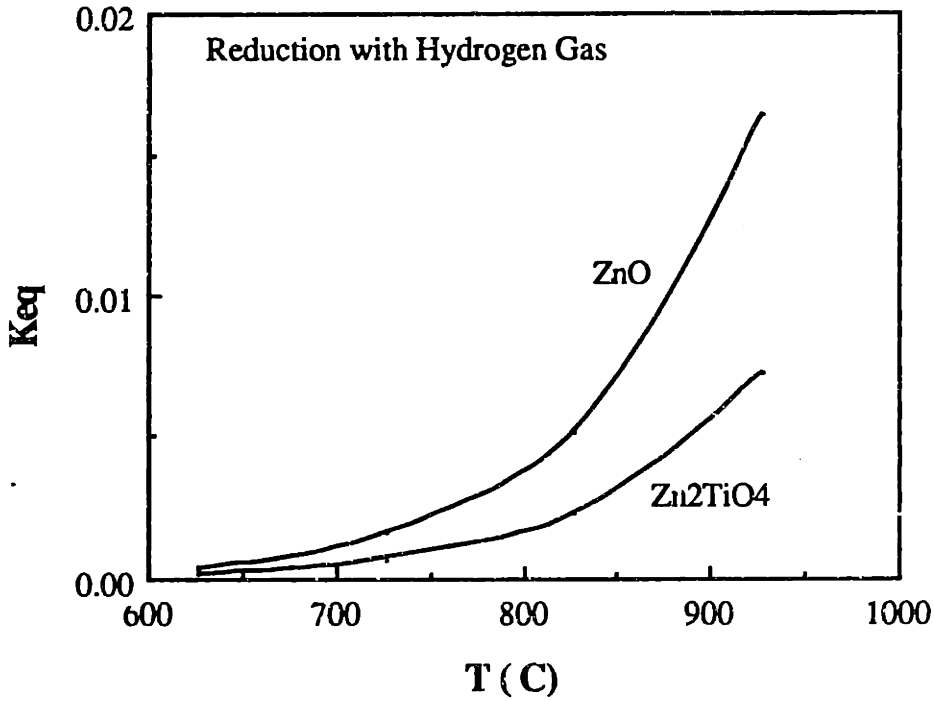

Figure 3.1 Equilibrium constants for ZnO and Zn2TiO4 reduction with hydrogen gas. (Barin and Knacke, 1973; Barin et al., 1976)

Table 3.1 Apparent activation energies and experimental conditions reported in the literature for ZnO reduction with (A) CO and (B) H_2.[1]

Reference	Pressure (Torr)	Temperature (°C)	Apparent Activation Energy (kcal/mol)		
			Powders	Sintered samples	Single crystals
Truesdale and Waring (1944)	760	750-1100		A: 20-25 B: 20-25	
Hegedus and Kiss (1966)	760	450-640	B: 27		
Guger and Manning (1971)	760	1000-1500		A: 38	
Gioia et al. (1977)	760	770-970		B: 29	
Grunze and Hirschwaid (1974; 1975)	10^{-1}-10^{-2} 10^{-2}-8 10^{-2}-4	500-700 415-800 500-800	A: 28	 A: 13-31 B: 19-29	
Gast et al. (1976)	10^{-2}-10^{-1}				A: $(000\bar{1})$: 14 A: (0001): 17 A: $(10\bar{1}0)$: 16
This work	760	550-1050	B: 23		

[1] modified table from Grunze (1981)

increased, the reduction rate decreased. However, when the amount of H_2O was increased further to 2.1% (16.2 Torr), no further change in the activation energy was observed. Flytzani-Stephanopoulos et al. (1987) also observed lower zinc oxide as well as zinc titanate reduction rates in the presence of H_2O vapor.

The first literature study to examine the reduction of Zn-Ti-O materials was performed by Flytzani-Stephanopoulos et al. (1987). A lower reduction rate by as much as five times was reported for Zn-Ti-O solids compared to ZnO. However, these experiments were carried out in a fixed bed reactor where mass transfer resistance may have been limiting. It has been reported by Hirschwald and Noack (1972) that it is possible to decrease the reducibility of ZnO by the inclusion of small amount of foreign atoms. They found that the reduction of ZnO can be inhibited by the addition of small amount (1 mol%) of Li_2O, Al_2O_3, or Ga_2O_3. They attributed this to a change in the electronic state of zinc oxide. However, no similar effects had been was reported about TiO_2.

A major objective of this thesis was to determine whether Zn-Ti-O materials are intrinsically more resistive to reduction than ZnO and to determine the composition of Zn-Ti-O needed to yield the lowest reduction rate. The mechanisms and kinetics of the reduction of Zn-Ti-O solids were studied and compared with ZnO reduction to elucidate the role of titanium in imparting greater resistivity to reduction reaction. Hydrogen reduction only was investigated. From the studies of others (Grunze and Hirschwald, 1974), reduction of ZnO in H_2 is faster than in CO. Thus, the reduction rates obtained with H_2 represent the maximum amount of zinc loss possible in a coal gas atmosphere. In addition, the effect of H_2O on the rate of reduction was examined since it is a major component in coal gases, and it was observed by others (Hegedus and Kiss, 1966;

Flytzani-Stephanopoulos et al., 1987) to have an inhibitory effect on the reduction of ZnO. The effect of H_2S on reduction was also investigated.

3.2 EXPERIMENTAL METHODS

Reduction experiments with solids containing various Zn/Ti atomic ratios were performed. The preparation and characterization of the solids were discussed in Chapter 2. The analytical techniques included BET-N_2 for surface area measurement, scanning electron microscopy (SEM) coupled with energy dispersive X-ray (EDS) analysis for surface morphology and elemental distribution determination, and X-ray diffraction (XRD) for crystalline phase identification. To ensure that rate measurements were performed in the absence of gas phase diffusion limitation or equilibrium limitation, small amounts (1-2 mg) of material was used in each test and several samples were sintered at 1000°C for 1 h to reduce their surface area. The chemical and physical properties of solids used in reduction experiments are shown in Table 3.2.

Kinetic experiments were performed in a Cahn System 113-X thermogravimetric analyzer (TGA) equipped with a Cahn 2000 electrobalance, a Micricon temperature controller, and a Bascom Turner data acquisition system. The TGA measured the weight loss as a function of the time required for with reduction to Zn followed by rapid zinc vaporization.

The reactant gas containing various concentrations of H_2, H_2O vapor, and N_2 was introduced into the apparatus through a side arm (Figure 3.2). Gas flow rates were set by passing H_2 and N_2 gases through Brooks Model 5850E mass flow controllers. A gas flow rate of 485 sccm was used in the experiments. Water vapor was added to the gas by bubbling nitrogen and hydrogen through a water saturator maintained at either

Table 3.2 Chemical and Physical Properties of Sorbents[1]

Sorbent	(Zn/Ti) (atomic ratio)	Calcination Temperature[2] (°C)	Surface Area (m^2/g)	Crystalline Phases (wt %)				
				ZnO	Zn_2TiO_4	$Zn_2Ti_3O_8$	$ZnTiO_3$	TiO_2
ZnO	---	1000, 1 h	0.68	100	0	0	0	0
Z9T	9/1	1000, 1 h	1.03	70	30	0	0	0
Z3T	3/1	1000, 1 h	0.94	25	75	0	0	0
Z2T	2/1	1000, 1 h	0.76	0	100	0	0	0
Z3T2	3/2	720, 12 h	2.18	0	68	14	18	0
ZT-a	1/1	1000, 1 h	0.40	0	75	0	0	25
ZT-b	1/1	720, 12 h	1.64	0	20	35	45	0
Z2T3-a	2/3	720, 12 h	2.29	0	0	16	65	19
Z2T3-b	2/3	700, 12 h	1.30	0	0	0	83	17

[1] Reduction experiments performed with 90-125 μm particles

[2] Sorbents calcined at 1000°C were first calcined at 720°C for 12 h

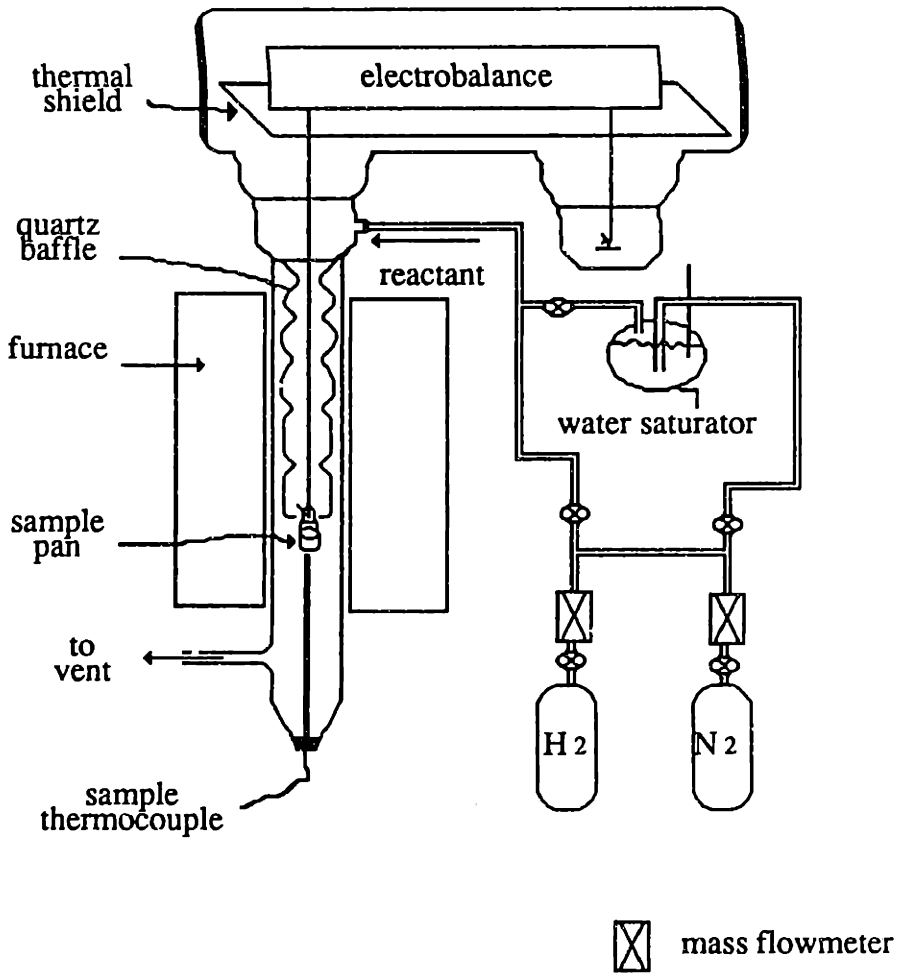

Figure 3.2 Schematic of the thermobalance reactor system.

25°C or 51°C in a three-neck flask assembly. The saturated gas stream entered the apparatus side arm through heated lines. A thin layer of sample (~1 mg and 90-125 μm size particles) was placed on a quartz pan suspended by a quartz hangdown wire. Isothermal reduction experiments were performed at temperatures between 550-1050°C. The sample was pretreated in a vacuum oven at 90°C for 1 h to remove any absorbed H_2O before it was reacted in the TGA.

It was not possible to directly examine the effect of hydrogen sulfide on reduction since in addition to reduction, sulfidation would also occur. To separate these effects, the solids were first partially sulfided (10-15%) in 2 mol% H_2S-1 mol% H_2-97 mol% N_2 and then reduced in 10 mol% H_2-90 mol% N_2. Sulfidation and reduction were performed at the same temperature.

3.3 PRESENTATION AND DISCUSSION OF REDUCTION RESULTS

3.3.1 Initial Reduction Rate of Bulk Zn-Ti-O Sorbents: Hydrogen-Nitrogen Mixtures

Initial rate experiments in the TGA were performed under isothermal conditions to determine the reduction reactivity of solids containing various atomic ratios of Zn:Ti and various chemical phases (e.g. ZnO, Zn_2TiO_4, $ZnTiO_3$, and $Zn_2Ti_3O_8$). Kinetic parameters (e.g. activation energies) were determined from these experiments. The possible overall reduction reactions are:

$$ZnO(s) + H_2(g) \text{---> } Zn(g) + H_2O(g) \quad (3.4)$$

$$1/2\ Zn_2TiO_4(s) + H_2(g) \text{---> } Zn(g) + H_2O(g) + 1/2\ TiO_2(s) \quad (3.5)$$

$$ZnTiO_3 + H_2(g) \text{---> } Zn(g) + H_2O(g) + TiO_2(s) \quad (3.6)$$

$$1/2\ Zn_2Ti_3O_8 + H_2(g) \text{---> } Zn(g) + H_2O(g) + 3/2\ TiO_2(s) \quad (3.7)$$

$$3\,TiO_2(s) + H_2(g) \text{---> } Ti_3O_5(s) + H_2O(g) \qquad (3.8)$$

At 1300 K, the K_{eq} for reaction (3.8) is 3.4×10^{-3} for the rutile form of TiO_2. Although this value is small, reduction of TiO_2 is possible. To check whether there is any reduction of TiO_2, both rutile (UCI 1090-113 extrusions crushed to 90-125 μm size particles) as well as anatase (obtained from Aldrich Chemical Co.) were reacted with H_2 at 700°C. The reduction of TiO_2 in hydrogen at elevated temperature can be observed by a change in color from white to bluish gray (Matsuda and Kato, 1983) due to the formation of Ti_3O_5. No weight change of either crystalline forms of TiO_2 was observed after 90 minutes in 10 mol% H_2-90 mol% N_2 at 700°C. Also the color of both materials remained white after the experiments. Thus, reduction of TiO_2 did not take place under these conditions.

In addition to the above overall reduction reactions, there is the possiblity of zinc loss by dissociative vaporization of ZnO according to the reactions:

$$ZnO(s) \text{--> } Zn(g) + 1/2\ O_2(g) \qquad (3.9)$$

$$1/2\ O_2(g) + H_2(g) \text{--> } H_2O(g) \qquad (3.10)$$

However, reaction (3.9) becomes significant only above 1300-1400°C (Hirschwald and Stolze, 1971). At 1300°C, the experimentally measured vapor pressure is only about 1 Torr. Several other investigators (Moore and Williams, 1959; Secco, 1960) have reported rapid vaporization of ZnO in a zinc vapor atmosphere at temperatures below 1300°C. However, Kodera et al. (1968) found that the apparently accelerated vaporization rates were due to the presence of carbonaceous impurities which reacted with ZnO to produce CO. Subsequently, CO reacted with ZnO. Most of the Zn-Ti-O materials used in this study were calcined at 1000°C. This ensured that no residual

carbon was present in the samples. However, it was neccessary to also have some Zn-Ti-O materials calcined at only 720°C to obtain reduction rate measurements for different zinc titanate phases.

The rate of zinc loss was measured at temperatures between 550-1050°C in various concentrations of hydrogen. It was assumed that this measured rate represents the rate of reduction. In this temperature range, zinc can exist either in a liquid or gas phase. At temperatures below 420°C, zinc exists in the solid phase. Between 420-911°C, zinc exists in the liquid phase (Barin and Knacke, 1973; Barin et al., 1976). Above 911°C, only gaseous zinc is formed. Although at 550°C, liquid zinc is formed, its vapor pressure (5.92 Torr) is high enough that it will completely evaporate. Thus, at temperatures below 911°C, the reactions for ZnO reduction are:

$$ZnO(s) + H_2(g) \rightarrow Zn(l) + H_2O(g) \qquad (3.11)$$

$$Zn(l) \rightarrow Zn(g) \qquad (3.12)$$

To determine whether the assumption that the rate of zinc evaporation (Eq. 3.12) is relatively rapid compare to the rate of reduction (Eq. 3.11), the rate of evaporation was calculated. Assuming reaction (3.11) is much faster than reaction (3.12), at 550°C with a gas flowrate of 485 sccm, the calculated rate of zinc loss is 3×10^{-6} mol Zn/s. In contrast, the measured rate of zinc loss of ZnO (calcined at 1000°C) in 10 mol% H_2-90 mol% N_2 at 550°C was approximately three orders of magnitude smaller. Consequently, the rate determining step is the reduction reaction (Eq. 3.11).

Reactions 3.4 and 3.5 are endothermic. At 1300 K, the heat of reaction for (3.4) is 51400 cal/mol and for reaction (3.5) is 51100 cal/mol (Barin and Knacke, 1973; Barin et al., 1976). Thermodynamic data were not available for $ZnTiO_3$ or $Zn_2Ti_3O_8$. With

the relatively high heats of reaction, there is some concern about possible cooling effects. A simple estimate of the maximum possible temperature drop using known methods discussed in Smith (1970) was made. The calculations are shown in Appendix A. At 1300 K, the calculated decrease in temperature across the gas film is only 1.8°C for ZnO in a gas containing 10 mol% H_2-90 mol% N_2. Thus, the isothermal assumption is valid for these experiments.

The initial reduction rate of various Zn-Ti-O materials listed in Tables 3.2 was measured in 10 mol% H_2-90 mol% N_2. The initial rate was calculated by:

$$R_o = \frac{\left.\frac{dW}{dt}\right|_{t=0}}{(81.3794)\, A_o} \qquad (3.13)$$

where the initial rate R_o [=] mmol cm^{-2} s^{-1}, $(dW/dt)_{t=0}$ [=] mg/s is the slope of the weight vs. time profile at t=0, 81.3794 is the molecular weight of ZnO, and A_o [=] cm^2 is the initial surface area of the reactant solid. Comparative plots of the inital reduction rates of solids containing various Zn:Ti atomic ratios reacted at 600 and 700°C are shown in Figure 3.3. At both 600 and 700°C, the rate of reduction of ZnO was greater than that of any of the Zn-Ti-O solids. With as little as 10 mol% TiO_2 (sorbent Z9T), there was still a significant (twofold) decrease in the rate of ZnO reduction. The reduction rate of ZnO was about 13 times greater than Zn-Ti-O solids with $(Zn/Ti)_{atomic\ ratio} \leq 3$ at 600°C and ten times greater at 700°C. When the relative amount of TiO_2 was increased above 25 mol%, no significant change in the reduction rate was observed. This implied that the presence of different zinc titanate phases had no significant effect on reduction. For example, the solid Z2T (2 Zn : 1 Ti) which contained only the

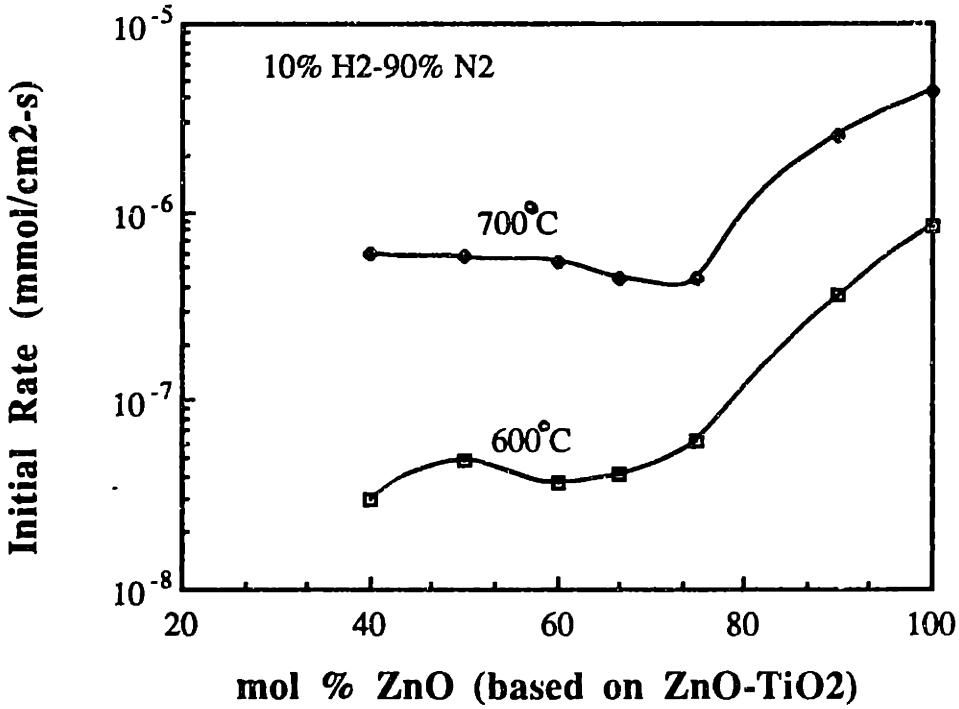

Figure 3.3 Comparative plots of the initial reduction rate of various Zn-Ti-O materials reacted at 600 and 700°C in 10% H2-90% N2.

crystalline phase Zn_2TiO_4 had approximately the same reduction rate as the solid Z2T3-b, which contained a mixture of $ZnTiO_3$ and TiO_2. Sorbent Z2T3-a (containing $Zn_2Ti_3O_8$, $ZnTiO_3$ and TiO_2) and Z2T3-b (containing $ZnTiO_3$ and TiO_2) did not differ appreciably in reduction rate. This is encouraging since it was difficult to obtain pure zinc titanate phases of the type $Zn_2Ti_3O_8$ or $ZnTiO_3$. Often mixtures of these phases were formed.

In order to elucidate the mechanism by which the presence of titanium in the solid inhibits the reduction reaction, further kinetic experiments were performed. In the absence of both diffusional and mass transfer resistances, an intrinsic initial heterogeneous rate expression of the form

$$R_o = k\, C_{H2}^{\,n} \qquad (3.14)$$

was used, where k [=] cm/s is the intrinsic rate constant, C_{H2} [=] mmol/cm^3 is the molar concentration of hydrogen gas, and n is the reaction order. The reaction order of ZnO and Z2T reduction was determined by varying the hydrogen gas concentration at 700°C as shown in Figure 3.4. From these results, the reaction orders for ZnO and Z2T reduction with hydrogen were determined with the equation

$$\ln R_o = \ln k + n \ln C_{H2} \qquad (3.15)$$

For ZnO, at 700°C the reaction order is 0.51 ± 0.05 while that of Z2T is 1. The former result is in agreement with the work of Grunze and Hirschwald (1974; 1975). These authors observed fractional reaction orders for ZnO reduction. At pressures in the range of 1-4 Torr, they found that the reaction order decreased from 0.77 at 800°C to 0.25 at 428°C. At 700°C, they reported a reaction order of 0.60. This is close to the value reported in this study. The somewhat smaller reaction order in this study is probably due to the higher reaction pressure (760 Torr). To confirm that there existed a

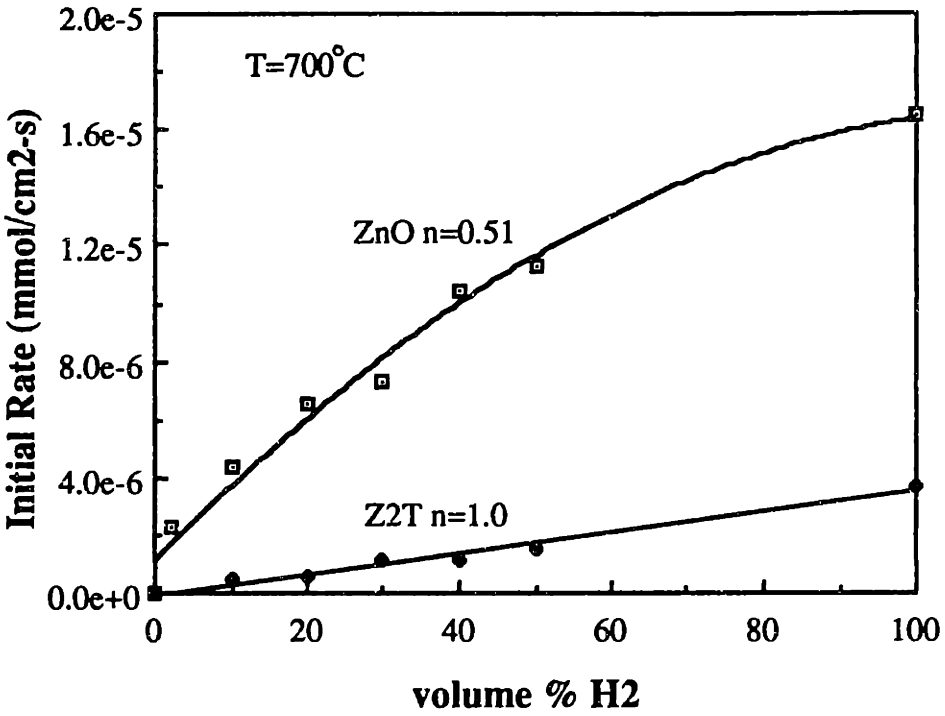

Figure 3.4 Effect of hydrogen concentration on the initial rate of reduction of ZnO and Z2T at 700 C.

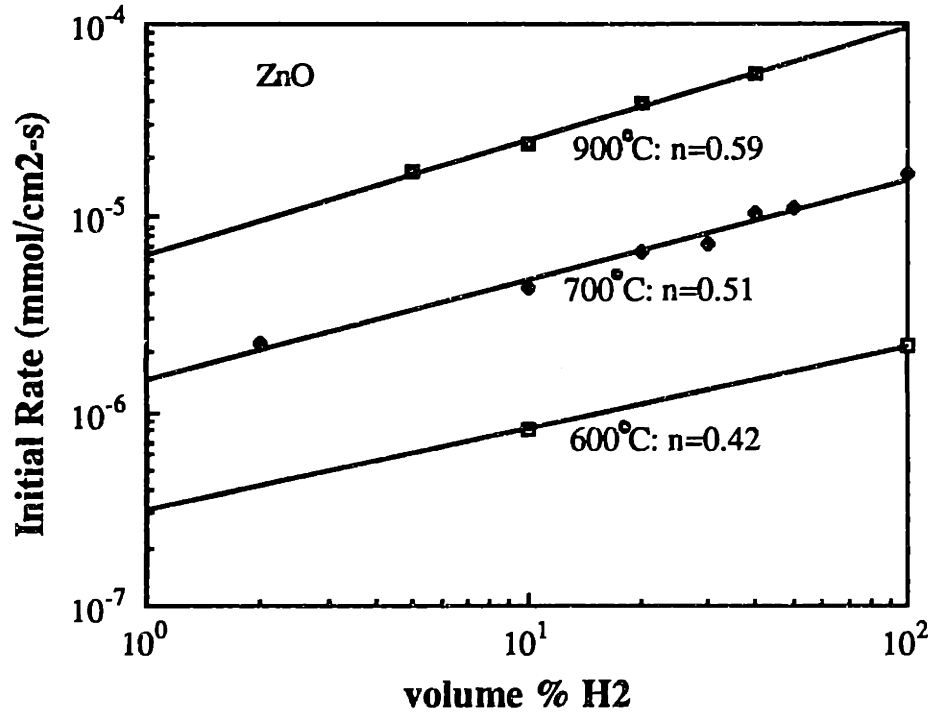

Figure 3.5 Effect of hydrogen concentration on the initial reduction of ZnO at various temperatures.

dependence of the apparent reaction order on the reduction temperature for ZnO, the reaction orders at several different temperatures were measured. The results are shown in Figure 3.5. The apparent reaction order increased somewhat from approximately 0.42 at 600°C to 0.59 at 900°C. This was consistent with a Langmuir-Hinshelwood expression:

$$R_o = \frac{KC_{H_2}}{\left(1 + \sqrt{K_{H_2}C_{H_2}}\right)^2} \qquad (3.16)$$

where K is a term which depends on the rate controlling step (e.g. $K = k_{sr}K_{H2}$ when the surface reaction is controlling; k_{sr} is the rate constant of the surface reaction) and K_{H2} is the hydrogen adsorption equilibrium constant. An adsorption process is almost always exothermic. Thus, K_{H2} decreases exponentially with increasing temperature by a factor of $e^{\lambda/RT}$ where λ (>0) is the heat of chemisorption. Consequently, as the temperature increases, the apparent reaction order increases to 1.

The rate can be expressed using an Arrhenius relationship, thus defining an activation energy:

$$R_o = k_r \exp(-E/RT) \qquad (3.17)$$

where k_r is a constant, E is the activation energy, R is the ideal gas constant, and T is the absolute temperature. Figure 3.6 shows the initial reduction rates of ZnO and Z2T on Arrhenius plots. At all temperatures (550-1050°C), the rate of reduction of ZnO was faster than Z2T. Based on this plot for ZnO, an activation energy of 22.9 $\pm$ 1.2 kcal/mol and k_r of 0.56 mmol/cm^2-s were obtained for reduction in 10 mol% H_2-90 mol% N_2. This activation energy was close to the values reported by others (Table 3.1). The reported values of the activation energy were 27-28 kcal/mol for ZnO

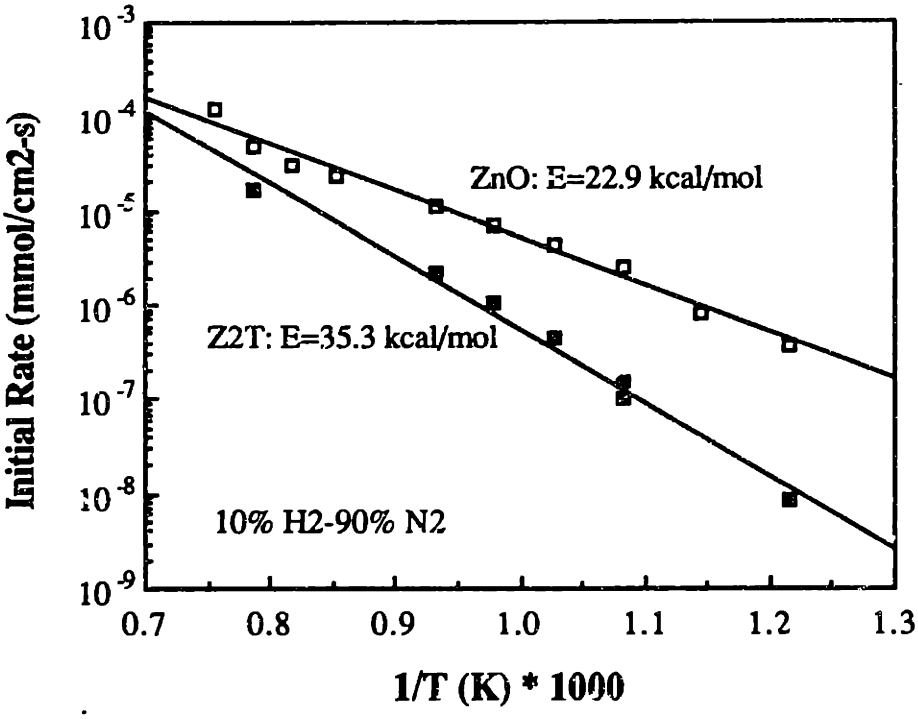

Figure 3.6 Arrhenius plots of the initial reduction rates of ZnO and Z2T.

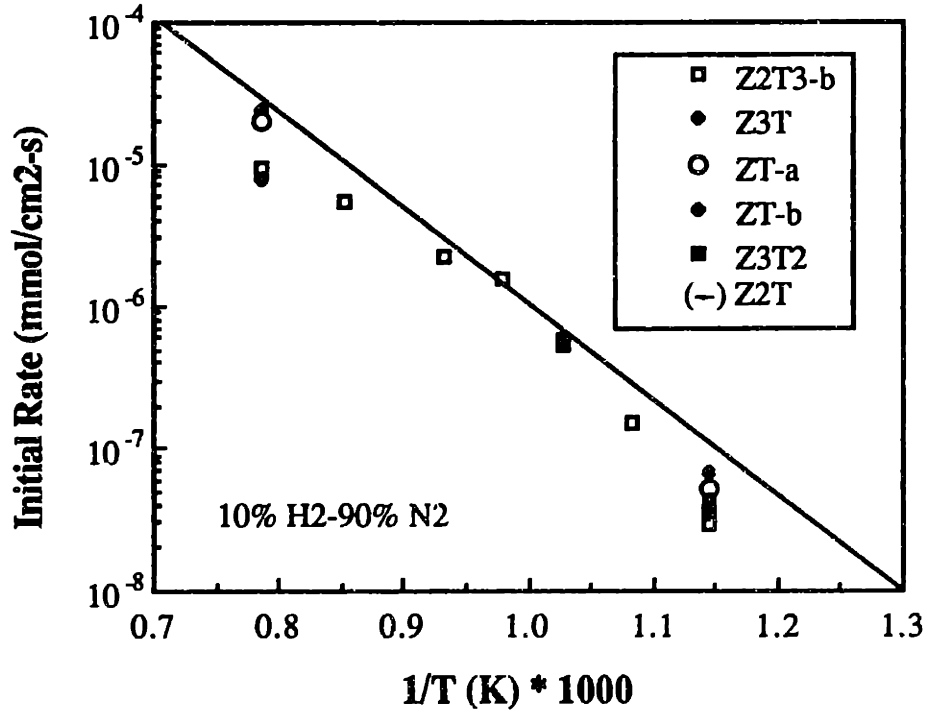

Figure 3.7 Arrhenius plots of the initial reduction rates for various Zn-Ti-O solids.

powders. For Z2T, the activation energy was 35.3 kcal/mol and k_r was 29.0 mmol/cm^2-s. There was no significant difference in the Arrhenius plots of other Zn-Ti-O materials reduction with $(Zn/Ti)_{atomic\ ratio} \leq 3$ as shown in Figure 3.7. The solid Z9T, on the other hand, behaves like ZnO. Figure 3.8 shows the Arrhenius plots of the initial reduction rates of ZnO and Z9T. The activation energy for Z9T was 23.7 kcal/mol, similar to the value obtained for ZnO. This indicated that the same reaction mechanism was involved in the reduction of ZnO and Z9T. This was not surprising considering that Z9T contains 70 wt% ZnO as well as 30 wt% Zn_2TiO_4 present as crystalline phases. The major difference between ZnO and Z9T was the constant k_r. For ZnO, k_r was 0.56 mmol/cm^2-s, while for Z9T it was 0.33 mmol/cm^2-s.

3.3.2 Initial Reduction Rate of Bulk Zn-Ti-O Sorbents: Effect of Water Vapor

Various amounts of water vapor were added to the reducing gas to determine if any inhibitory effect on the reduction rate was present. For ZnO, a dramatic effect of H_2O on reduction was observed. Figure 3.9 shows the Arrhenius plots of ZnO reduction in the presence of various amounts of water vapor. The inclusion of 1 mol% H_2O in the gassignificantly decreased the reduction rate of ZnO. However, when the amount of water vapor was increased to 3 or 8 mol%, the reduction rate did not decrease much further. The activation energy drastically changed with the presence of water vapor. With a gas containing 10 mol% H_2-3 mol% H_2O-87 mol% N_2, the activation energy was 41.6 kcal/mol and k_r was 366.6 mmol/cm^2-s. In contrast, with no H_2O vapor present, the activation energy was only 22.9 kcal/mol.

H_2O also had an inhibitory effect on the reduction of Zn-Ti-O solids. Figure 3.10 shows the Arrhenius plots of Z2T reduction in the presence of 0, 3 and 8 mol% H_2O. Unlike ZnO, the effect of water vapor was smaller on the reduction kinetics of Z2T.

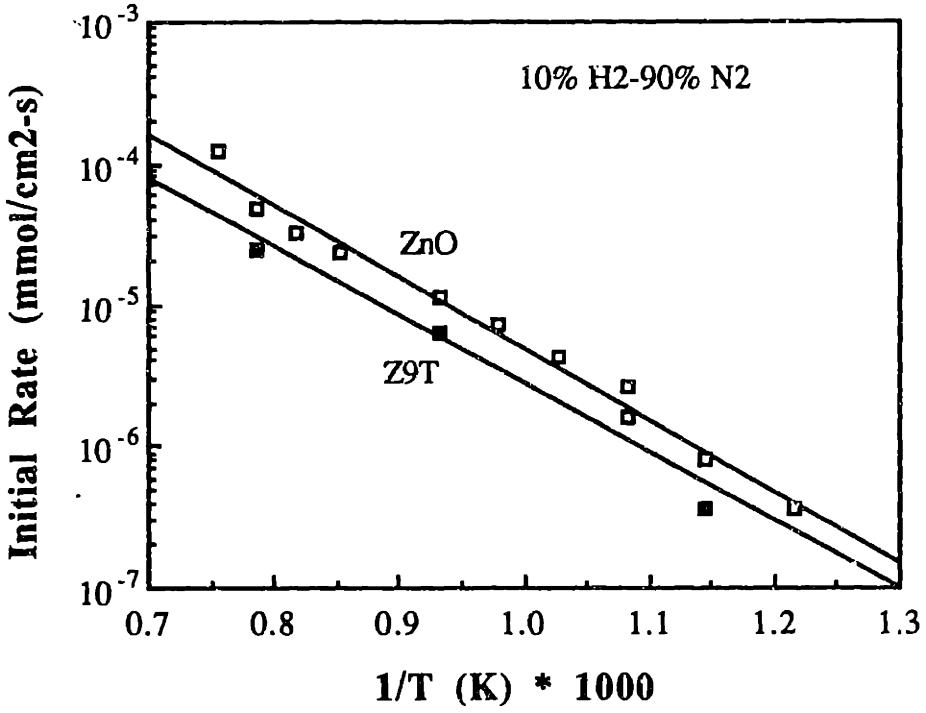

Figure 3.8 Arrhenius plots of the initial reduction rates of ZnO and Z9T.

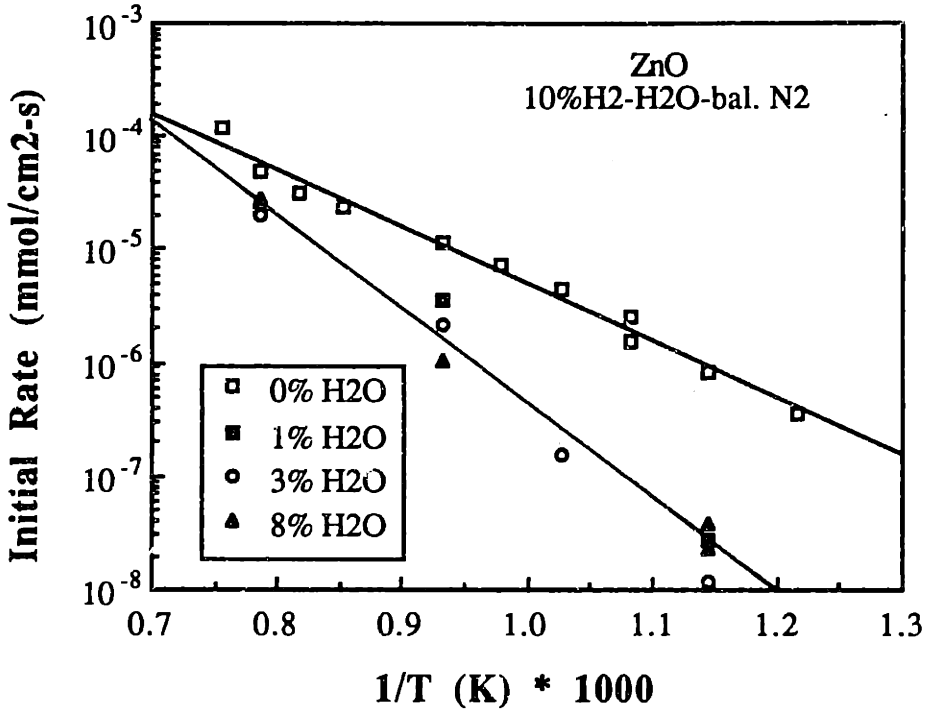

Figure 3.9 Arrhenius plots of the initial reduction rates of ZnO in the presence of various amounts of H2O vapor.

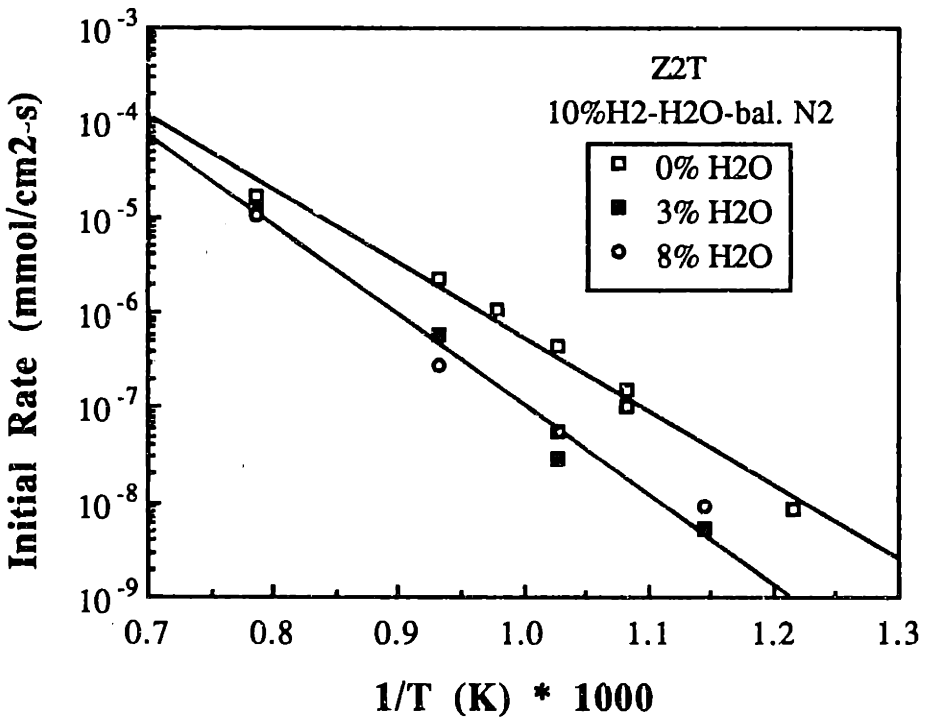

Figure 3.10 Arrhenius plots of the initial reduction rates of Z2T in the presence of various amounts of H2O vapor.

The activation energy increased from 35.3 to 41.3 kcal/mol and k_r changed to 110.7 mmol/cm^2-s. The new activation energy was approximately the same as the value attained for ZnO reduction (41.6 kcal/mol) in the presence of 3 mol% H_2O. The only difference was that the constant, k_r, for Z2T was 3.3 times smaller than that of ZnO. Like ZnO, no effect on the reduction of Z2T was observed when a larger amount (8 mol%) of H_2O was introduced into the reactant gases.

For ZnO, there was a concomitant change in the reaction order in the presence of water vapor. Figure 3.11 shows the effect of hydrogen concentration on the initial reduction rate of ZnO and Z2T in the presence of 3 mol% H_2O at 700°C. The reaction order of ZnO changed to 1 while in the absence of H_2O, it was only 0.51. In contrast, there was no change in the reaction order of Z2T which remained first order.

A comparative plot of the initial reduction rates of various Zn-Ti-O materials at 700°C in 10 mol% H_2-3 mol% H_2O-87 mol% N_2 is shown in Figure 3.12. Lower reduction rates were obtained for Zn-Ti-O solids than for pure ZnO. However, unlike the case when H_2O was not present (Figure 3.3), there was not a sharp drop in the rate of reduction from ZnO to solid with $(Zn/Ti)_{atomic\ ratio} \approx 3$ followed by a plateau for $(Zn/Ti)_{atomic\ ratio} < 3$. Instead, as seen in Figure 3.12, the reduction rate steadily decreased as the relative amount of TiO_2 in the solid increased. Comparative Arrhenius plots of ZnO, Z2T and Z2T3-b in the presence of H_2O are shown in Figure 3.13. The activation energies of all solids were approximately the same (~41 kcal/mol). The difference in reactivity lies in the constant, k_r, as listed in Table 3.3. For Z2T3-b, the value of k_r was 8.7 times smaller than for ZnO.

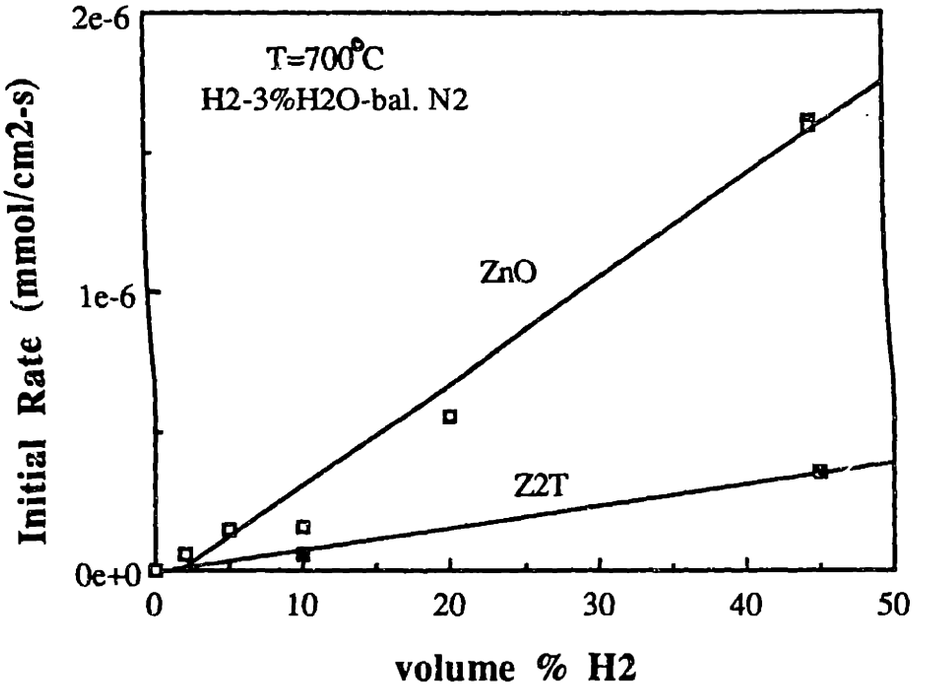

Figure 3.11 Effect of hydrogen concentration on the initial reduction rate of ZnO and Z2T in the presence of 3% H2O at 700°C.

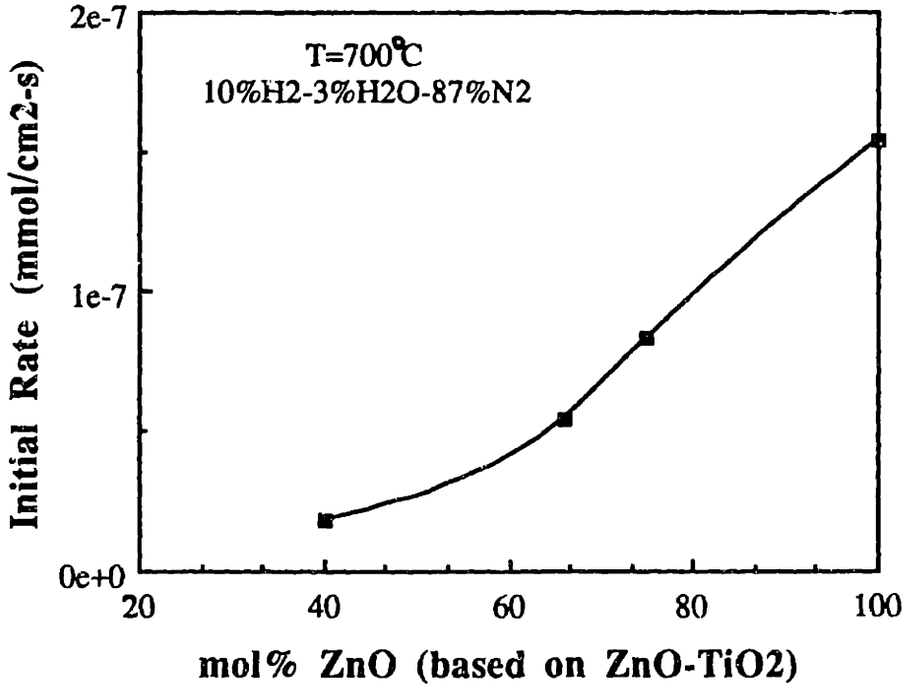

Figure 3.12 A comparative plot of the initial reduction rates of various Zn-Ti-O materials reacted at 700°C in 10%H2-3%H2O-87%N2.

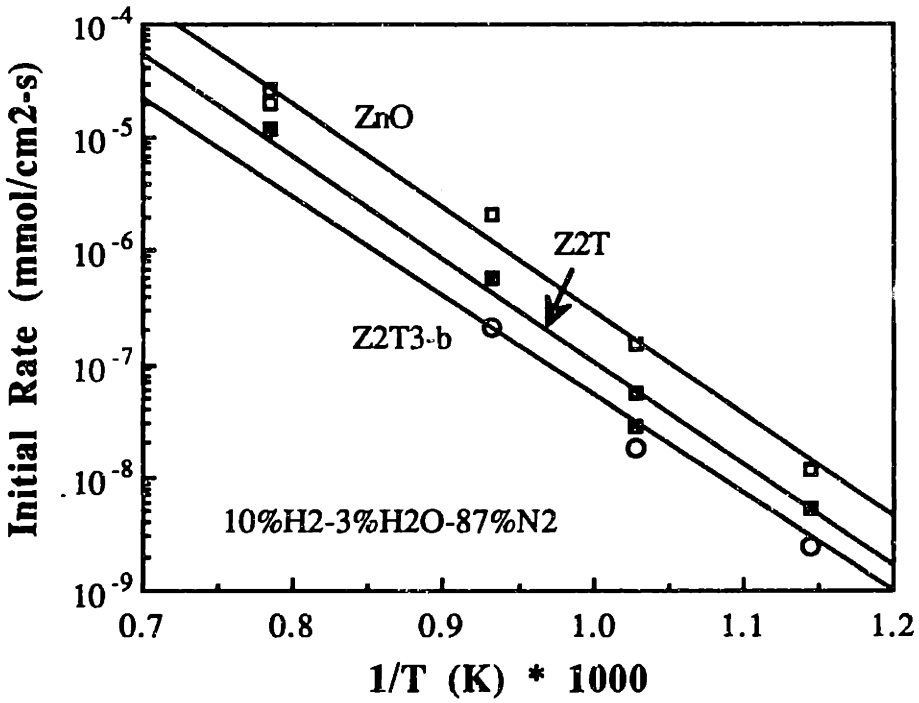

Figure 3.13 Arrhenius plots of the initial reduction rates of ZnO, Z2T and Z2T3 in 10%H2-3%H2O-87%N2.

Table 3.3 Values of k_r for ZnO, Z2T and Z2T3.

	k_r (mmol/cm^2-s)
ZnO	366.6
Z2T	110.7
Z2T3-b	41.9

3.3.3 Initial Reduction Rate of Bulk Zn-Ti-O Sorbents: Effect of Hydrogen Sulfide

ZnO and Z2T were sulfided 10-15% between 600 and 700°C. Reduction of the partially sulfided solids in 10 mol% H_2-90 mol% N_2 showed a lower initial reduction rate than reduction of the unsulfided solids. In these experiments, only the oxides were reduced. No reduction of ZnS was observed by measuring the weight change. As shown in Figure 3.14, there appeared to be a similar inhibitory effect on reduction by hydrogen sulfide as was found with water vapor. Figure 3.14b shows the reduction profiles. A sigmoidal shape profile is found for ZnO which has been partially sulfided. Initially (< 10 min) the reduction profiles of ZnO partially sulfided and the profile of ZnO reduced in the presence of 3% H_2O virtually overlap. As the reactant surface recedes from the sulfided layer, sites which are more reactive are exposed and a corresponding increase in rate is observed. The initial rates shown in Figure 3.14a were measured from the early part of the reduction profiles. Because of some contribution from the more reactive sites and the change in weight is small, the initial rate measurements for the partially sulfided solid tend to be on the high side and have a some degree of error . In the following section, the reduction mechansim and the role of water vapor will be discussed. Hydrogen sulfide appears to play a similar role as water vapor.

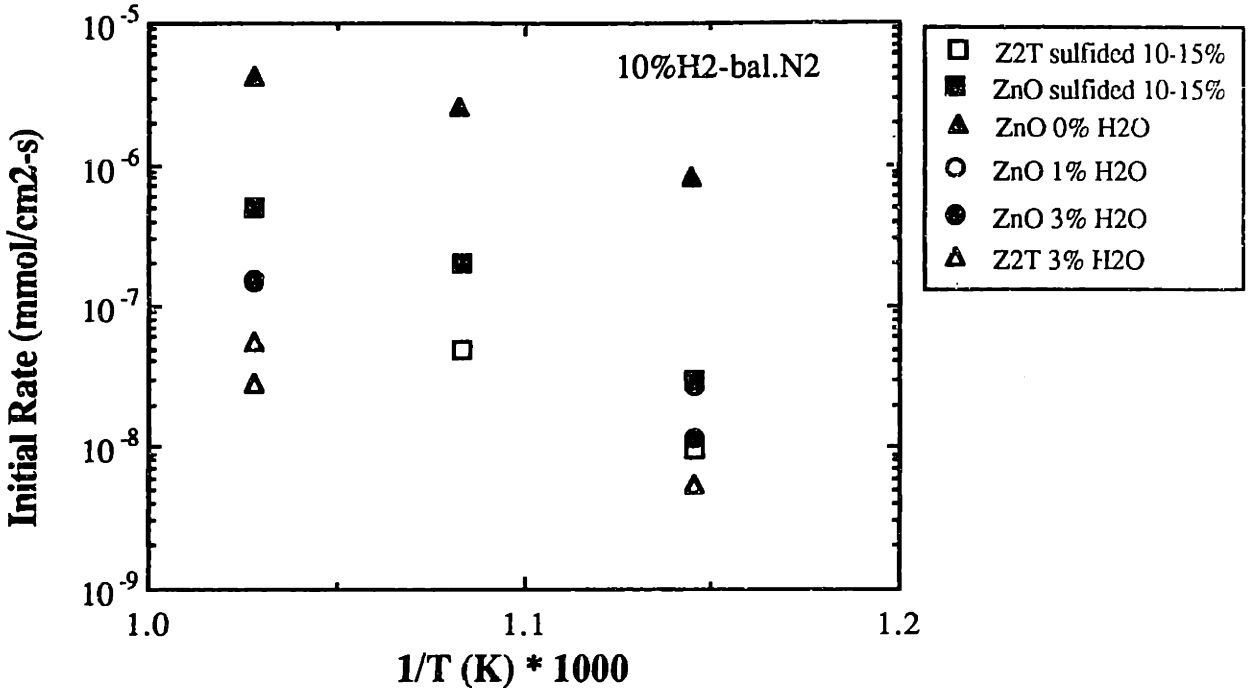

a)

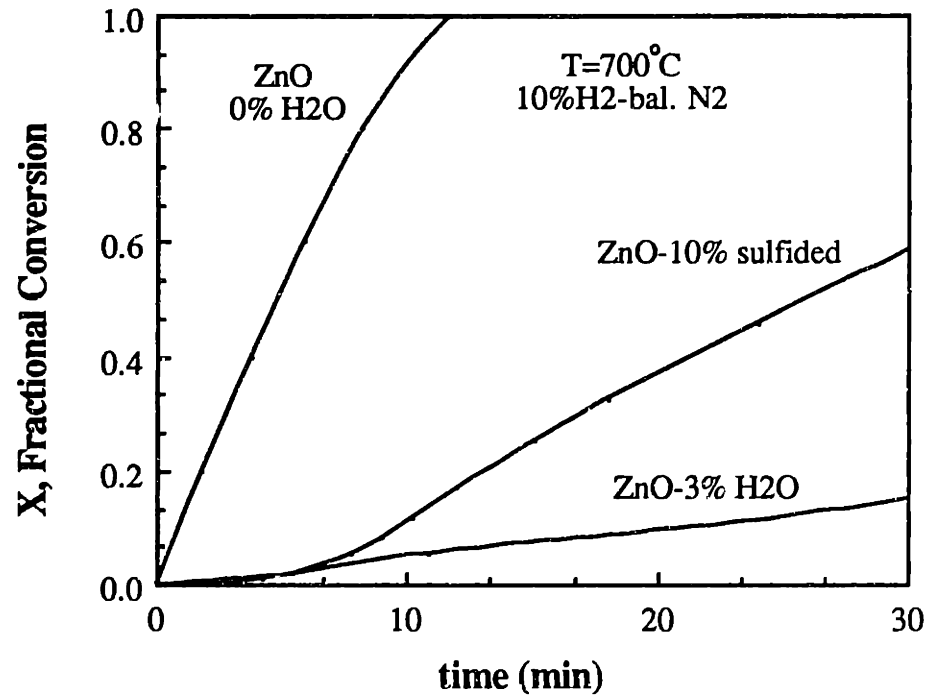

b)

Figure 3.14 Reduction of partially sulfided solid a) comparison of the Arrhenius plots of the initial rate and b) comparison of reduction profiles.

3.3.4 Reduction Mechanism

From the kinetic measurements described in the above section, a mechanism for ZnO reduction and the means by which titanium dioxide inhibits reduction can be proposed. The inhibition pattern observed with water vapor suggests that two very different types of reaction sites are involved in ZnO reduction. The existence of multiple reaction sites for ZnO reduction has been shown in the literature for the (low temperature) hydrogen chemisorption on ZnO (Eischens et al., 1962; Dent and Kokes, 1969; Boccuzzi et al., 1978).

Hydrogen adsorption on ZnO is a complex process and has been the subject of numerous investigations. At room temperature, there exist at least two types of hydrogen adsorption sites on ZnO (Eischens et al., 1962; Dent and Kokes, 1969; Boccuzzi et al., 1978). By a combination of infrared spectrometry and volumetric measurements, it was possible to distinguish between different adsorption sites and structures. Type I sites are characterized by weak, fast, and reversible hydrogen adsorption. Surface OH and ZnH groups are formed by:

$$\text{Zn--O} + \text{H}_{2\,(g)} \rightarrow \begin{matrix} \text{H} & \text{H} \\ | & | \\ \text{Zn} & \text{O} \end{matrix} \qquad (3.18)$$

Water vapor acts as a poison to type I sites (Dent and Kokes, 1969). Type I sites are confined in densely populated patches on the surface, and the Zn-H and O-H groups strongly interact via a long range effect (Boccuzzi et al., 1978). In contrast, for type II sites, hydrogen adsorption is irreversible and occurs rapidly initially but slowly in later stages. Chemisorption on type II sites involves hydrogen bonding and bridged structures (Boccuzzi et al., 1978). For the OH groups, the structure is:

$$O\text{-}H \cdots O \qquad (3.19)$$

where the OH groups are hydrogen bonded to adjacent oxygen ions. For the ZnH groups, the bridged structure is:

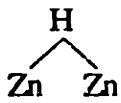

(3.20)

It has been hypothesized that this type of sites is located in the subsurface cavities of ZnO (Dent and Kokes, 1969). The maxima in adsorption of type I and II sites occur at 60 and 300°C. Not as much is known about H_2 adsorption at higher temperatures. Kesavulu and Taylor (1960) observed hydrogen adsorption on sites different from either type I or II at 250°C. Because it (the other sites) is opaque to infrared spectroscopy, they were not able to determine the structure of these sites.

Since the experiments performed in this thesis all took place at much higher temperatures ($\geq$ 550°C) than the chemisorption studies performed by others, it was not possible to directly apply the knowledge gained in those previous work to the analysis of this system. However, some insight is gained from the previous studies. From those early studies, multiple sites for hydrogen adsorption were found in ZnO. Very different behavior (e.g rate of H_2 adsorption and effect of H_2O) were observed for each type of sites. At higher temperatures, it is possible that there are still multiple hydrogen adsorption sites, though not necessarily type I or II sites.

For ZnO reduction at 550-1050°C, two reaction sites are proposed. One type, called type A sites, is characterized by rapid reduction rate but is poisoned by water vapor. The other type of sites, called type B, has a slower reaction rate but is unaffected by H_2O. Since no change in the reduction rate is observed after a single monolayer has been reacted, it is assumed that the relative concentration of each type of sites is

conserved in the successive monolayers. Each type of sites can be expressed in terms of a Langmuir-Hinshelwood equation. For type A sites, the following expression is obtained:

$$R_{o,A} = \frac{K_A C_{H_2}}{\left(1 + \sqrt{K_{H_2,A} C_{H_2}} + \sqrt{K_{H_2O,A} C_{H_2O}}\right)^2} \qquad (3.21)$$

where K_A is a constant related to the rate controlling step for the reaction, $K_{H2,A}$ and $K_{H2O,A}$ are the hydrogen and water adsorption equilibrium constants on type A sites, respectively. From the apparent reaction order of ZnO reduction in the absence of H_2O ($n \sim 0.51$ at 700°C), $(K_{H2,A}C_{H2})^{0.5}$ must be the same order of magnitude as 1. In the presence of H_2O, sites A are poisoned. This is equivalent to $(K_{H2O,A}\, C_{H2O})^{0.5} >> 1$ or $(K_{H2,A}C_{H2})^{0.5}$. Thus, $R_{o,A}$ becomes small. For type B sites, a similar Langmuir-Hinshelwood equation is obtained

$$R_{o,B} = \frac{K_B C_{H_2}}{\left(1 + \sqrt{K_{H_2,B} C_{H_2}} + \sqrt{K_{H_2O,B} C_{H_2O}}\right)^2} \qquad (3.22)$$

However, since the apparent reaction order of ZnO reduction in the presence of H_2O was unity and there was no significant effect on the reduction rate when the amount of H_2O was increased from 1 to 8 mol% H_2O, then $(K_{H2,B}C_{H2})^{0.5}$ and $(K_{H2O,B}C_{H2O})^{0.5} << 1$. Consequently, Eq. 3.22 reduces to

$$R_{o,B} = K_B C_{H_2} \qquad (3.23)$$

The reaction rate is equal to the sum of the reactions on type A and B sites:

$$R_o = R_{o,A} + R_{o,B} \qquad (3.24)$$

In the absence of H_2O, reaction on type A sites is much faster than on type B sites. Thus, $R_o \approx R_{o,A}$. The constants in Eq. 3.21 can be determined by rearranging the equation to:

$$\frac{1}{\sqrt{R_{o,A}}} = \frac{1}{\sqrt{K_A}} \frac{1}{\sqrt{C_{H_2}}} + \sqrt{\frac{K_{H_2}}{K_A}} \qquad (3.25)$$

At 700°C, using a least squares fit of the initial rates obtained at various hydrogen concentrations, the values of the constants are calculated and Eq. (3.21) for $R_{o,A}$ becomes:

$$R_{o,A} = \frac{\{1.27 \times 10^{-2} [cm/s]\} C_{H_2}}{(1 + \sqrt{509.0 [cm^3/mmol] C_{H_2}})^2} \qquad (3.26)$$

In the presence of H_2O, $R_{o,A} \approx 0$ and $R_o \approx R_{o,B}$. For ZnO with the experimental results obtained with 10 mol% H_2-3 mol% H_2O-87 mol% N_2, Eq. 3.23 becomes:

$$R_{o,B} = 9.27 \times 10^5 [cm/s] e^{-43.9 [kcal/mol]/RT} C_{H_2} \qquad (3.27)$$

For Zn-Ti-O solids, the presence of titanium appears to either eliminate type A sites or modify their reactivity. The observation that the presence of H_2O decreases the reduction rate of Zn-Ti-O solids suggests that in the absence of H_2O either a modified type A sites with lower reactivity or different sites are reacting. The tenfold lower rate of reduction of solids with $(Zn/Ti)_{atomic\ ratio} \leq 3$ at 700°C implies type A sites are very sensitive to the presence of titanium. A solid (i.e. Z9T) with only 10 mol% TiO_2 (based on ZnO-TiO_2 stochiometry) has a reduction rate 1.7 times slower than the reduction rate of pure ZnO in the absence of H_2O. Because its (Z9T) activation energy is the same as pure ZnO and only the pre-exponential factor is different, this suggests that titanium eliminates type A sites. If there is a simple linear relationship between the relative

amount of titanium and the number of of type A sites eliminated, based on the observed reduction rate of Z9T, all type A sites can be eliminated in a solid containing 24.3 mol% TiO_2. Experimentally, it was observed that there was no effect on the reduction rate when the relative amount of titanium was above 25 mol%. For solids with $(Zn/Ti)_{atomic\ ratio} \leq 3$, most likely another type of sites is operating which is not affected by the presence of titanium. Similar to type A sites, these sites are poisoned by H_2O. For Zn-Ti-O solids, in the absence of H_2O, the rate expression is:

$$R_o = 6.30 \times 10^4\ [cm/s]\ e^{-37.3\ [kcal/mol]/RT}\ C_{H_2} \qquad (3.28)$$

In the presence of H_2O, reduction of Zn-Ti-O solids occurs by type B sites. This conclusion is drawn because of the similarity in activation energies of Zn-Ti-O and ZnO solids. The effect of titanium is to decrease the pre-exponential constant of the rate expression. As shown in Figure 3.12, the reduction rate decreased as the amount of titanium dioxide increased from 0% to 60 mol%. This is very different from the situation without H_2O (Figure 3.3). This indicates type B sites are much less sensitive to the presence of titanium than type A sites. Consequently, a higher relative amount of titanium is needed to obtain lower reduction rates. The difference in sensitivity may be explained geometrically by hypothesizing that type A sites are composed of groups or ensembles of atoms. The effect of titanium would be greatest on sites requiring the greatest number of nearby atoms.

3.3.5 Reduction Conversion Profiles of Bulk Zn-Ti-O Solids

Typical experimental conversion-time profiles for ZnO and Z2T at 650 and 700°C are shown in Figures 3.15 and 3.16 (square symbols), respectively. The fractional conversion is defined as follows:

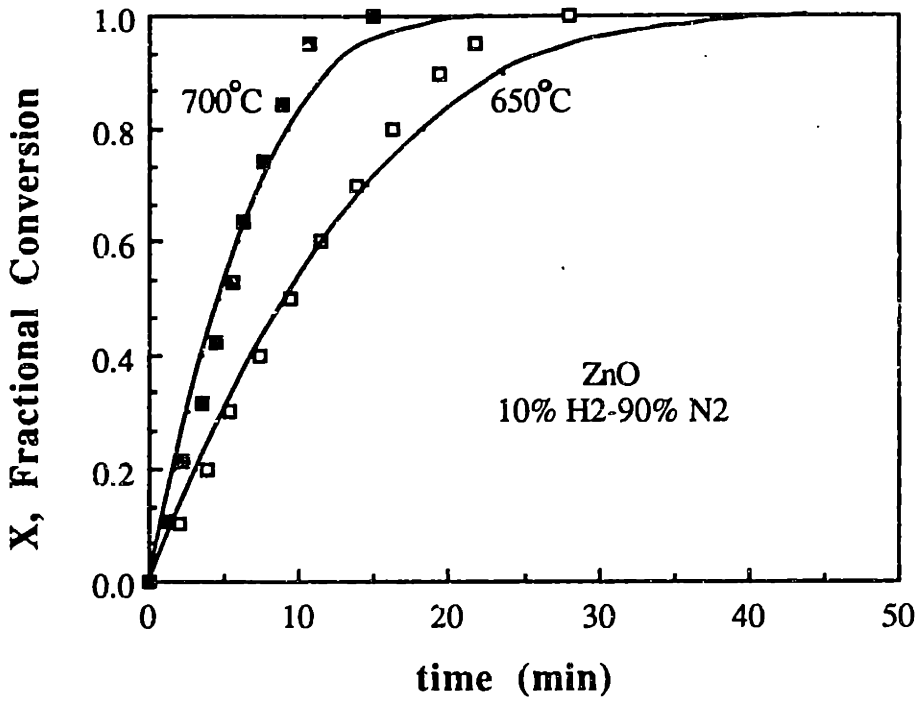

Figure 3.15 Comparison of experimental conversion profiles of ZnO reduced in 10%H2-90%N2 with profiles predicted from the grain model.

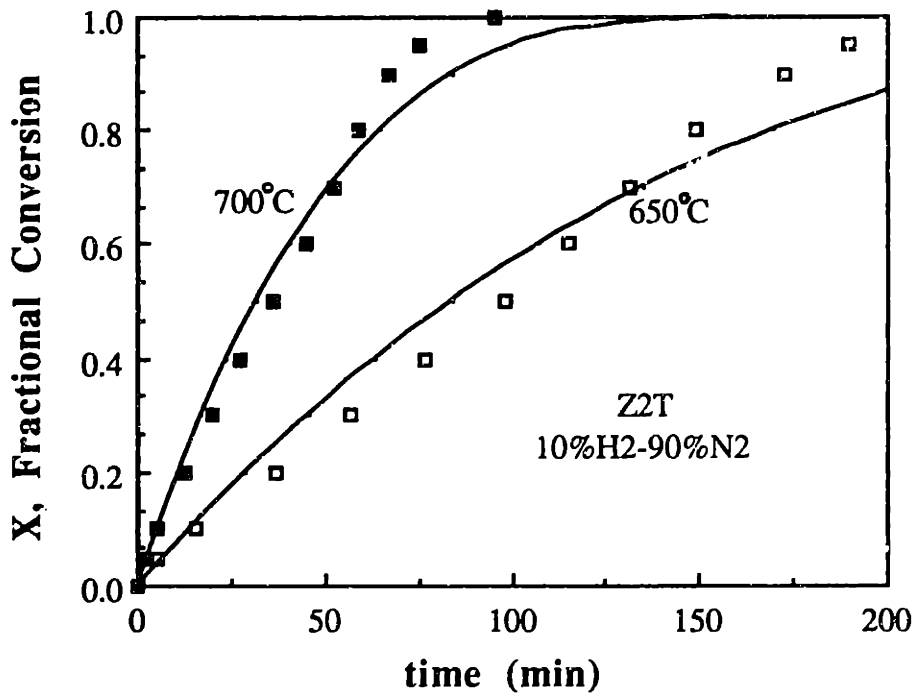

Figure 3.16 Comparison of experimental conversion profiles of Z2T reduced in 10%H2-90%N2 with profiles predicted from the grain model.

$$X = (W_i - W)/(W_i - W_f^J) \tag{3.29}$$

where W is the weight, W_i is the initial weight, and W_f^J is the final weight at complete conversion. For ZnO, W_f^J is equal to zero. W_f^J is the weight of the remaining TiO_2 for Zn-Ti-O solids. For both ZnO and Z2T, the reaction rates remained relatively constant up to a high level of conversion. At approximately 0.8-0.9 conversion, the reaction rate decreased. The experimental conversion profiles can be adequately described by the heterogeneous, gas-solid reaction of shrinking, nonporous spherical grains. In contrast as discussed in Chapter 5, a discrete bimodal grain size distribution was needed to describe sulfidation of Z2T. The different requirements are found because during reduction the thick "skin" of low porosity breaks up into smaller pieces due to the escape of Zn and H_2O vapor and the lower molar volume of the solid product. During sulfidation, the "skin" remains relatively intact. Figure 17 and 18 show SEM micrographs of Z2T (calcined 720 C) after ~10% reduction and after 25% sulfidation, respectively. The beginning of fragmentation of the "skin" is evident in Figure 17. The following equations are obtained (Szekely et al., 1976) for reaction A(g) + *b*B(s) --> *c*C(g) + *d*D(s) assuming the reaction is only chemically controlled:

$$t^* = 1-(1-X)^{1/3} \tag{3.30}$$

$$= (b/\rho_s r_o)\, R_o\, t \tag{3.31}$$

$$r_o = \frac{3}{A_o \rho_s} \tag{3.32}$$

where t^* is the dimensionless reaction time, ρ_s is the molar density of the solid B, r_o is the initial grain radius, R_o is the initial reaction rate, and A_o is the initial surface area of the solid B. As shown in Figures 3.15 and 3.16, the agreement between the predicted conversion profiles and the experimental profiles is good. For Z2T reduction, a product

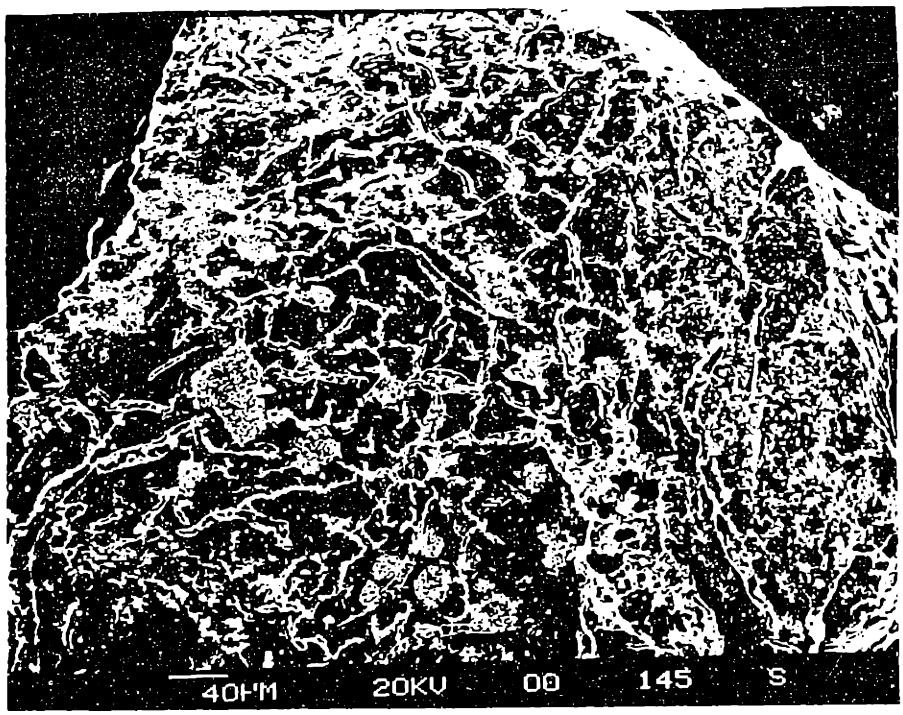

a)

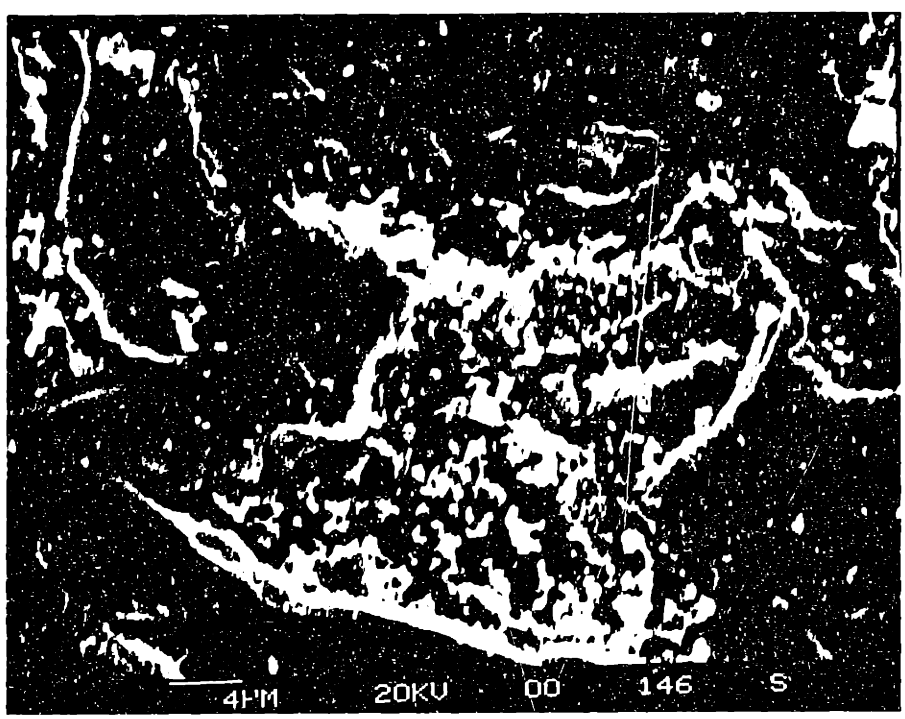

b)

Figure 3.17 SEM micrographs of Z2T calcined at 720°C a) partially reduced (~10%) at 650°C in 10% H_2-90% N_2 b) magnification.

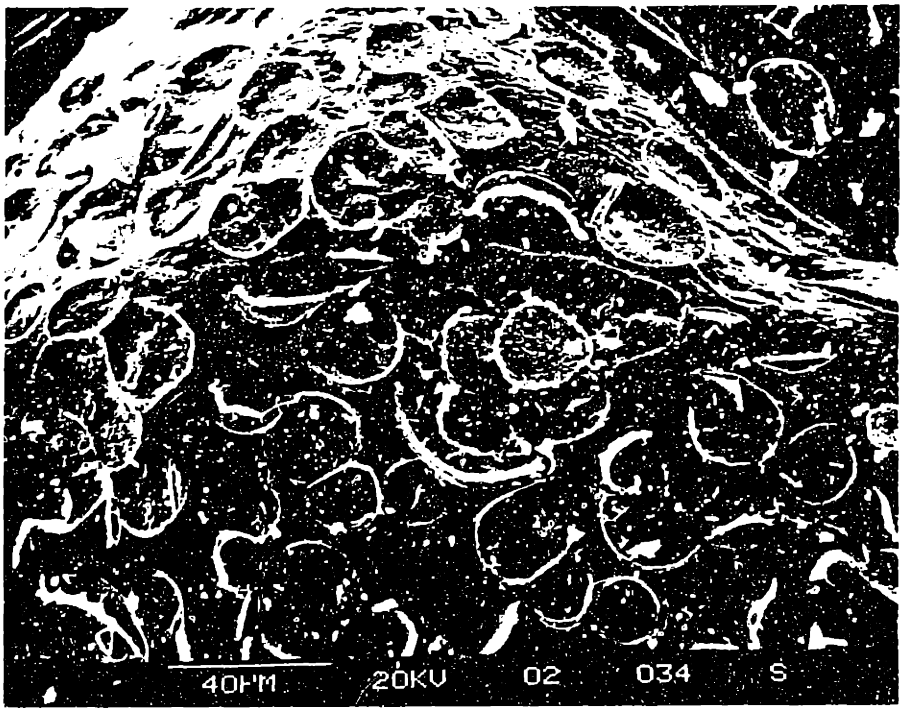

Figure 3.18 SEM micrograph of Z2T (calcined at 720°C) partially sulfided (~25%) at 650°C in 2% H_2S-1 H_2%-98% N_2.

layer of TiO_2 is formed. Since the ratio of the solid product molar volume to the solid reactant molar volume is only 0.41, a porous product layer is formed. From the conversion profiles, this product layer poses no hindrance to reaction.

To determine the chemical phase transformations of the Zn-Ti-O solids during reduction, partially reacted solids were examined by XRD analyses. To obtain sufficient quantities of materials for analyses, 40-50 mg of solids were reacted in the TGA. Table 3.4 lists the results of the XRD analyses of various partially reduced solids. The reactions were performed at 650°C in 10 mol% H_2-90 mol% N_2. For Z2T, the following phase transformations were observed:

$$Zn_2TiO_4(s) + 2\,H_2(g) \rightarrow 2\,Zn(g) + TiO_2(s) + 2\,H_2O(g) \qquad (3.33)$$

$$1/2\,Zn_2TiO_4(s) + TiO_2(s) \rightarrow 1/2\,Zn_2Ti_3O_8(s) \qquad (3.34)$$

No coresponding change in the reaction rate accompanied the phase change from Zn_2TiO_4 to $Zn_2Ti_3O_8$. At conversion higher than 66%, the only reactive phase present was $Zn_2Ti_3O_8$. As shown in Figure 3.16, no noticeable change in the reduction rate was observed. For Z2T3-b, $ZnTiO_3$ reacted directly with H_2 to form Zn(g) and TiO_2(s). No intermediate chemical phases were detected. Although these XRD analyses revealed that the chemical phase transformations of Zn_2TiO_4 and $ZnTiO_3$ were different, from the results of the initial rate measurements discussed in Section 3.3.1, these differences did not affect the reduction rate.

After partial reduction of Zn-Ti-O solids, changes in the color of the solids were observed. ZnO which was initially white in color stayed the same color after partial reduction. However, Zn-Ti-O solids which were also initially white took on a grey color after partial reduction. Fully reduced Zn-Ti-O solids also had a grey color. This

Table 3.4 XRD analyses of reduced Zn-Ti-O solids.[1]

Sample	Crystalline Phase (wt%)			
	Zn_2TiO_4	$Zn_2Ti_3O_8$	$ZnTiO_3$	TiO_2 (rutile)
Z2T, 31% reduced	76	24	0	0
Z2T, 74% reduced	0	85	0	15
Z2T, 100% reduced	0	0	0	100
Z3T, 53% reduced	75	25	0	0
Z2T3-b, 69% reduced	0	0	33	67

[1] reduced in the TGA at 650°C in 10 mol% H_2-90 mol% N_2

grey pigment was probably due to some surface reduction of TiO_2. Ti_3O_5 has a blue-black color. No reduced TiO_2 phase was detected by XRD analyses which indicated that no bulk reduction of TiO_2 took place. In addition, the weight loss was not signifcantly different (within 5%) from what would be expected from the loss of only ZnO.

The structural changes occurring with reduction were examined with a scanning electron microscope. Figure 3.19 shows the surfaces of ZnO unreacted and 31% reduced in 10 mol% H_2-90 mol% N_2 at 650°C. The solid which was calcined at 1000°C is very sintered. The unreacted solid is composed of overlapping grains with an average radius of 0.6-0.75 μm. Because of the overlapping grain structure, the predicted grain radius by Eq. 3.32 is greater (0.79 μm) than the observed radius. After 31% reduction, the grain radius is smaller (~ 0.4-0.6 μm). This is consistent with a heterogeneous gas-solid reaction where the solid is composed of shrinking nonporous grains.

Figures 3.20 and 3.21 show the SEM micrographs of Z2T, calcined at 1000°C, unreacted and partially reduced (31%) at 650°C in 10 mol% H_2-90% N_2, respectively. As shown in Figure 3.20, Z2T is highly sintered. Overlapping grains between 0.3-0.4 μm are present. After reaction (Figure 3.21), the size of the grains is smaller (~ 0.2-0.3 μm). On the surface of these grains is a porous crystalline layer which is the TiO_2 product layer. The formation of a porous product layer where diffusion is rapid is consistent with the conversion profile. No decrease in reaction rate due to slow diffusion through the developing product layer was observed.

The reduction of Z9T which is composed of a mixture of ZnO and Zn_2TiO_4 is structurally interesting. Figure 3.22 shows the SEM micrographs of unreacted and

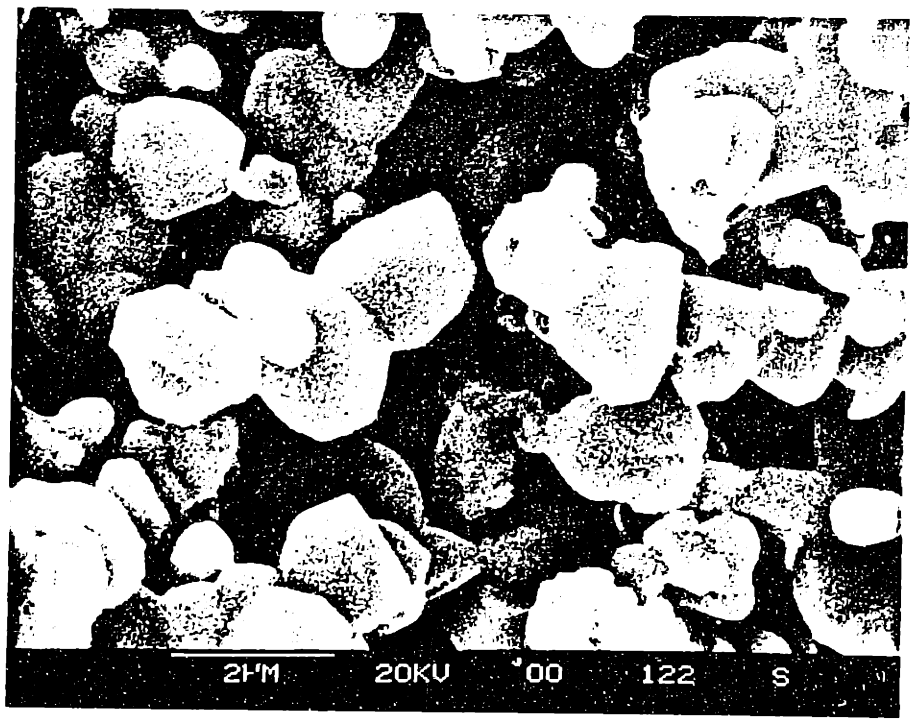

a)

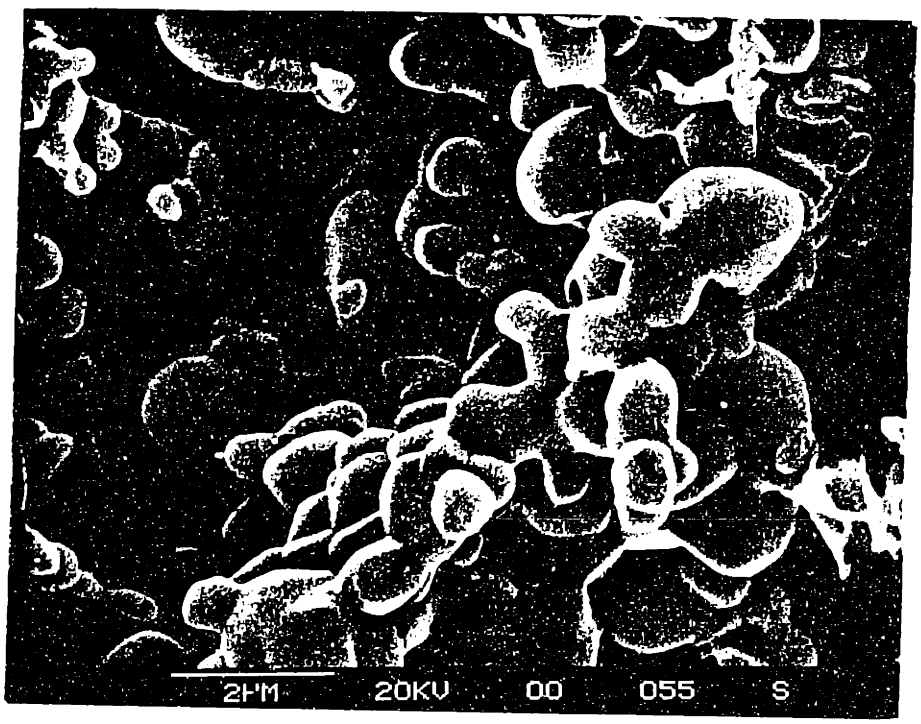

b)

Figure 3.19 SEM micrographs of ZnO calcined at 1000°C a) unreacted and b) 31% reduced at 650°C in 10% H_2-90% N_2.

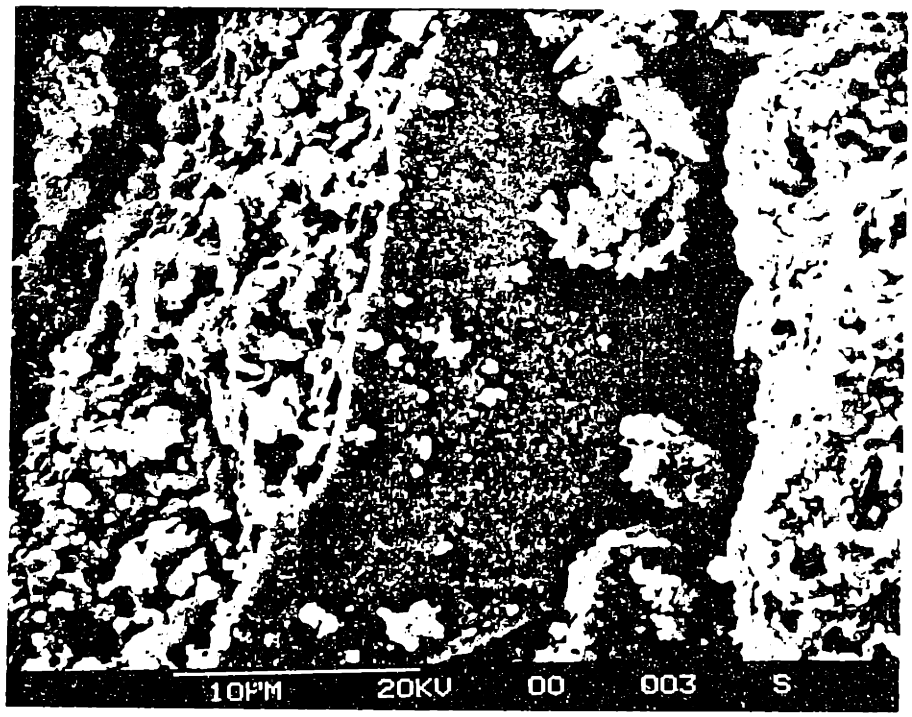

a)

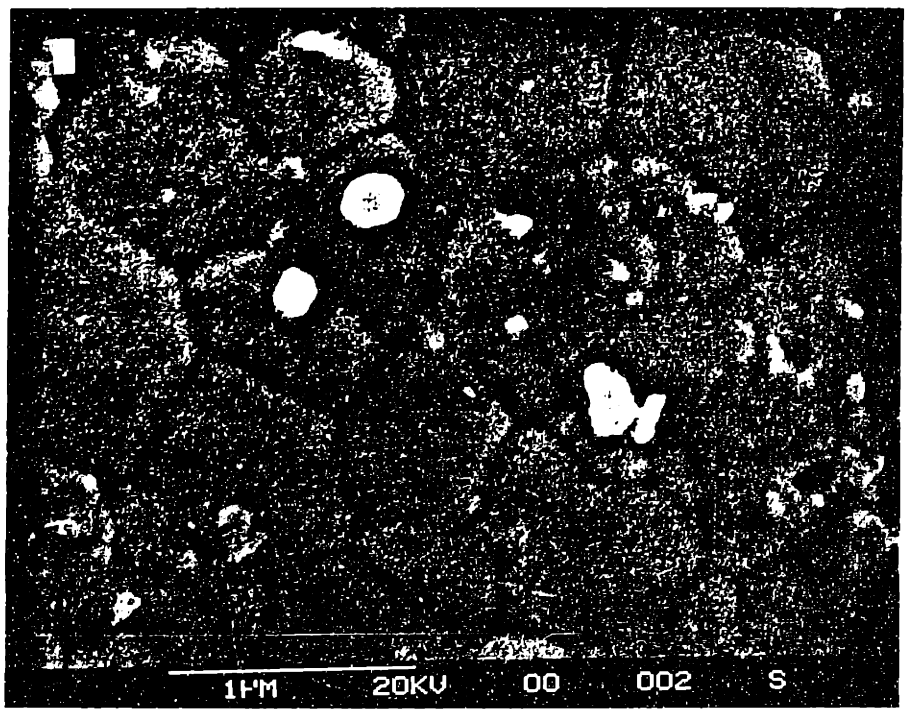

b)

Figure 3.20 SEM micrographs of a) unreacted Z2T calcined at 1000°C and b) magnification of (a).

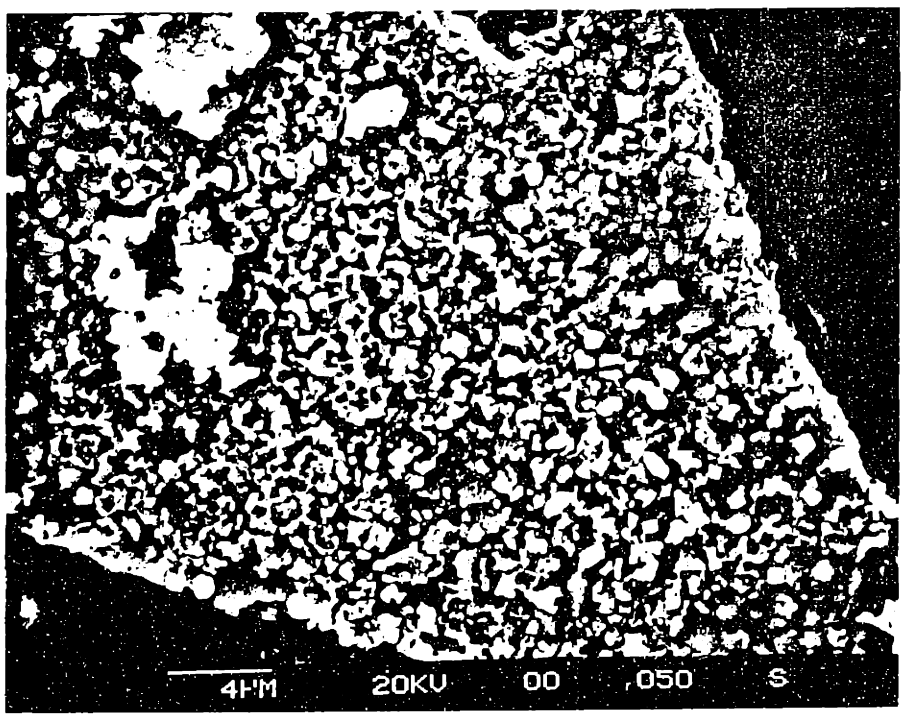

a)

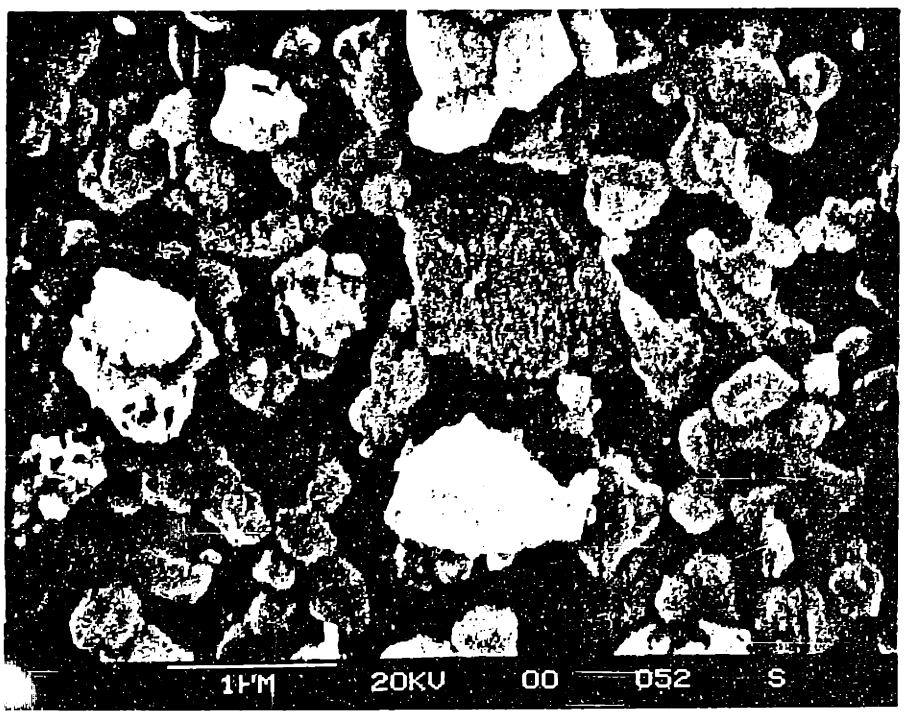

b)

Figure 3.21 SEM micrographs of a) Z2T (calcined at 1000°C) after 31% reduction at 650°C in 10% H_2-90% N_2 and b) magnification of (a)

a)

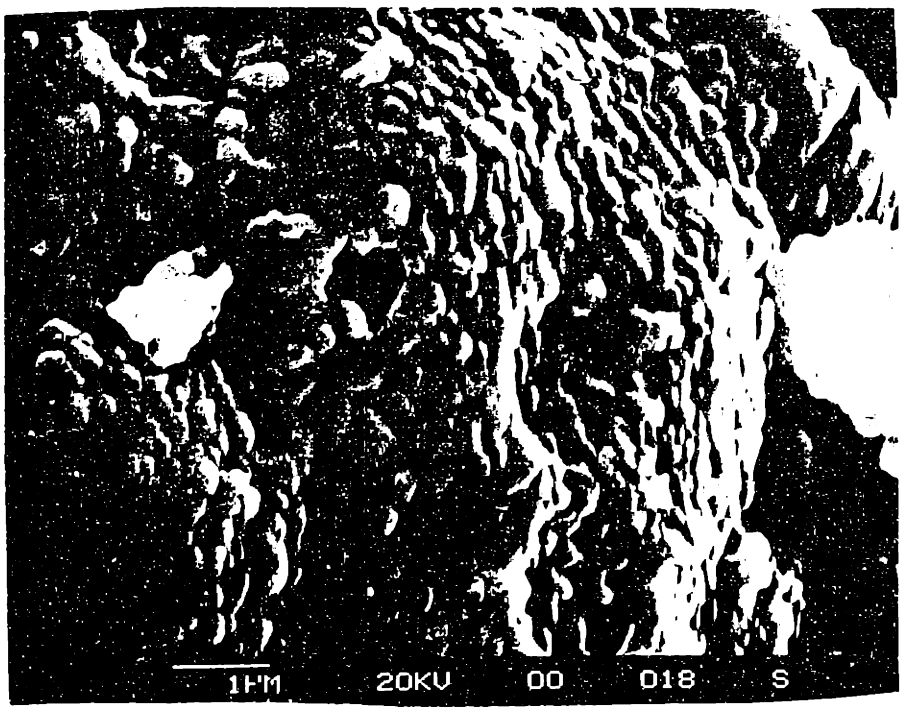

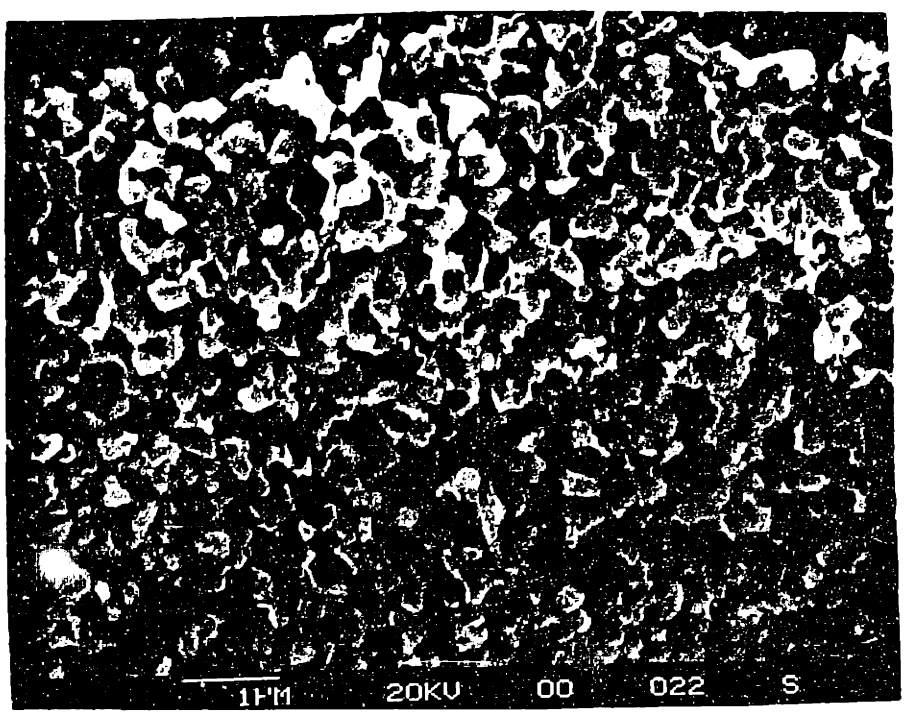

b)

Figure 3.22 SEM micrographs of Z9T calcined at 1000°C a) unreacted and b) 45% reduced at 650°C in 10% H_2-90% N_2.

partially reduced (45%) at 650°C in 10 mol% H_2-90 mol% N_2, respectively. The unreacted solid is composed of closely packed crystals (0.1-0.2 μm radius). After partial reduction (Figure 3.22b), it is apparent that some crystals were more reactive than others. Holes which are approximately hexagonal in shape were left where these crystals had reacted with H_2. This is consistent with the finding that ZnO is more reactive in reduction than Zn_2TiO_4. ZnO crystallizes in the close-packed hexagonal system. The cubic Zn_2TiO_4 crystals, however, react much slower than ZnO and, as seen in Figure 3.22b, the sizes of the remaining crystals were relatively unchanged after 45% conversion.

3.3.6 Reduction of TiO_2-Coated Single Crystals of ZnO

The reduction of a ZnO single crystal completely coated with a thin layer of TiO_2 was examined. The purpose of these experiments was to determine whether resistance to reduction comparable to bulk Zn-Ti-O can be obtained by this preparation method. If this method is successful, a solid with a comparatively lower amount of TiO_2 than in the bulk Zn-Ti-O solids can be used for desulfurization.

Single ZnO crystals (orientation $000\bar{1}$, oxygen-riched face) were obtained from Atomergic Chemetals Corporation. These crystals were plate-like in shape and were obtained in two different sizes, 2x2x1 mm and 6x6x1 mm. The coating of the ZnO crystal with TiO_2 was performed by a dip-coating method (Takahashi and Matsuoka, 1988) using a solution of titanium isopropoxide (TTIP)-diethanolamine (DEA)-H_2O-isopropanol (i-PrOH). The ZnO single crystal was dipped in the solution, slowly pulled out, dried in air for 24 h (25°C), and then heated for 30 min at 600°C. A thin film of approximately 0.3 μm in thickness was formed. The coating cycle was repeated to

produce a uniform film of approximately 0.75 μm in thickness. The TiO_2-coated ZnO will be called TiO_2/ZnO in the following discussion.

ZnO and ZnO/TiO_2 single crystals were reacted at 600°C in 10 mol% H_2-90 mol% N_2. The reduction rate profiles of ZnO and TiO_2/ZnO single crystals are shown in Figures 3.23 and 3.24, respectively. The amounts of solid reacted were relatively low compared to the bulk Zn-Ti-O and ZnO solids because of their relatively low specific surface area (ZnO single crystal=8.2×10^{-4} m^2/g; TiO_2/ZnO single crystal=5.5×10^{-4} m^2/g). After 3 h, the ZnO single crystal was reduced only 1.2%, while after 4 h, the TiO_2/ZnO single crystal was reduced 1.5×10^{-2}%. As shown in Figure 3.23, the rate of ZnO reduction is relatively constant up to 1.2% conversion. The reduction rate is approximately 1.75×10^{-6} mmol ZnO/cm^2-s. In comparison, the reduction rate measured with the polycrystalline ZnO was 1.03×10^{-6} mmol ZnO/cm^2-s. This finding is consistent with the results of Gast et al. (1976), who observed that the reduction rate in carbon monoxide is dependent on the crystallographic orientation of ZnO. At 600°C, from their reported Arrhenius constants, the reduction rate of the $(000\bar{1})$ face (oxygen-rich face) is approximately 1.77 times faster than the $(10\bar{1}0)$ face (stoichiometric face) and 1.79 times faster than the (0001) face (zinc-rich face). For polycrystalline ZnO, all three crystallographic orientation may be present. Consequently, the measured reduction rate should be lower than the reduction rate of crystals with a $(000\bar{1})$ crystallographic orientation.

The reduction rate of TiO_2/ZnO (Figure 3.24) was much slower than that of ZnO single crystal. Initially, the rate of ZnO loss was approximately 1.3×10^{-7} mmol ZnO/cm^2-s. However, this rate rapidly decreased to approximately 1×10^{-6} mmol ZnO/cm^2-s at higher conversion. The initially high rate of reduction is believed to be cause by the

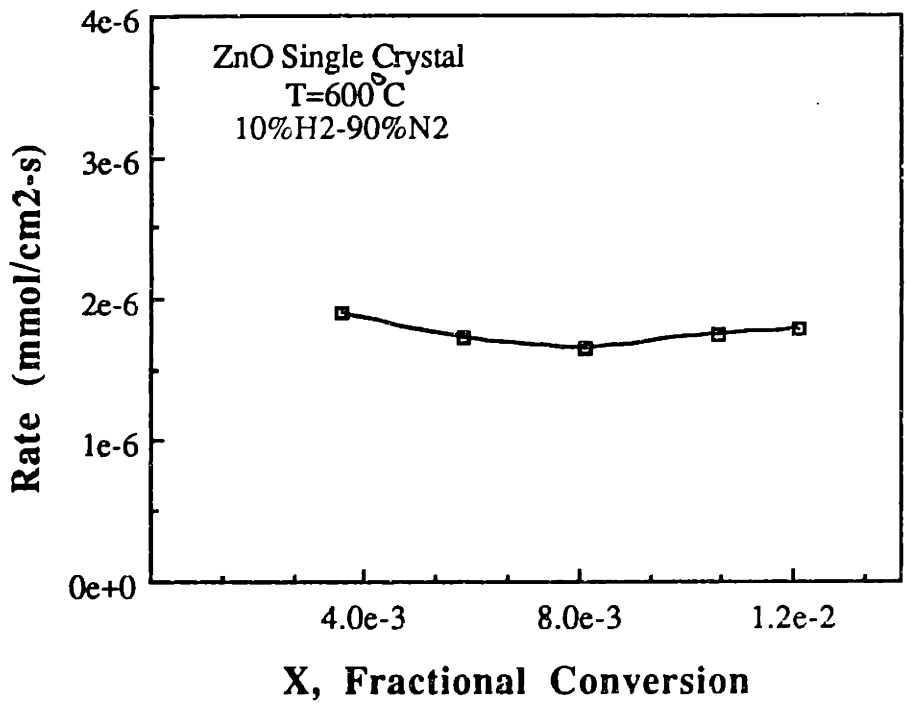

Figure 3.23 Reduction rate profile of ZnO single crystal $(000\bar{1})$ at 600 C in 10%H2-90%N2.

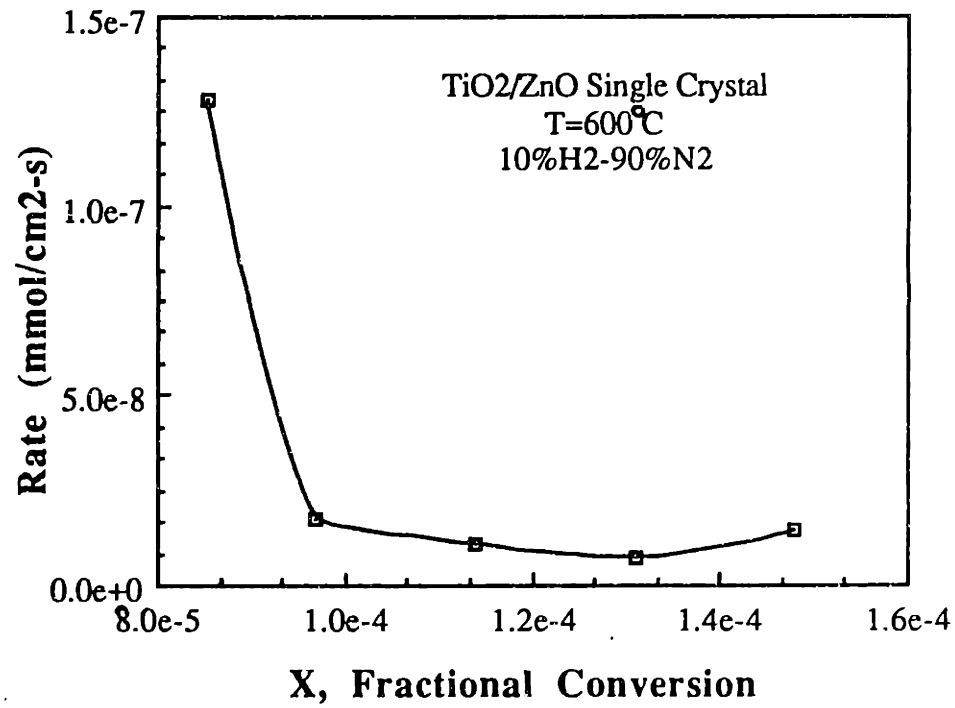

Figure 3.24 Reduction rate profile of TiO2/ZnO single crystal at 600 C in 10%H2-90%N2.

presence of some zinc on the surface of the TiO_2 coating. During the calcination step, there is probably some degree of interdiffusion between zinc and titanium ions. After this surface zinc completely reacts, the reaction is controlled by the diffusion across the TiO_2 coating, and a corresponding drop in the reduction rate is observed.

From the results of Figure 3.24, it appears that coating ZnO with TiO_2 can significantly inhibit the rate of reduction. However, if a similar degree of inhibition is observed in the sulfidation of TiO_2/ZnO, nothing is gained by this method. The function of the TiO_2 layer is to decrease the diffusion rate of the diffusion species. To compare the effect of TiO_2 on sulfidation and reduction, the diffusion coefficient of the rate-limiting species was determined. For the reduction of TiO_2/ZnO, the rate-limiting species is probably either Zn cations or OH anions. Hydrogen cations because of their relatively small size diffuse rapidly. To determine the diffusion coefficient, it was assumed that the reaction rate was controlled by the diffusion across the TiO_2 layer. This is a good assumption considering that the reaction rate of ZnO single crystal is approximately 100 times faster than the rate of TiO_2/ZnO. Since the actual conversion is low, the solid can be modeled as an infinite slab. The conversion-time profile can be determined by:

$$X = \frac{b\, D_e (C_i - C_{i,o})}{\rho_s\, h\, r_o}\, t \qquad (3.35)$$

where D_e is the diffusion coefficient, C_i is the concentration of the rate-limiting ion (Zn or OH ions) at the ZnO-TiO_2 interface, $C_{i,o}$ is its concentration at the TiO_2-gas interface, ρ_s is the molar density of ZnO, h is the thickness of the TiO_2 layer, and r_o is the half-thickness of the ZnO slab. The reaction at the surface of ZnO is:

$$ZnO + H^+ = Zn^{2+} + OH^- \qquad (3.36)$$

At equilibrium:

$$K_{eq} = \frac{C_{Zn^{2+}} C_{OH^-}}{C_{H^+}} \tag{3.37}$$

Since the diffusion of hydrogen cations is fast,

$$C_{H+} \approx C_{H+,o} \tag{3.38}$$

where C_{H+} and $C_{H+,o}$ are the concentrations of hydrogen cations at the ZnO-TiO_2 interface and the TiO_2-gas interface, respectively. The adsorption of hydrogen gas is by the reaction:

$$H_2(g) = 2\,H^+ \text{(adsorbed)} \tag{3.39}$$

At equilibrium,

$$C_{H^+,o} = \frac{\sqrt{K_{H_2} C_{H_2}}}{1 + \sqrt{K_{H_2} C_{H_2}}} \tag{3.40}$$

From the earlier discussed data of reduction of bulk Zn-Ti-O solids, $(K_{H2}\, C_{H2})^{0.5} << 1$. Assuming a similar relationship for adsorption on TiO_2, then:

$$C_{H^+,o} = \sqrt{K_{H_2} C_{H_2}} \tag{3.41}$$

Assuming rapid removal of the rate-limiting species, $C_{i,o} \approx 0$. Thus, eq. (3.35) becomes:

$$X = \frac{b\, D_e K\, C_{H_2}^{1/4}}{\rho_s h\, r_o} t \tag{3.42}$$

where $K = K_{eq}^{0.5}\, K_{H2}^{0.25}$. With $r_o = 0.033$ cm, the area of the solid=5.46×10^{-4} m^2/g and the reaction rate of TiO_2/ZnO = 1×10^{-8} mmol ZnO/cm^2-s, the calculated value of $D_eK = 3.9 \times 10^{-12}\, cm^{2.75}\, s^{-1}\, mmol^{-0.25}$.

Sulfidation of ZnO and TiO_2/ZnO single crystals was performed at 600°C in 2 mol% H_2S-1 mol% H_2-97 mol% N_2 to determine the effects of the TiO_2 layer. The results are discussed in more detail in Chapter 5. The results are plotted in Figures 3.25 and 3.26. The sulfidation rate of ZnO single crystal decreased from $4.2x10^{-6}$ mmol ZnS formed/cm^2-s at X=0.0001 to $1x10^{-7}$ mmol/cm^2-s at X=0.003. The formation of the ZnS product layer caused the rate decrease. The rate of sulfidation of TiO_2/ZnO single crystal was much slower. At X=0.0001, the rate was $1.4x10^{-8}$ cm^2/s. Thus, the TiO_2 coating decreased the sulfidation rate 300 times. In contrast, the reduction rate was decreased only approximately 175 times. The difference in the relative effect of TiO_2 on the rate is due to differences in the rate-limiting diffusing species. For reduction, the rate-limiting diffusing species is either Zn^{2+} or OH^-. while for sulfidation it is S^{2-}. In chapter 5; analyses of these results are provided. The calculated diffusion coefficient for S^{2-} through TiO_2 is $K_{H2S}D_{S,TiO2} = 9x10^{-10}$ cm^2/s, where K_{H2S} is the adsorption coefficient of H_2S on TiO_2. It was not possible to directly compare the diffusion coefficient calculated in reduction and sulfidation because values of the adsorption constants were not known.

3.4 CONCLUSIONS

1. In the absence of water vapor, Zn-Ti-O solids have a lower reduction rate than ZnO at temperature between 550-1050°C. When the solid contained $(Zn/Ti)_{atomic\ ratio} \leq 3$, the reduction rate was ten times slower than that of ZnO at 700°C.

2. All zinc titanate phases (i.e. Zn_2TiO_4, $Zn_2Ti_3O_8$ and $ZnTiO_3$) had the same rate of reduction in the absence of H_2O. Increasing the amount of TiO_2 beyond 25 mol% (75 mol% ZnO) did not correspondingly decrease the reduction rate.

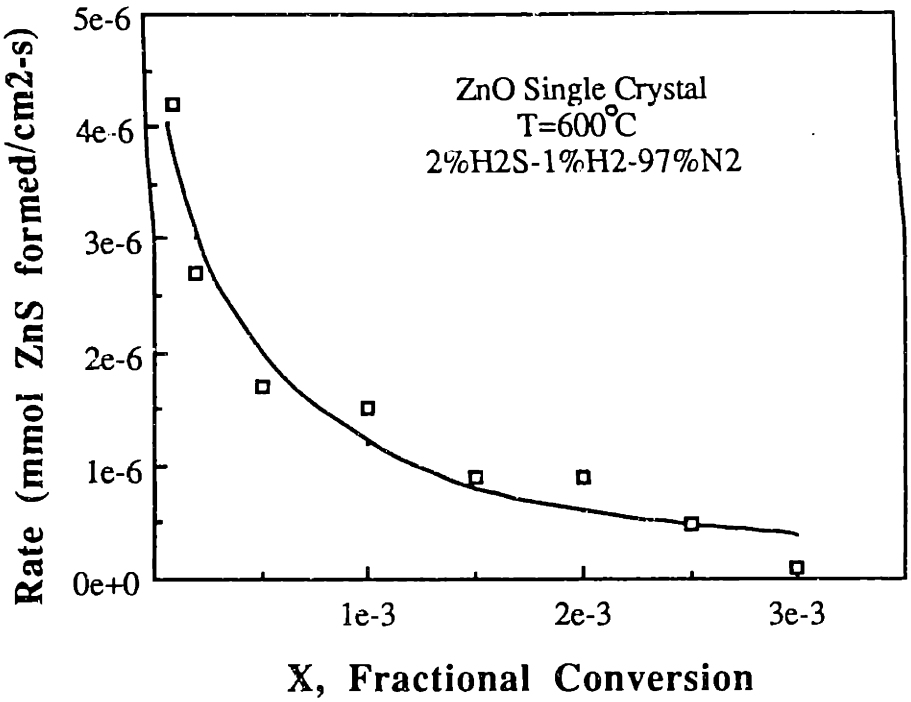

Figure 3.25 Sulfidation rate profile of ZnO single crystal $(000\bar{1})$ at at 600 C in 2%H2S-1%H2-97%N2.

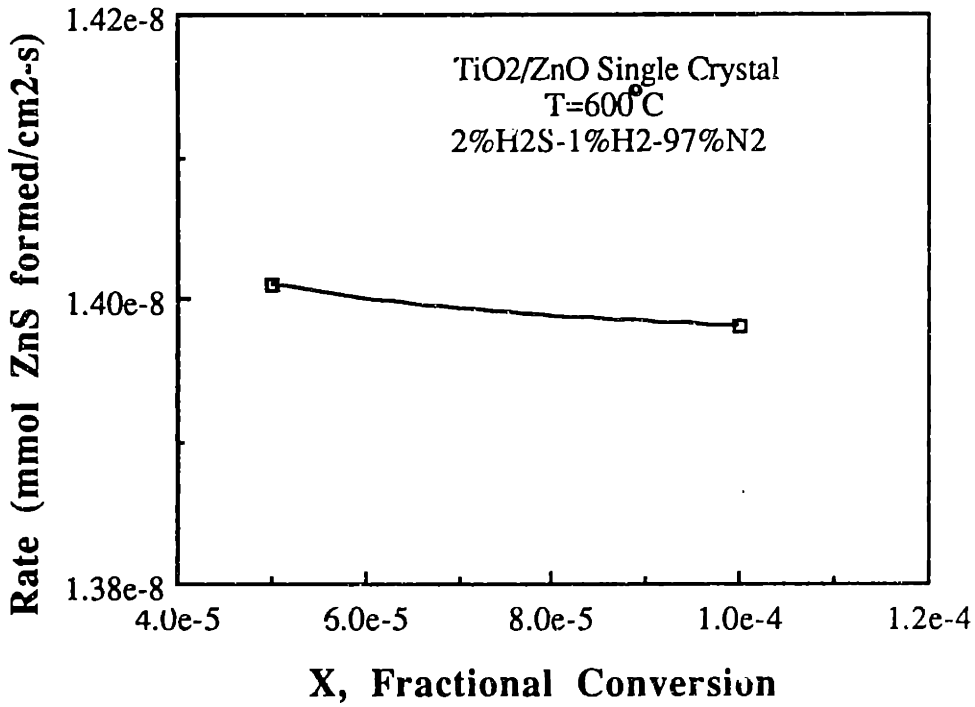

Figure 3.26 Sulfidation rate profile of TiO2/ZnO single crystal at 600°C in 2%H2S-1%H2-97%N2.

3. Water vapor and hydrogen sulfide inhibit the reduction rate of ZnO and Zn-Ti-O solids. This effect is largest in ZnO. Unlike the situation with no water vapor present, increasing the relative amount of TiO_2 from 0 mol% to 60 mol% was accompanied by a corresponding decrease in the reduction rate.

4. Two reduction sites are proposed for ZnO reduction. Type A sites which are very reactive but can be poisoned by H_2O and H_2S and type B sites which are less reactive.

5. Titanium dioxide eliminates Type A sites. Approximately 25 mol% TiO_2 (with 75 mol% ZnO) will completely eliminate Type A sites. With $(Zn/Ti)_{atomic\ ratio} \leq 3$, another type of reaction sites, less reactive than type A sites, is involved in reduction. In the presence of H_2O or H_2S, these sites are eliminated and type B sites take over reduction. Type B sites are less sensitive to titanium than type A sites. Thus, higher relative amount of TiO_2 is needed to affect type B sites.

6. As will be discussed in Chapter 4, suppression of reduction has two benefits. First, lower zinc loss and second, better structural integrity. Reduction followed by the evolution of Zn(g) and H_2O(g) can cause cracks and fissure in the solid.

7. No advantage is gained by coating ZnO with TiO_2 to inhibit reduction because it will suppress the rate of sulfidation to a higher degree. Thus, the only desirable way TiO_2-induced reduction inhibition is by interaction with the reaction sites and not by acting as a physical barrier against reduction. Consequently, Zn-Ti-O solids should be prepared in bulk form where the zinc and titanium ions are intimately associated.

CHAPTER 4

SULFIDATION OF ZN-TI-O MATERIALS

4.1 INTRODUCTION

A large portion of the early work in coal gas desulfurization has focused primarily on single metal oxides (e.g. MERC, 1978; Grindley and Steinfeld, 1981). Comparative evaluations of various metal oxide sorbents for hot gas desulfurization have been reported (Westmoreland and Harrison, 1976; Westmoreland et al., 1977, MERC, 1978, Tamhankar et al., 1981). The sorbents tested included oxides of zinc, iron, copper, calcium, magnesium, vanadium, manganese, nickel, cobalt, tin, lead, bismuth, cadmium, niobium, tantalum, molybdenum, tungsten, and chromium. Each of these oxides has some advantages and disadvantages for hot gas cleanup. Westmoreland et al. (1977) and Tamhankar et al. (1981) published some kinetic data on several selected metal oxides. The relative initial sulfidation rate was $Fe_2O_3 > MnO > CaO \approx ZnO > V_2O_5$. Figure 4.1 shows equilibrium H_2S levels expected in desulfurization of a gas containing 13 mol% H_2 and 19 mol% H_2O. Equilibrium constants were computed from

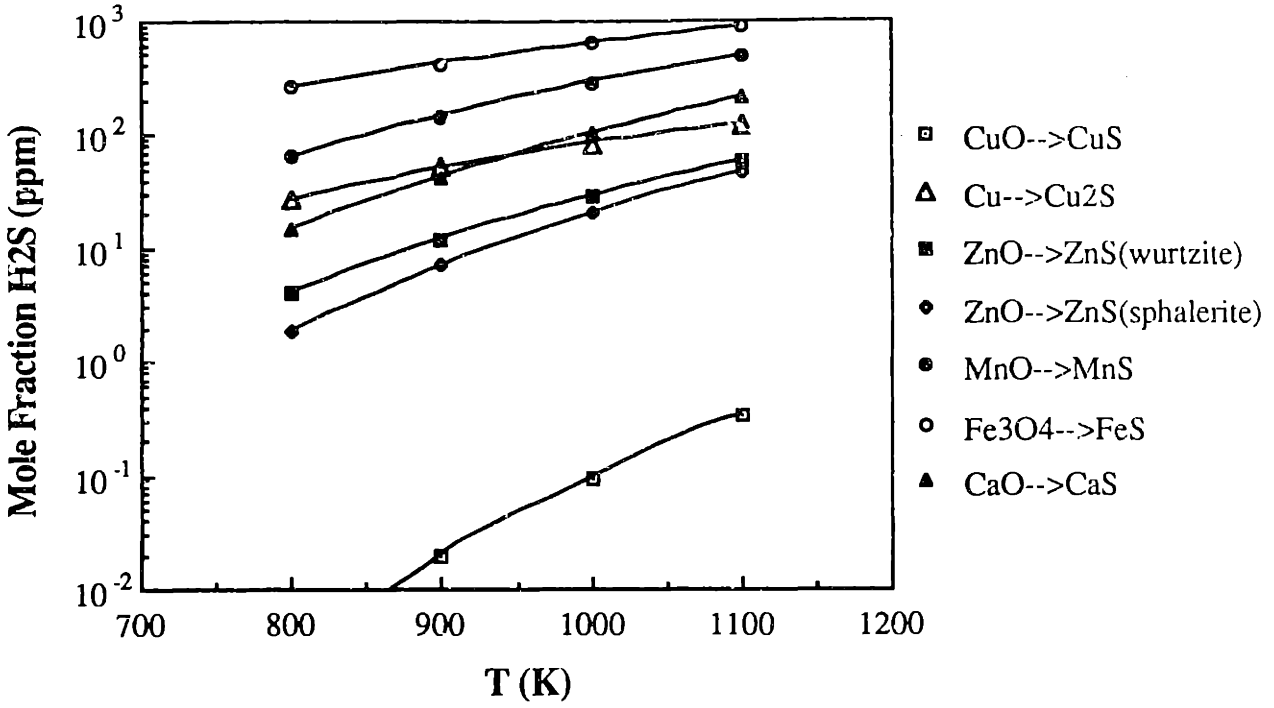

Figure 4.1 Equilibrium H2S levels for various metal oxide sorbents with [H2]/[H2O]=13/19. (Barin and Knacke, 1973; Barin et al., 1976)

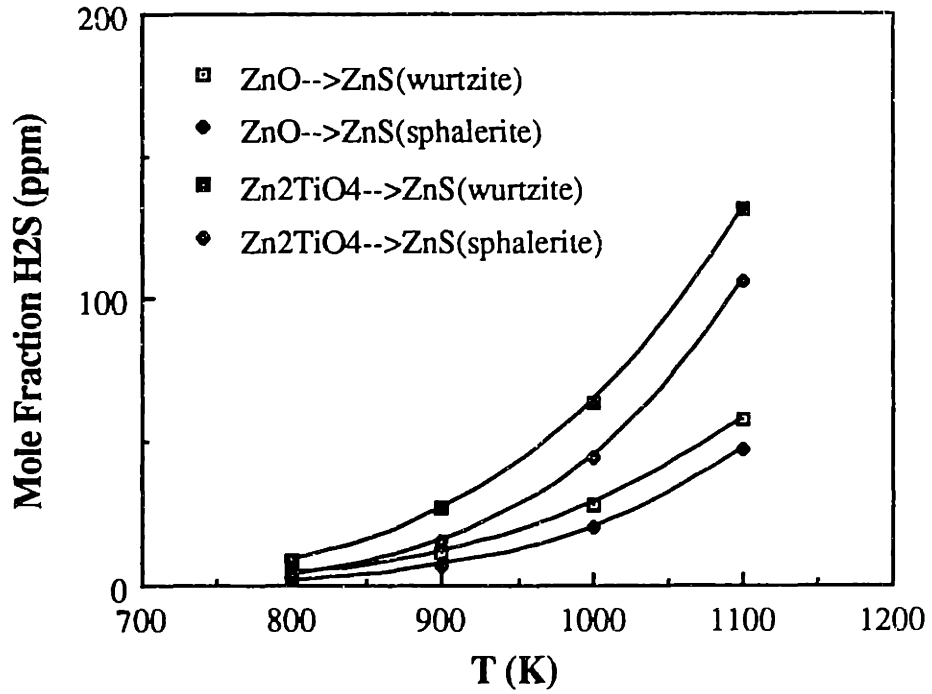

Figure 4.2 Equilibrium H2S levels for ZnO and Zn2TiO4 with [H2]/[H2O]=13/19. (Barin and Knacke, 1973; Barin et al., 1976)

free energy data given in Barin and Knacke (1973) and Barin et al. (1976). Although iron oxide has the most rapid sulfidation kinetics, its thermodynamic equilibrium is unfavorable for removing hydrogen sulfide to the level required for downstream processes such as power generation using molten carbonate fuel cells. Calcium oxide has a slightly higher initial sulfidation rate than ZnO and its thermodynamic efficiency is better than iron oxide, but its overall sulfidation rate will decrease rapidly because of the formation of a nonporous sulfide product layer and the deposition of carbon. Copper oxide possesses the highest H_2S removal efficiency but it will be rapidly reduced to metallic copper in the coal-gas atmosphere. Metallic copper has much lower sulfidation equilibria than its oxides, CuO and Cu_2O.

Extensive desulfurization research has been performed with zinc oxide. ZnO has been used as a non-regenerable sulfur sorbent in "guard beds" to protect downstream water-gas shift or methanol synthesis catalysts from trace sulfur impurities. Zinc oxide has more recently been tested for regenerative hot gas desulfurization (MERC, 1978; Giner, 1981; Grindley and Steinfeld, 1981). Kinetic studies using single pellets of zinc oxide were also performed (Gibson and Harrison, 1980; Ranade and Harrison, 1981). The thermodynamic equilibrium for H_2S removal is very favorable with ZnO. Hydrogen sulfide levels down to a few parts per million (ppm) can be attained (Figure 4.1). However, the sulfidation kinetics of ZnO are slower than those of iron oxide. The regeneration of ZnS is somewhat restricted by the formation of zinc sulfate at low regeneration temperature and the loss of surface area at high regeneration temperature. Also, as discussed in the previous chapter, reduction of zinc oxide to volatile elemental zinc at temperatures above 600°C is a serious problem in zinc-based sorbents.

Recent research has shifted from pure metal oxides to mixed oxides in the hope of eliminating some of the disadvantages associated with single metal oxides. To stabilize CuO against reduction to metallic copper, mixed $CuO-Al_2O_3$ sorbents were investigated (Flytzani-Stephanopoulos et al., 1985; Tamhankar et al., 1986; Flytzani-Stephanopoulos et al., 1987; Patrick, 1988; Patrick et al., 1989). Also $CuO-Fe_2O_3$, $CuO-Fe_2O_3-Al_2O_3$, and $ZnO-Fe_2O_3$ were examined (Stephanopoulos et al., 1985; Tamhankar et al., 1986; Stephanopoulos et al., 1987; Focht et al., 1988; Sa et al., 1989; Ayala et al., 1989). The addition of Fe_2O_3 was for the purpose of producing a sorbent with rapid sulfidation kinetics associated with the presence of Fe_2O_3 and high H_2S removal efficiency due to the presence of CuO or ZnO. $CuO-Fe_2O_3-Al_2O_3$, and $ZnO-Fe_2O_3$ sorbents were found to be very promising sorbents for hot gas cleanup. However, the addition of Fe_2O_3 imparted no resistance against zinc loss in zinc-based sorbents (Flytzani-Stephanopoulos et al., 1987). Additionally, Fe_2O_3 was found to segregate out of the zinc ferrite sorbent in the less efficient FeO form (Focht et al., 1988). Under some conditions, iron carbides could also be formed which were structurally detrimental to the ZnO sorbent.

This research has focused on Zn-Ti-O sorbents for high temperature desulfurization. Zinc titanate promoted with hydrodesulfurization catalysts was reported (Farha, Jr. and Gardner, 1982) to convert organic sulfur liquids to H_2S and to remove H_2S by absorption (over the temperature range of 205-583°C). The sulfided material also was observed to be easier regenerated in air than bulk ZnO. Zinc sulfate was not formed during regeneration at 650°C. From the free energy data given in Barin and Knacke (1973) and Barin et al. (1976), the zinc orthotitanate phase, Zn_2TiO_4, has slightly lower H_2S removal efficiency than ZnO. Figure 4.2 shows the equilibrium hydrogen sulfide level for ZnO and Zn_2TiO_4 in a gas containing 13 mol% H_2 and 19 mol% H_2O.

No thermodynamic data were found for the other possible zinc titanate phases (i.e. $ZnTiO_3$ and $Zn_2Ti_3O_8$). Recently, cyclic sulfidation-regeneration tests with various compositions of Zn-Ti-O sorbents were performed in laboratory packed-bed reactors (Flytzani-Stephanopoulos et al., 1987; Lew, 1987; Lew et al., 1989). Hydrogen sulfide removal efficiencies were found to be comparable to those of ZnO. In other work, zinc titanates prepared and tested in pellet form were found to have much higher crush strength than other type of pellets (e.g. $CuO-Al_2O_3$, $CuO-Fe_2O_3-Al_2O_3$, and $ZnO-CuO-Fe_2O_3$) and were able to retain their strength after sulfidation (Gangwal, 1989).

The objectives of the sulfidation research conducted in this thesis were to (1) measure the sulfidation kinetics of various compositions of bulk Zn-Ti-O sorbents and compare them to results obtained for ZnO, (2) examine the structural and chemical changes of sorbents during sulfidation, (3) determine the effect of hydrogen and water vapor in the reactant stream, and (4) identify the range of Zn-Ti-O compositions that has the most desirable overall sulfidation performance.

4.2 EXPERIMENTAL METHODS

Sulfidation experiments with sorbents containing various Zn/Ti ratios were performed. The preparation and characterization of the sorbents were discussed in Chapter 2. The reacted sorbents were characterized by various physical and chemical techniques which were also discussed in Chapter 2. These analytical techniques include BET-N_2 desorption for surface area measurement, mercury porosimetry for pore volume measurement, scanning electron microscopy (SEM) coupled with energy dispersive X-ray (EDS) analysis for surface morphology and elemental distribution determination, and X-ray diffraction for crystalline phase identification. The chemical and physical

properties of the sorbents used in sulfidation are shown in Tables 4.1 and 4.2, respectively.

Kinetic experiments were performed in a Cahn System 113-X thermogravimetric analyzer (TGA) equipped with a Cahn 2000 electrobalance, a Micricon temperature controller, and a Bascom Turner data acquisition system. The TGA measures the weight increase as a function of time associated with hydrogen sulfide uptake. The reactant gas was introduced into the apparatus through a side arm (Figure 4.3). The balance section of the TGA was constantly purged with a protective nitrogen gas flow (~200 cm^3/min) which also served as a diluent for the reactant stream. Gas flow rates were set by Brooks Model 5850E mass flow controllers. To accomodate corrosive gases such as hydrogen sulfide, the sample was placed on a quartz pan suspended by a quartz hangdown wire. Previously, a Nichrome hangdown wire was used. However, H_2S was observed to corrode the wire. Platinum pans were not used because it is known that platinum catalyzes the H_2S decomposition (Fukuda et al., 1978; Bartholomew et al., 1982; Patrick, 1988). In regards to gas diffusion problems, it was experimentally verified that a gas flow rate of typically between 300-400 sccm with a sample size between 1-3 mg minimized external mass transfer effects. Particle sizes needed to minimize pore diffusional effects were typically between 88-125 μm (120-170 mesh).

For sulfidation, a reactant gas mixture containing H_2S-H_2-N_2 was used. In several experiments, H_2O vapor was added. Various compositions were used to determine the effects of H_2 and H_2O on sulfidation. Water vapor was added to the gas by bubbling nitrogen and hydrogen through a water saturator maintained at room temperature

Table 4.1 Chemical Properties of Sorbents Used in Sulfidation Experiments [1]

Sorbent	(Zn/Ti) (atomic ratio)	Crystalline Phases (wt %)				
		ZnO	Zn_2TiO_4	$ZnTiO_3$	$Zn_2Ti_3O_8$	TiO_2
Z3T7 [2]	3/7	0	0	69	0	31
Z2T3-a	2/3	0	0	65	16	19
Z2T3-b	2/3	0	0	83	0	17
ZT	1/1	0	20	45	35	0
Z3T2	3/2	0	68	18	14	0
Z2T-a	2/1	0	100	0	0	0
Z2T-b [3]	2/1	0	100	0	0	0
Z3T	3/1	28	72	0	0	0
ZnO	---	100	0	0	0	0

[1] Prepared from zinc acetate and titanium (IV) i-propoxide with 1:1 mole ratio of metal ions to citric acid (unless otherwise noted). Calcined at 720°C for 12 h.

[2] Prepared with titanium tetrachloride.

[3] Prepared with 1:2 mole ratio of metal ions to citric acid.

Table 4.2 Physical Properties of Sorbents Used in Sulfidation Experiments [1]

Sorbent	Surface Area (m^2/g)	Pore Volume (cm^3/g)	Pore Size Distribution [2] (%), μm (diameter)
Z3T7 [3]	5.4	1.26	16.0%, > 25 μm 69.5%, 25-1 μm 13.3%, 1-0.1 μm 1.2%, 0.1-0.003 μm
Z2T3-a	2.3	0.47	58.5%, >25 μm 21.8%, 25-1 μm 10.8%, 1-0.1 μm 8.9%, 0.1-0.003μm
Z2T3-b	1.3	0.29	44.8%, >25 μm 25.4%, 25-1 μm 12.6%, 1-0.1 μm 17.2%, 0.1-0.003μm
ZT	1.6	0.57	15.7%, >25 μm 67.2%, 25-1 μm 7.9%, 1-0.1 μm 9.2%, 0.1-0.003μm
Z3T2	2.2	0.72	44.2%, >25 μm 38.4%, 25-1 μm 10.5%, 1-0.1 μm 6.9%, 0.1-0.003μm

Table 4.2 Physical Properties of Sorbents Used in Sulfidation Experiments [1] (cont'd)

Sorbent	Surface Area (m^2/g)	Pore Volume (cm^3g)	Pore Size Distribution [2] (%), μm (diameter)
Z2T-a	4.1	0.73	56.2%, >25 μm 28.1%, 25-1 μm 5.8%, 1-0.1 μm 9.9%, 0.1-0.003μm
Z2T-b [4]	13.9	1.13	10.0%, >25 μm 53.4%, 25-1 μm 15.3%, 1-0.1 μm 21.3%, 0.1-0.003μm
Z3T	7.6	0.93	19.6%, >25 μm 54.6%, 25-1 μm 10.0%, 1-0.1 μm 15.8%, 0.1-0.003μm
ZnO	2.4	1.20	15.0%, >25 μm 62.2%, 25-1 μm 21.1%, 1-0.1 μm 1.7%, 0.1-0.003μm

[1] Prepared from zinc acetate and titanium (IV) i-propoxide with 1:1 mole ratio of metal ions to citric acid. Calcined at 720°C for 12 h. (unless otherwise noted)

[2] Pore size distribution for 90-125 μm particles except for Z2T3-b with 420-840 μm particles.

[3] Prepared with titanium tetrachloride.

[4] Prepared with 1:2 mole ratio of metal ions to citric acid.

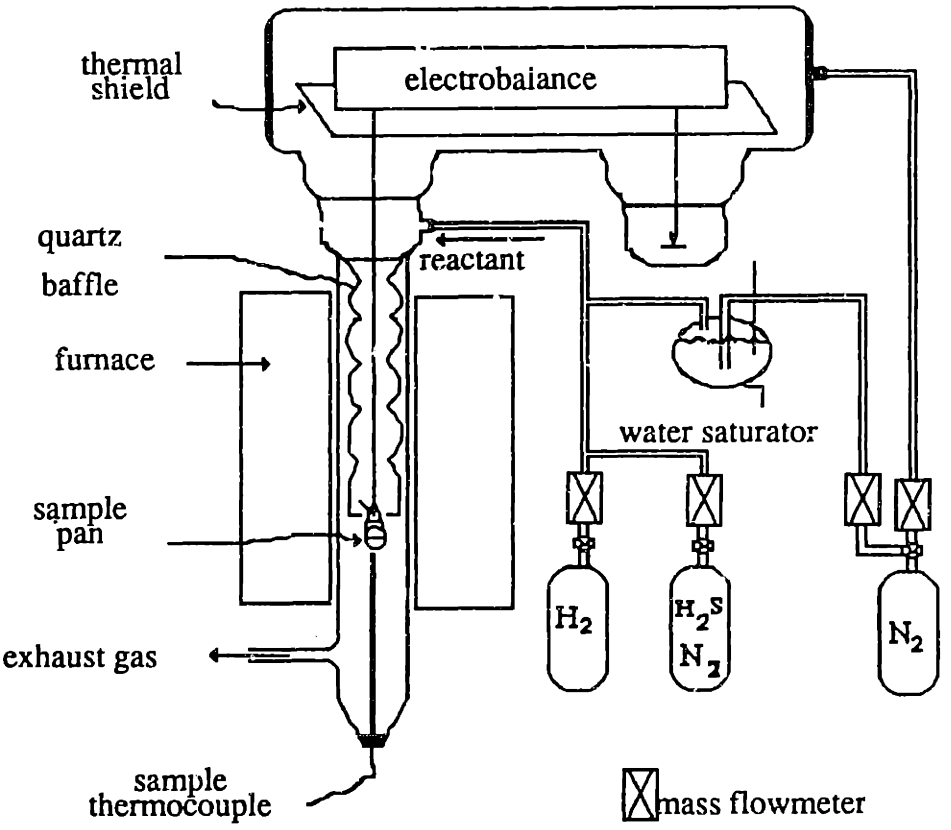

Figure 4.3 Schematic of TGA reactor system.

(25°C) in a three-neck flask assembly. The saturated gas stream was then mixed with the H_2S-N_2 gas stream and entered the reactor through the side arm.

4.3 PRESENTATION AND DISCUSSION OF SULFIDATION RESULTS

4.3.1 Initial Sulfidation Rate of Bulk Zn-Ti-O Sorbents

Initial rate experiments in the TGA were performed under isothermal conditions to determine the sulfidation reactivity of sorbents containing various atomic ratios of Zn:Ti and various chemical phases (e.g. ZnO, Zn_2TiO_4, $ZnTiO_3$, and $Zn_2Ti_3O_8$). Kinetic parameters (e.g. activation energies) were determined from these experiments. The possible overall reactions in sulfidation are:

$$ZnO + H_2S \text{ ----> } \alpha,\beta\text{-}ZnS + H_2O \quad (4.1)$$

$$1/2\ Zn_2TiO_4 + H_2S \text{ ---> } \alpha,\beta\text{-}ZnS + 1/2\ TiO_{2(rutile)} + H_2O \quad (4.2)$$

$$ZnTiO_3 + H_2S \text{ ---> } \alpha,\beta\text{-}ZnS + TiO_{2(rutile)} + H_2O \quad (4.3)$$

$$1/2\ Zn_2Ti_3O_8 + H_2S \text{ ---> } \alpha,\beta\text{-}ZnS + 3/2\ TiO_{2(rutile)} + H_2O \quad (4.4)$$

$$1/2\ TiO_{2(anatase,rutile)} + H_2S \text{ ---> } 1/2\ TiS_2 + H_2O \quad (4.5)$$

Table 4.3 lists the K_{eq} for these reactions. No thermodynamic data were found for either $ZnTiO_3$ or $Zn_2Ti_3O_8$. Two types of ZnS may form. One is β-ZnS (sphalerite) which exists in a cubic crystalline form. The other is α-ZnS (wurtzite) which exists in a hexagonal crystalline form. At temperatures above 1020°C, β-ZnS is transformed to α-ZnS. Formation of β-ZnS is slightly more thermodynamically favorable yielding higher K_{eq}. The reaction of titanium dioxide with hydrogen sulfide (reaction 4.5) is thermodynamically unfavorable. At 1000 K, the K_{eq} for reaction (4.5) is 5.67×10^{-9} for anatase and 1.53×10^{-9} for rutile. Anatase is a metastable high surface area structure which upon heating above 750°C, transforms into the denser rutile structure. This

Table 4.3 Equilibrium Constants and Heats of Reaction for Sulfidation Reactions at 727°C

Reaction	Thermodynamic Constants	
	K_{eq}	ΔH, kcal/mol
$ZnO + H_2S = \beta\text{-}ZnS + H_2O$	1.03×10^{4}	-18.97
$ZnO + H_2S = \alpha\text{-}ZnS + H_2O$	7.21×10^{4}	-15.81
$1/2Zn_2TiO_4 + H_2S = \beta\text{-}ZnS + 1/2TiO_2 + H_2O$	4.61×10^{3}	-18.98
$1/2Zn_2TiO_4 + H_2S = \alpha\text{-}ZnS + 1/2TiO_2 + H_2O$	3.22×10^{3}	-15.82
$1/2TiO_2(\text{anatase}) + H_2S = 1/2TiS_2 + H_2O$	5.67×10^{-9}	18.76
$1/2TiO_2(\text{rutile}) + H_2S = 1/2TiS_2 + H_2O$	1.53×10^{-9}	20.35

transformation is associated with a significant surface area loss. To check whether there was any absorption of H_2S on TiO_2, 2 mol% H_2S-1 mol% H_2-97 mol% N_2 was passed over TiO_2 at 700°C. Figure 4.4 shows the results of experiments with both the anatase (from Aldrich Chemical Co.) and rutile (UCI 1090-113 extrusions crush to 90-125 μm size particles) forms of titanium dioxide. Neglible weight change was measured for either type of TiO_2.

Reactions 4.1 and 4.2 are exothermic. In Table 4.3, the heats of reaction at 1000 K are also listed. Since these reactions are exothermic, it is necessary to investigate the possible temperature excursion which may occur during the reaction. A method for estimating the maximum possible temperature increase is provided in Appendix A. Calculations were based on reaction with a gas containing 2 mol% H_2S-1 mol% H_2-97 mol% N_2 at 1000 K. Because the gas contains mainly N_2, the properties of the reactant gas (i.e. viscosity, density, and heat capacity) were assumed to be the same as those for pure N_2. The inside diameter of the reactor is 1.6 cm, and the particle diameter is 1.25×10^{-2} cm. To calculate the Reynolds number, a typical gas flowrate of 350 sccm was used. The maximum possible temperature increase for reactions (4.1) and (4.2) assuming β-ZnS as a product is less than 1°C. For α-ZnS formation, the temperature change is smaller. It was, therefore, concluded that the isothermal assumption was valid.

The reactant gas used in these experiments contained 2 mol% H_2S-1 mol% H_2-97 mol% N_2. Hydrogen was added to the gas to inhibit the decomposition of H_2S. The decomposition reaction is:

$$2H_2S = 2H_2 + S_2 \qquad (4.6)$$

At 1000 K and a gas flowrate of 350 cm^3/min, the equilibrium decomposition rate due

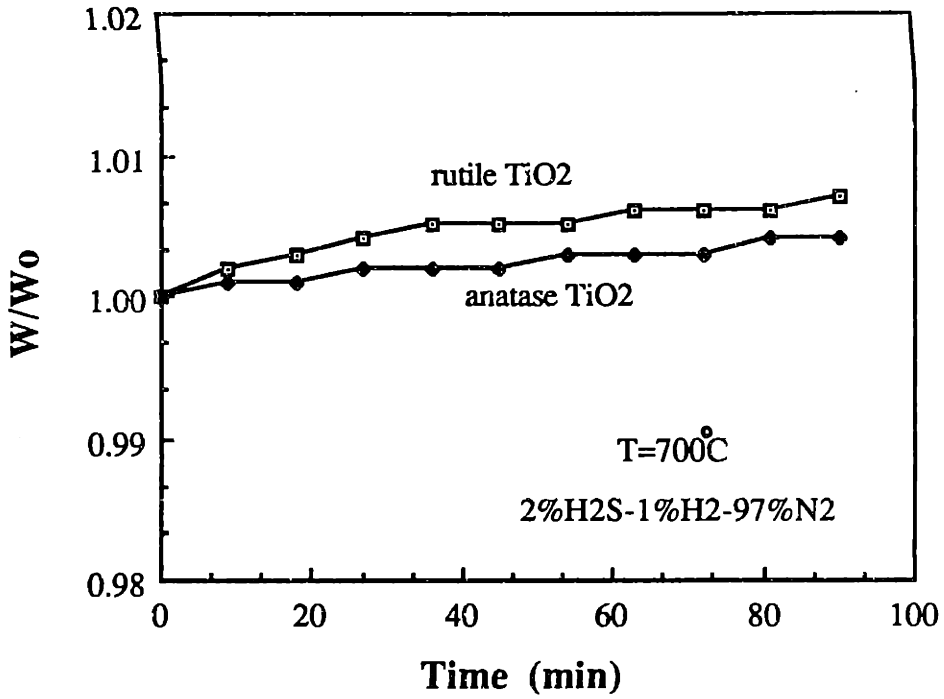

Figure 4.4 Reaction of TiO2 with H2S at 700°C.

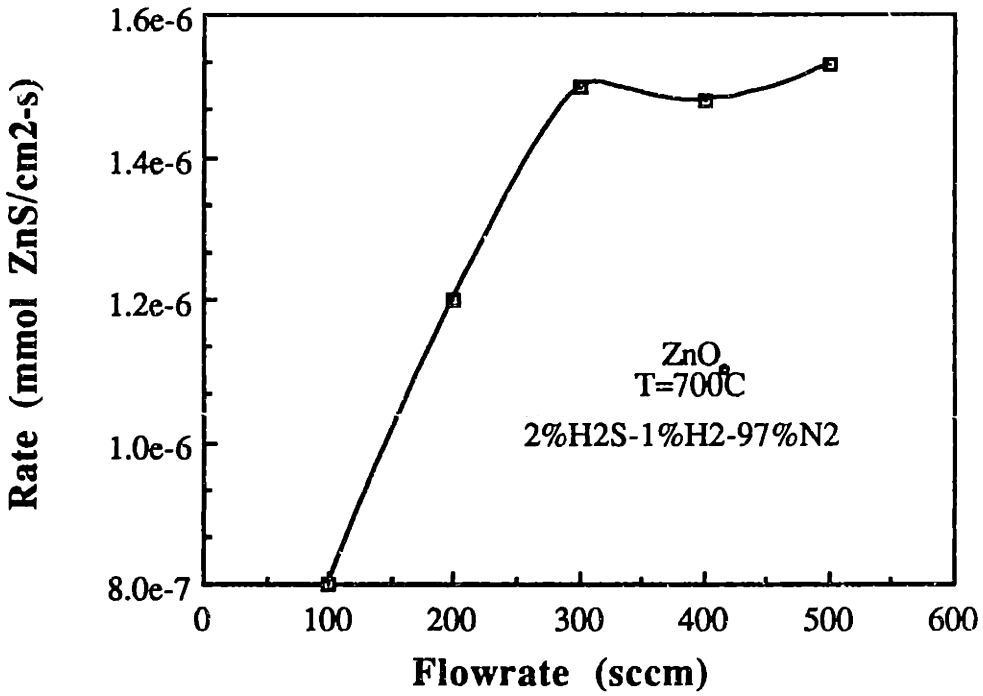

Figure 4.5 Effect of gas flowrate on the initial reaction rate of ZnO at 700°C.

to reaction (4.6) is 93 mg S_2/h in the absence of hydrogen. The sulfur will deposit on the cooler section of the reactor downstream of the sample pan. With 1 mol% H_2 in the gas stream, the rate decreases to 11 mg S_2/h. This decomposition rate is low compare to the total H_2S in the reactant gas (549 mg S_2/h). The presence of 10 mol% H_2 will decrease the rate of decomposition even further (0.1 mg S_2/h). However, as will be discussed in Section 4.3.4, no significant difference in the sulfidation profiles was observed in the presence of different concentrations of hydrogen at temperatures up to and including 700°C. This indicates that the effect of gaseous S_2 is neglible.

To ensure that these results were obtained in the absence of diffusional limitations, either external (i.e. gas-film diffusion) or internal (i.e. intra-particle diffusion), the gas flow rate, the sample size, and the particle size were varied. In preliminary experiments, the effect of gas flow rate on the reaction rates was examined. Approximately 1-3 mg of sample were used. The results for ZnO sulfidation are depicted in Figure 4.5, which shows that above approximately 300 sccm the gas flow rate has no effect on the initial reaction rate at 700°C. Similar results were obtained for the sulfidation of the other sorbents. This indicates that above 300 sccm external mass transfer effects were eliminated. All sulfidation experiments were subsequently conducted with a gas flow rate of 350 sccm.

Different particle sizes were examined to minimize the effect of internal mass transfer. In Figure 4.6, the result for this set of sulfidation experiments is shown for two ranges of particle sizes, 420-840 μm and 90-125 μm, with sorbents ZnO, Z2T-a, and Z2T3-a These experiments were performed at 700°C. The results are shown in terms of fractional conversion (X) versus reaction time (minutes). The fractional conversion is based on conversion to ZnS. The data from these experiments appear to show little

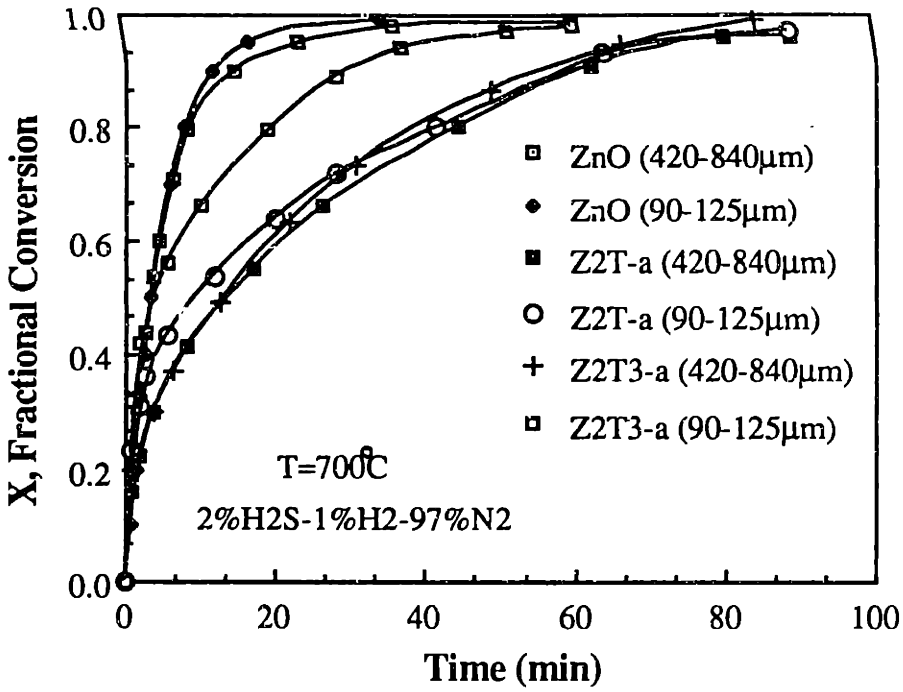

Figure 4.6 Effect of particle sizes, 420-840 and 90-125 μm, for sorbents ZnO, Z2T-a and Z2T3-a on sulfidation conversion profiles.

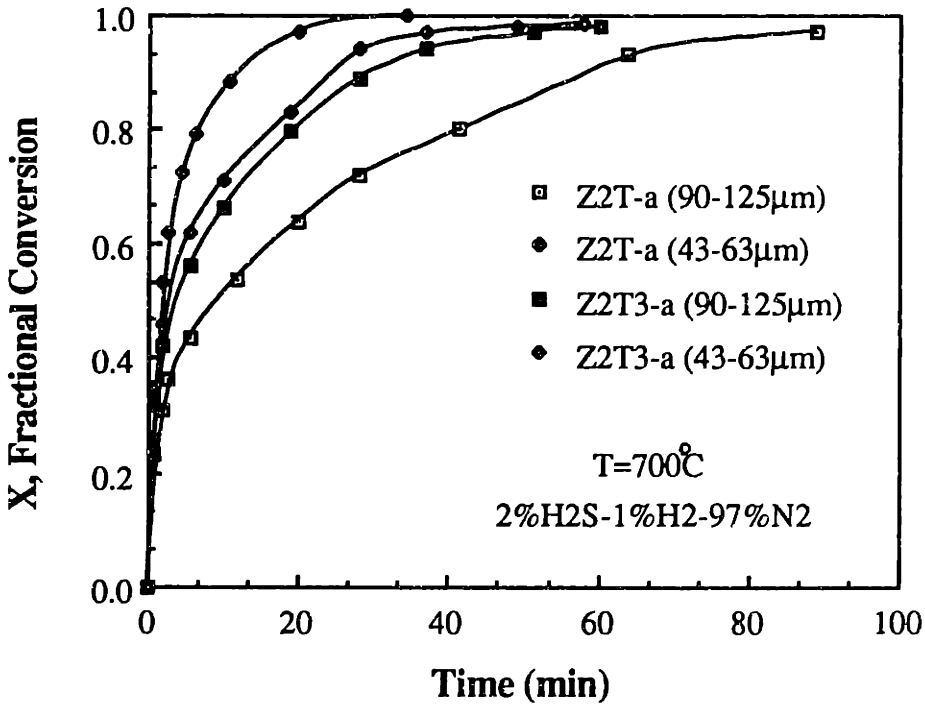

Figure 4.7 Effect of particle sizes, 90-125 and 43-63 μm, for sorbents Z2T-a and Z2T3-a on sulfidation conversion profiles.

effect on the rate of reaction for all sorbents except Z2T3-a. However, when even smaller particle sizes (43-63 μm) were used for Z2T-a as shown in Figure 4.7, although no change in the initial sulfidation rate occurred, a significant effect was seen at higher fractional conversion. No difference in the sulfidation profile was observed with 43-63 μm particles for Z2T3-a. For these experiments, 90-125 μm size particles were used for all sorbents except Z2T-a, for which 43-63 μm size particles were used.

Initial rate measurements were performed with the sorbents listed in Tables 4.1 and 4.2. The results of these experiments at 600 and 700°C in 2 mol% H_2S-1 mol% H_2-97 mol% N_2 are shown in Figure 4.8. The initial rate is expressed in mmole ZnS formed/cm2-s. The rate was normalized with the initial surface area of the sorbent. The initial rate of sulfidation for ZnO at 700°C is approximately 1.2-1.8 times higher than for all Zn-Ti-O sorbents containing $\geq$ 25 mol% Ti (based on Zn-Ti stochiometry). At 600°C, the ZnO sulfidation rate is approximately 1.5 times higher than that of Zn-Ti-O sorbents.

A significant finding of this work is that the initial sulfidation rate was similar for different zinc titanate phases. Sorbents with different Zn-Ti compositions will form different zinc titanate phases as shown in Table 4.2. A sorbent with 30 mol% ZnO-70 mol% TiO_2 forms a mixture of $ZnTiO_3$ and TiO_2 while a sorbent with 75 mol% ZnO-25 mol% TiO_2 forms a mixture of Zn_2TiO_4 and ZnO. However, both of these sorbents had approximately the same initial sulfidation rates (Figure 4.8).

Since all Zn-Ti-O sorbents containing $\geq$ 25 mol% Ti (based on Zn-Ti stochiometry) had approximately the same initial sulfidation rate, further kinetic experiments were performed with just two different typess of Zn-Ti-O sorbents. Experiments were performed with Z2T-a, a sorbent prepared with 2:1 atomic ratio of Zn:Ti, and Z2T3-a

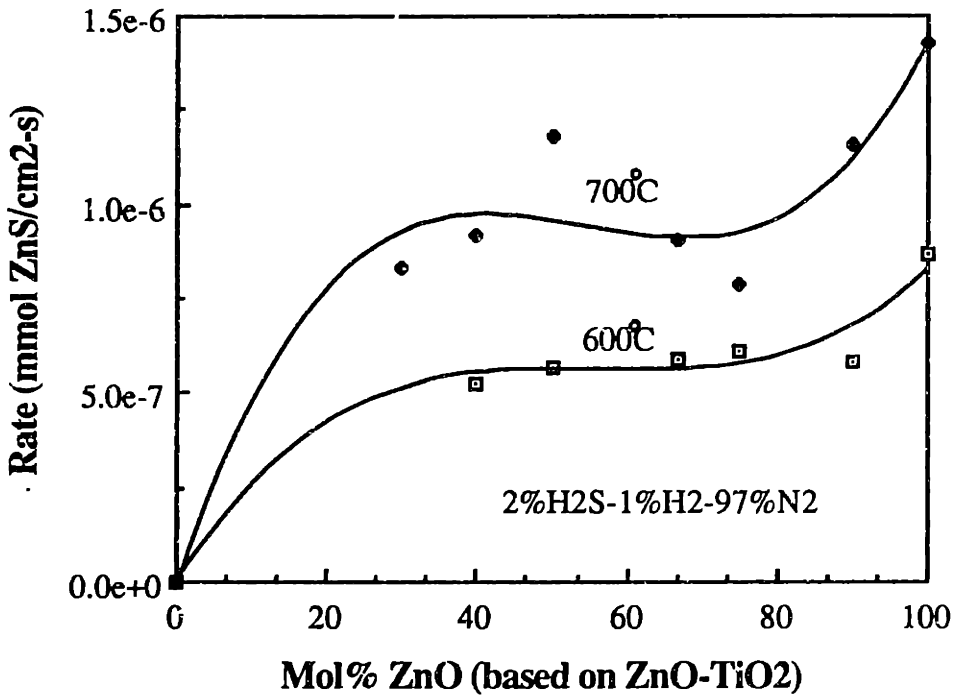

Figure 4.8 Initial sulfidation rate of several Zn-Ti-O sorbents in 2%H2S-1% H2-97%N2 at 600 and 700°C.

which was prepared with 2:3 atomic ratio of Zn:Ti. Zn_2TiO_4 was the only crystalline phase determined by XRD in Z2T-a, while Z2T3-a contained a mixture of $ZnTiO_3$, $Zn_2Ti_3O_8$ and TiO_2. As shown in the X-ray diffractogram of Z2T-a (Figure 4.9), the peaks are very narrow which is consistent with a highly crystalline material. For the purpose of comparison and in order to establish a base line sulfidation performance level to meet or perhaps exceed, similar kinetic experiments were also performed with ZnO.

In the absence of both diffusional and mass transfer resistances, an intrinsic initial heterogeneous rate expression of the form

$$R_o = k\, C^n_{H_2S} \qquad (4.7)$$

was used, where R_o is the initial molar rate of ZnS formation per unit surface area of the solid reactant [mmol/cm^2-s], k is the intrinsic rate constant [cm/s], C_{H2S} is the molar concentration of hydrogen sulfide [mmol/cm^3], and n is the reaction order. An Arrhenius relationship can be used to express the intrinsic rate constant as

$$k = k_o \exp[-E/RT] \qquad (4.8)$$

In equation (4.8), k_o is the Arrhenius frequency factor [cm/s], E is the activation energy [kcal/mol], R is the gas constant [1.987x10^{-3} kcal/mol-K], and T is the temperature [K].

The reaction orders (n) for ZnO and Z2T-a sulfidation were both determined to be one. Figure 4.10 illustrates the results obtained for ZnO and Z2T-a sulfidation. The linearity of the variation in initial sulfidation rate with changing hydrogen sulfide concentration indicates a reaction order of one. This agrees with the data reported by Westmoreland et al. (1977) for zinc oxide.

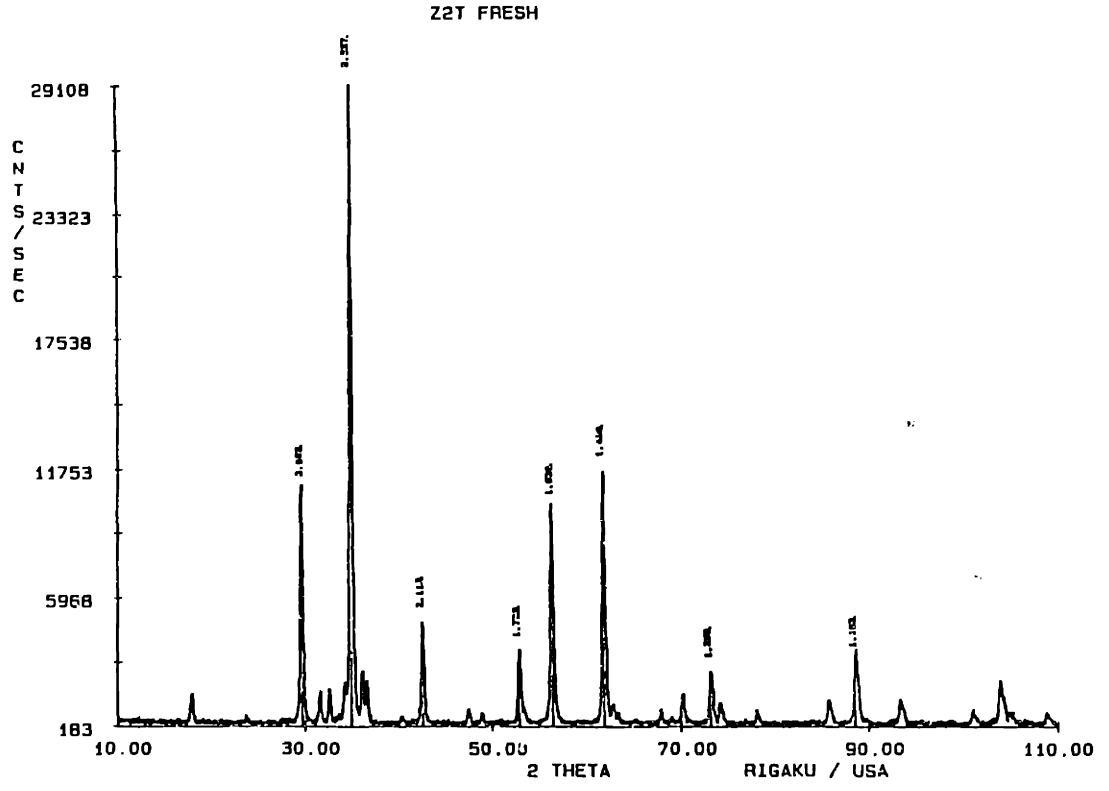

Figure 4.9 X-ray diffractogram of sorbent Z2T-a (2 Zn : 1 Ti) calcined at 720°C.

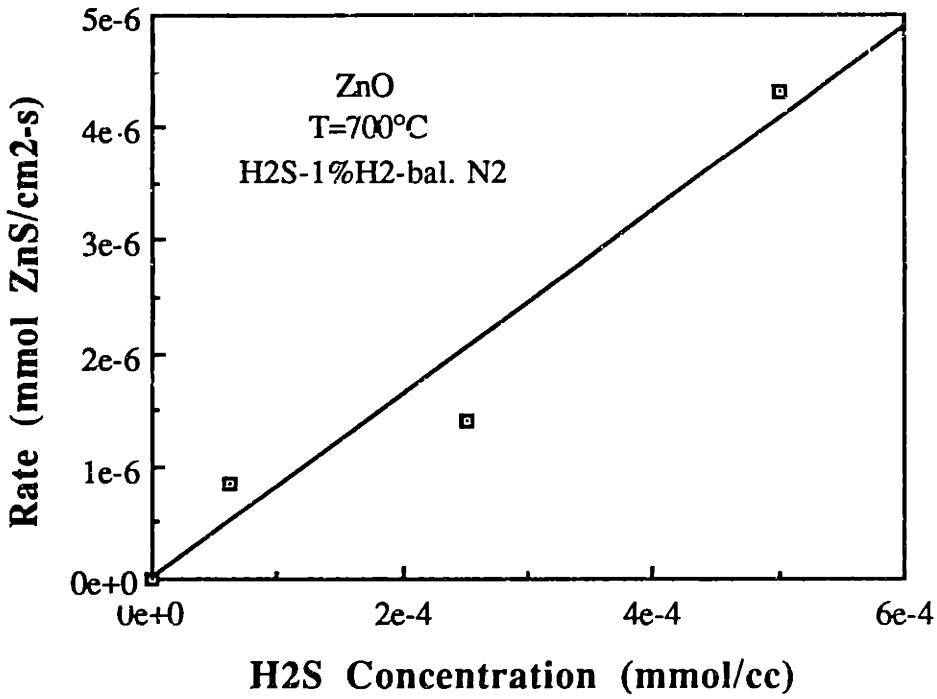

a) ZnO-H2S

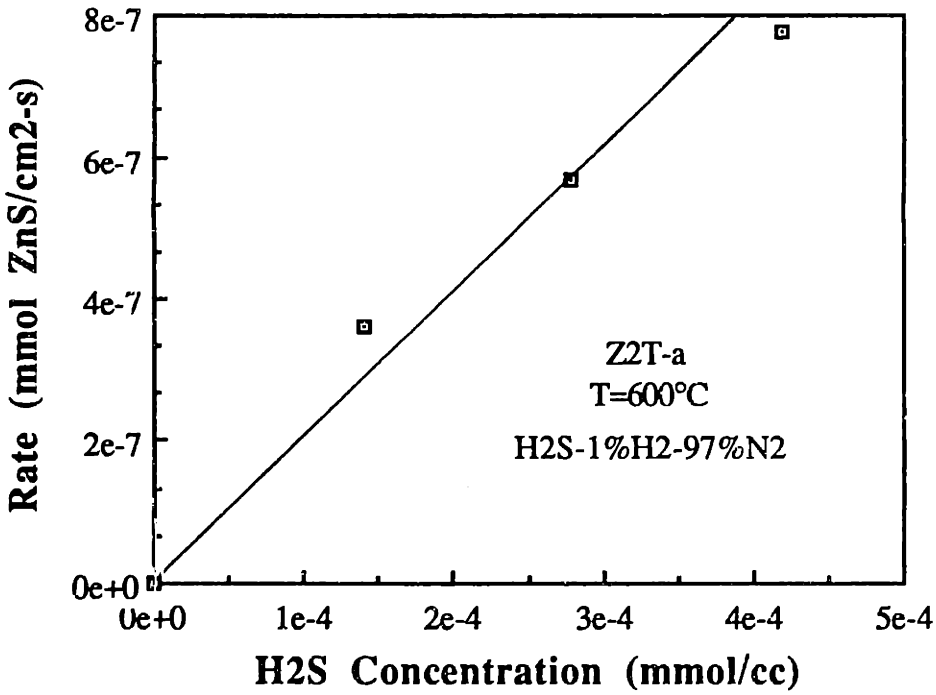

b) Z2T-H2S

Figure 4.10 Determination of reaction order for a) ZnO-H2S and b) Z2T-H2S reactions.

The Arrhenius dependence for ZnO-H_2S and Z2T-H_2S reactions was determined by measuring the initial sulfidation rate as a function of temperature. The experiments were performed in 2 mol% H_2S-1 mol% H_2-97 mol% N_2. Figure 4.11 shows the resultant Arrhenius plots for ZnO and Z2T-a sulfidations. The intrinsic sulfidation rate for ZnO is greater than Z2T-a at all temperatures between 400-700°C. Kinetic constants obtained for the ZnO-H_2S and Z2T-H_2S systems are listed in Table 4.4. The activation energies for both ZnO and Z2T-a sulfidation are approximately the same (10.3 kcal/mol and 9.3 kcal/mol, respectively). The major difference is in the frequency factors. The frequency factor for ZnO sulfidation is approximately three times greater than for Z2T-a. The lower frequency factor for the latter is probably caused by fewer reaction sites on the surface of the reactant solid due to the presence of titanium on the surface. Thus, the lower values for the initial rate is somewhat deceptive because the surface area used in the calculation of the frequency factor is the total surface area (ZnO+TiO_2) and not the specific surface area (ZnO only). Also, another possible reason for the lower initial rate may be the interaction of titanium with a reactive site to decrease its reactivity. What is important to note is that sorbents prepared with higher amount of TiO_2 do not have correspondingly lower initial reaction rates as shown in Figure 4.8. Thus, as the concentration of TiO_2 in the sorbent increases, there is not a corresponding decrease in the number of reactive sites. As shown in Figure 4.12, sorbent Z2T3-a has nearly an identical Arrhenius plot as sorbent Z2T-a.

Table 4.4 lists the values for the sulfidation reaction constants reported by Westmoreland et al. (1977). The initial sulfidation rate reported in the present study is approximately twice as fast as that reported by Westmoreland et al. To discover the reason for this, an attempt was made to perform sulfidation experiments with the same source of zinc oxide as that used by Westmoreland et al. However, the Matheson

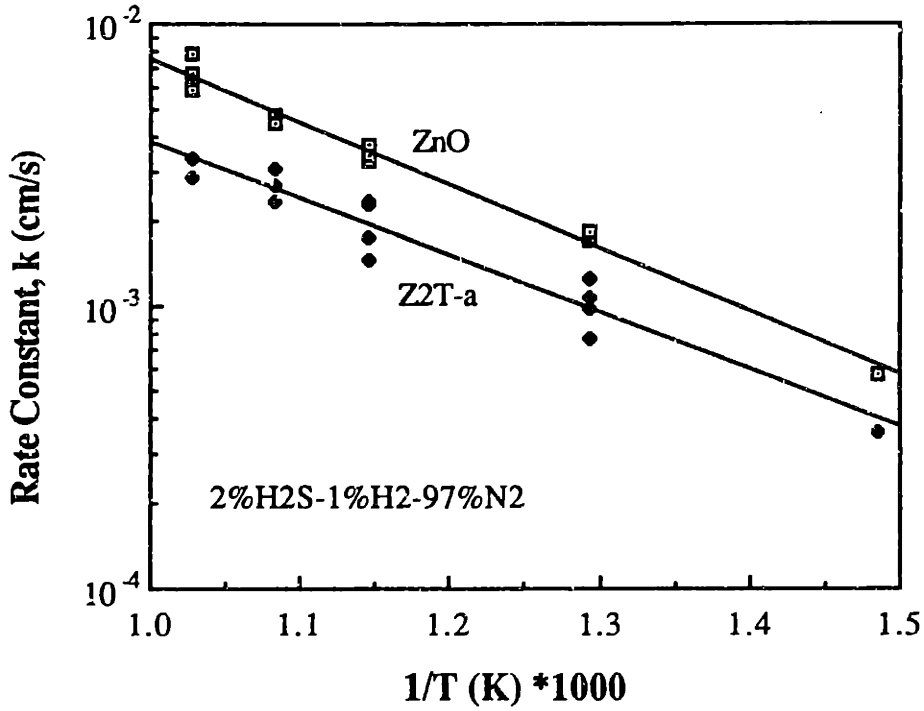

Figure 4.11 Comparative Arrhenius plots for ZnO-H2S and Z2T-H2S reactions.

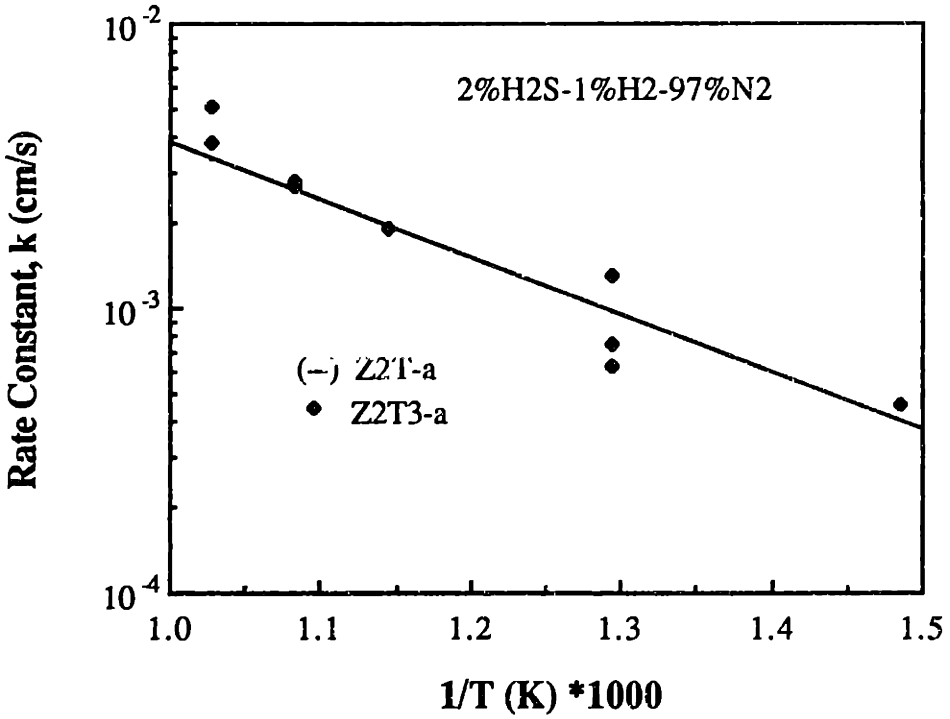

Figure 4.12 Comparative Arrhenius plots for Z2T3-H2S and Z2T-H2S reactions.

Table 4.4 Arrhenius Constants for Sulfidation Reactions

Reaction	Temp. Range °C	Arrhenius Constants	
		k_o, cm/s	E, kcal/mol
$ZnO + H_2S \rightarrow ZnS + H_2O$	400-700	1.31	10.3
$ZnO + H_2S \rightarrow ZnS + H_2O$ (Westmoreland et al., 1977)	300-750	0.11	7.2
$1/2Zn_2TiO_4 + H_2S \rightarrow ZnS + 1/2TiO_2 + H_2O$	400-700	0.40	9.3

Table 4.5 Specific Surface Areas of ZnO Samples

Source	Surface Area, m^2/g
amorphous citrate technique, calcined at 720°C, 12h	2.4
EM Science	3.7
Matheson Coleman & Bell (Westmoreland et al., 1977)	4.9

Coleman & Bell zinc oxide used by these authors was no longer available. Instead, zinc oxide was purchased from EM Science which took over most of Matheson Coleman & Bell production. This source of zinc oxide was as close as possible to that of Westmoreland et al. In Table 4.5, the specific surface areas of these zinc oxide samples are listed. Comparative Arrhenius plots of the different types of ZnO are shown in Figure 4.13. The experimental results with the ZnO from EM Science are much closer to the data of Westmoreland et al. than the ZnO prepared in this work by the amorphous citrate technique. The activation energy and the frequency factor (7.5 kcal/mol and 0.18 cm/s) are close to the value reported in the literature (Table 4.4). It is known that exposure of different ZnO crystal faces can be obtained by varying the precursor (Krebs and Littbarski, 1981; Hindermann et al., 1988). Such variations in exposed crystal faces may explain the somewhat different reactivity obtained from two different sources of ZnO. To determine whether any dissimilarity in crystal geometry and, thus, perhaps, crystal orientation is present, the surfaces of the ZnO prepared by the amorphous citrate technique and the one obtained from EM Science were examined with the scanning electron microscope. The SEM micrographs for ZnO (EM Science) and ZnO (amorphous citrate technique) are shown in Figures 4.14 and 4.15, respectively. As can be seen in these two figures, different crystal geometries are present in each. The (EM Science) ZnO has a majority of rectangular crystals, while the ZnO prepared by the amorphous citrate technique comprises mostly of spherical crystals.

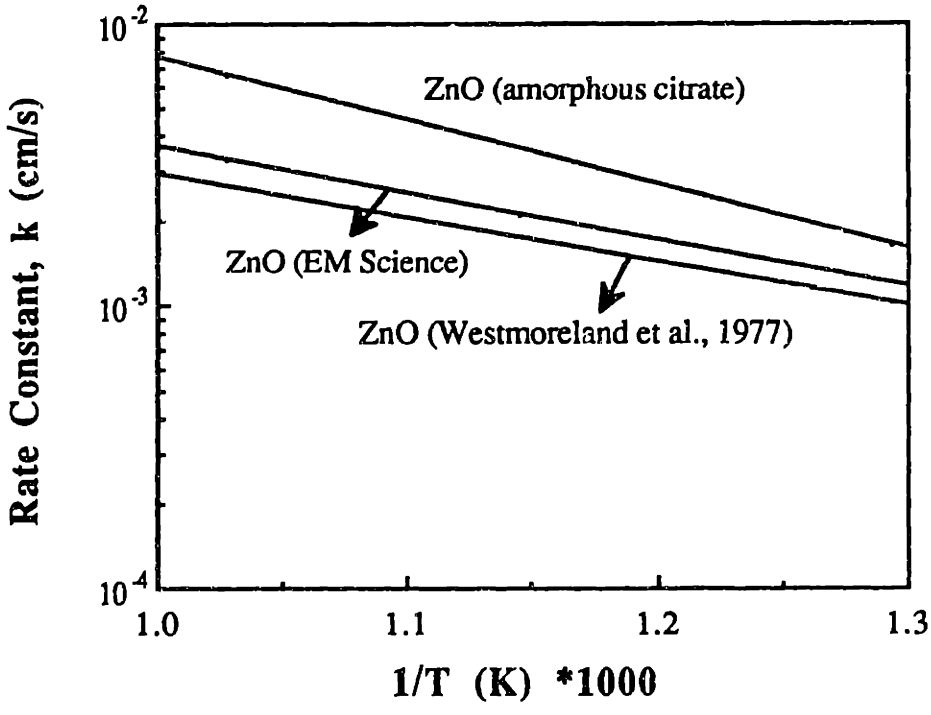

Figure 4.13 Comparative Arrhenius plots for several ZnO samples.

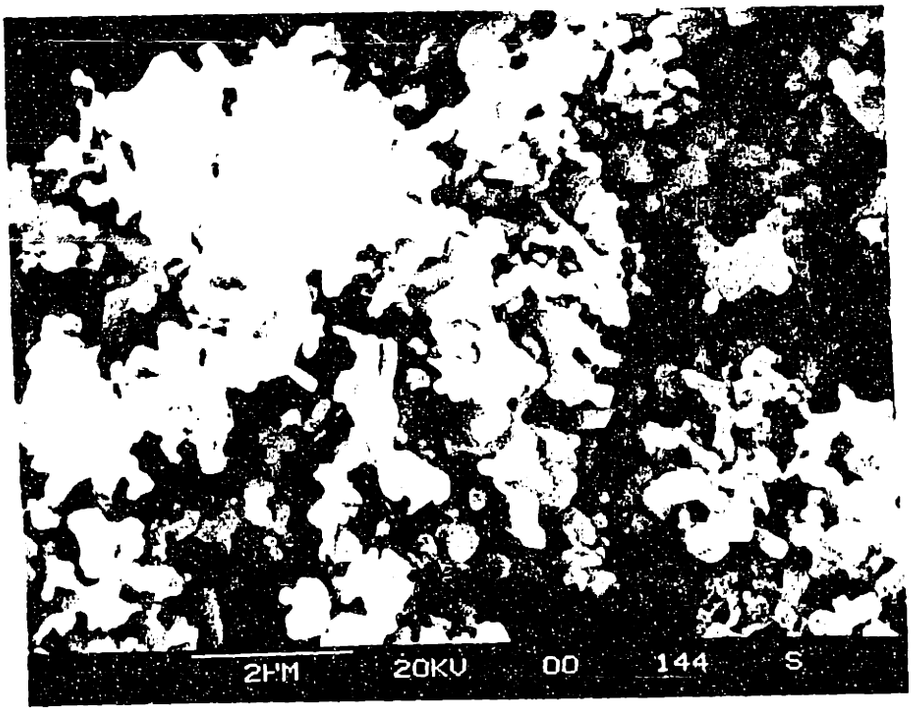

a) 5000x

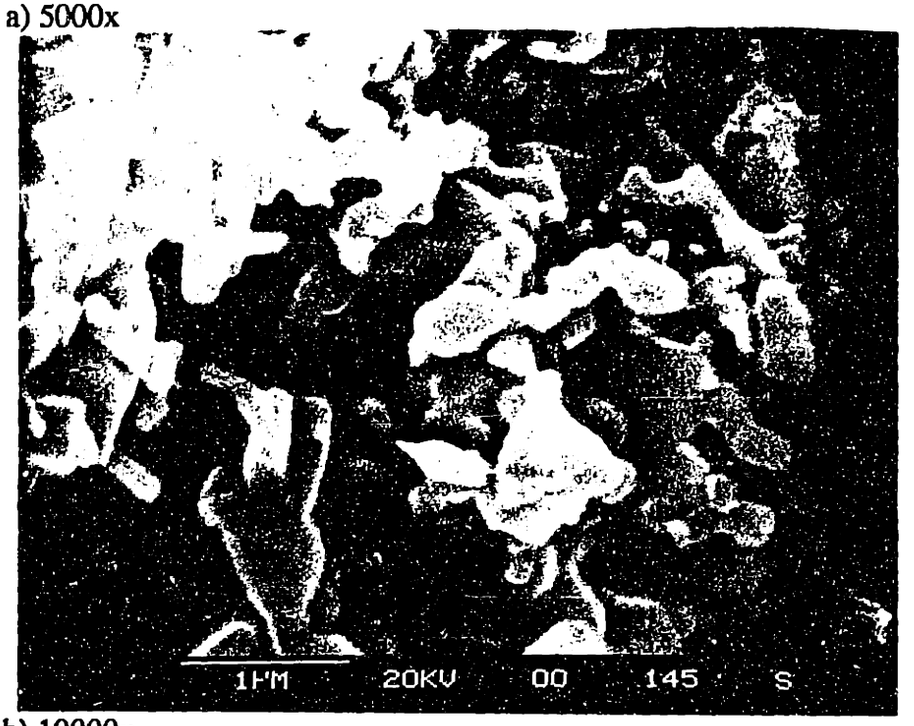

b) 10000x

Figure 4.14 SEM micrographs of ZnO (EM Science) a) 5000x and b) 10000x.

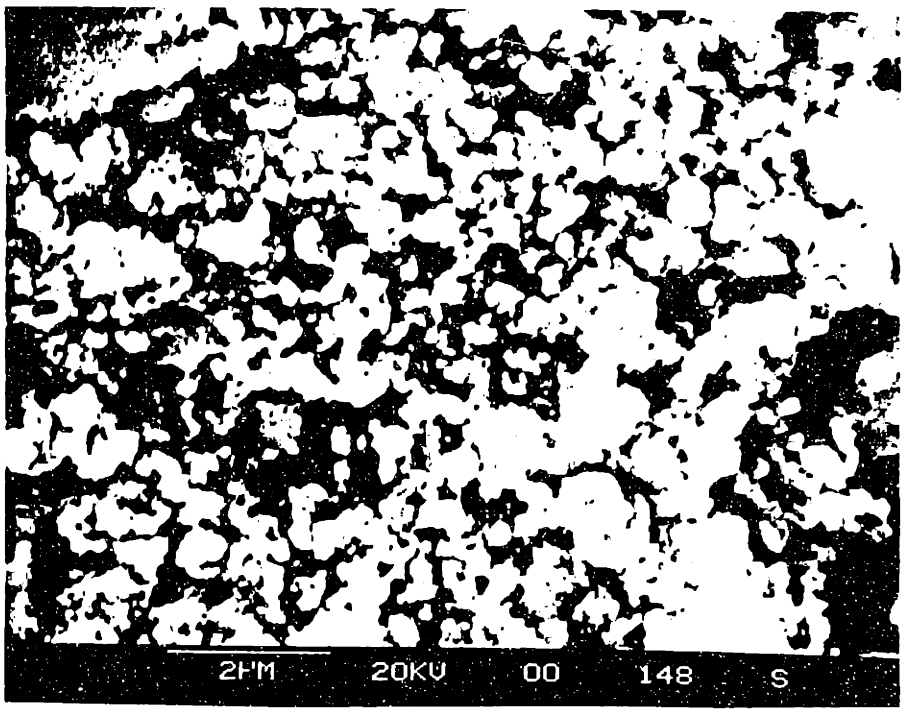

a) 5000x

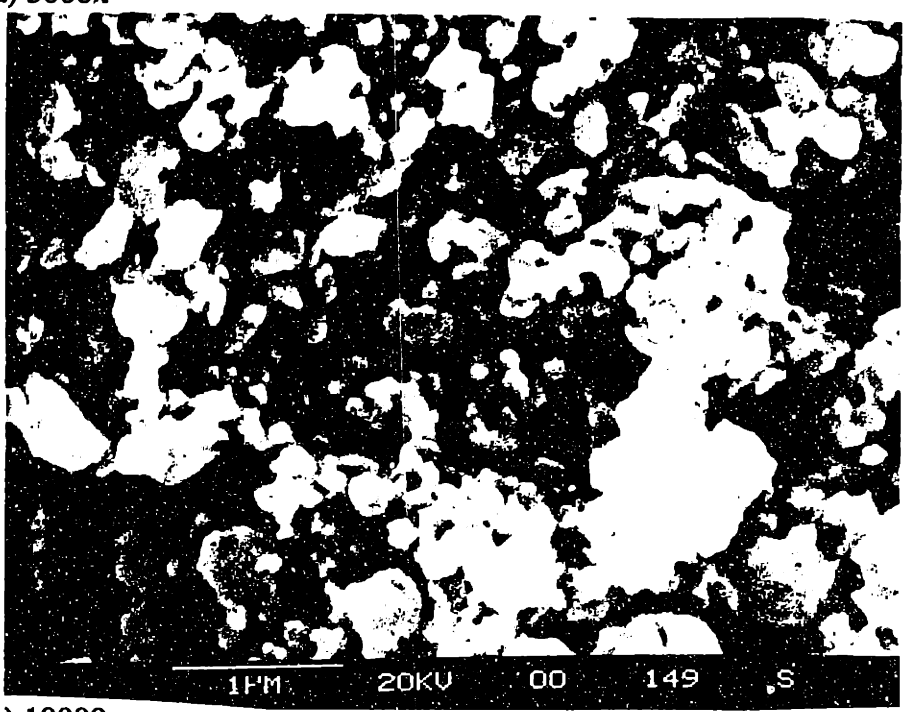

b) 10000x

Figure 4.15 SEM micrographs of ZnO (amorphous citrate technique, calcined at 720°C) a) 5000x and b) 10000x.

4.3.2 Conversion Profiles of Bulk Zn-Ti-O Sorbents

The sulfidation reactions of three sorbents, ZnO, Z2T-a, and Z2T3-a were studied in detail. Figure 4.16 shows the conversion profiles for these sorbents at 650°C. Conversion was defined as follows

$$X = (W_i - W)/(W_i - W_f^J) \qquad (4.9)$$

where W is the weight, W_i is the initial weight and W_f^J is the final weight at complete conversion assuming that the sorbent reacts completely to form ZnS and TiO_2 (for the Zn-Ti-O sorbents).

To gain complementary information, the data of Figure 4.16 are plotted in the form of the reaction rate as a function of conversion in Figure 4.17. The reaction rate decreases with conversion. The decreasing reaction rate is due both to formation of the product layer (ZnS + TiO_2) as well as to a decrease in the reaction surface area. The latter statement is generally true if the sorbents are not comprised of plate-shaped grains. In the case of ideal plate-shaped grains of infinite length, no change in the reaction surface area will occur until the sorbent is completely reacted. For Z2T3-a, the drop in the reaction rate is much more pronounced than for ZnO . As will be discussed in Chapter 5, this is due to non-uniformity in the grain size distribution and slower diffusion through the product layer of ZnS and TiO_2 than for just ZnS alone.

In Section 4.3.1, it was shown that the initial sulfidation rates of sorbents composed of $(Zn/Ti)_{atomic} \leq$ 3/1 were approximately the same. To determine whether this similarity in rates is due to reaction of similar intermediate phases, XRD analyses were performed on partially sulfided samples. The samples were sulfided in the TGA at 650°C in 2 mol% H_2S-1 mol% H_2- 97 mol% N_2. To provide sufficient amount of samples for analysis, 20-30 mg were used. This is a much larger quantity than what was used for

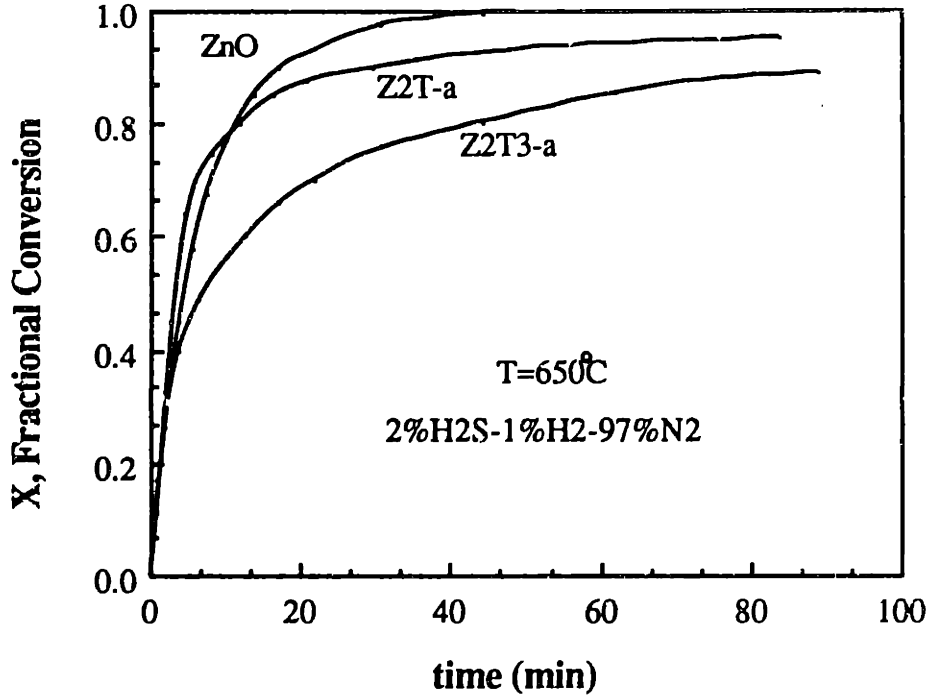

Figure 4.16 Comparative conversion profiles for sorbents ZnO, Z2T-a and Z2T3-a.

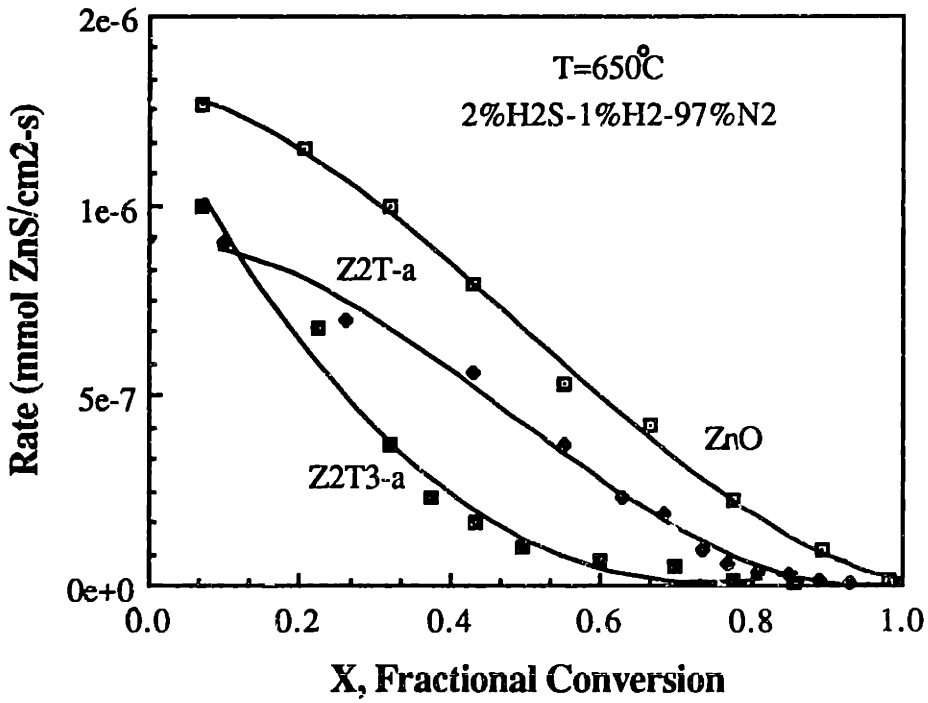

Figure 4.17 Comparative plots of reaction rates for sorbents ZnO, Z2T-a and Z2T3-a.

kinetic experiments (1-3 mg). The results of these analyses are shown in Table 4.6. Because Z2T3-a contained two zinc titanate phases (i.e. $ZnTiO_3$ and $Zn_2Ti_3O_8$), it was difficult to analyze the phase changes. After partial sulfidation, its XRD-analysis showed $ZnTiO_3$, $Zn_2Ti_3O_8$, ZnS, and TiO_2. It was unclear whether $Zn_2Ti_3O_8$ was being formed during sulfidation. Another sorbent with $(Zn/Ti)_{atomic}$ =2/3, designated Z2T3-b contained only a mixture of $ZnTiO_3$ and TiO_2. The X-ray diffractograms showing the transformation of ZnO to a fully sulfided sorbent and Z2T3-b to a partially sulfided (~35%) sorbent are shown in Figures 4.18 and 4.19. ZnO formed α-ZnS and β-ZnS upon sulfidation. $ZnTiO_3$ reacts directly with H_2S to form α-ZnS and rutile TiO_2 by:

$$ZnTiO_3 + H_2S \rightarrow ZnS + TiO_2 \qquad (4.10)$$

No intermediate zinc titanate phases were detected.

The sulfidation of Z2T-a is more complex. During sulfidation, $Zn_2Ti_3O_8$, α-ZnS and β-ZnS are formed. As shown in Figure 4.20, nearly overlapping XRD patterns (from Powder Diffraction Files) of Zn_2TiO_4 and $Zn_2Ti_3O_8$ make it difficult to determine the relative amounts of each compound. The reason for the similar XRD patterns is that both phases exist in a similar crystalline form. Zn_2TiO_4 exists as a cubic spinel while $Zn_2Ti_3O_8$ has a defect spinel structure. It is proposed that the abstraction of Zn from Zn_2TiO_4 to form ZnS produces the defect spinel phase. The reactions which occur for Zn_2TiO_4 are then:

$$Zn_2TiO_4 + 4/3\ H_2S = 1/3\ Zn_2Ti_3O_8 + 4/3\ ZnS + 4/3\ H_2O \qquad (4.11)$$

$$Zn_2Ti_3O_8 + 2\ H_2S = 2\ ZnS + 3\ TiO_2 + 2\ H_2O \qquad (4.12)$$

No significant amount of free TiO_2 was detected for the Z2T-a sample sulfided to 48%. This appears to indicate that $Zn_2Ti_3O_8$ reacts much slower than Zn_2TiO_4. If this was

Table 4.6 XRD Analyses of Sulfided Sorbents [1]

Sample	Crystalline Phases (wt %)						
	ZnO	Zn_2TiO_4	$Zn_2Ti_3O_8$	$ZnTiO_3$	α-ZnS	β-ZnS	TiO_2(anatase)
Z2T -a							
48% sulfided	0	23	35	0	16	26	negligible
95% sulfided	0	0	6	0	17	53	24
Z2T3-b							
35% sulfided	0	0	0	48	15	0	37
ZnO							
100% sulfided	0	0	0	0	33	67	0

[1] Sulfided at 650°C in 2% H_2S-1% H_2-97% N_2.

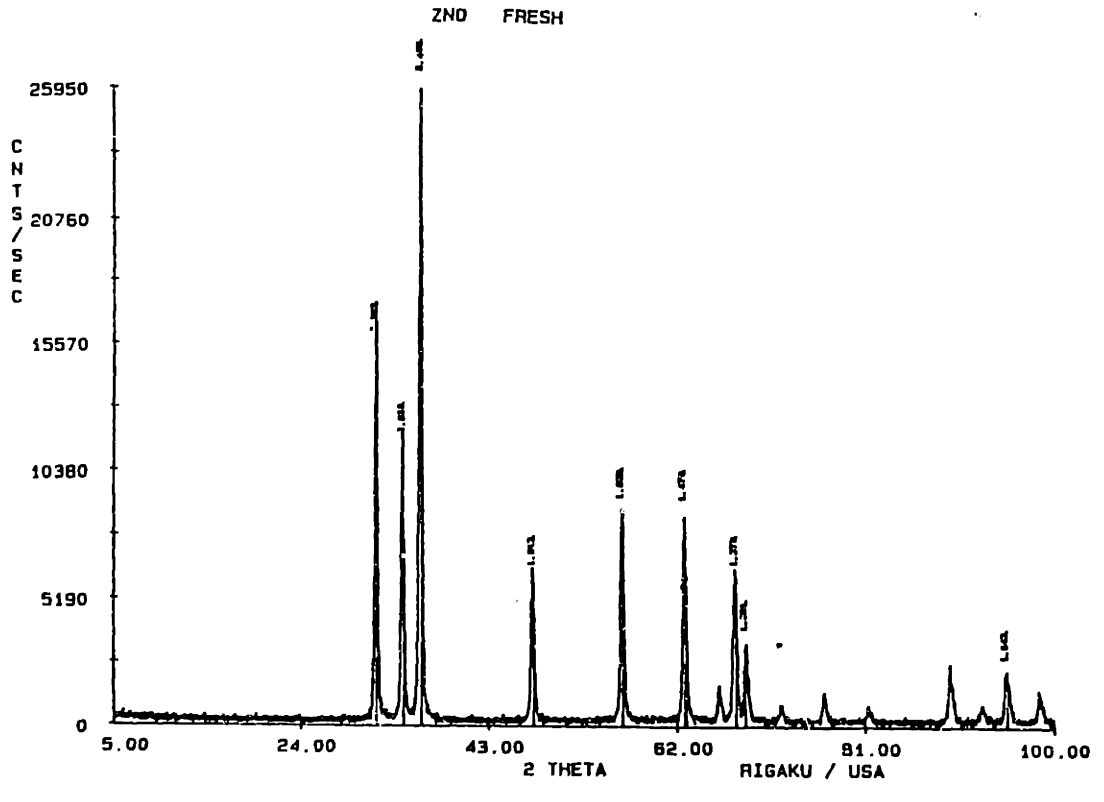

a)

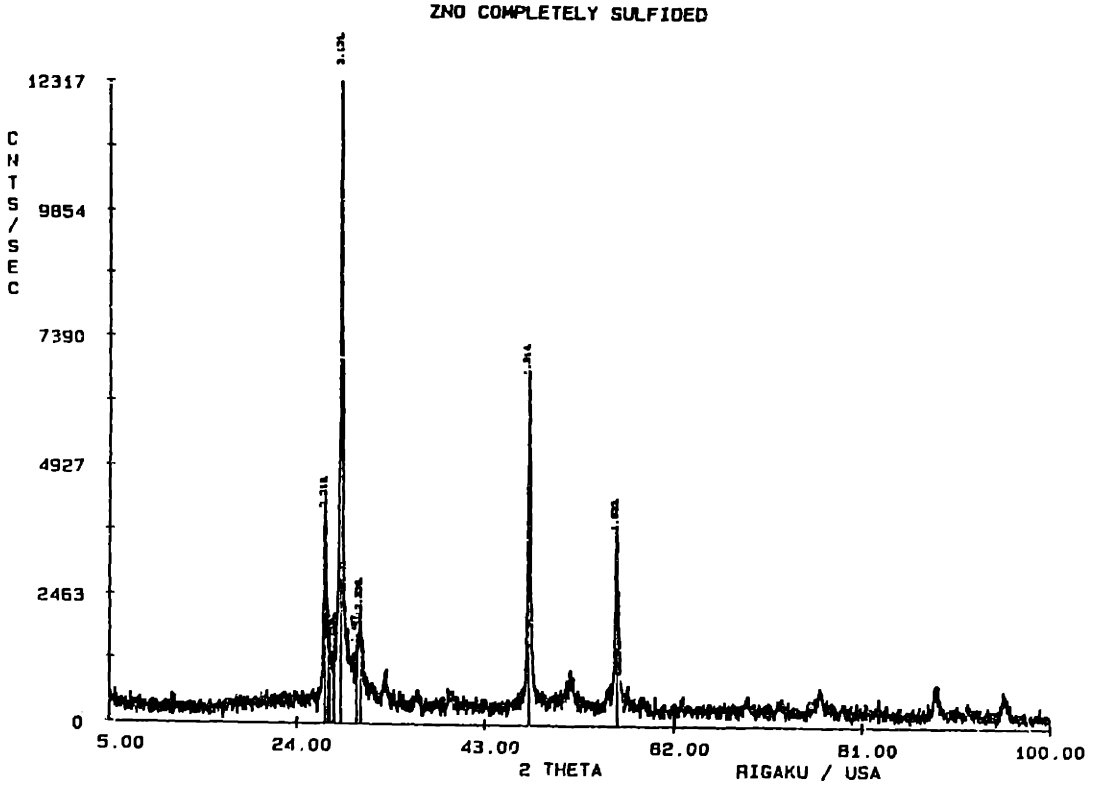

b)

Figure 4.18 X-ray diffractograms of a) unreacted ZnO calcined at 720°C and b) fully sulfided ZnO at 650°C in 2%H_2S-1%H_2-97%N_2.

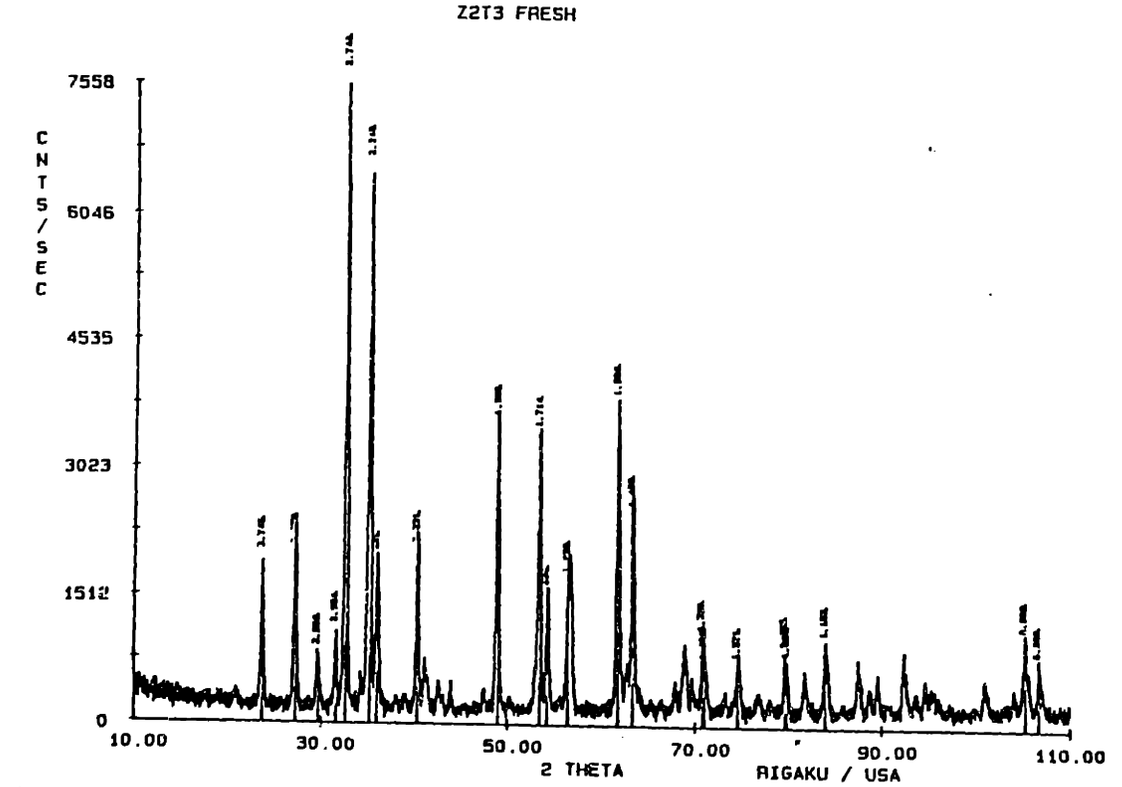

a)

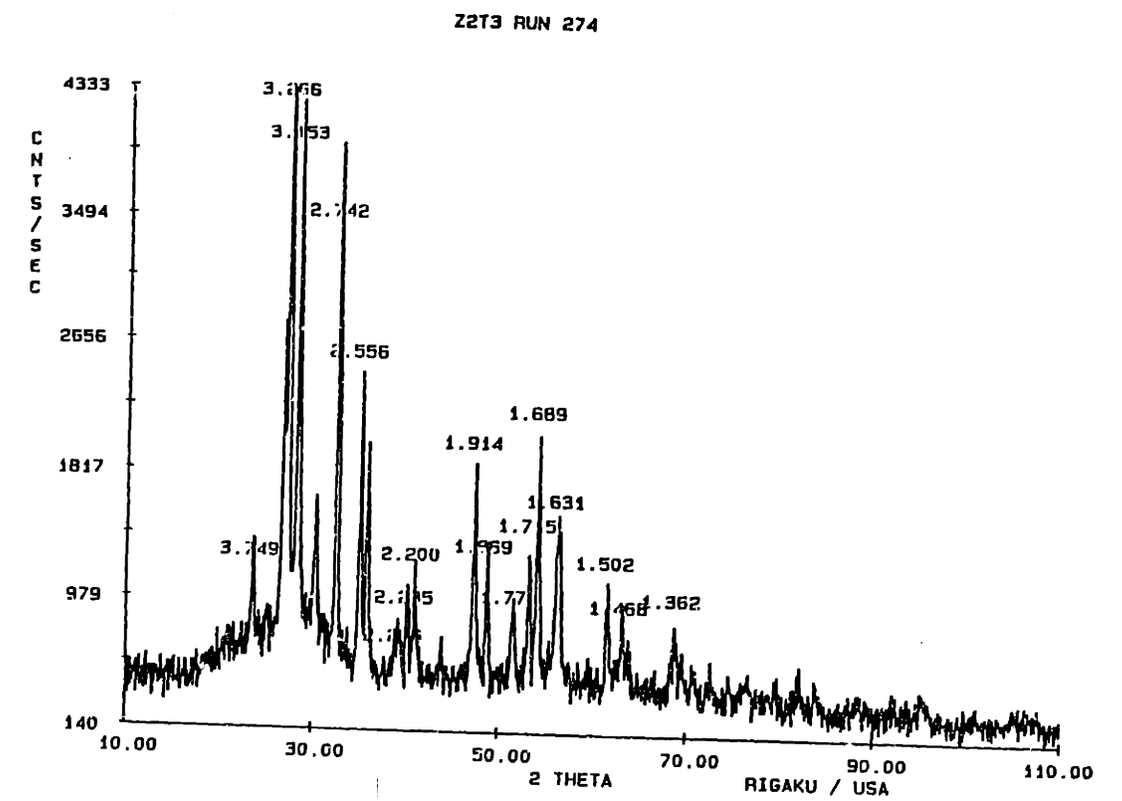

b)

Figure 4.19 X-ray diffractograms of a) unreacted Z2T3-b calcined at 720°C and b) 35% sulfided Z2T3-b at 650°C in 2%H_2S-1%H_2-97%N_2.

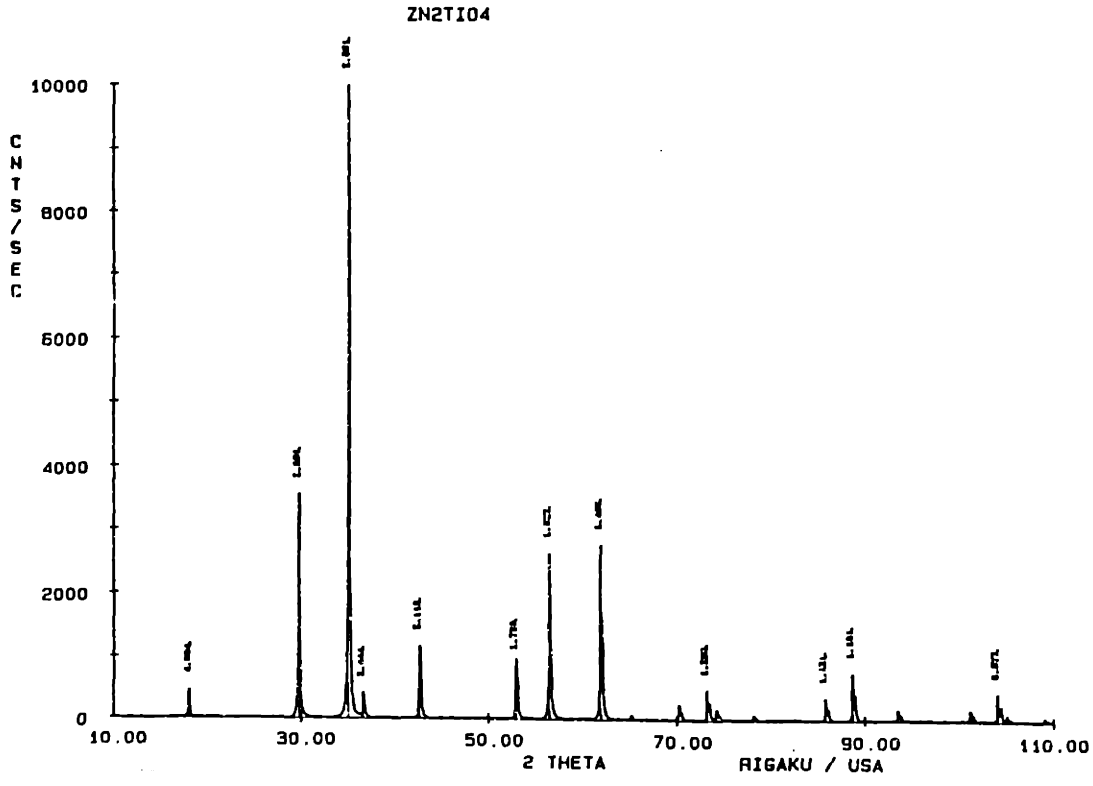

a)

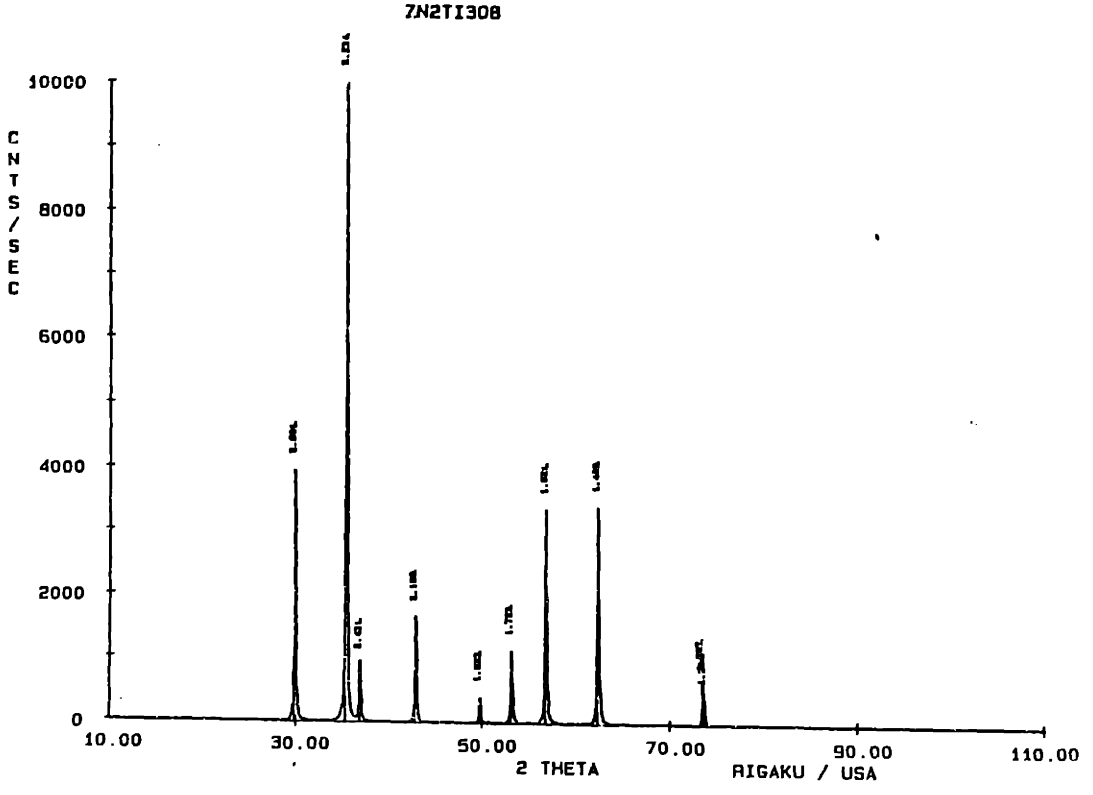

b)

Figure 4.20 X-ray diffractograms of a) Zn_2TiO_4 and b) $Zn_2Ti_3O_8$ from Powder Diffraction Files.

true, a noticeable drop in the reaction rate would be observed at 66% conversion (complete conversion to $Zn_2Ti_3O_8$ and ZnS based on stochimetry). To determine the validity of this argument, experiments were performed with a different sample, Z2T-b. Z2T-b consists of 100% Zn_2TiO_4, similar to Z2T-a. However, it was prepared with a more uniform grain structure (by doubling the citric acid/metal ratio in the precursor solution). Figure 4.21 shows the difference in grain structure of Z2T-a and Z2T-b. Z2T-a has very non-uniform grain size distribution. Both small grains (radius, r=0.05 μm) and much larger grains (r~0.1-0.2 μm) are present. The size of the large grains in Z2T-a were difficult to estimate from the SEM micrographs (Figure 4.21a). They appear to be large plates whose thickness are hard to estimate. Z2T-b, on the other hand, has more uniform grains of approximately 0.02 μm radius. Also on Z2T-a, the formation of a "skin" of relatively low porosity was observed (discussed in Chapter 2). Crushing the sorbent to smaller particle sizes exposed the more porous interior. This "skin" had lower reactivity than the interior. Figure 4.22 shows an SEM micrograph of Z2T-a ~90% sulfided with 2 mol% H_2S-1 mol% H_2-97 mol% N_2 at 650°C. Part of the surface "skin" had been removed (perhaps, by crushing the sorbent) prior to sulfidation. EDS analyses of the ~90% sulfided sorbent of Figure 4.22 found that the exposed interior was more sulfided (S/Zn=1.0, Zn/Ti=2.3) than the "skin" (S/Zn=0.7, Zn/Ti=2.4). Thus, a combination of the "skin" effect and variation in particle sizes can explain changes in the reaction rate of Z2T-a. Z2T-b was chosen because it would be easier to determine whether changes in the reaction rate were due to changes in its chemical phases and not its physical structure. As shown in the conversion profile for Z2T-b in Figure 4.23, the slope of the curve remained constant up to approximately 90% conversion. Thus, $Zn_2Ti_3O_8$ has approximately the same sulfidation rate as Zn_2TiO_4. This agrees with the initial rate measurements performed with sorbents

a)

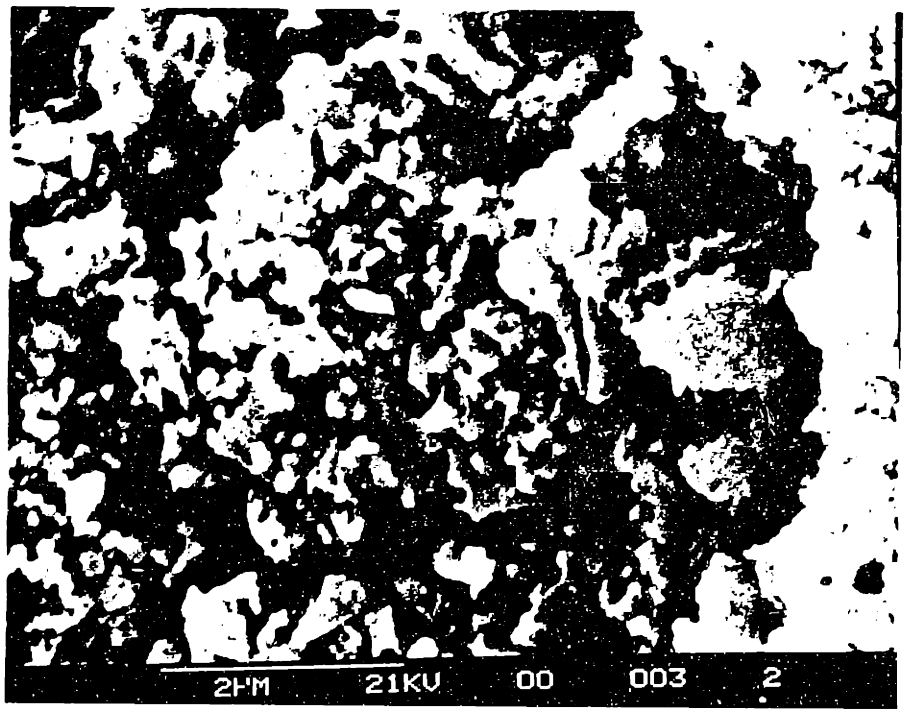

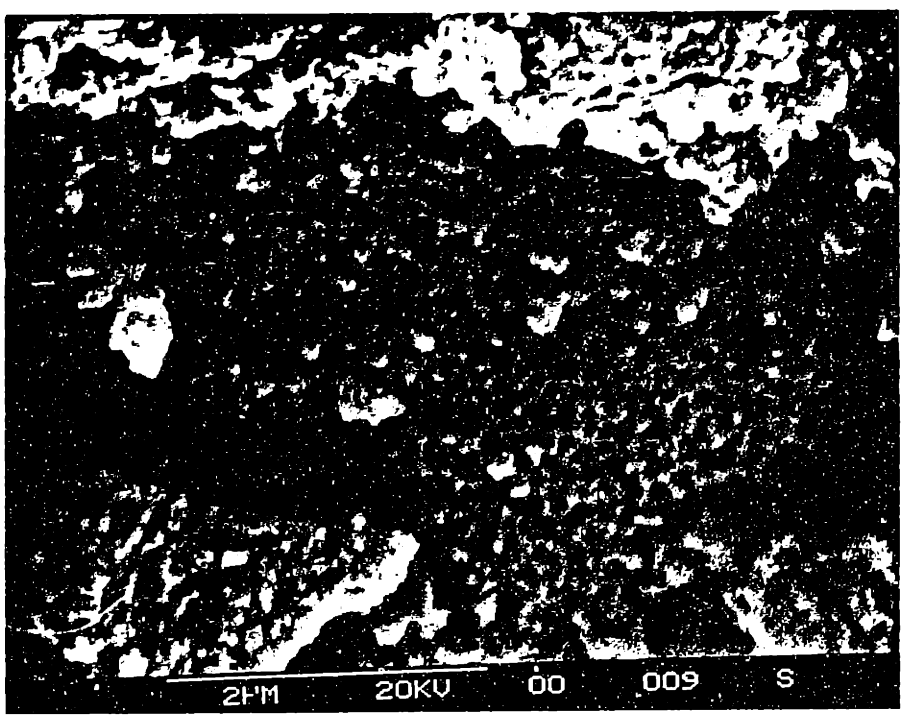

b)

Figure 4.21 SEM micrographs of unreacted (calcined at 720°C) a) Z2T-a and b) Z2T-b.

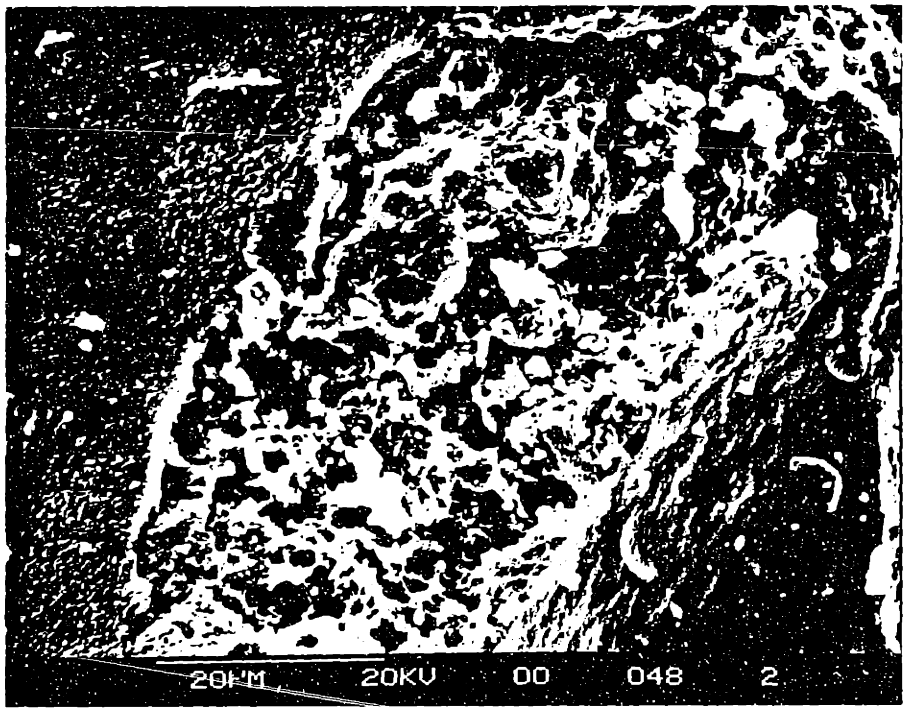

Figure 4.22 SEM micrograph of 90% sulfided Z2T-a at 650^0C in 2% H_2S-1% H_2-97% N_2. (Interior: S/Zn=1.0 and "Skin": S/Zn=0.7)

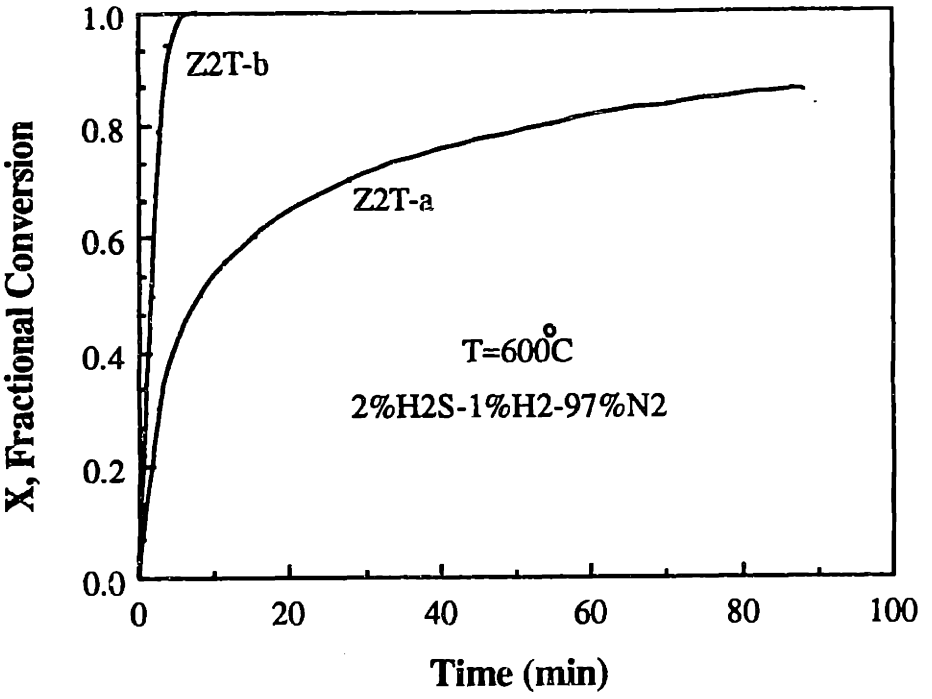

Figure 4.23 Sulfidation conversion profiles for Z2T-a and Z2T-b.

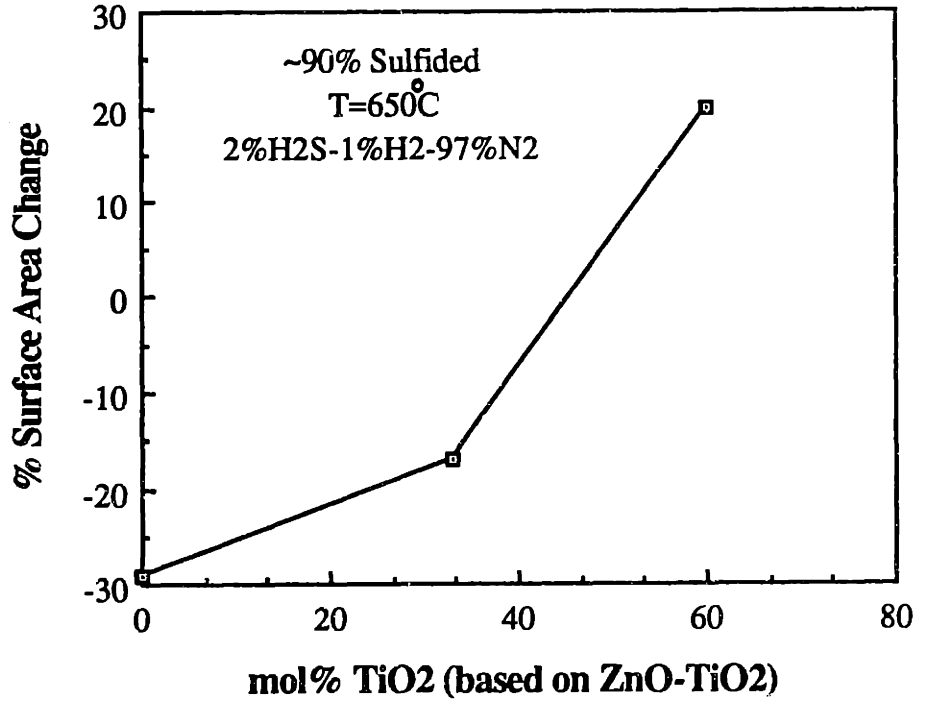

Figure 4.24 Surface area change (based on initial surface area) of sorbents after 90% sulfidation.

containing different chemical phases. Sorbent ZT which contained 55 wt% $Zn_2Ti_3O_8$ and 45 wt% $ZnTiO_3$ did not have significantly different initial sulfidation rate than sorbent Z2T-b (100 wt% Zn_2TiO_4) The reason that no significant amount of free TiO_2 was detected is that any free TiO_2 reacts rapidly with Zn_2TiO_4 to form $Zn_2Ti_3O_8$ according to the reaction

$$Zn_2TiO_4 + 2TiO_2 = Zn_2Ti_3O_8 \qquad (4.13)$$

4.3.3 Physical Changes of Sorbents During Sulfidation

This section examines the structural effects of sulfidation. Surface area changes along with morphological changes were examined. The samples were sulfided in the TGA at 650°C with 2 mol% H_2S-1 mol% H_2- 97 mol% N_2. Again to obtain sufficient quantity of samples for accurate measurements of the surface area, a large amount (40-60 mg) of sample was used. The samples were sulfided to approximately 90% conversion, and the surface areas were measured. Figure 4.24 shows the changes in surface area due to sulfidation. Lower surface area (29% lower than the initial area) was measured for ZnO after sulfidation. This can be attributed to a combination of sintering and grain overlapping in the product layer. If no sintering occurred and the sorbent was composed of non-interacting isolated grains (i.e. with non-overlapping product layers of different grains), the surface area should increase by 16%. However, if overlapping of the product layer is allowed, this would contribute to the observed surface area decrease. The Tamman temperature of ZnO is 849°C while that of α-ZnS is 713°C. Thus, α-ZnS sinters at a lower temperature than ZnO. The surface area of Zn-Ti-O sorbents after sulfidation does not decrease as much as for ZnO. As the amount of TiO_2 increases from 0 mol% to 60 mol%, sintering decreases concomitantly. Z2T3 (60 mol% TiO_2) after 90% sulfidation had a 20% higher surface area. However, Figure

4.24 is somewhat deceptive. When sulfidation of higher surface area-materials was performed, the percentage loss in surface area after sulfidation (~90% sulfided, 90 min) was approximately the same with ZnO and a Zn-Ti-O sorbent. For example, Z2T-b with an initial surface area of 13.9 m^2/g saw a 40% (8.4 m^2/g) drop in its surface area after sulfidation at 650°C. Correspondingly, a higher surface area ZnO (5.2 m^2/g) had a 38% (3.2 m^2/g) drop in its surface area after sulfidation. Similarly, sorbent Z3T with an initial surface area of 7.6 m^2/g decreased by 44% to 4.2 m^2/g after sulfidation. Thus, the sintering rate is approximately the same. From surface area measurements of sulfided sorbents with initially low surface area, the conclusion is drawn that although the sintering rate is similar, the equlibrium surface area of the final product tends to be higher with the presence of TiO_2. This is shown in Figure 4.25. Higher surface area is attained with TiO_2 present. The initial values of the surface area of the sorbents shown in Figure 4.25 are listed in Table 4.7. Finally, the greater increase in surface area of Zn-Ti-O sorbents after sulfidation is not due to the formation of free TiO_2 with a higher surface area. When TiO_2 was calcined at the same temperature and for the same length of time as ZnO, the surface area of ZnO was 1.3 times higher than TiO_2.

Although sulfidation of several sorbents, such as Z3T, was accompanied by a loss in surface area, after regeneration the surface area recovered and exceeded it original value. Using sorbent Z3T, sulfidation was performed in 2 mol% H_2S-1 mol% H_2-97 mol% N_2 at 650°C. A gas mixture containing 21 mol% O_2-79 mol% N_2 was used to regenerate the sorbent, also at 650°C. Three cycles of sulfidation-regeneration were performed. As shown in Figure 4.26, after the first cycle, the surface area of Z3T increased from 7.6 m^2/g to 12.0 m^2/g. After the succeeding cycles, the surface area decreased slightly. In comparison, the increase in surface area of ZnO (initial surface

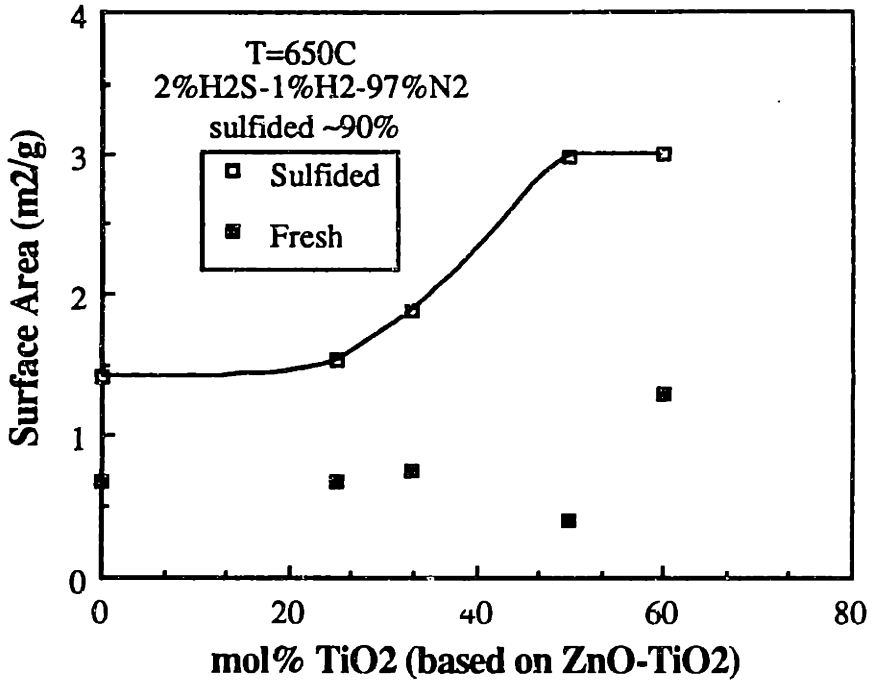

Figure 4.25 Surface area of sorbents before and after sulfidation.

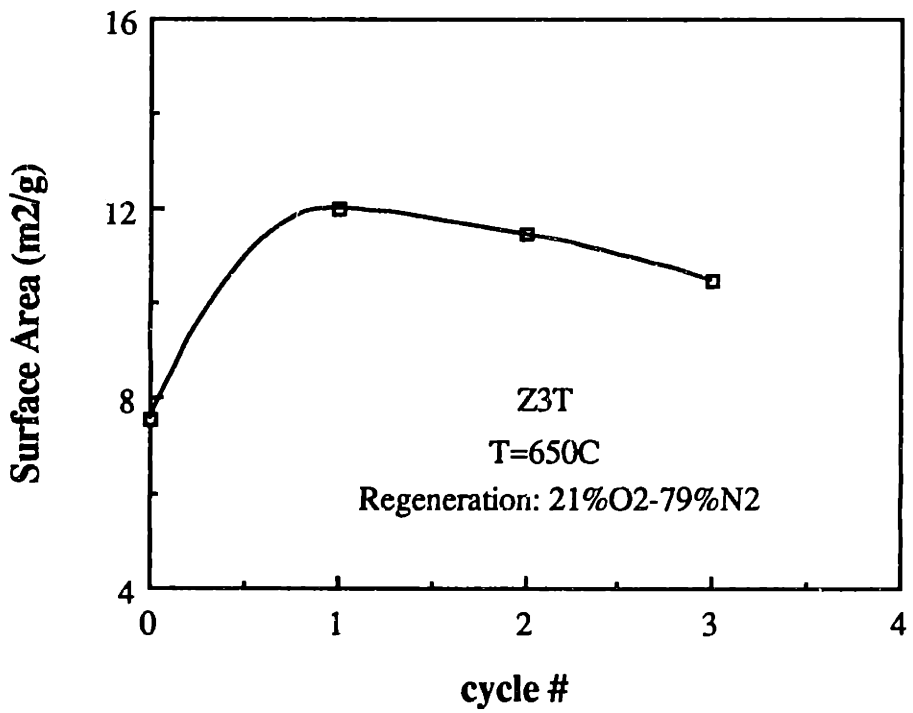

Figure 4.26 Surface area of sorbent Z3T after successive sulfidation/regeneration. cycles.

Table 4.7 Initial surface areas of the sorbents shown in Figure 4.25 [1]

Zn/Ti	mol% TiO_2	Surface Area, (m^2/g)
ZnO	0	0.68
3/1	25	0.68
2/1	33	0.76
1/1	50	0.40
2/3 (Z2T3-b)	60	1.30

[1] Surface area was decreased by heating all solid (calcined at 720°C, 12 h) except for Z2T3-b at 1000°C for 1 h. No further heat treatment of solid Z2T3-b except for the calcination at 720°C for 12 h was performed.

area 2.4 m^2/g) was greater (13.1 m^2/g) after regeneration in one cycle. This increase in surface area for the regenerated ZnO is in agreement with previous observations (Flytzani-Stephanopoulos et al., 1987).

Scanning electron micrographs of unreacted (2.4 m^2/g) and sulfided ZnO are shown in Figure 4.27. The assumption of isolated grains is incorrect, as can be seen in Figure 4.27a by the presence of overlapping grains of approximately 0.08-0.1 μm radius. After ~90% sulfidation, large agglomerates due to the overlapping of the product layer are present (Figure 4.27b). The sizes of these agglomerates are in the range ~0.5-1 μm radius. As shown in Figure 4.28, these agglomerates are composed of closely packed grains (0.05-0.1 μm radius). Surface area measurements were also performed on ZnO sulfided at 400°C to determine whether the observed decrease in surface area is due to sintering or overlapping of the product layer. At this low temperature (400°C), sintering is neglible. The measured surface area for ZnO 50% sulfided is 2.4 m^2/g. Comparatively, at 650°C, the surface area for ZnO 50% sulfided is 2.0 m^2/g. At 650°C, some sintering takes place.

The SEM photographs of unreacted (2.3 m^2/g) and 90-95% sulfided Z2T3-a are shown in Figure 4.29a and 4.29b, respectively. The unreacted Z2T3-a is composed of small grains (~0.09 μm radius). Larger agglomerates (~0.4-0.6 μm radius) where individual grains are together are also present. EDS elemental analysis of the surface in Figure 4.29a estimates a ratio of $(Zn/Ti)_{atomic} = 0.77$. This is more enriched in zinc than expected (Zn/Ti=0.67 from stochiometry). After sulfidation, as shown in Figure 4.29b, much larger agglomerates are present on the surface. Higher TiO_2 content plays a role in preventing sintering of the ZnS phase and, thus, keeping agglomerates from forming and growing. In Figure 4.29b, the small isolated grains on the left and right

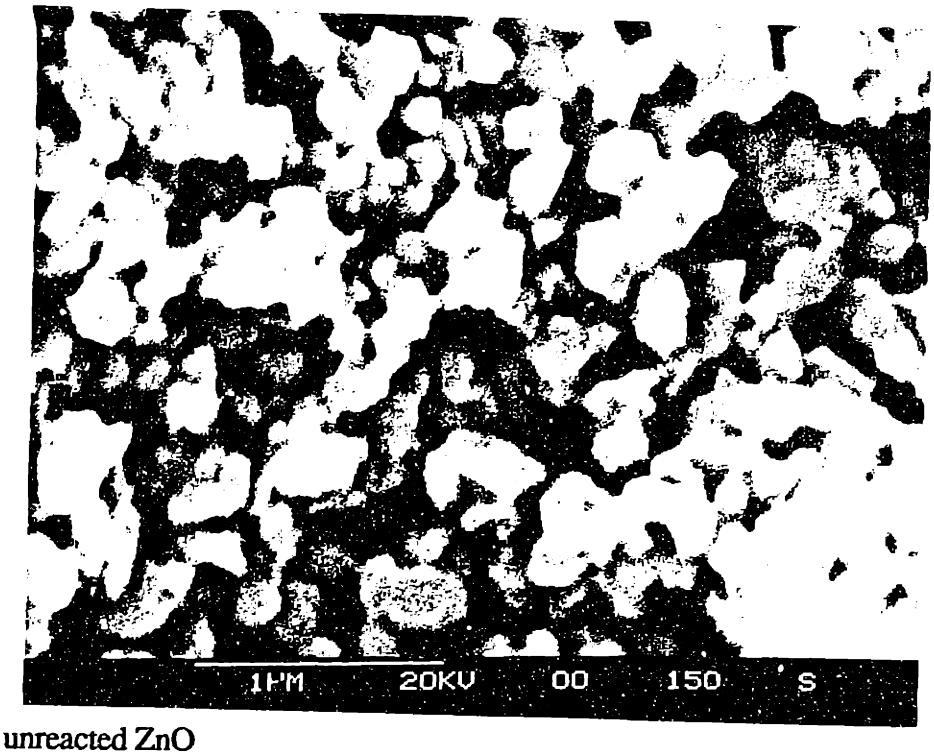

a) unreacted ZnO

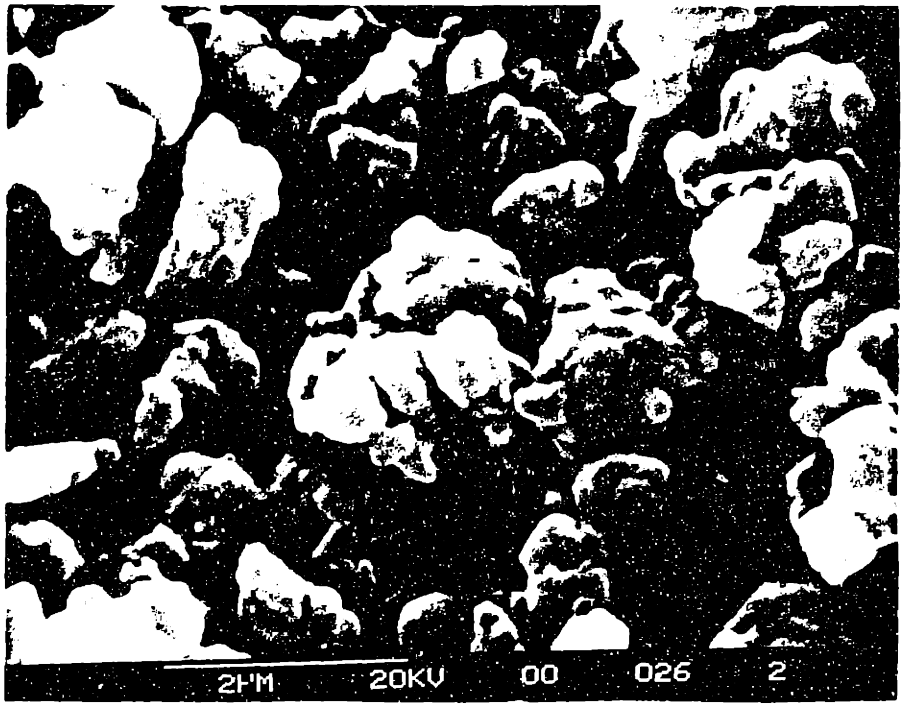

b) 54% sulfided ZnO

Figure 4.27 SEM micrographs of a) unreacted ZnO (calcined at 720°C) and b) 54% sulfided ZnO at 650°C in 2% H_2S-1% H_2-97% N_2.

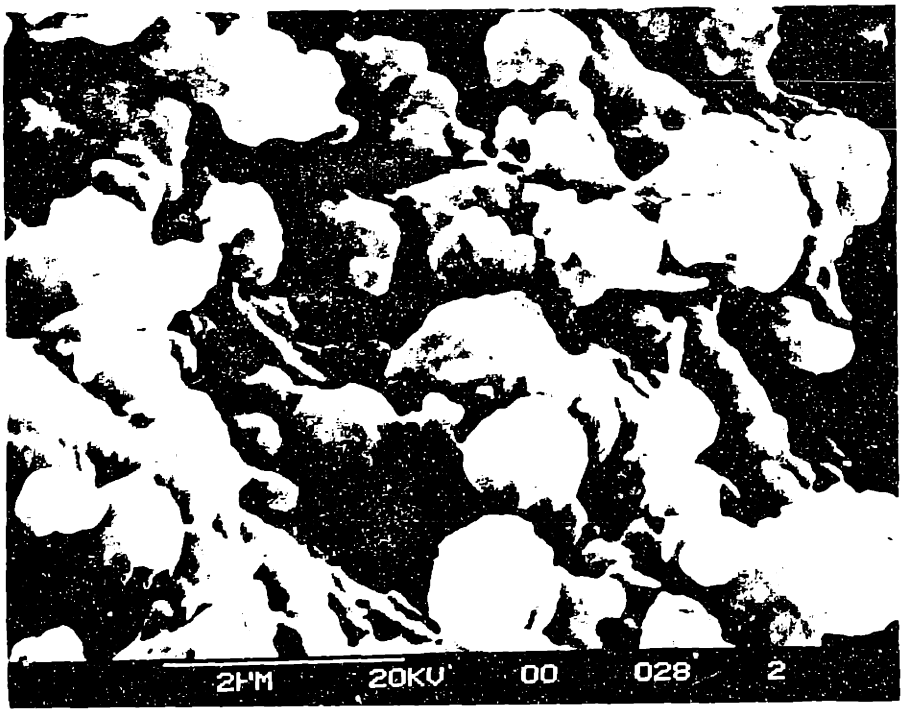

a) 15000x

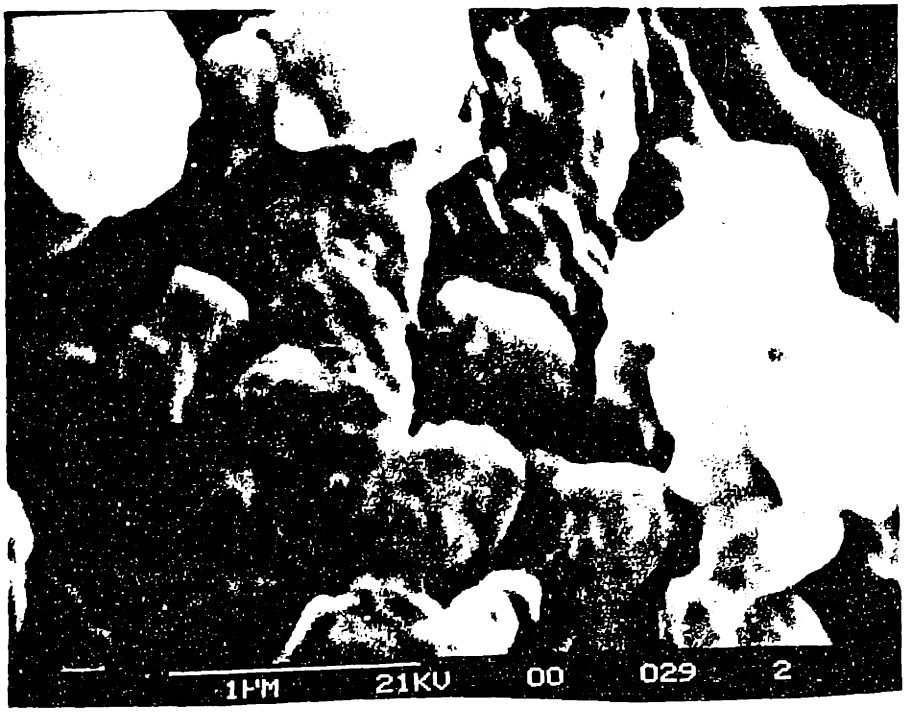

b) 30000x

Figure 4.28 SEM micrographs of 75% sulfided ZnO a) 15000x and b) 30000x.

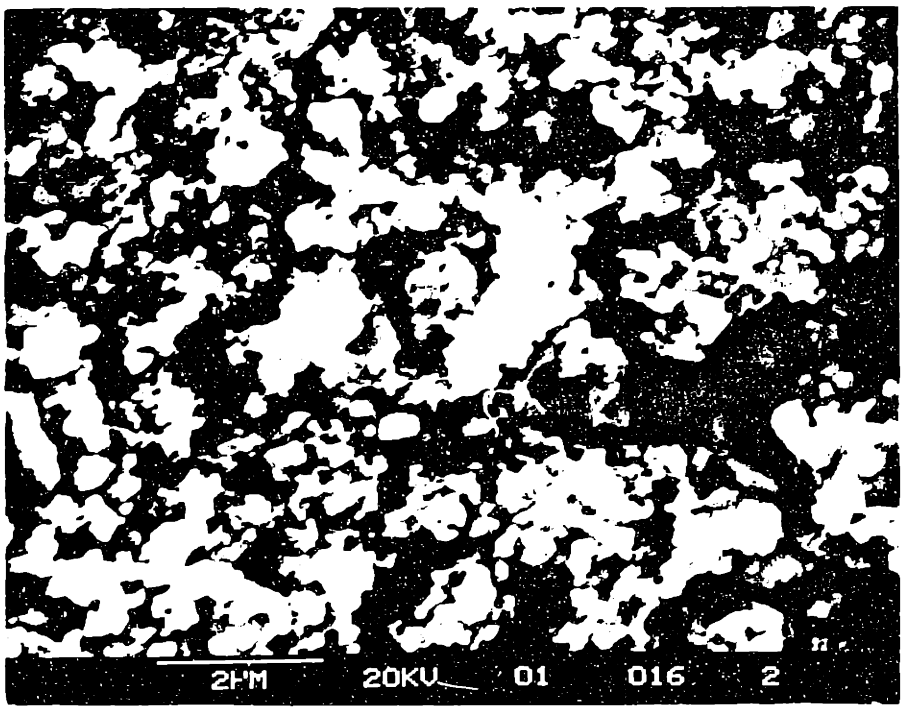

a) 5000x

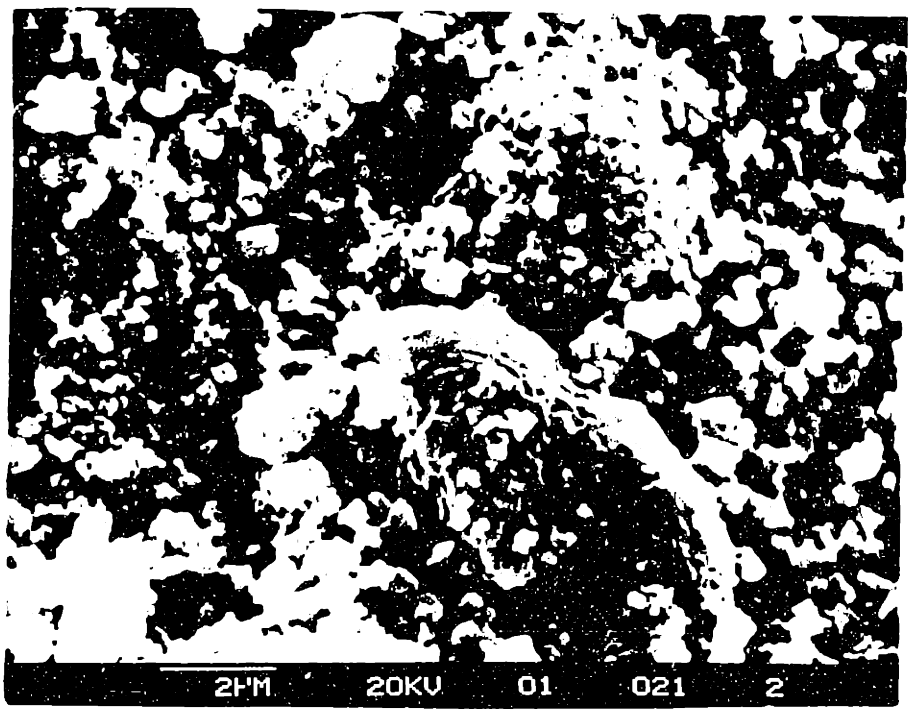

b) 10000x

Figure 4.29 SEM micrographs of a) unreacted Z2T3-a (calcined at 720°C) and b) ~90-95% sulfided Z2T3 at 650°C in 2% H_2S-1% H_2-97% N_2.

side of the micrograph are composed mainly of TiO_2 (Zn/Ti=9x10-2 and S/Zn=0.94). The two large agglomerates in the middle of the photograph are shown in Figure 4.30a and 4.30b at higher magnification. Figure 4.30a shows the agglomerate in the upper portion of Figure 4.29b, while Figure 4.30b shows the one in the lower portion of that photograph. In Figure 4.30a, the agglomerate is made up of flat grains (0.08-0.14 μm radius). The composition of this agglomerate is $(Zn/Ti)_{atomic} = 0.32$ and $(S/Zn)_{atomic} = 1.0$. In Figure 4.30b, the agglomerate appears more sintered. The individual grains are fused to one another. This agglomerate contains much less titanium than the previous one. Its composition is $(Zn/Ti)_{atomic} = 1.8$ and $(S/Zn)_{atomic} = 1.0$. From these photographs, it is evident that ZnS tends to sinter while TiO_2 can inhibit this sintering by, acting as a physical barrier to prevent coalescence of ZnS.

4.3.4 Effect of H_2

Comparative plots of the initial reduction rate (shown in Chapter 3) and the initial sulfidation rate are depicted in Figure 4.31. The reduction rate is shown for a gas containing 2 mol% H_2-98 mol% N_2 at 700°C. The reduction rate was calculated from the kinetic constants obtained in Chapter 3. The sulfidation rate is shown for a gas containing 2 mol% H_2S-1 mol% H_2-97 mol% N_2 at 700°C. As will be discussed later in this section, eliminating the 1 mol% H_2 from the reactant gas caused no significant change in the initial sulfidation rate. For single ZnO, the reduction rate is approximately 1.3 times higher than the sulfidation rate. However, for Zn-Ti-O sorbents reduction will occur at a much slower rate (about tenfold slower) than sulfidation.

Various concentrations of H_2 were added to the reactant gas to determine what effects hydrogen has on sorbent sulfidation. The effect of H_2 on the initial rate was first examined. Arrhenius plots for ZnO and Z2T-a sulfidation for various H_2 concentrations

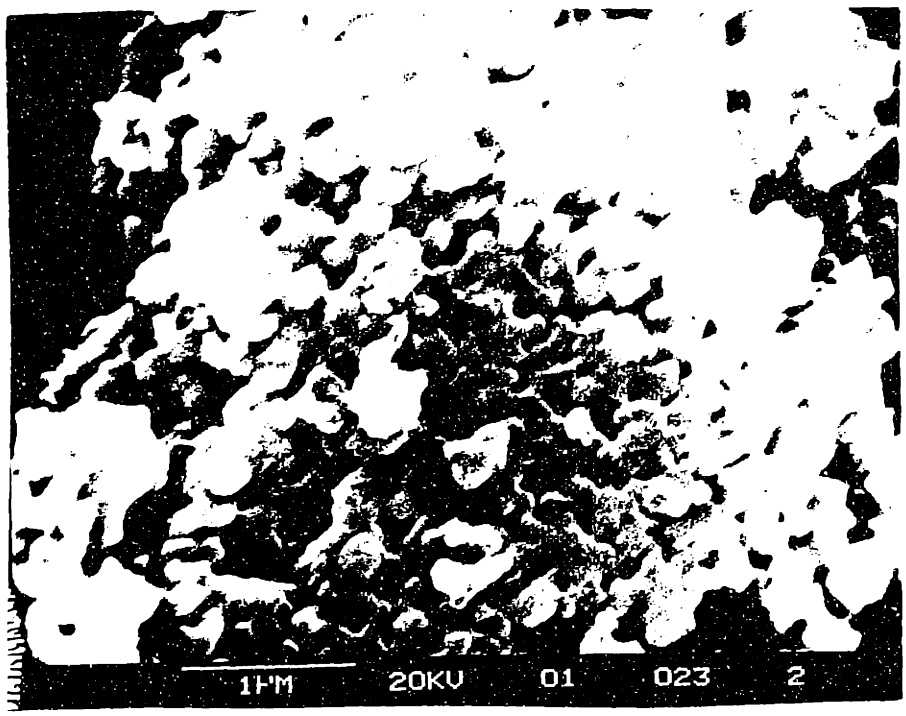

a) 5000x

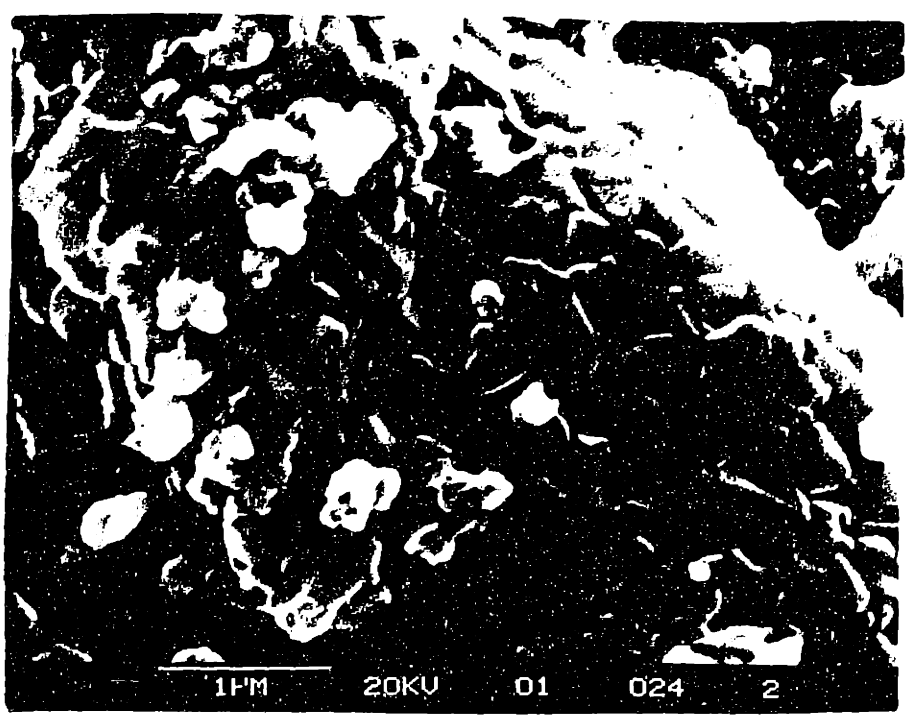

b) 10000x

Figure 4.30 SEM micrographs at higher magnification of large agglomerates observed in Figure 4.29b a) agglomerate in upper portion and b) agglomerate in lower portion of Figure 4.29b.

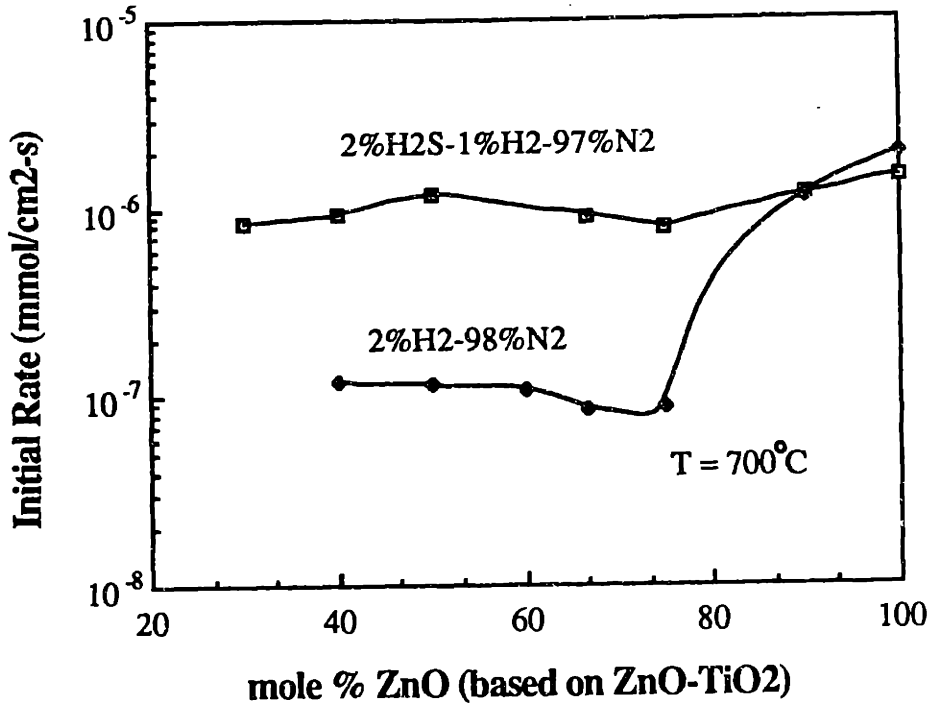

Figure 4.31 Comparative plots of the initial reduction and sulfidation rates.

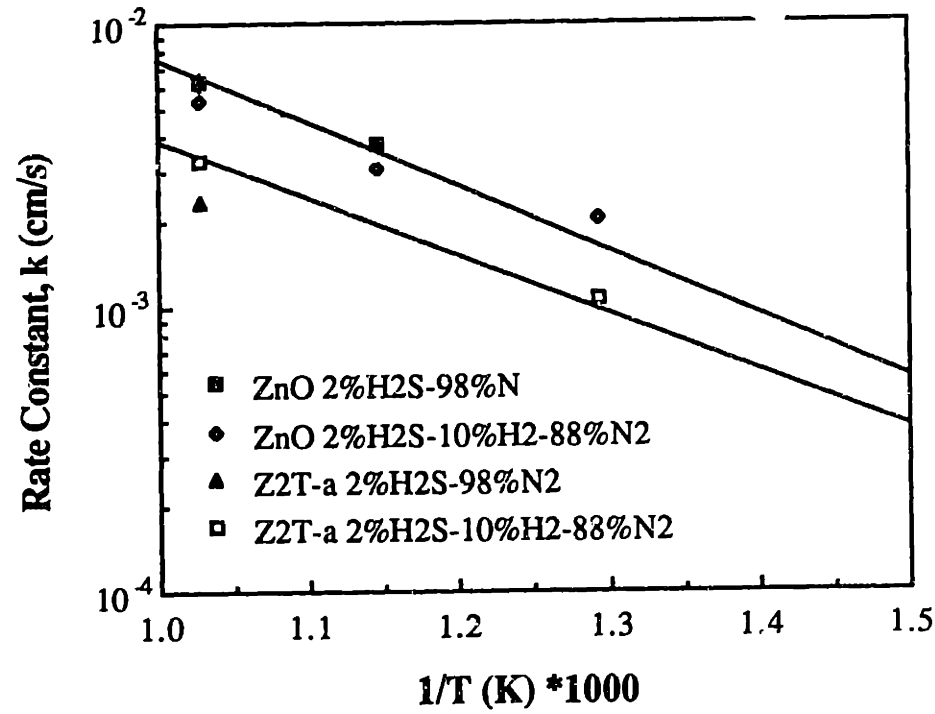

Figure 4.32 Arrhenius plots of ZnO and Z2T-a sulfidation for various hydrogen concentrations. (— 2%H2S-1%H2-97%N2)

(0, 1, and 10 mol%) are shown in Figure 4.32. No discernible difference was observed. The conversion profiles of sorbents ZnO, Z2T-a, and Z2T3-a were then examined to see if any noticeable effect of H_2 can be observed after the initial period of sulfidation. These results are displayed in Figure 4.33. Again very little difference is observed when the hydrogen concentration is changed from 1 mol% to 10 mol% at temperatures $\leq$ 700°C.

However, in the presence of hydrogen and temperatures greater than 600°C, a small jump (~5% conversion) in the conversion profile was occasionally observed for both ZnO and Zn-Ti oxides. An example for Z2T-a is shown in Figure 4.34. The following explanation is proposed for this behavior. At high sulfidation temperatures and in the presence of hydrogen, reduction takes place and zinc vapor diffuses out of the particle. As the solid sulfidation product layer is formed zinc vapor will accumulate in the particle until the pressure is sufficient to cause the product layer to crack. At that point, reaction will occur rapidly and the jump in conversion profile will be observed. The reason why this was not observed in all experiments performed under similar conditions is probably because the physical properties of the sorbents were not completely uniform. As discussed in Chapter 2, during the sorbent preparation, especially during drying, the heating process may produce a surface "skin" such that pores at the surface are smaller than those in the interior. This effect is reduced by crushing the material to a small size. However, there are some non-uniformities among different particles. Some particles may have a greater proportion of the "skin" than others. For these particles, it would be more likely to observe the jump in conversion profile. In such a case, zinc vapor diffusing out of the particle will react with H_2S to form solid product (ZnS) deposits, which effectively block the pores. Zinc vapor building up in the particle causes cracks to form. It was difficult to determine the

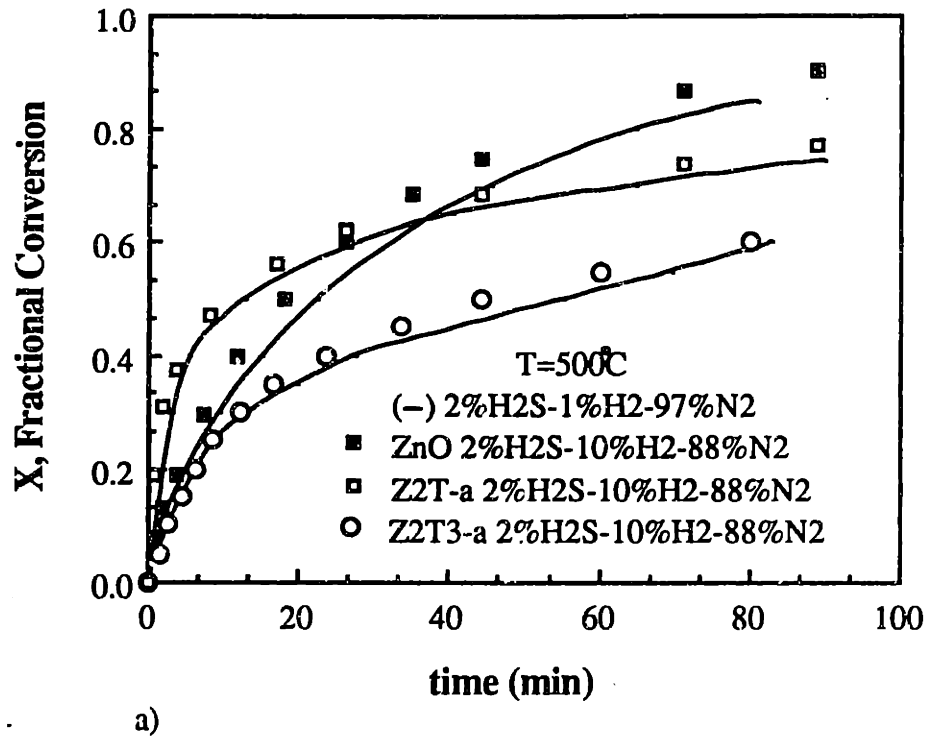

a)

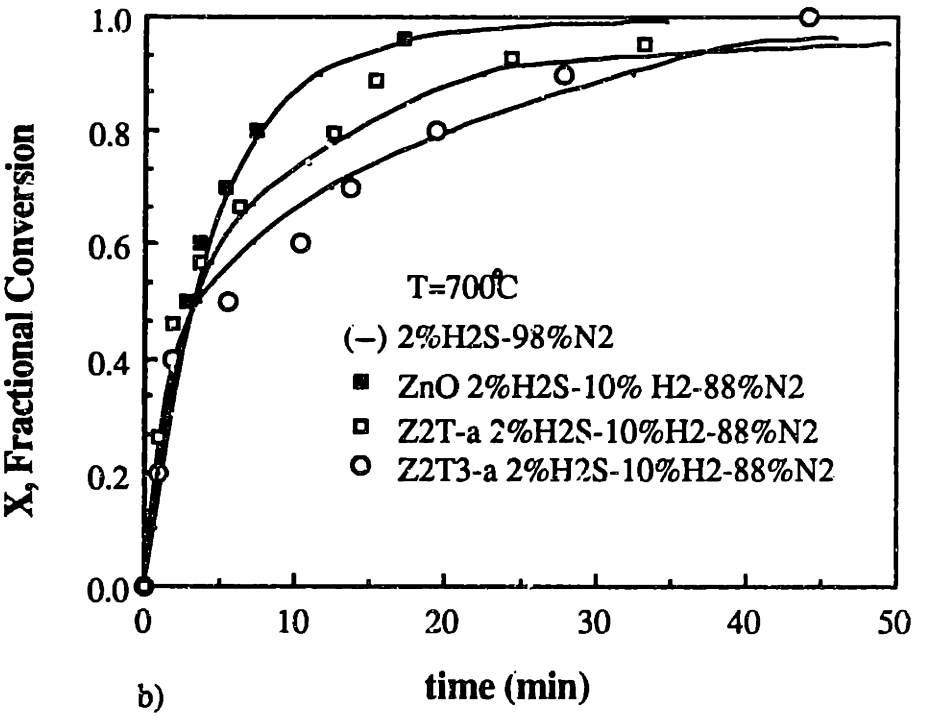

b)

Figure 4.33 Conversion profiles with various hydrogen concentrations at a) 500°C and b) 700°C.

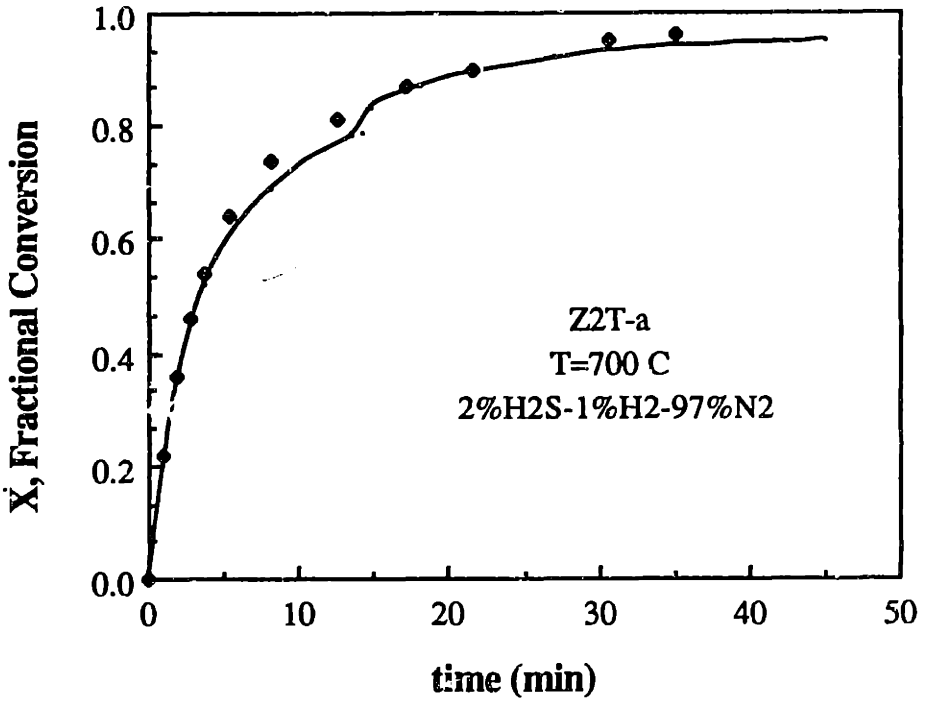

Figure 4.34 Conversion profiles for Z2T-a sulfidation. Two experimental profiles are shown, one represented by the (—) and the other by the points.

validity of this explanation when the sulfided sorbents were examined with a scanning electron microscope because this effect (i.e. the jump) is relatively small. Thus, it was hard to visually confirm the presence of cracks after the conversion jump. However, recent data from sulfidation of $ZnO-Fe_2O_3$ pellets have confirmed the generation of cracks and zinc migration (Flytzani-Stephanopoulos and Shao, 1988).

Except for the small conversion jump described in the preceeding paragraph, no significant difference in sulfidation was observed with 0% H_2 and with 10% H_2 at various temperatures as shown in Figure 4.33. This appears to contradict the results shown in Figure 4.31. The reduction rate of ZnO (with H_2 and N_2) is comparable to its sulfidation rate. Thus, significant zinc loss should have occurred during sulfidation in 2 mol% H_2S-10 mol% H_2-88 mol% N_2 at 700°C. However, the reason no zinc loss (within 5%) was observed is because zinc diffusing out will react with H_2S to form ZnS. A faint white film was observed on the quartz pan. Analysis of the film by atomic absorption spectroscopy identified the presence of zinc. The formation of the film is likely due to reaction of (escaped) Zn(g) formed by reduction of the sorbent and H_2S. Figure 4.35a shows the small, rounded crystals formed as a result of the reaction of H_2S with Zn vapor leaving the sorbent Z2T-a from a crater-like hole on the surface. Figure 4.35b shows the same sorbent after 10% reduction.in 10 mol% H_2-90 mol% N_2 Holes are present on the surface where Zn vapor had escaped. Consequently, desulfulfurization in a reducing atmosphere with ZnO can proceed by two routes operating in parallel. First, there is the direct sulfidation of solid ZnO by

$$ZnO(s) + H_2S(g) \rightarrow ZnS(s) + H_2O(g) \qquad (4.14)$$

Secondly, there is the gas phase sulfidation of zinc vapor produced by reduction of ZnO

$$ZnO(s) + H_2(g) \rightarrow Zn(g) + H_2O(g) \qquad (4.15)$$

a)

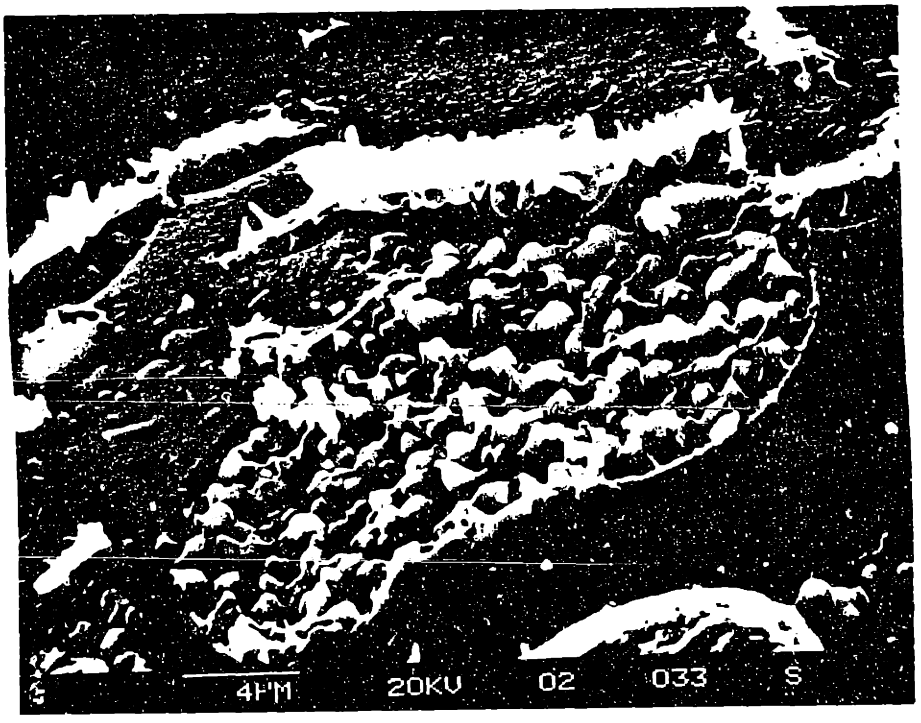

b)

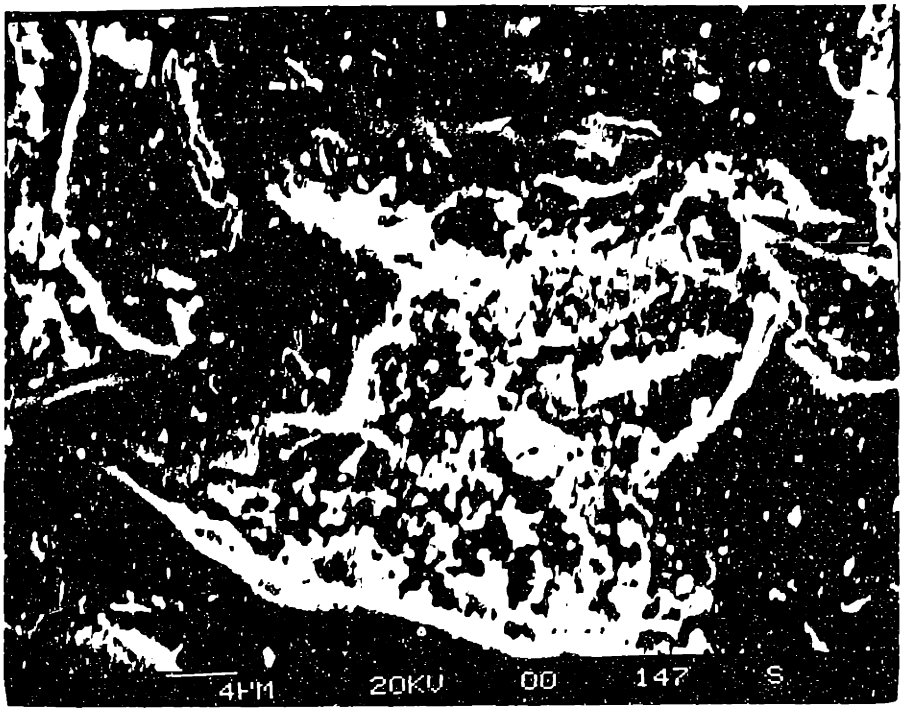

Figure 4.35 SEM micrographs of sorbent Z2T-a showing a) crystals formed by the gas-phase Zn-H_2S reaction at 700°C in 2%H_2S-10%H_2-88%N_2 and b) surface after 10% reduction at 700°C in 10%H_2-90%N_2.

$$Zn(g) + H_2S(g) \rightarrow ZnS(s) + H_2(g) \quad (4.16)$$

Although there was no significant difference in the sulfidation profiles with varying concentration of H_2, the surface morphology of the reacted sorbents was different. Figures 4.36 and 4.37 show ZnO and Z2T-a, respectively, sulfided in 2 mol% H_2S-98 mol% N_2 and in 2 mol% H_2S-10 mol% H_2-88 mol% N_2 at 650°C. For ZnO (Figure 4.36), no noticeable difference is evident between sulfidation in the absence of H_2 and in its presence. For Z2T-a (Figure 4.37), a noticeable change is present. Sulfidation in 2 mol% H_2S-10 mol% H_2-88 mol% N_2 (Figure 4.37b) produced a material with more dispersed crystals (~0.09 μm radius). In the absence of H_2, these crystals do not form. Instead, agglomerates (Figure 4.37a) are present with only faint grain boundaries visible.

The surface area of the sorbents sulfided in the TGA in the presence of various concentrations of hydrogen was measured to determine whether hydrogen increases the dispersion of the sulfided materials. Figure 4.38 shows that with 10 mol% H_2 in the gas, less sintering occurred than when 1 mol% H_2 was present. This effect is more dramatic in sorbent Z2T-a than in ZnO. With 2 mol% H_2S-10 mol% H_2-88 mol% N_2, the surface area of Z2T-a increased 1.7% after sulfidation while with only 1 mol% H_2, the surface area decreased 17%. The differences in the surface areas after sulfidation can be explained by two opposing effects: (1) increase in surface area due to reduction of sorbent and reaction of Zn with H_2S to form small small crystallites (e.g. Figure 4.35a) and (2) decrease in surface area due to ZnS sintering. During reduction, the surface area will increase as $1/r$ (r=radius). Also, the reaction of Zn vapor and H_2S will produce small ZnS crystals. However, it has been observed that the presence of Zn vapor phase will enhanced the grain growth kinetics (Sainamthip and Amarakoon,

a)

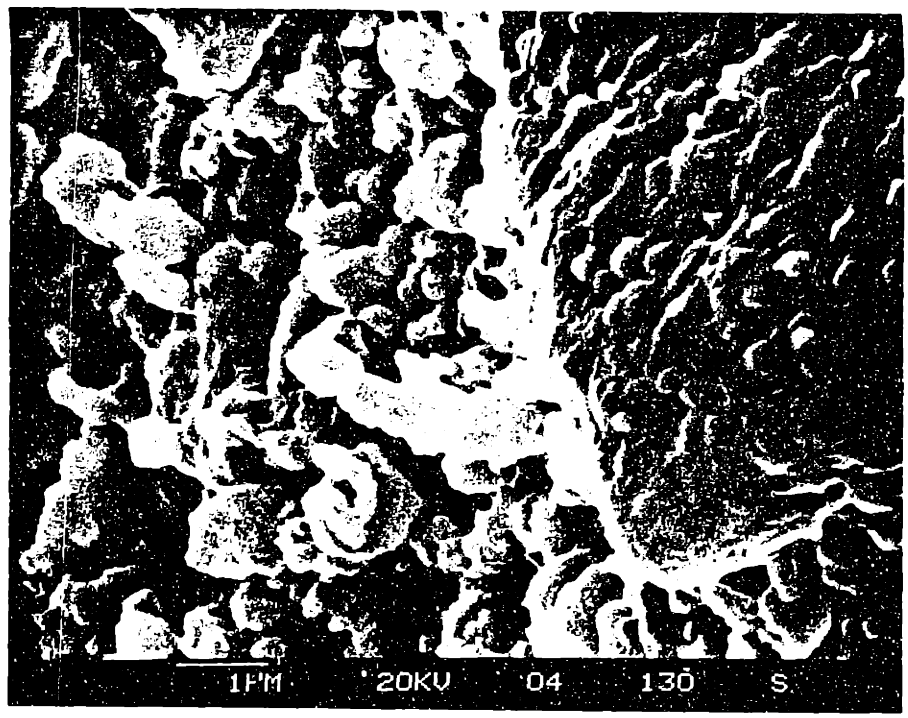

b)

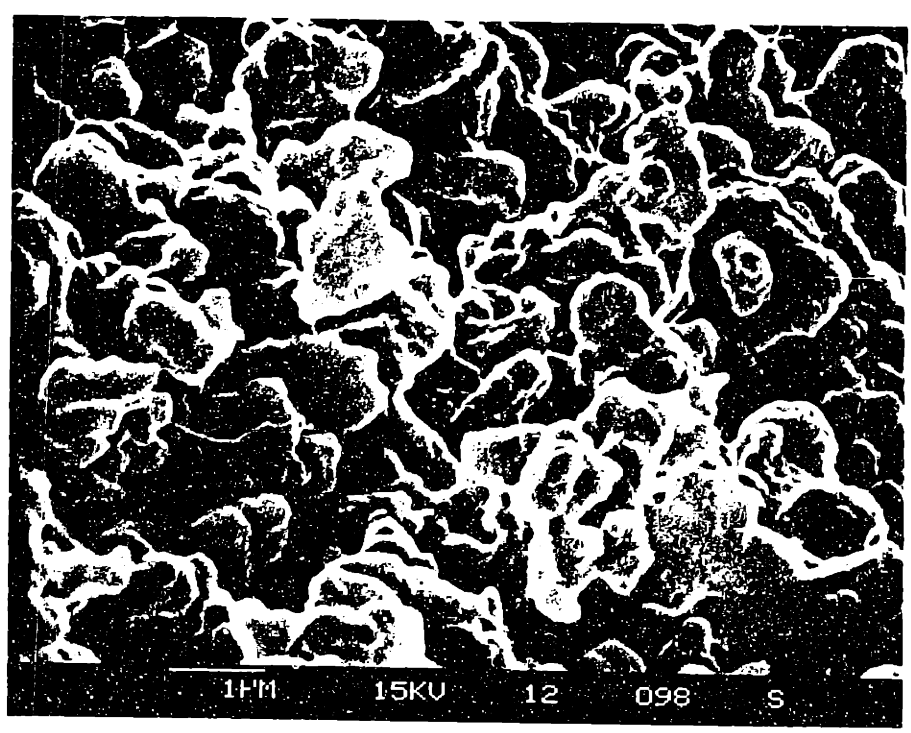

Figure 4.36 SEM micrographs of ZnO sulfided (~90%) at 650°C with a) 2% H_2S-98% N_2 and b) 2% H_2S-10% H_2-88% N_2.

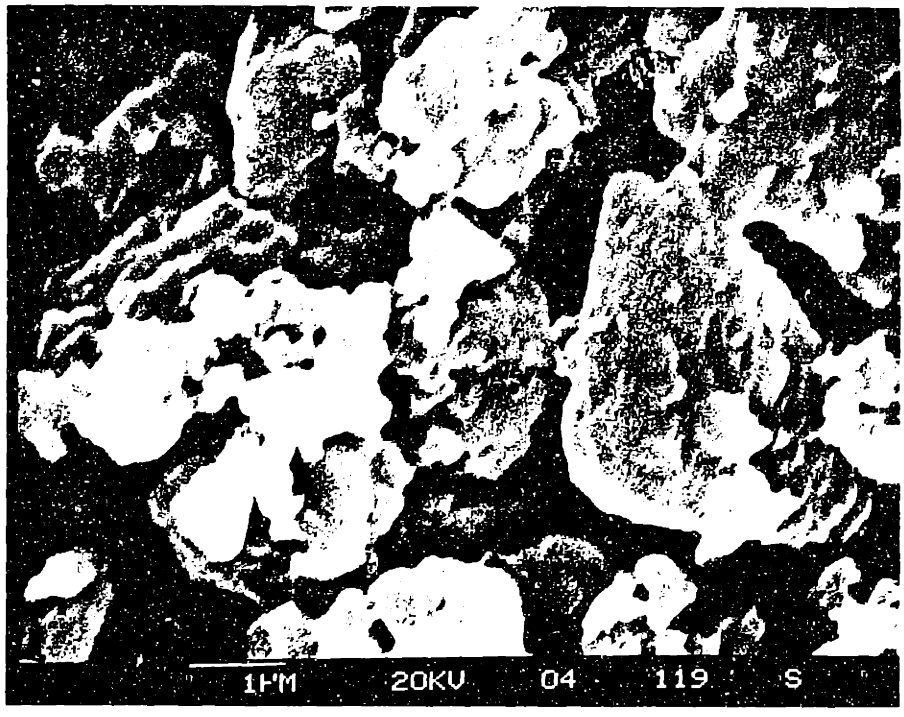

a)

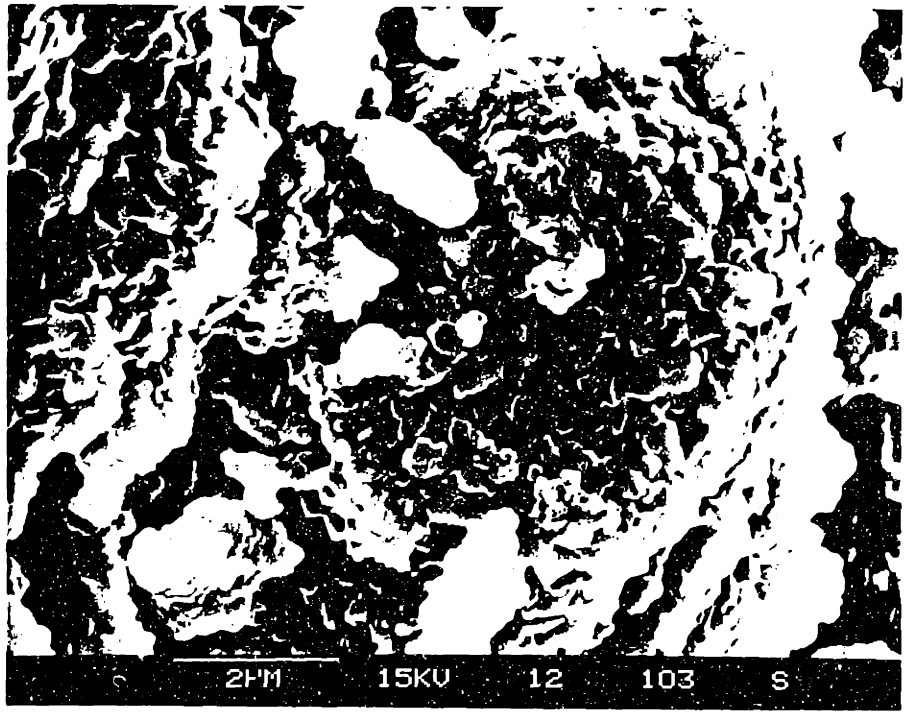

b)

Figure 4.37 SEM micrographs of Z2T-a (~90%) sulfided at 650°C with a) 2% H_2S-98% N_2 and b) 2% H_2S-10% H_2-88% N_2.

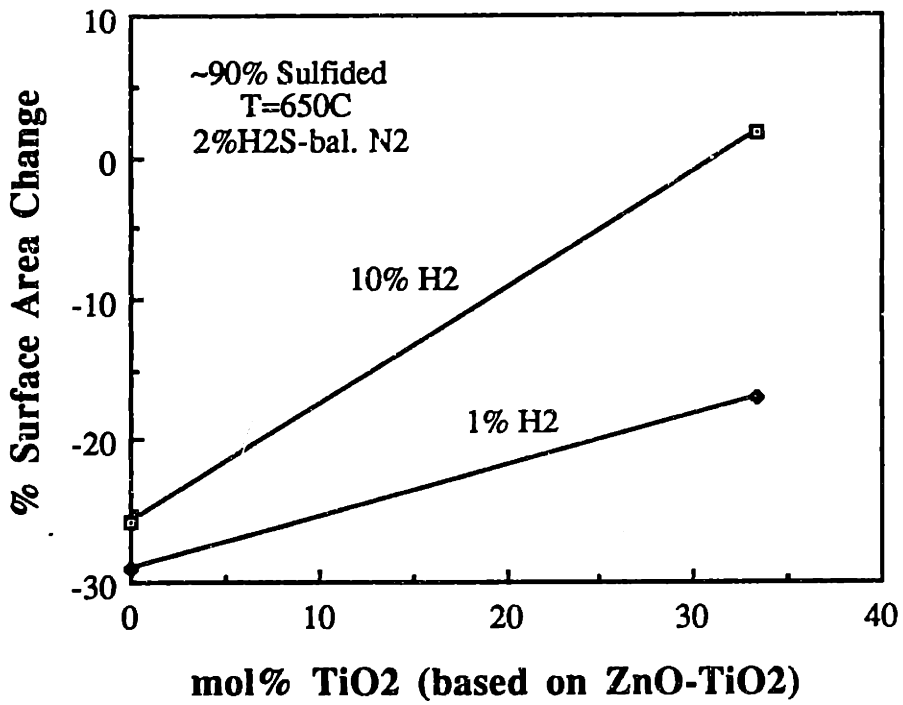

Figure 4.38 Comparison of surface area change of sorbents in 2%H2S-1%H2-97%N2 and 2%H2S-10%H2-88%N2 gas mixtures.

1988). For Z2T, the increase in surface area is due to the effect of reduction and the presence of TiO_2 which inhibits the formation of ZnS agglomerates.

Sulfidation was performed at a higher temperature (800°C) to examine potential changes in the sulfidation profiles as well as the sorbent physical structure. At this temperature, reduction will play a major role during sulfidation in a gas containing both H_2S and H_2. Reactions were performed with 2 mol% H_2S-H_2-bal. N_2. The H_2 content of the gas mixture was varied (1, 10, and 20 mol%). In Table 4.8, the initial sulfidation and reduction rates at 800°C with various gas compositions are listed for ZnO and Z2T-a sorbents. At this temperature, reduction by the more reactive sites (type A) is much faster than the rate of ZnO sulfidation. Thus, if reduction takes place by type A sites, either significant zinc loss should be observed or the initial sulfidation rate should be significantly greater than the sulfidation rate extrapolated from data obtained at lower temperatures (400-700°C). A higher initial sulfidation rate would imply that the gas-phase sulfidation rate of Zn(g) is faster than the reduction rate by type A sites. The initial sulfidation rates were calculated from the Arrhenius parameters obtained from experiments performed at 400-700°C. With 10 mol% H_2, the reduction rate is approximately 4.8 times faster than the extrapolated sulfidation rate (with 2 mol% H_2S) for ZnO. For Z2T-a, it is only 1.6 times faster than the initial sulfidation rate. The results of sulfidation experiments performed at 800°C are shown in Figure 4.39 and 4.40 for sorbent ZnO and Z2T-a, respectively. The experimentally measured initial sulfidation rate at 800°C for reaction in the presence of 2 mol% H_2S-1 mol% H_2-97 mol% N_2 is approximately the same (within 95% confidence) as the rate extrapolated with Arrhenius parameters obtained from data in the range of 400-700°C. Again, for both ZnO and Z2T-a, no noticeable zinc loss took place. Both sorbents were completely sulfided (based on the initial sorbent weight). However, after sulfidation was

Table 4.8 Initial Sorbent Sulfidation and Reduction Rate at 800°C

	Initial Rate (mmol/cm2-s)	
	ZnO	Z2T
Sulfidation [1]		
2% H_2S-1% H_2-97% N_2	$2.4x10^{-6}$	$1.2x10^{-6}$ mmol ZnS formed/cm^2-s
Reduction [2]		
1% H_2-99% N_2	$4.6x10^{-6}$	$1.9x10^{-7}$ mmol Zn lost/cm2-s
10% H_2-90% N_2	$1.2x10^{-5}$	$1.9x10^{-6}$
20% H_2-80% N_2	$1.7x10^{-5}$	$3.7x10^{-6}$
1% H_2-3% H_2O-96% N_2	$1.2x10^{-7}$	$6.0x10^{-8}$
10% H_2-3 %H_2O-87% N_2	$1.2x10^{-6}$	$6.0x10^{-7}$
20% H_2-3% H_2O-77% N_2	$2.4x10^{-6}$	$1.2x10^{-6}$

[1] Calculated from Arrhenius parameters taken from data at 400-700°C with 2%H_2S-1%H_2-97%N_2.

[2] Calculated from Arrhenius parameters taken from data at 600-1000°C with either 10%H_2-90%N_2 or 10%H_2-3%H_2O-87%N_2.

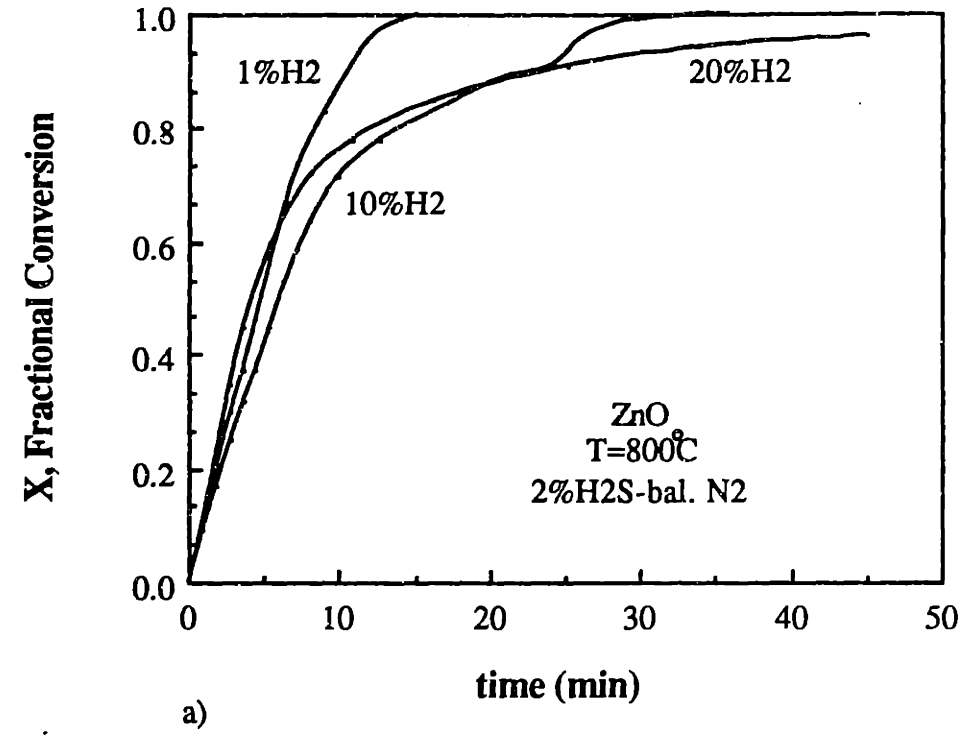

a)

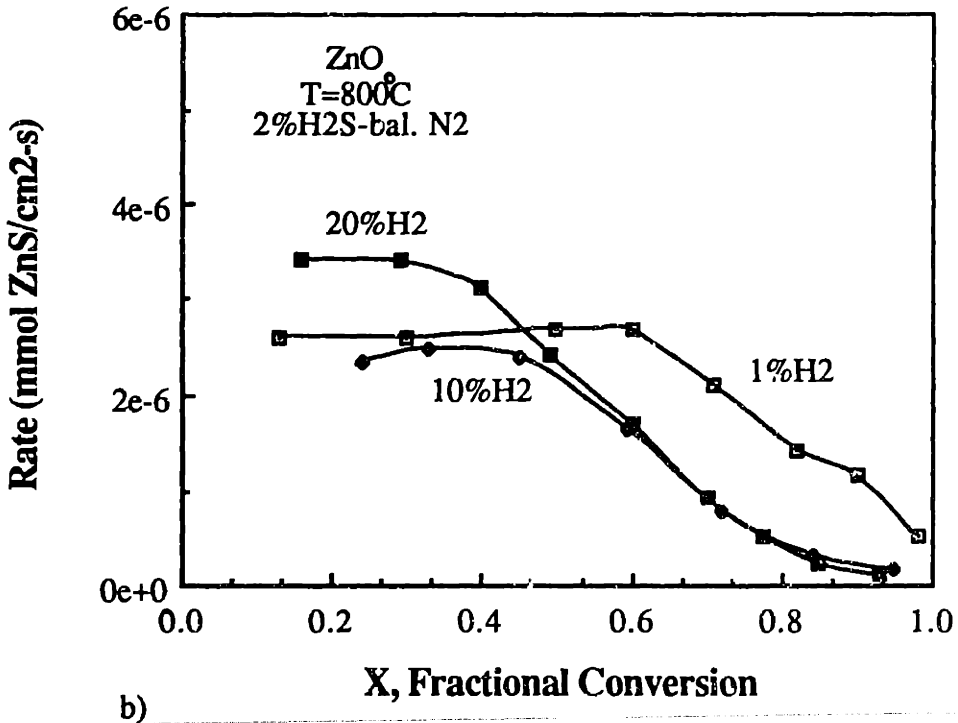

b)

Figure 4.39 Effect of H2 on ZnO sulfidation at 800°C a) conversion profiles and b) reaction rates.

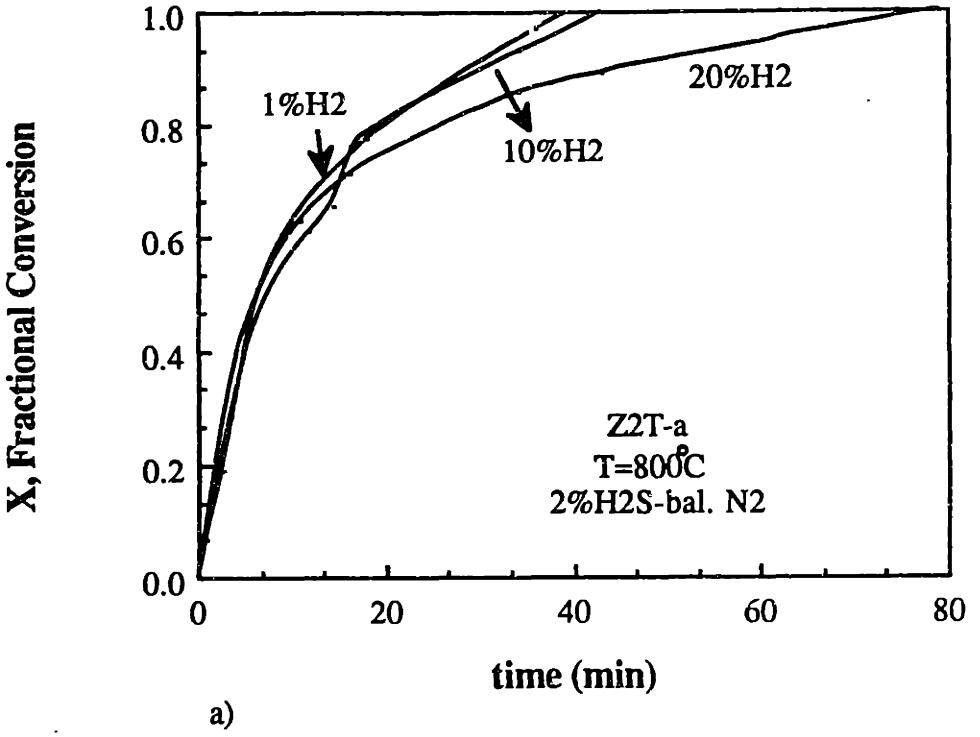

a)

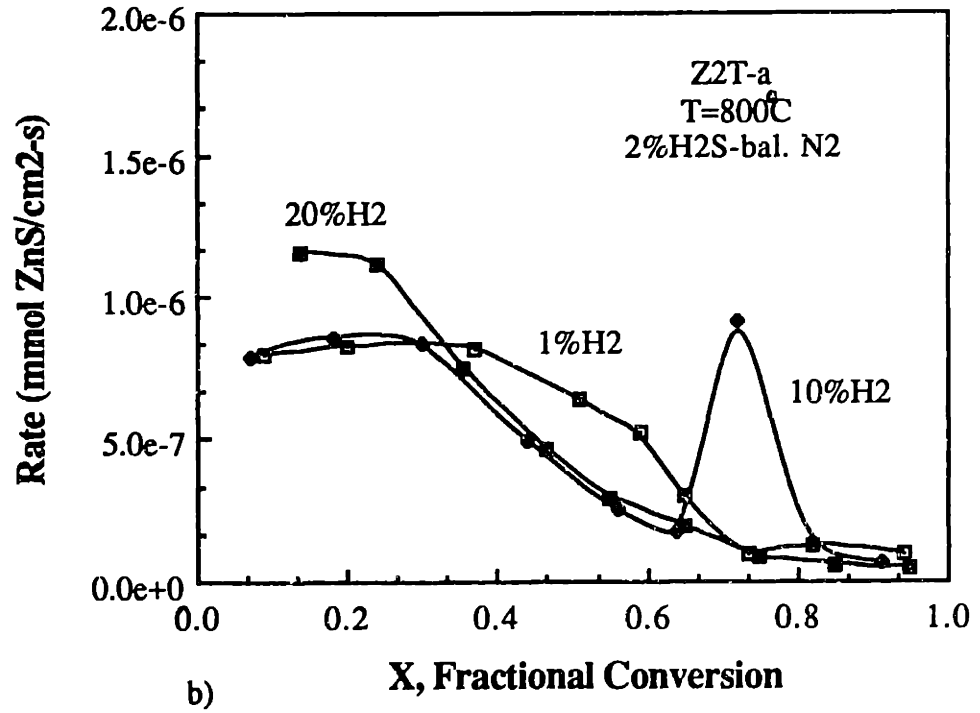

b)

Figure 4.40 Effect of H2 on Z2T-a sulfidation at 800°C a) conversion profiles and b) reaction rates.

completed, again a white film due to the reaction of Zn(g) and H_2S(g) was observed on the sample pan. As Figure 4.39 shows, up to approximately 50% conversion, the reaction rates of ZnO stayed relatively constant with different gas compositions. Above 50% conversion, the reaction rate dropped when sulfidation was performed with a gas containing either 10 or 20 mol% H_2.When sulfidation was performed with 1 mol% H_2, the rate remained relatively constant until approximately 70% conversion where it dropped off. A possible explanation for the faster decrease in the reaction rate for experiments performed in the presence of either 10 or 20 mol% H_2 is pore blockage due to the deposit of solid product from the vapor phase reaction between Zn(g) and H_2S(g). What is interesting to note is that the initial sulfidation rate in the presence of 20 mol% H_2 is slightly greater (1.25 times) than in the presence of either 1 or 10 mol% H_2. This slightly higher rate is due to the contribution of the gas phase sulfidation reaction to the initial sulfidation rate.

The initial sulfidation rates at 800°C provide some information about the reactivity of the different reaction sites involved in reduction (discussed in Chapter 3). Two different types of sites plays a role in ZnO reduction. Highly reactive sites (type A) which can be easily poisoned by H_2O vapor and sites of lower reactivity (type B). Type A sites have initial reduction rate 4.8 times faster than the initial sulfidation rate in 2 mol% H_2S-10 mol% H_2-88 mol% N_2. Since no zinc loss was evident, the reaction of Zn(g) with H_2S(g) must have occurred. Then, the initial sulfidation rate must be comparable to the initial reduction rate. Since this was not found, it implies that reduction by Type A sites did not occur. Thus, this verified that H_2S poisons Type A sites as was concluded in Chapter 3 from the reduction of partially sulfided solids. Reduction by the less reactive sites (type B) occurred. At 800°C with 2 mol% H_2S-10 mol% H_2-88 mol% N_2, the

predicted initial sulfidation rate is approximately twice as fast as the predicted initial reduction rate by type B sites.

Similar to ZnO, the initial sulfidation rate of Z2T-a at 800°C remained unchanged in the presence of either 1 or 10 mol% H_2 (Figure 4.40). But, sulfidation in the presence of 20 mol% H_2 resulted in an initial rate 1.4 times faster than either in 1 or 10 mol% H_2. Again similar to ZnO sulfidation, there is a faster decrease in the reaction rate at the higher H_2 mole fractions (10 and 20 mol%).

The reacted sorbents were examined by SEM to identify any differences due to more extensive sorbent reduction as the hydrogen content was increased. No considerable difference can be observed on the surface of ZnO reacted at 800°C (Figure 4.41) in 2 mol% H_2S-1 mol% H_2-97 mol% N_2 and at 650°C (Figure 4.36a) in 2 mol% H_2S-98 mol% N_2. However, at 800°C, the sorbent appeared to be more crystalline. Hexagonal crystals (~0.25 μm radius) characteristic of ZnS formation are present on the sorbent surface. With 2 mol% H_2S- 10 mol% H_2-88 mol% N_2, cracks and fissures are evident on the particle (Figure 4.42) which were probably caused by Zn(g) and H_2O(g) escaping from the particle. Deposited on the original surface are small crystals (0.05-0.2 μm radius) formed as a result of the reaction between Zn(g) and H_2S(g). Thus, for ZnO, reduction not only causes zinc loss under certain conditions but can also lead to weakening of the strength of the material by crack and fissure formations and the formation of fines. With higher H_2 content (20 mol%), similar features were observed on the surface as those shown for reaction with 10 mol% H_2 (Figure 4.42). A larger amount of crystal formations due to the reaction of Zn(g) and H_2S(g) are observed. In addition, large spherical agglomerates (0.7-1.3 μm radius) were also observed on the surface (Figure 4.43) of several of the examined particles. The agglomerates are

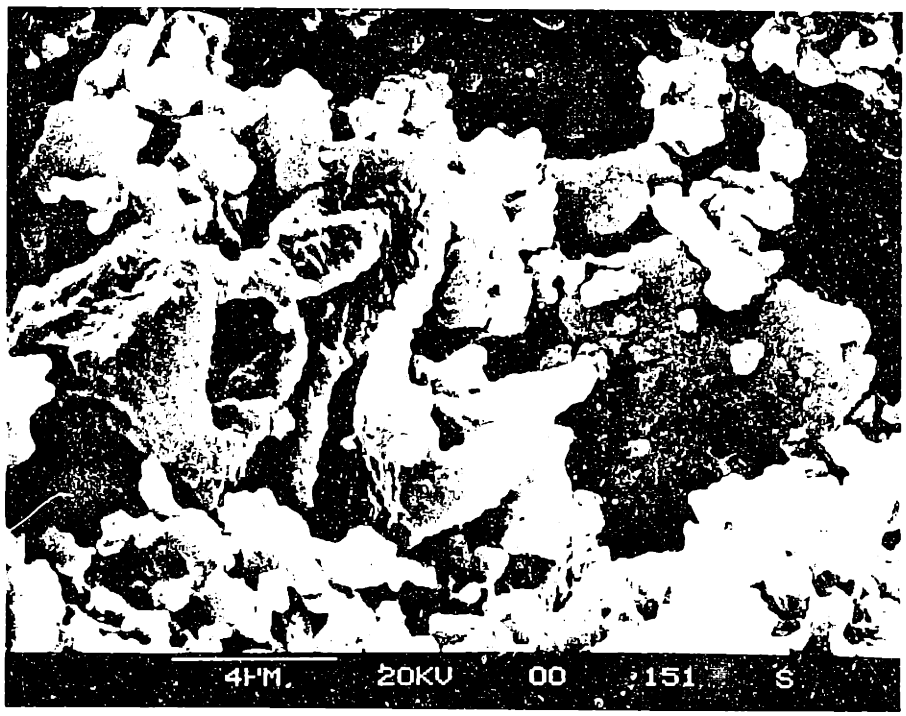

a) 5000x

b) 10000x

Figure 4.41 SEM micrographs of ZnO sulfided at 800°C with 2% H_2S-1% H_2-97% N_2 a)5000x and b) 10000x.

Figure 4.42 SEM micrographs of ZnO sulfided at 800°C with 2% H_2S-10% H_2-88% N_2.

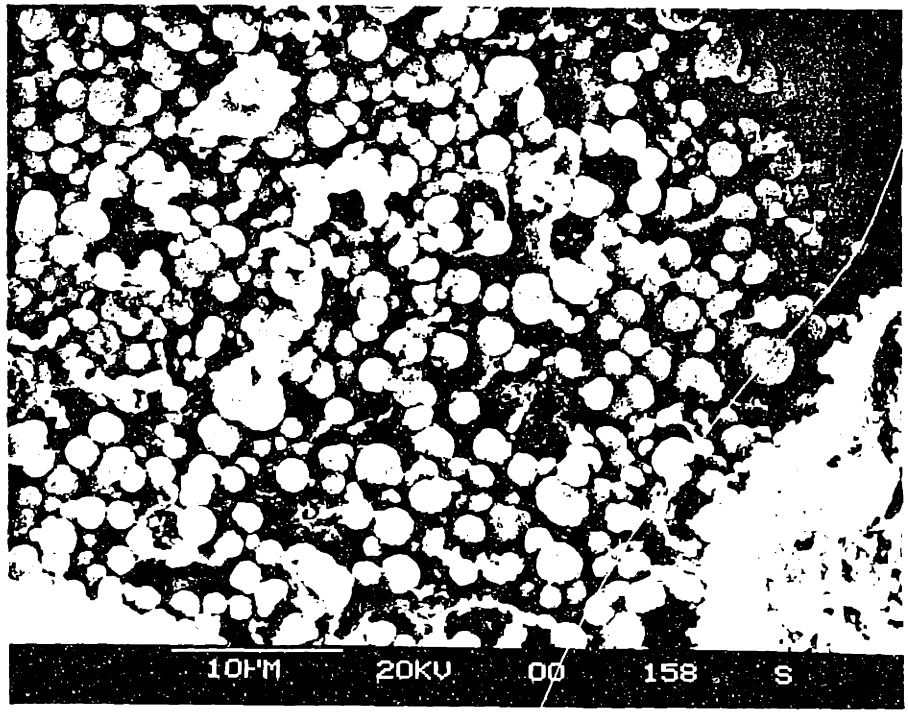

a) 4000x

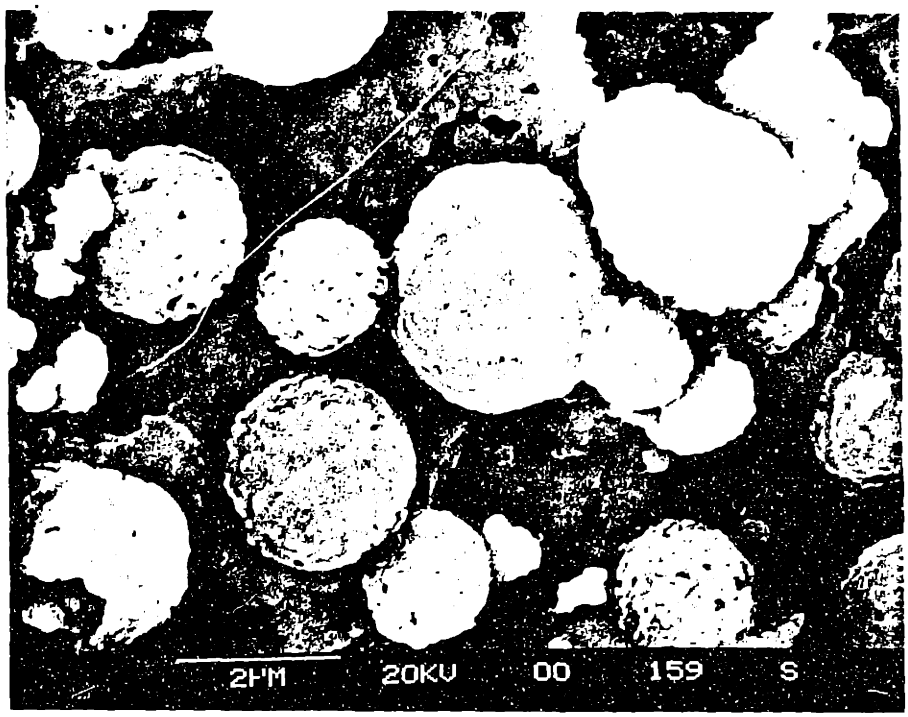

b) 10000x

Figure 4.43 SEM micrographs of ZnO sulfided at 800°C with 2% H_2S-20% H_2-78% N_2 a) 4000x and b) 10000x.

composed of smaller crystals (~0.04 μm radius). Thus, the higher Zn vapor phase concentration when reaction is performed with 20 mol% H_2 leads to enhance sintering. Sainamthip and Amarakoon (1988) also saw enhanced grain growth in Zn vapor.

Unlike the physical transformation observed for ZnO, no gross morphological changes were evident for Z2T-a sulfidation at 800°C with various H_2 concentrations. A lower degree of change with increasing hydrogen concentrations is in agreement with the findings that Zn-Ti-O sorbents are more resistive to reduction than ZnO. Figure 4.44 shows SEM micrographs of Z2T-a after sulfidation. With higher hydrogen concentrations, the grain boundaries can be more clearly seen. This is consistent with zinc volatilization preferentially occurring along grain boundaries (Sainamthip and Amarakoon, 1988).

These observations offer interesting possibilities for reactor design. Desulfurization in a fixed-bed reactor will lead to zinc loss. As illustrated in Figure 4.45, H_2S will react with the top of the sorbent bed. Any zinc vapor formed will also react with H_2S. The downstream part of the sorbent bed will be in contact only with H_2S-free reducing gas, thus, resulting in zinc losses.On the other hand, desulfurization in a fluidized bed reactor offers the possibility of eliminating zinc loss. The disadvantages of this reactor configuration, however, are lower H_2S removal efficiency (due to bubbling) as well as the fact that the vapor phase reaction between H_2S and Zn will produce fines and will lead to sorbent loss and elutriation. Thus, Zn-Ti oxides would still be preferable as sorbents over ZnO because of decrease particle cracking and fines production.

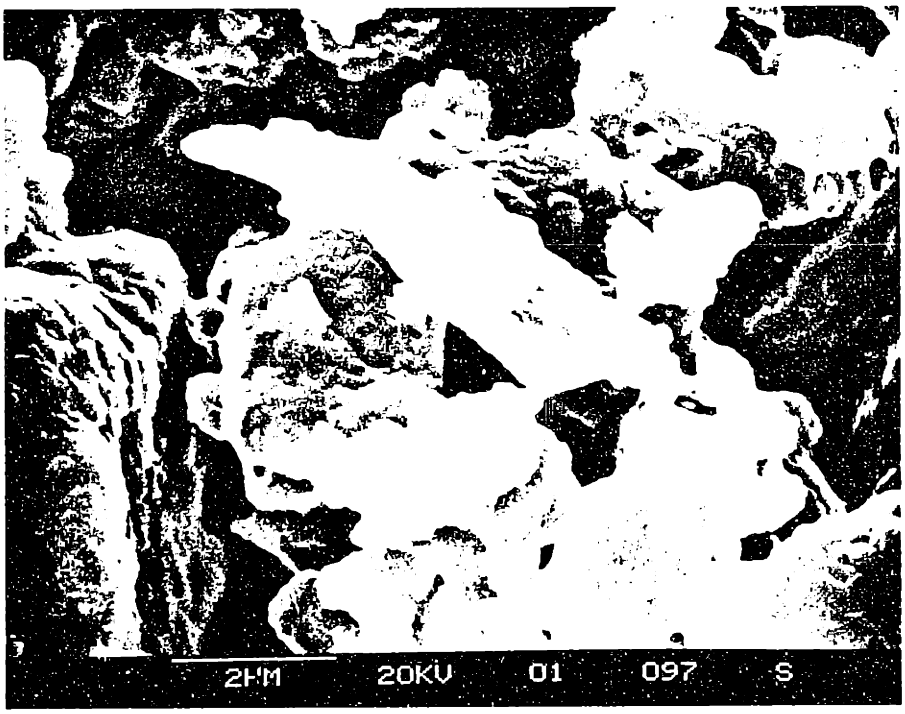

a)

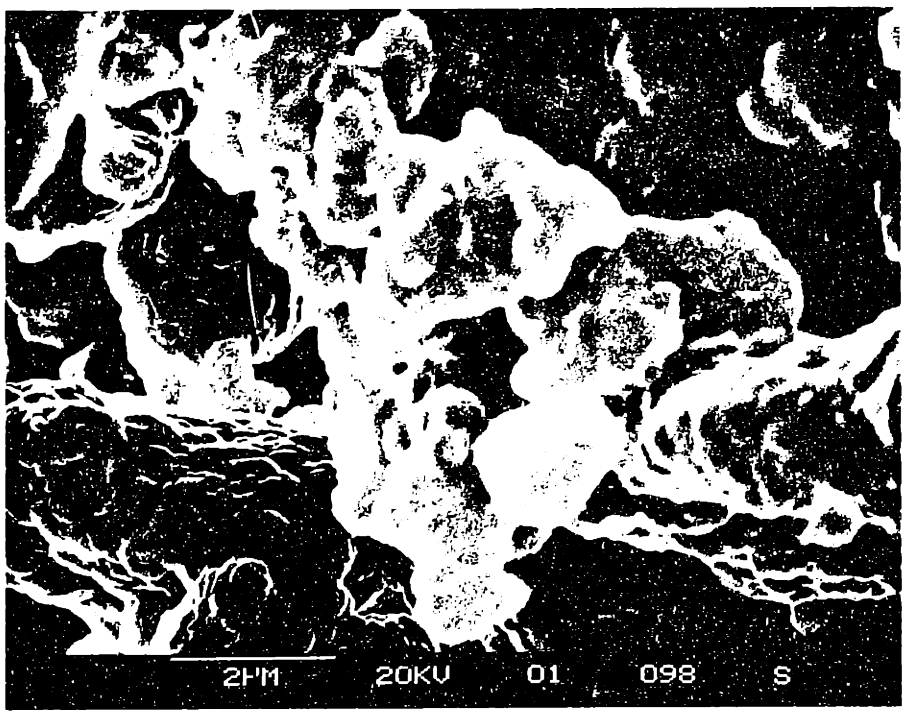

b)

Figure 4.44 SEM micrographs of Z2T-a sulfided at 800°C with various hydrogen concentrations a) 2% H_2S-1% H_2-97% N_2 b) 2% H_2S-10% H_2-88% N_2 and c) 2% H_2S-20% H_2-78% N_2.

c)

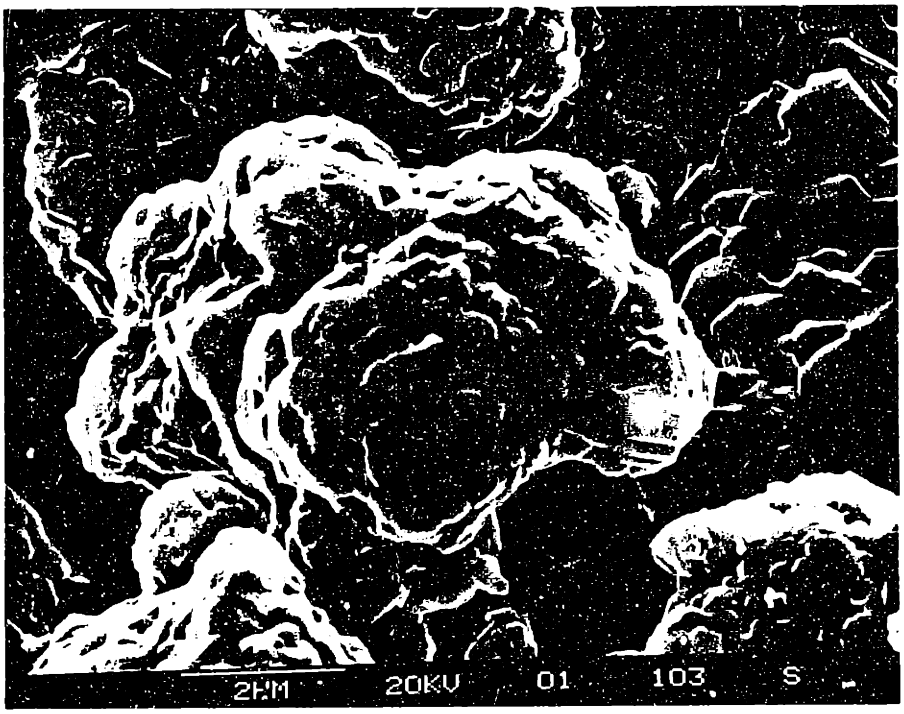

Figure 4.44(cont'd) SEM micrographs of Z2T-a sulfided at 800°C with various hydrogen concentrations a) 2% H_2S-1% H_2-97% N_2 b) 2% H_2S-10% H_2-88% N_2 and c) 2% H_2S-20% H_2-78% N_2.

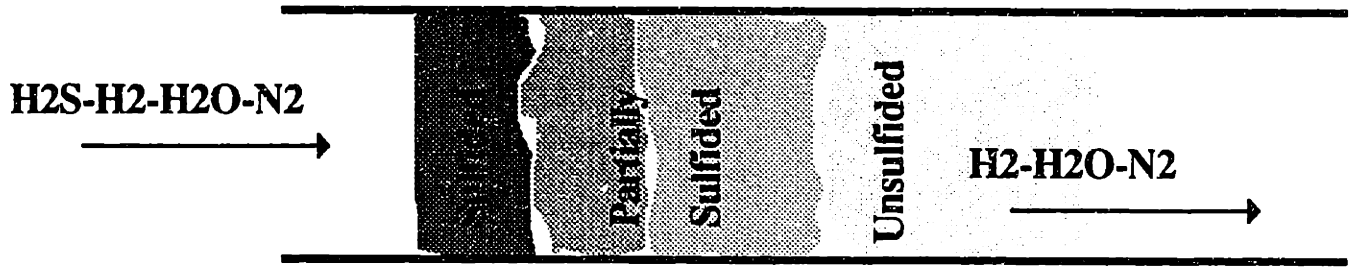

Figure 4.45 Desulfurization in a fixed-bed reactor.

4.3.5 Effect of H_2O

The next parameter investigated in Zn-Ti-O sulfidation was H_2O. As discussed in Chapter 3, the presence of water vapor has the beneficial effect of significantly inhibiting the reduction of ZnO and subsequent zinc loss. Water vapor was added to the reactant gas stream to examine whether any effects similar to those found in reduction may also be present in sulfidation.

Experiments were performed in a gas mixture consisting of 2 mol% H_2S-1 mol% H_2O-1 mol% H_2-96 mol% N_2. For these experiments, a nitrogen-hydrogen gas stream was saturated with water vapor at room temperature (25°C). The saturated gas stream and a H_2S-N_2 stream were mixed and entered the reactor through a side arm. Nitrogen was also continuously passed into the balance to prevent the corrosive gas from reaching the balance mechanism. When water vapor is absent from the reactant gas stream, the calculated concentration of H_2O (produced during sulfidation) in the external film of the particle is approximately zero. Therefore, although the 1 mol% H_2O used here is a smaller amount than what is typically found in coal-derived fuel gases (e.g. 50 mol% from a fixed-bed Lurgi gasifier and 10 mol% from a fluidized bed KRW gasifier-values from Halow, 1986), it is much higher than what was found in the external film. Thus, any inhibition effect that water vapor may have on sulfidation should be readily apparent in a gas containing 1 mol% H_2O.

The conversion profiles of ZnO, Z2T-a, and Z2T3-a were examined. As illustrated in Figure 4.46, no significant effect was observed by the presence of water vapor at either 400 or 700°C. Thus, no inhibition effects on either the initial sulfidation rate or diffusion through the sulfidation product layer were present when 1 mol% H_2O was added to the reactant gases. While the presence of water vapor can significantly change

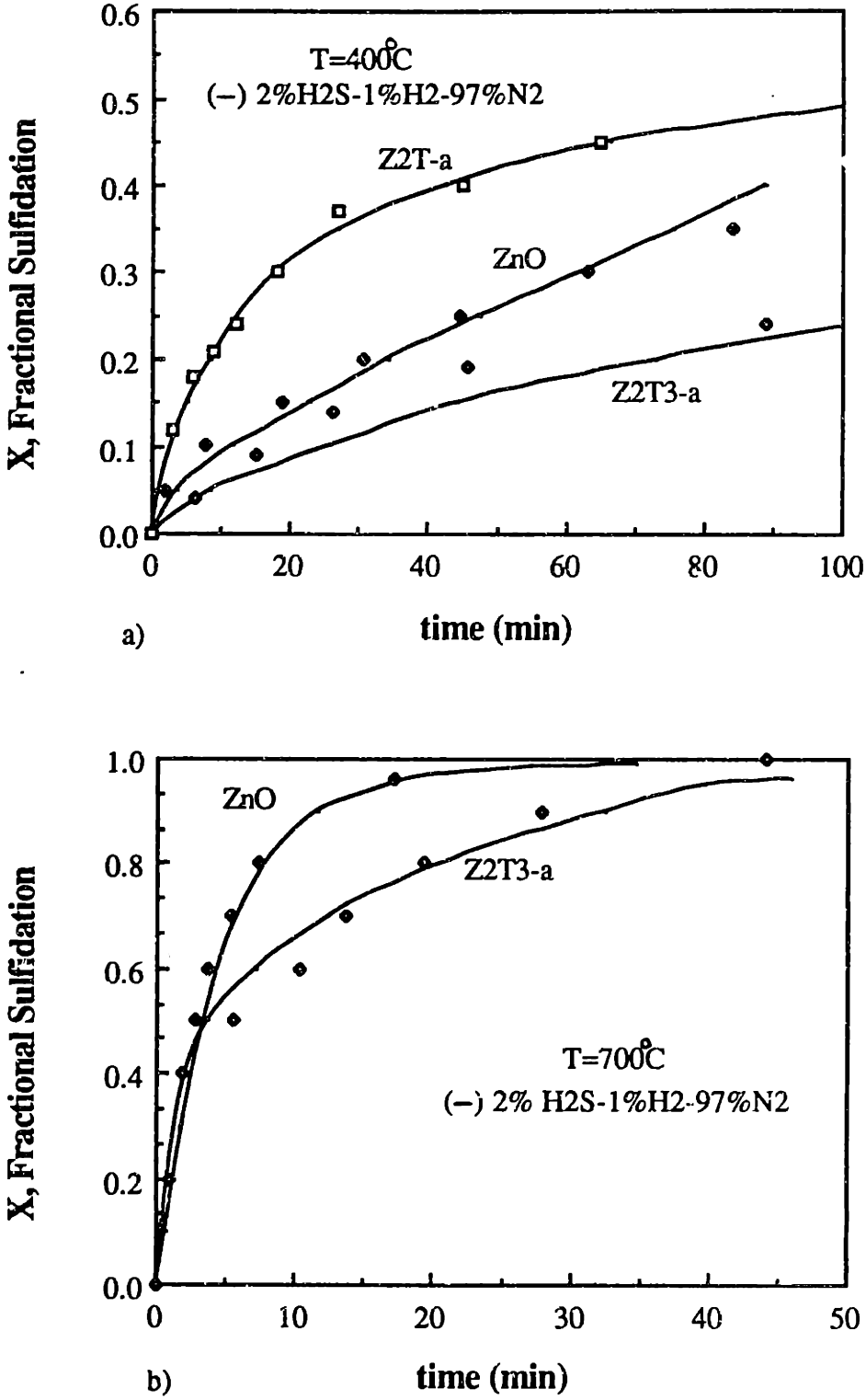

Figure 4.46 Comparison of conversion profiles for various sorbents reacted in 2%H2S-1%H2O-1%H2-96%N2 and 2%H2S-1%H2-97%N2 at a) 400°C and b) 700°C. (Data points for reaction in H2O)

the initial reduction rate, no such effect is found in sulfidation. Comparison of the initial reduction and sulfidation rate at 700°C is shown in Figure 4.47. The initial reduction rate was calculated from the Arrhenius parameters obtained from experiments with 10 mol% H_2-3 mol% H_2O-87 mol% N_2. The initial sulfidation rate was obtained from experiments with 2 mol% H_2S-1 mol% H_2-97 mol% N_2. In the presence of water vapor, the reduction rate for all sorbents examined was significantly lower than the sulfidation rate. For ZnO, the initial sulfidation rate is approximately 43 times greater than its reduction rate in the presence of H_2O. In contrast, when no H_2O is present, the reduction rate is approximately 1.4 times faster. Comparing these values to sorbent Z2T-a, in the presence of H_2O, the sulfidation rate is 64 times faster than the initial reduction rate, while in the absence of H_2O, it is only 10 times greater. Unlike the situation in the absence of water vapor, varying the amount of titanium in the Zn-Ti-O sorbents did have a noticeably change on the reduction rate. For the case of sorbent Z2T3-a, the sulfidation rate is 422 times faster than the reduction rate in the presence of H_2O, while in its absence, it is only 8 times greater.When the ratio of H_2O to H_2S was increased from 1:2 to 3.8:1, no visible changes in the conversion profiles (Figure 4.48) were apparent for either ZnO or Z2T3-a. The solid lines shows the results of experiments with 0.5 mol% H_2S-1 mol% H_2-98.5 mol% N_2 and the data points are for reaction in 0.5 mol% H_2S-1.9 mol% H_2O-1 mol% H_2-96.6 mol% N_2 at 700°C.

From the results of sulfidation experiments with H_2O, some indications of the reaction sites involved in sulfidation can be drawn. Two types of sites (Type A and Type B sites) were identified in reduction of ZnO. Type A sites were found to be poisoned by H_2O and H_2S. Type A sites, thus were not involved in sulfidation. The number of Type B sites decreased with increasing relative amount of TiO_2 in the sorbent. No decrease in the initial sulfidation rate was observed when the relative amount of TiO_2

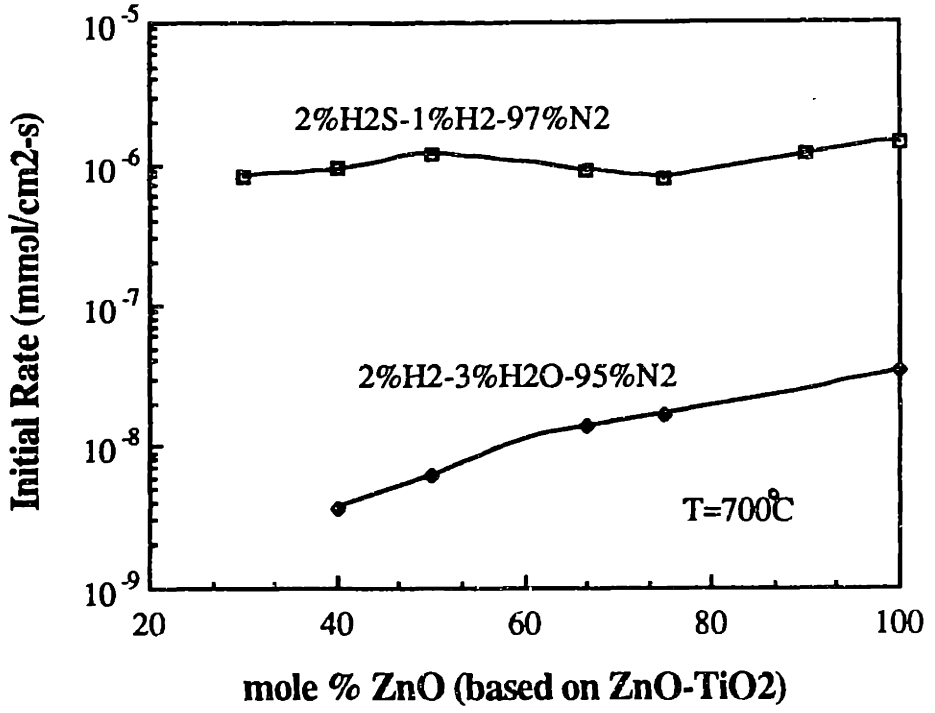

Figure 4.47 Comparison of initial reduction (2%H2-3%H2O-95%N2) and sulfidation (2%H2S-1%H2-97%N2) rates at 700°C.

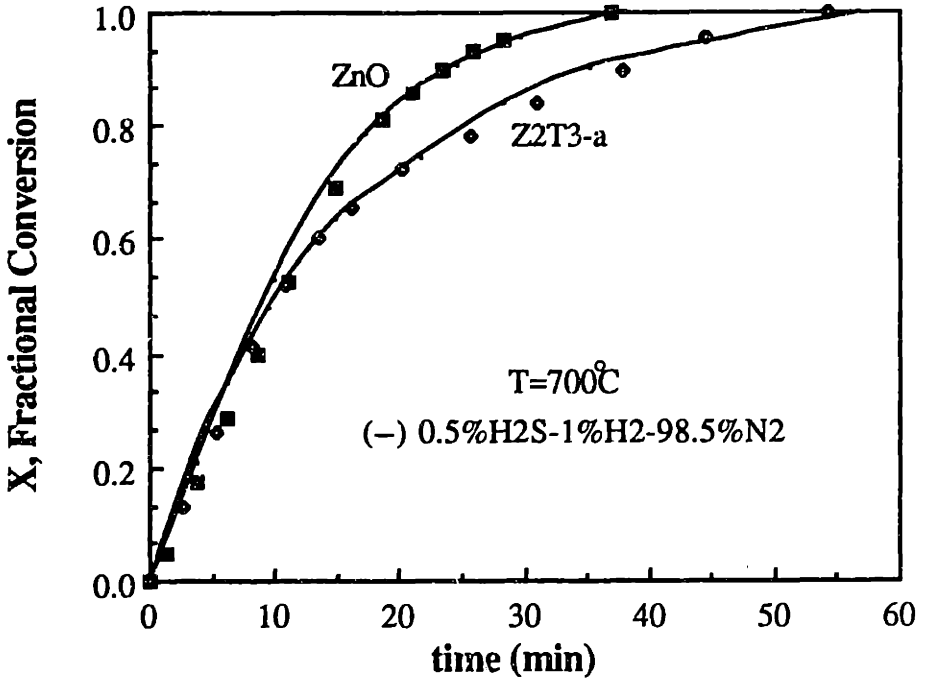

Figure 4.48 Comparison of conversion profiles of sorbent ZnO and Z2T3-a sulfided in 0.5%H2S-1.9%H2O-1%H2-96.6%N2 and 0.5%H2S-1%H2-98.5%N2 at 700°C. (Data points for reaction in H2O)

was increased from 25 mol% to 60 mol%. Thus, Type B sites were also not involved in sulfidation. Consequently, reduction and sulfidation must proceed on different reaction sites, independent of each other.

Although there were no discernible differences in the sulfidation profiles with the addition of water vapor, physical changes were readily apparent when the reacted sorbents were examined under the SEM. ZnO and Z2T-a (Figures 4.49 and 4.50, respectively) were reacted in 2 mol% H_2S-1 mol% H_2O-1 mol% H_2-96 mol% N_2 at 700°C. As shown in both Figures 4.49 and 4.50, the presence of water vapor enhanced the sintering of the sorbent. The surface areas of a few reacted sorbents were measured to determine the extent of sintering which occurred in the presence of water vapor. These results are shown in Figure 4.51. For ZnO, after ~90% sulfidation, the surface area decreased 43% from its original value. In contrast, in the absence of H_2O, the surface area decreased only 29%. Sorbent Z2T3-a for which an increase of surface area (20%) take place after dry sulfidation showed only 11% increase in surface area in the presence of H_2O.

4.4 CONCLUSIONS

1) At temperatures between 400-700°C, similar activation energies are observed for both Zn-Ti-O sorbents and ZnO sorbents, while lower frequency factors are measured as a result of the presence of titanium in the sorbents. Therefore, it is proposed that sulfidation of Zn-Ti-O proceeds by the same mechanism as ZnO sulfidation, but the presence of titanium serves to eliminate reaction sites.

a)

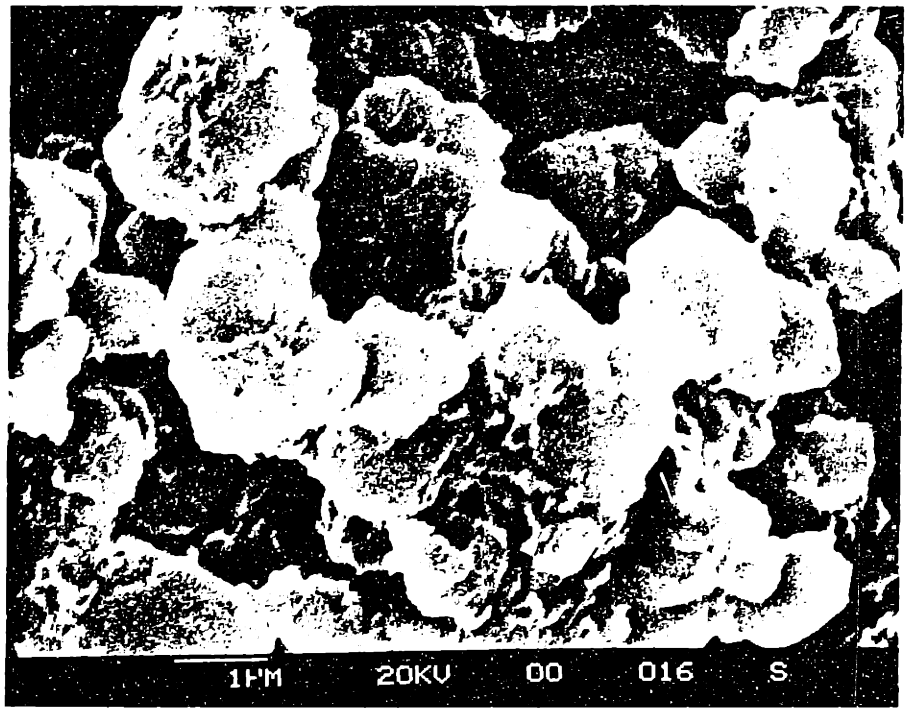

b)

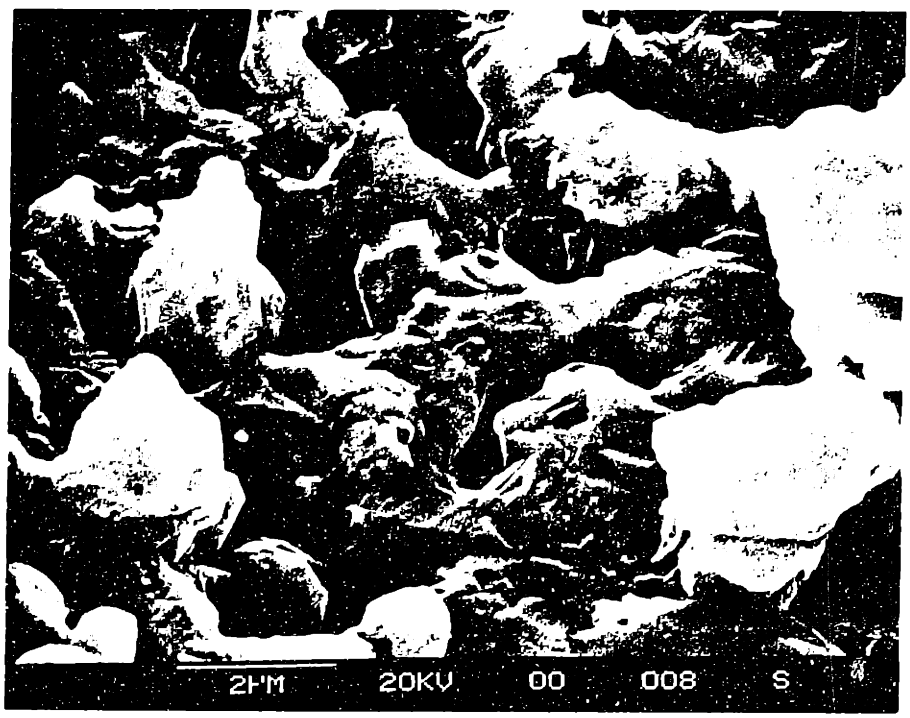

Figure 4.49 SEM micrographs of ZnO sulfided at 700°C with a) 2% H_2S-1% H_2-97% N_2 and b) 2% H_2S-2% H_2O-1% H_2-95% N_2.

a)

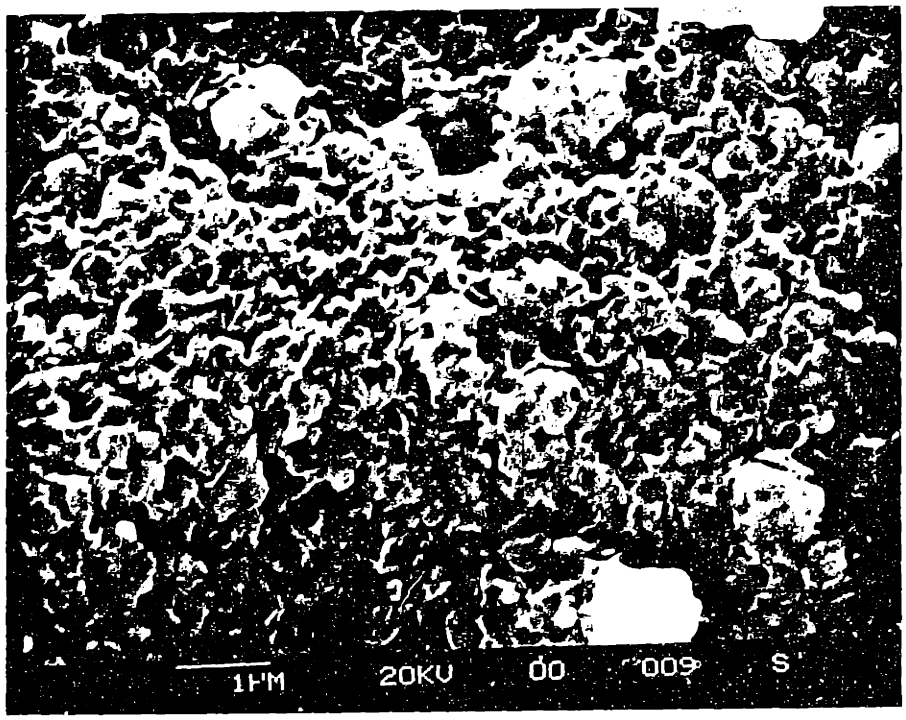

b)

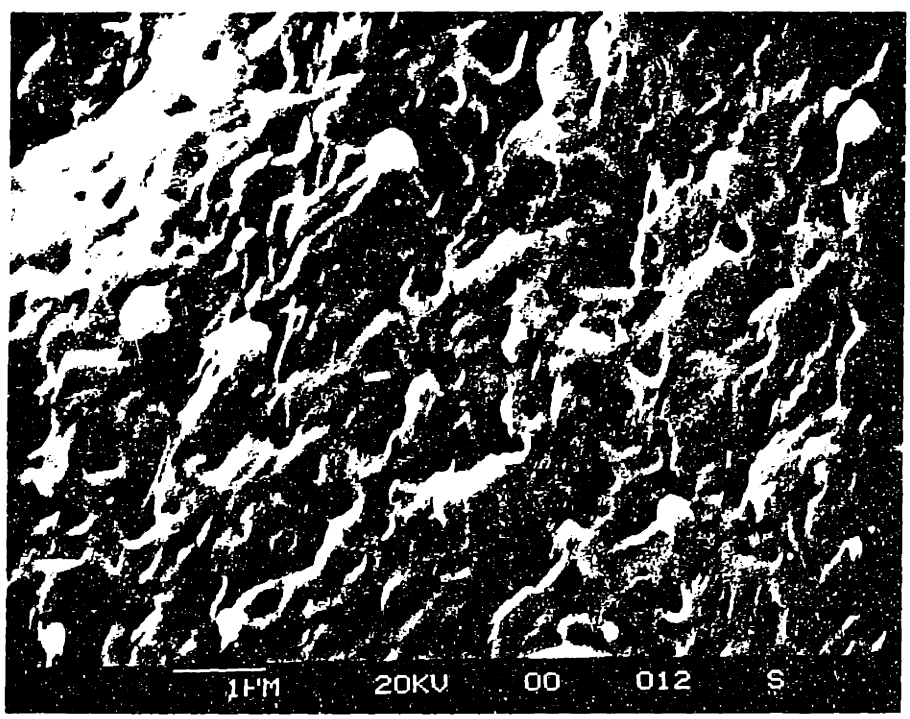

Figure 4.50 SEM micrographs of Z2T sulfided at 700°C with a) 2% H_2S-1% H_2-97% N_2 and b) 2% H_2S-2% H_2O-1% H_2-95% N_2.

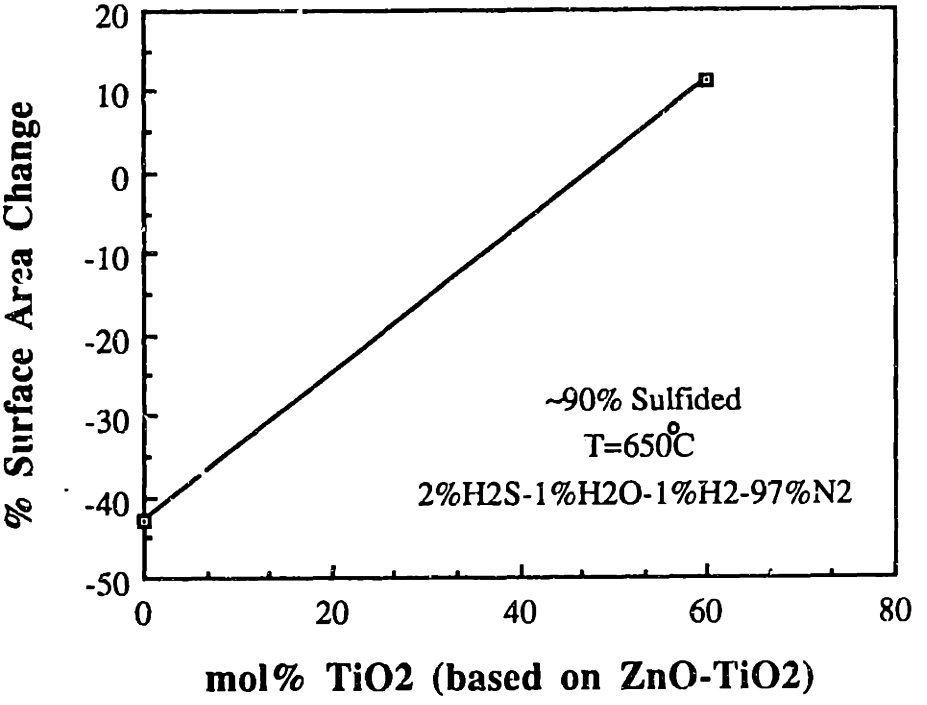

Figure 4.51 Surface area change after sulfidation at 650°C with 2%H2S-1%H2O-1%H2-96%N2.

2) Only a certain number of reaction sites for sulfidation will be eliminated by titanium. Increasing titanium content of the sorbents above 25 mol% (based on Zn-Ti stochiometry) does not lead to a corresponding decrease in the frequency factor.

3) No differences in the sulfidation kinetics were observed by the presence of different zinc titanate phases (i.e. Zn_2TiO_4, $Zn_2Ti_3O_8$, and $ZnTiO_3$).

4) No effect of hydrogen on the sulfidation kinetics was observed for temperatures in the range of 400-700°C. However, at 800°C, an increase in the initial reaction rate was observed with H_2/H_2S=20/2. This effect is believed to be due to the reaction between Zn(g) produced by reduction and H_2S. No zinc loss was evident for either ZnO or sorbent Z2T-a. However, a noticeable development of cracks and fissures was observed in ZnO as a result of the reduction of ZnO and the evolution of Zn vapor.

5) No effect of water vapor on the sulfidation kinetics was observed for temperatures in the range of 400-700°C. However, the presence of H_2O enhanced the sintering of both ZnO and Zn-Ti-O sorbents.

6) From these results, it is concluded that the optimum sorbent composition for desulfurization should be based only on the amount of reduction tolerated and the sulfur loading desired. In the absence of H_2O, the best sorbent composition for operation in a fixed-bed reactor is one with an atomic ratio of $(Zn/Ti)_{atomic} \approx 3/1$. A higher percentage of titanium yields no improvement in decreasing the reduction rate and decreases the sulfur loading. Howerver, in the presence of H_2O or for operation in a fluidized bed reactor, a higher percentage of titanium will decrease the reduction rate.

CHAPTER 5

MODELING OF SULFIDATION

5.1 INTRODUCTION

Various mathematical models have been presented in the literature for gas-solid reactions. They can generally be classified as either grain models representing the structure as an assemblage of very small grains, usually spherical in shape, or as pore models representing the porous solid by a collection of capillaries. As would be expected, very different reaction profiles are calculated depending on the structural model employed.

One of the earliest gas-solid reactions model described a solid with overlapping pores of uniform size randomly distributed in space (Petersen,1957). Further refinements of the model were introduced to more closely describe the physical structure of the solid.

This model was extended to include the possibility of solid product formation which changes the surface area and porosity of the solid (Cavelo and Cunningham, 1970; Ramachandran and Smith, 1977[1]). Recently. the model was expanded to describe a pore size distribution with randomly overlapping pores (Gavalas, 1980; Bhatia and Perlmutter, 1980; Bhatia and Perlmutter, 1983). Concurrently, variable property grain models allowing for solid product formation and sintering have also been proposed (Hartman and Coughlin, 1976; Szekely, 1976; Georgakis et al., 1979; Ramachandran and Smith, 1977[2]; Ranade and Harrison, 1981). In these models, the solid was represented by non-overlapping uniform size grains. Several different grain shapes (e.g. spheres, plates, and cylinders) were used. More recently, an overlapping grain model with a grain size distribution was developed for gas-solid reaction (Sotirchos and Yu, 1988). To facilitate this discussion, the non-overlapping grain model will be designated as the grain model while the overlapping one will be called the random grain model.

The fundamental difference between the pore model and grain model is in the representation of the solid structure, its reactant surface area, and its pore surface area. General schematic representations for the random pore, grain and random grain models are shown in Figure 5.1. The reactant surface area will influence both the rate of chemical reaction as will as the diffusion through the product layer. The pore surface area will only affect the product layer diffusion. The random pore model and grain model give very different expressions for the reactant and pore surface area, and this will correspondingly affect the reaction profile. The grain model predicts a monotonically decreasing reaction surface area (S(X)) with increasing conversion for spherical and cylindrical shape grains:

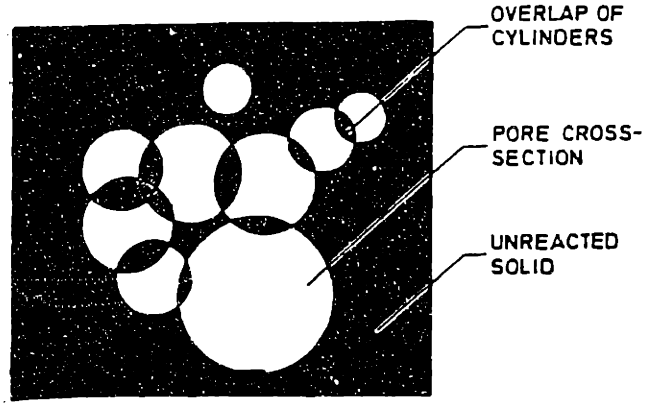

a) Random Pore Model with a distributed pore size
(from Bhatia and Perlmutter, 1980)

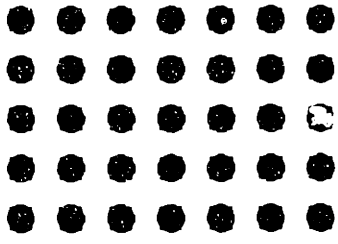

b) Grain Model

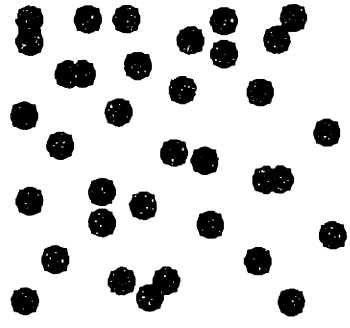

c) Random Grain Model
(uniform spherical grains)

● unreacted solid

Figure 5.1 Schematic representations of the reacting porous solid by a) random pore b) grain and c) random grain models.

$$S^*(X) = (1-X)^m \qquad (5.1)$$

where $S^*(X)$ is the normalized reaction surface area $[S(X)/S_o]$, m is the shape factor (sphere = 2/3; cylinder = 1/2), and X is the fractional conversion. S(X) is the reaction surface area per unit volume and S_o is the surface area per unit volume at X=0. For flat plate, the reaction surface area remains constant with conversion.

The random pore model is more versatile in describing the reaction surface area because with certain values of the structural parameters, it is possible to observe a maximum in the surface area. Some systems, such as the gasification of coal and char have been known to exhibit a maximum in the reaction rate (Dutta et al., 1977; Dutta and Wen, 1977). The maximum in reaction rate has been attributed to a maximum in the reaction surface area. This maximum can arise from two opposing effects: 1) the growth of the reaction surface as the pores radius increases and 2) the decrease in reaction surface as pores progressively collapse by intersection. For the random pore model with uniform cylindrical pores, the reaction surface area is

$$S^*(X) = (1-X)\sqrt{1-\psi \ln(1-X)} \qquad (5.2)$$

where ψ is a structural parameter equal to $4\pi L_{Eo}/S_{Eo}^2$, L_{Eo} is the total length of non-overlapping cylindrical surface per unit volume at t=0, and S_{Eo} is the surface area per unit volume at t=0. Depending on the value of ψ, a maximum may be present in the value of $S^*(X)$.

Like the reaction surface area, the expressions for the pore surface area are very different for the random pore and the grain model. For the grain model, the pore surface area is

$$S_p^*(X) = [1+(Z-1)X]^m \qquad (5.3)$$

For the random pore model, it is

$$S_p^*(X) = [1+(Z-1)X]\sqrt{1-\psi\ln(1+(Z-1)X)} \qquad (5.4)$$

where Z is the volume of product formed per unit volume of reactant. The grain model produces the anomaly of a monotomically increasing pore surface area even when the porosity reduces to zero. This produces a discontinuity in the reaction profile at the point where the porosity reaches zero. On the other hand, the random pore model more realistically predicts that as the porosity goes to zero the pore surface area also goes to zero. The porosity is customarily assumed to vary linearly with conversion according to

$$\varepsilon = \varepsilon_o-(1-\varepsilon_o)(Z-1)X \qquad (5.5)$$

Due to the inadequacies of the grain model in certain areas (e.g. reaction and pore surface area prediction), further refinements of the model were developed. One basic problem with the grain model is the assumption that the individual grains grow independently with no overlapping. This would be true for $Z \leq 1$ or very porous material (ε_o large). To obtain a more realistic and flexible model, Lindner and Simonsson (1981) in their partially sintered sphere model (PSSM) represented the initial solid structure as an aggregate of truncated spheres (i.e. overlapping spheres) in contact with each other in an initial stage of sintering. In the PSSM-model, the pore reaction surface area tends to zero with decreasing porosity. Depending on the values of the structural parameters, λ (initial degree of sintering of spheres estimated from microscopic pictures of the solid structure) and ε (porosity), the PSSM-model can predict an initial increase of the reaction surface area with conversion. In general, however, the degree of overlapping of spheres is not uniform throughout the solid structure. Thus, one value for λ cannot be used. Sotirchos and Yu (1988) further refined this model by allowing grains of different shapes (e.g. sphere, cylinder, and

plate) to randomly overlap with each other. Since many solid structures do not have a uniform grain size, these authors also allowed for the possibility of a grain size distribution. The resulting expressions obtained for the reaction and pore surface area are

$$S^* = \frac{\varepsilon_r \int_{Y(t)}^{r_{o,max}} r_r^{F_g-1}\, n_o(r_o)\, dr_o}{\varepsilon_o \int_{r_{o,min}}^{r_{o,max}} r_o^{F_g-1}\, n_o(r_o)\, dr_o} \qquad (5.6)$$

$$S_p^* = \frac{\varepsilon_p \int_{r_{o,min}}^{r_{o,max}} r_p^{F_g-1}\, n_o(r_o)\, dr_o}{\varepsilon_o \int_{r_{o,min}}^{r_{o,max}} r_o^{F_g-1}\, n_o(r_o)\, dr_o} \qquad (5.7)$$

where

ε_r = porosity of reactant solid

ε_p = porosity of pore solid (reactant + product)

r_o = initial grain size (radius for spheres and cylinders or half-thickness for plate)

$r_{o,max,min}$ = initial upper and lower limit of grain size range

$r_{r,p}$ = size of grain of initial size r_o at the reactant (r) and pore surface (p) at time t

Y(t) = lower limit of active grain size range

$n_o(r_o)\, dr_o$ = number of grains per unit volume with size in the initial size range $[r_o, r_o+dr_o]$

F_g = grain shape factor (3 for a sphere, 2 for a cylinder, and 1 for a plate)

A better description of the solid structure is obtained with this model than for the grain model. The overlapping grain (random grain) model is more flexible and powerful than

grain model in that various behaviors (e.g. a maximum in the rate-conversion profile) can be adequately predicted by this model. This type of model has been successful in predicting the deactivation in hydrodemetallation catalysts (Van Eekelen, 1973; Smith, 1988). However, as with all models which try to closely approximate realistic behavior, the computational complexity of the random grain model is greater than that of the grain model.

In this thesis, SEM micrographs of the fresh sorbents used in sulfidation experiments (e.g. Figures 4.15, 4.21, 4.27 and 4.29) show that the solids can be more closely described as aggregates of individual grains rather than a solid structure with well-defined pores. Modeling of the sulfidation of these systems was, therefore, undertaken with the grain model. In comparison, the random grain model was also used to examine whether this could better predict the experimental reaction profiles. Results from this analysis are presented in the following sections.

5.2 THE GRAIN MODEL

Several different desulfurization systems have been modeled with the grain model. Gibson and Harrison (1980) and Ranade and Harrison (1981) used the grain model to describe the ZnO-H_2S reaction system. The Fe_2O_3-H_2S system was also analyzed with the grain model (Tamhankar et al., 1981). The resistances in the latter system were due to chemical reaction and pore diffusion and, thus, application of the constant property (i.e. no structural changes due to reaction and/or sintering) grain model was good. For the ZnO-H_2S system poorer agreement with the constant grain model was observed (Gibson and Harrison, 1980) which was later improved by incorporating structural changes due to reaction and sintering (Ranade and Harrison, 1981).

The gas-solid sulfidation reaction can be represented by the general stoichiometry

$$A(g) + bB(s) \text{ ---> } cC(g) + dD(s) \qquad (5.8)$$

The solid reactant is visualized as being composed of a large number of non-porous grains of regular geometry (i.e. sphere, cylinder, or plate). Each grain reacts like a shrinking core. As the reaction proceeds, the unreacted core decreases in size while maintaining its original geometric shape. Around the unreacted core, a solid product layer which may be porous or nonporous is developed. Depending on the relative density of the solid product and reactant, the overall size of the grain may change.

There are several possible resistances to the gas-solid reaction rate, such as resistances due to mass transfer, pore diffusion, product layer diffusion, and chemical (surface) reaction. In the experiments performed in this study, both mass transfer and pore diffusional limitations were eliminated by suitable choices of gas flowrate, sample quantity, and particle size and macroporosity. Only product layer diffusion and chemical reaction resistances were important.

The expressions derived for the grain model (Szekely et al., 1976) are based on the assumptions of: 1. isothermal reaction; 2. first order intrinsic reaction rate with respect to gas concentration 3. irreversible reaction 4. equimolar counter-diffusion 5. pseudo-steady state approximation and 6. structural changes due only to reaction (i.e. no sintering).

The rate of disappearance of reactant A by an irreversible first order surface chemical reaction is

$$R_s = kC_{As} \qquad (5.9)$$

where R_s is the reaction rate (e.g. moles of A per unit time per unit surface area), k is the heterogeneous rate constant, and C_{As} is the concentration of the reactant gas at the reaction surface.

Assuming equimolar counter-diffusion of the reactants and product species, the diffusion rate through the product layer is

$$-A_x D_e dC_A/dr = A_x D_e dC_C/dr \qquad (5.10)$$

where A_x is the cross-sectional diffusion area. This yield the equation

$$R_s = \frac{D_e(C_{Ao}-C_{As})}{A_r \int_{r_p}^{r_r} \frac{dr}{A_{r,p}}} \qquad (5.11)$$

where C_{Ao} is the concentration of the reactant gas in the bulk, $A_{r,p}$ is the reaction and pore surface area, respectively, $r_{r,p}$ is the distance from the center (sphere), axis (cylinder), or plane of symmetry (plate) to the reaction and pore surface of the grain, respectively. For solid state diffusion, Eq (5.9) and (5.11) would have to be modified with the concentration of the diffusing ions replacing the concentration of the reactant gas. In this study, it was assumed that the H_2S concentration is equivalent (or proportional) to the concentration of the diffusing ions. This was verified by sulfidation experiments performed with various H_2S concentration. It was determined that the product layer diffusion rate had a first-order dependence on the bulk H_2S concentration (discussed later in Section 5.4.1). With the assumption of pseudo-steady state conditions, these two equations (5.9 and 5.11) can be combined resulting in

$$R_s = -\frac{C_{Ao}}{\frac{1}{k} + \frac{A_r}{D_e}\int_{r_p}^{r_r} \frac{dr}{A_{r,p}}} \qquad (5.12)$$

The rate of reaction of A can be expressed in terms of the rate of disappearance of B by

$$bR_s = \rho_s dr_r/dt \tag{5.13}$$

The fractional conversion (X), r_p, and r_o are related by

$$X = 1 - (r_r/r_o)^{Fg} \tag{5.14}$$

$$r_p^{Fg} = Zr_o^{Fg} + (1-Z)r_r^{Fg} \tag{5.15}$$

$$r_o = \frac{F_g}{A_{o,s}\rho_s} \tag{5.16}$$

Combining these equations (5.13-5.16), the following simplified equations can be derived

$$t^* = g_{Fg}(X) + \sigma_s^2 p_{Fg}(X) \tag{5.17}$$

where

t^* = dimensionless time

$$= \left(\frac{bk}{\rho_s r_o}\right) C_{A_o} t \tag{5.18}$$

$g_{Fg}(X)$ = resistance due to chemical reaction

$$= 1-(1-X)^{1/Fg} \tag{5.19}$$

$p_{Fg}(X)$ = resistance due to diffusion through the product layer

$$= 3\left\{\frac{Z-[Z+(1-Z)(1-X)]^{2/3}}{Z-1} - (1-X)^{2/3}\right\}, \text{ sphere} \tag{5.20}$$

$$= \frac{[Z+(1-Z)(1-X)]\ln[Z+(1-Z)(1-X)]}{Z-1} + (1-X)\ln(1-X), \text{ cylinder} \tag{5.21}$$

$$= ZX^2, \text{ plate} \tag{5.22}$$

σ_s^2 = product layer diffusion resistance / chemical reaction resistance

$$= kr_o/2F_gDe \tag{5.23}$$

where k is the intrinsic rate constant (cm/s); ρ_s is the solid reactant density (mmol/cm^3); r_o is the initial grain radius (initial half-thickness for plate) (cm); A_{os} is the initial specific surface area (cm^2/mmol); C_{Ao} is the concentration of the gaseous reactant in the bulk gas (mmol/cm^3); F_g is the shape factor (3=sphere; 2=cylinder; 1=plate); Z is the ratio of the product to reactant molar volume; and De is the product layer diffusion coefficient (cm^2/s).

The sulfidation conversion profiles of several Zn-Ti-O and ZnO sorbents were analyzed with the grain model. The goal of this analysis was to understand the role that TiO_2 plays in affecting the reaction after a certain extent of conversion. Consequently, it was necessary to determine the effect of TiO_2 on the product layer diffusion. The diffusion coefficient (De) was the fitting parameter in this model. The values of k, the intrinsic rate constant, were obtained from the Arrhenius constants (Table 4.4) calculated from initial rate experiments. The sulfidation data were obtained from experiments conducted with 2 mol% H_2S-1 mol% H_2-97 mol% N_2. Experimental data with higher concentrations of H_2 were not used for this part of the study because at higher temperature (e.g. 800°C) the vapor phase reaction between Zn and H_2S can result in pore plugging. This can lead to an unexpected decrease in the reaction rate.

A comparison of the experimental results and the predicted conversion profiles is shown in Figures 5.2 and 5.3 for ZnO at a low (400-600°C) and high (700-800°C) temperature range. The values of the parameters used in the model are listed in Table 5.1. Also listed in Table 5.1 are the calculated diffusion coefficients. The grains were assumed to have a spherical shape (F_g=3), which was confirmed after examining the material under a scanning electron microscope. The initial grain radius was calculated from Eq. (5.16) for F_g=3.

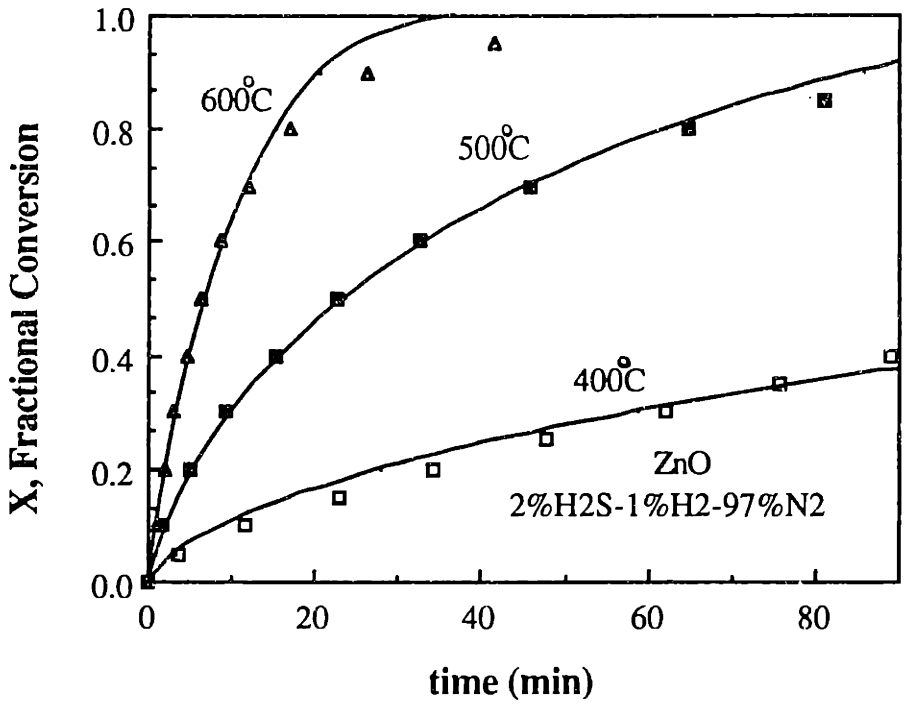

Figure 5.2 Comparison of experimental sulfidation profiles of ZnO at 400-600°C (2%H2S-1%H2-97%N2) with calculated profiles from grain model.

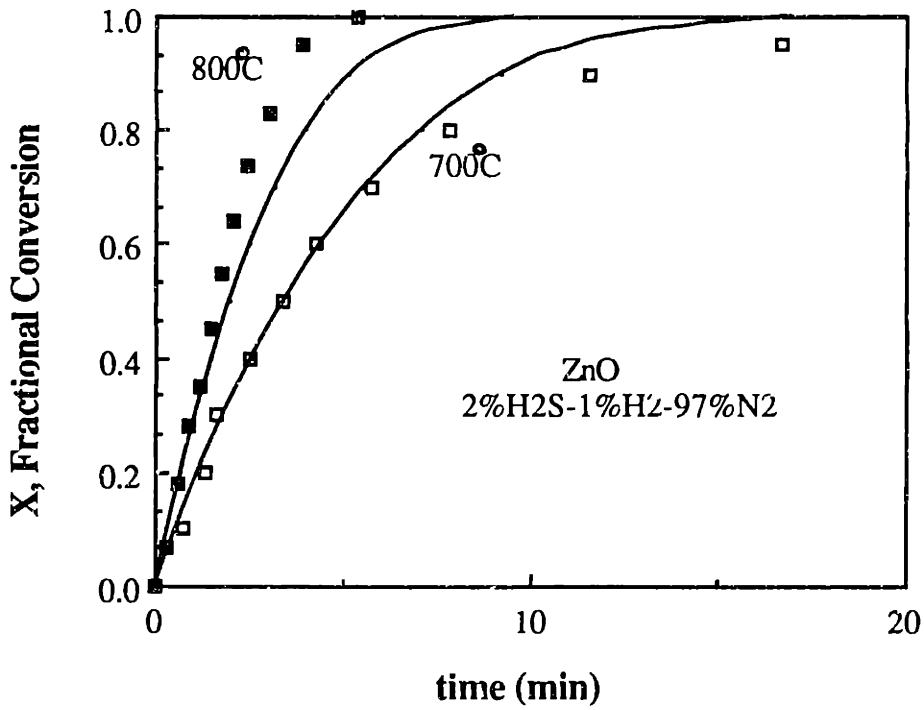

Figure 5.3 Comparison of experimental sulfidation profiles of ZnO at 700 and 800°C (2%H2S-1%H2-97%N2) with calculated profiles from the grain model.

Table 5.1 Parameter values used to calculate ZnO conversion profiles in Figures 5.2 and 5.3

$A_{o,s}$ (surface area, $cm^2/mmol$)	1961
ρ_s (density, $mmol/cm^3$)	68.9
k (rate constant, cm/s)	1.3exp[10.3kcal/mol/RT]
Molar Gas Composition	2% H_2S-1% H_2-97% N_2
Z	1.64
F_g	3
b	1
De (cm^2/s) - 400°C	$3.8x10^{-10}$
500°C	$3.5x10^{-9}$
600°C	$3.5x10^{-8}$
700°C	$3.0x10^{-7}$

However, the calculated grain radius was larger than the grain radius observed in SEM micrographs of ZnO (Figures 4.15 and 4.27). Figure 5.4a shows the grain size distribution of ZnO (surface area = 2.41 m^2/g, calcined at 720°C for 4 h) measured from SEM micrographs. The discrepancy between the calculated grain radius and the measured grain radius was even greater with more sintered materials. Figure 5.4b shows the grain size distribution of ZnO (surface area = 1.33 m^2/g) calcined at the same temperature for a longer period of time (12 h). The calculated grain radius was 0.40 μm while the measured grain size distribution had a peak centered at ~0.15 μm. The SEM micrograph of this sintered ZnO is shown in Figure 5.5. The solid structure is characterized by overlapping grains which causes the error in the calculated grain radius.

At 400°C ($\sigma_s^2 \geq 10$), the system was controlled by the diffusion through the product layer except during the intial period of the reaction. At 500 and 600°C, both chemical reaction and product layer diffusion were controlling. Chemical reaction alone controlled the system at 700 and 800°C ($\sigma_s^2 < 0.1$).

The agreement between the predicted and the experimental results was quite good at temperatures up to 700°C considering that the reduction in surface area due to the ov apping of product layer and sintering which was observed for ZnO (Figures 5.2 and 5.3) was ignored in the model. The grain model predicted an increasing surface area with sulfidation while the experimental results found a decrease in the surface area for sulfidation at 650°C (Figure 5.6). Sintering appears to have no effect on the conversion profiles as indicated by the relatively good fit between the model prediction and the experimental profiles. Some sintering takes place at 650°C, However, at this temperature, product layer diffusion resistance has a relatively minor effect. Ranade and

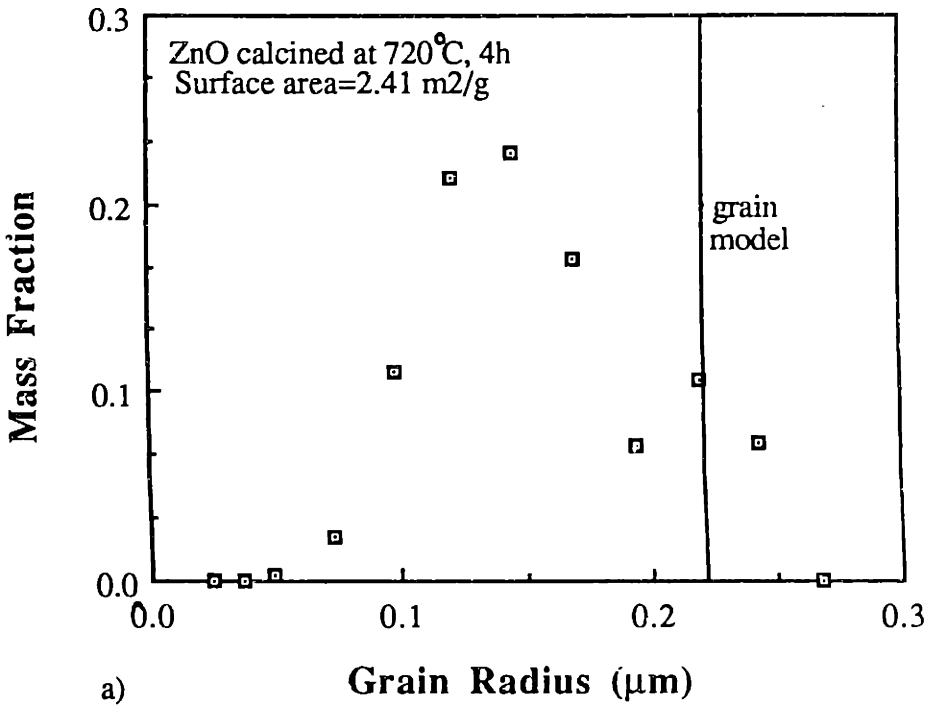

a)

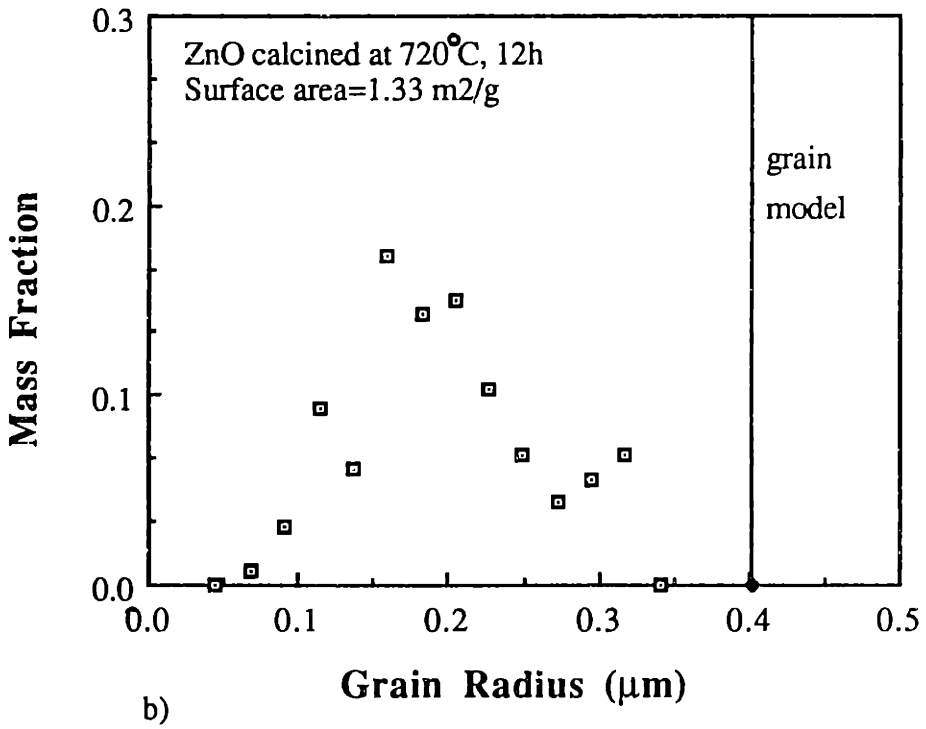

b)

Figure 5.4 Grain size distribution of a) ZnO, 2.41 m2/g and b) ZnO, 1.33 m2/g. (Comparison with the grain model)

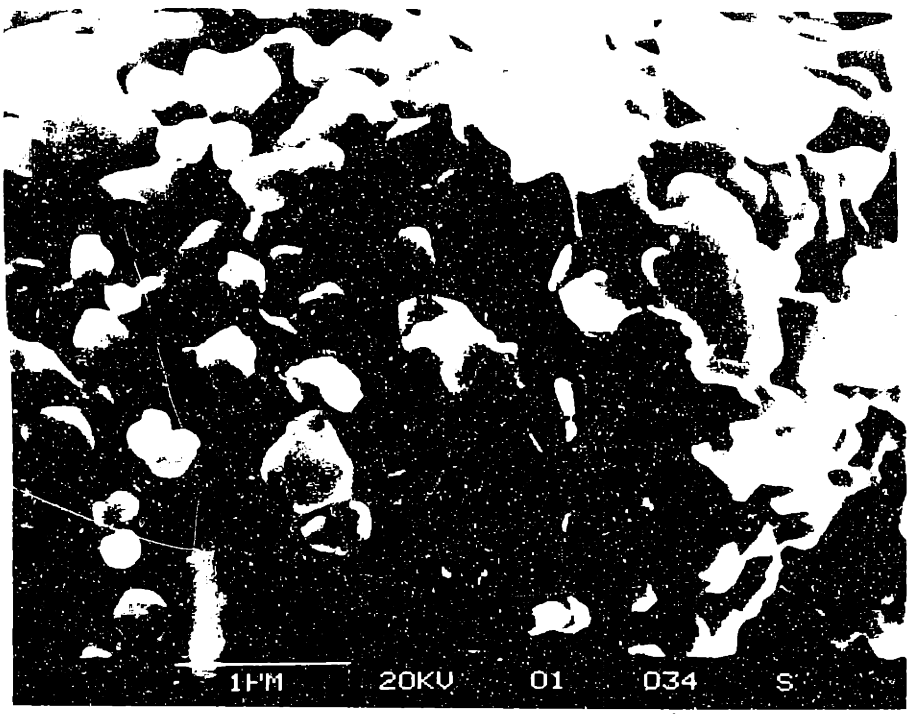

Figure 5.5 SEM micrograph of ZnO calcined at 720°C, 12 h. (Surface area: 1.33 m^2/g)

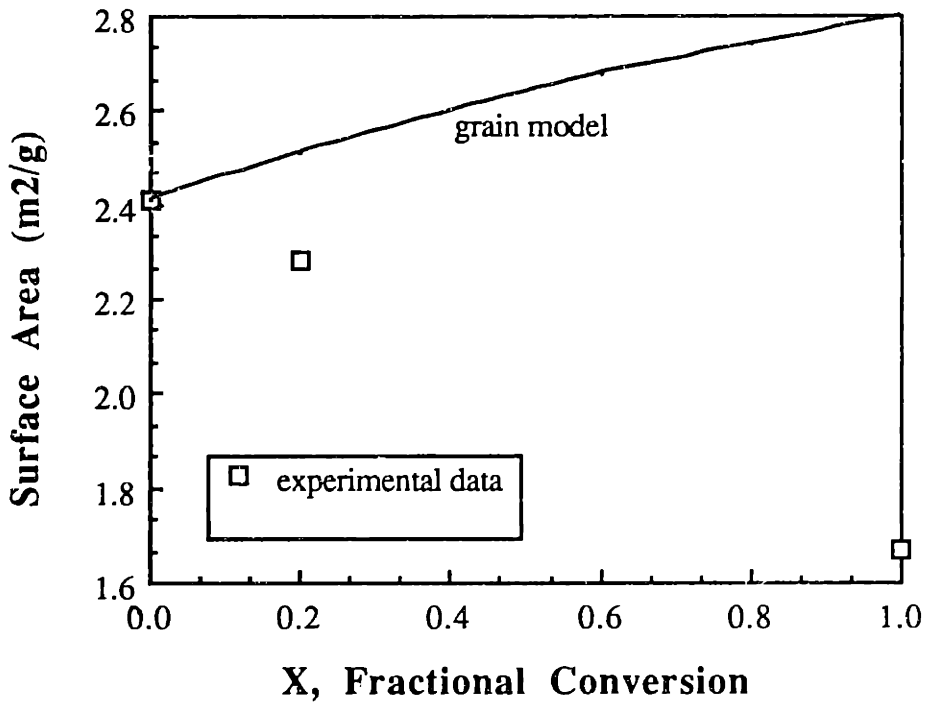

Figure 5.6 Comparison of the predicted surface area change from the grain model with the experimental data at 650°C (2% H2S-1%H2-97%N2) for ZnO.

Harrison (1980) observed similar results with ZnO. When they incorporated sintering into the model, it had very little effect on the predicted time-conversion profiles, because at temperatures where sintering is important grain diffusion resistance is negligible.

At 800°C, the model tends to underpredict the experimental results (Figure 5.3). At this temperature, however, there may be enhancement of the actual reaction rate by the homogeneous reaction, $Zn(g)+H_2S(g)=ZnS(s)+H_2(g)$ (discussed in Chapter 4).

The grain model was also used to describe the sulfidation of the Zn-Ti-O solids. The predicted valuess from the grain model and the experimental results for both sorbent Z2T-a (Figures 5.7 and 5.8) and Z2T3 (Figure 5.9) were not as close as for sorbent ZnO. Physical properties and product layer diffusion coefficients for the Zn-Ti-O sorbents are listed in Table 5.2. The modeling was based on spherical grains. The calculated sulfidation profiles underpredicted the experimental results at low conversion and overpredicted them at higher conversion. Sintering was eliminated as a cause of this decrease in the reaction rate since the surface area of sulfided Z2T3 and Z2T-a changed only slightly from the fresh sorbent value.

The poor agreement between the grain model and the experimental results was due either to unaccounted intrinsic chemistry of the Zn-Ti-O system or to the physical properties of the material. The term intrinsic chemistry of the Zn-Ti-O system is used to indicate a potential decrease in the reaction rate after a certain extent of sulfidation similar in all Zn-Ti-O sorbents. This can occur by a change in the chemical phase

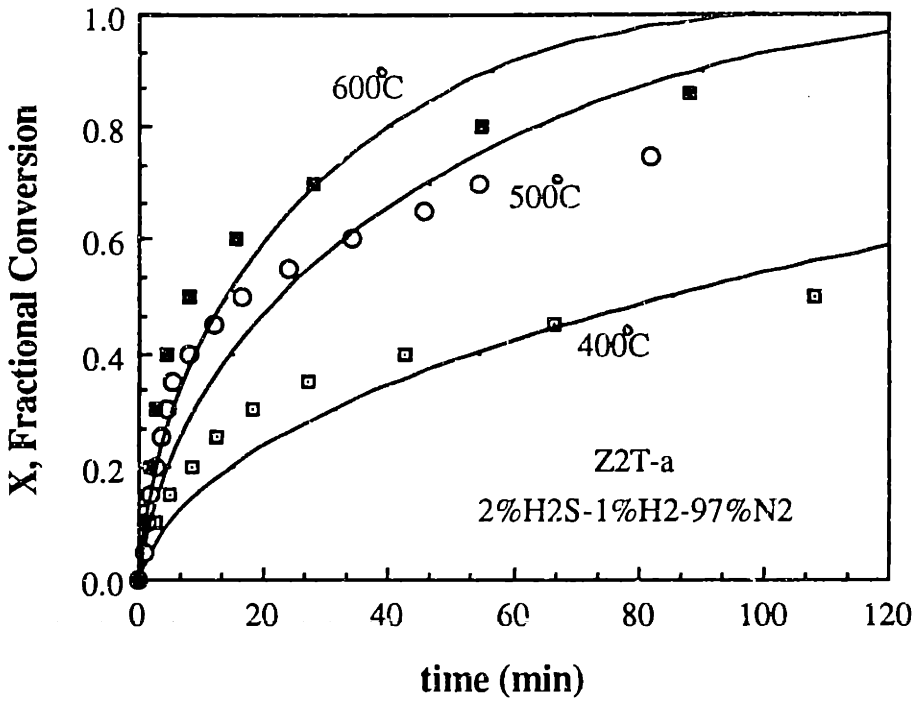

Figure 5.7 Comparison of experimental sulfidation profiles of Z2T-a at 400-600°C (2%H2S-1%H2-97%N2) with calculated profiles from the grain model.

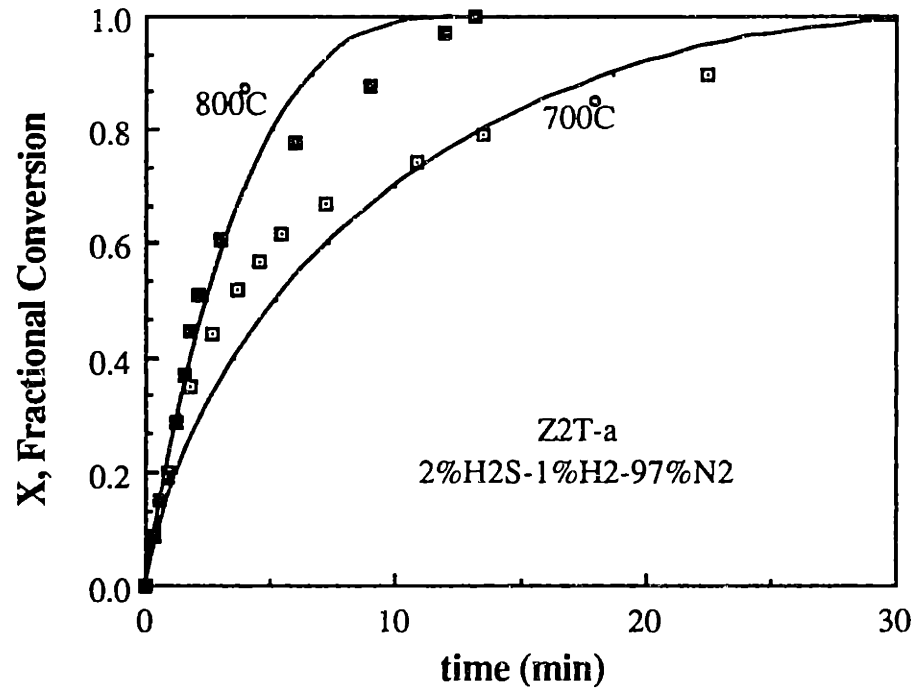

Figure 5.8 Comparison of experimental sulfidation profiles of Z2T-a at 700 and 800°C (2%H2S-1%H2-97%N2) with calculated profiles from the grain model.

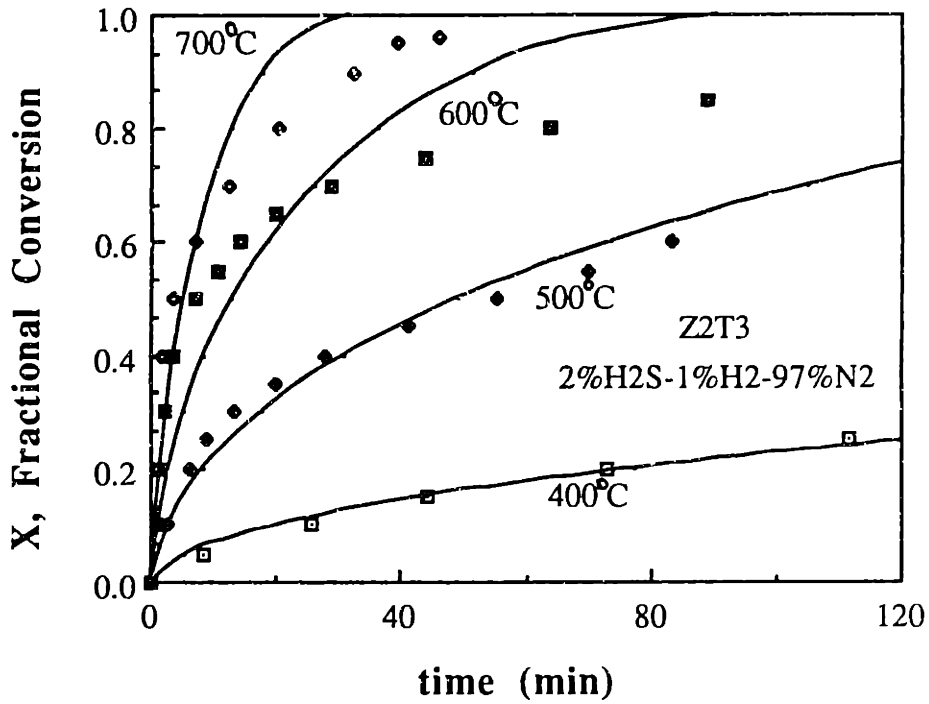

Figure 5.9 Comparison of experimental sulfidation profiles of Z2T3 at 400-700°C (2%H2S-1%H2-97%N2) with calculated profiles from the grain model.

Table 5.2 Parameter values used to calculate conversion profiles in Figures 5.7, 5.8 and 5.9

Z2T	
$A_{o,s}$ (surface area, $cm^2/mmol$)	9973
ρ_s (density, $mmol/cm^3$)	21.8
k (rate constant, cm/s)	0.40exp[9.3kcal/mol/RT]
Molar Gas Composition	2% H_2S-1% H_2-97% N_2
Z	1.45
F_g	3
b	0.5
De (cm^2/s) - 400°C	$1.3x10^{-10}$
500°C	$6.7x10^{-10}$
600°C	$1.2x10^{-9}$
700°C	$5.0x10^{-9}$
Z2T3	
$A_{o,s}$ (surface area, $cm^2/mmol$)	9216
ρ_s (density, $mmol/cm^3$)	11.7
k (rate constant, cm/s)	0.40exp[9.3kcal/mol/RT]
Molar Gas Composition	2% H_2S-1% H_2-97% N_2
Z	1.22
F_g	3
b	0.5
De (cm^2/s) - 400°C	$4.2x10^{-11}$
500°C	$6.0x10^{-10}$
600°C	$3.3x10^{-9}$
700°C	$1.5x10^{-8}$

after a certain extent of sulfidation to a much less reactive phase than the initial phase. During sulfidation sorbent Z2T-a, which contained only the phase Zn_2TiO_4, formed $Zn_2Ti_3O_8$ and ZnS. After 67% conversion, only the phases $Zn_2Ti_3O_8$ and ZnS were present. Experiments with Z2T-b were also performed. Z2T-b, like Z2T-a, contained only Zn_2TiO_4. However, its physical properties were very different from Z2T-a. It had a higher surface area (13.9 m^2/g) and a more uniform grain size (Figure 4.21). As shown in Figure 5.10, the agreement between the calculated conversion profiles and the experimental results for Z2T-b was much better than for Z2T-a. The observed differences in the progress of reaction for Z2T-a and Z2T-b can then be attributed to the difference in their grain morphology (i.e. grain size distribution). Varying the grain size distribution has been shown to have a substantial effect on the conversion profile (Bartlett et al., 1973; Szekely and Propster, 1975; Sotirchos and Yu, 1988).

The grain model, although successful in predicting the conversion evolution of ZnO has several drawbacks. First, based on the assumption that the solid was composed of non-overlapping grains, the calculated grain radius was larger than the grain radius measured from SEM micrographs. The solid structures observed in the photographs were composed of overlapping grains. Second, it failed to predict the surface area changes observed for ZnO. The possibility of overlapping product layer which will decrease the surface area was not taken into account. Last, in order to model Zn-Ti-O solids such as Z2T-a and Z2T3, non-uniform grain sizes must be used.

5.3 THE RANDOM GRAIN MODEL

In order to more closely simulate the solid structure of ZnO and Zn-Ti-O, a random grain model will be used. The porous solid is simulated as an assemblage of grains randomly distributed in space. The centers of the grains are randomly placed in space

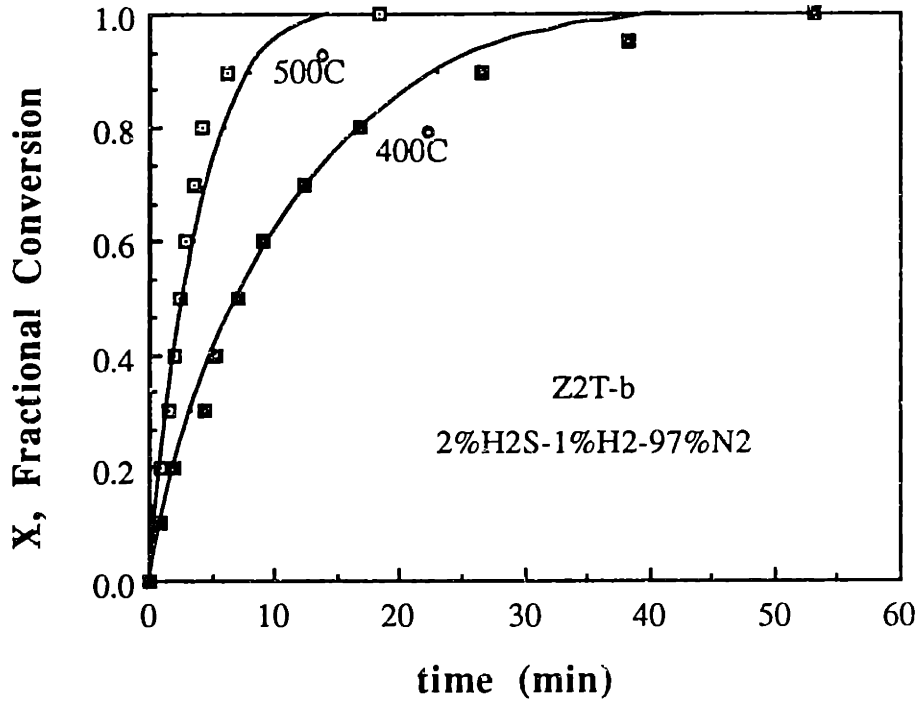

Figure 5.10 Comparison of experimental sulfidation profiles of Z2T-b at 400 and 500°C (2%H2S-1%H2-97%N2) with calculated profiles from the grain model.

and overlapping of the grains is permitted. This is consistent with the observed solid structures of the sorbents studied in this thesis. If the solid product occupies more volume than a stoichiometrically equal volume of reactant, then overlapping of the product resulting in pore closure is possible. Contributions from particle sintering are ignored in using this model. Since the solid reactants were calcined at 720°C for 4-12 h, sintering of the reactants is minimal except at higher reaction temperatures where product layer diffusion is neglible. As discussed previously, Ranade and Harrison (1980) found that incorporating sintering into the grain model for ZnO sulfidation did not effect the predicted time-conversion profile because at temperatures where sintering is important , product layer diffusion is relatively unimportant.

Early models based on random grains were limited to only spherical grain shape (Weissberg, 1963; Haller, 1965; Van Eekelen, 1973). These model was further extended to include various grain shapes and solid product formation by Sotirchos and Yu (1988). As discussed in Section 5.1, the porosity (ε) and the surface area (S) are uniquely defined by this model. The expressions for the initial porosity (ε_o) and the initial surface area per unit volume (S_o) of grains randomly distributed in space are

$$\varepsilon_o = \exp(-\varphi_{ox}) \tag{5.24}$$

$$S_o = \varepsilon_o S_{ox} \tag{5.25}$$

$$S_{ox} = F_g f \int_{r_{o,min}}^{r_{o,max}} r_o^{F_g - 1} n_o(r_o)\, dr_o \tag{5.26}$$

$$\varphi_{ox} = f \int_{r_{o,min}}^{r_{o,max}} r_o^{F_g} n_o(r_o)\, dr_o \tag{5.27}$$

where φ_{ox} and S_{ox} are the total volume and specific surface area (cm^2/cm^3) of grains at time t without correction for overlapping, respectively; F_g is the grain shape factor (sphere=3; cylinder=2; plate=1); r_o is the initial grain radius; f is the grain geometric factor (sphere=$4\pi/3$; cylinder=πL_{avg}; plate=$2A_{avg}$), L_{avg} and A_{avg} are the average grain length of the cylinder and average grain surface area of plate-like grains, respectively; $n_o(r_o)dr_o$ is the number of grains per unit volume with size in the initial size range $[r_o, r_o+dr_o]$. The initial specific surface area (S_o) is obtained by the fact that the probability of any random point not lying within a grain is equal to the initial porosity (ε_o). Therefore, only a fraction (ε_o) of the surface (S_{ox}) has a probability of lying outside the solid volume.

For a reactive system, equations similar to Eq. 5.24-5.27 can be derived for both the reaction surface and the pore surface. The assumption was made that the number of grains per unit volume does not change with the reaction. For the reaction and pore surface at time t, the expressions are

$$\varepsilon_r = \exp\left[-f\int_{Y(t)}^{r_{o,max}} r_r^{F_g} n_o(r_o)\, dr_o\right] \tag{5.28}$$

$$S_r = F_g f \varepsilon_r \int_{Y(t)}^{r_{o,max}} r_r^{F_g-1} n_o(r_o)\, dr_o \tag{5.29}$$

$$\varepsilon_p = \exp\left[-f\int_{r_{o,min}}^{r_{o,max}} r_p^{F_g} n_o(r_o)\, dr_o\right] \tag{5.30}$$

$$S_p = F_g f \varepsilon_p \int_{r_{o,min}}^{r_{o,max}} r_p^{F_g-1} n_o(r_o)\, dr_o \tag{5.31}$$

These expressions for the solid structure can then be incorporated into the rate expressions (5.12 and 5.13) with $S_{r,p}$ (total surface area per unit volume) replacing $A_{r,p}$ (total surface area per unit mass) to yield

$$\frac{dr_r}{dt} = \frac{\frac{-bkC_{Ao}}{\rho_s}}{1+\frac{k}{D_e}\varepsilon_f r_r^{F_g-1}\int_{r_p}^{r_r}\frac{dr}{\varepsilon_{r,p}(t')r^{F_g-1}}} \tag{5.32}$$

The change in the pore radius (r_p) is related to the reaction surface radius of the grain (r_r) by

$$\frac{dr_p}{dt} = -\frac{dr_r}{dt}\left[(Z-1)\frac{\varepsilon_f r_r^{F_g-1}}{\varepsilon_f r_p^{F_g-1}}\right] \tag{5.33}$$

The porosity of the solid (product + reactant) is found by

$$\varepsilon_p = \varepsilon_o-(Z-1)(\varepsilon_f-\varepsilon_o) \tag{5.34}$$

The fractional conversion is calculated with

$$X = \frac{\varepsilon_o-\varepsilon_p}{(Z-1)(1-\varepsilon_o)} \tag{5.35}$$

Equations (5.32)-(5.35) can be used to model a gas-solid reaction system. Again, the effective product layer diffusion coefficient (D_e) is used as a fitting parameter. Different grain size distributions can be incorporated by varying $n_o(r_o)$. This model is much more flexible than the grain model because it can describe various grain structures. For example, with certain values of the physical parameters (i.e. ε_o and S_o), it can predict a

maximum in the reaction rate associated with a maximum in the reaction surface area. With other values of the physical parameters, it can predict a monotomically decreasing reaction rate. However, this model does produce more complex equations than the grain model.

5.4 APPLICATION TO ZnO AND Zn-Ti-O SULFIDATION

5.4.1 ZnO Modeling

For ZnO, based on Figure 5.11, a uniform size of spherical grains was used for the random grain model. Using Eq. (5.24), the initial porosity of the system for spheres is

$$\varepsilon_o = \exp\left[-\frac{4}{3}\pi r_o^3 n_o\right] \tag{5.36}$$

The specific surface area is

$$S_o = n_o 4\pi r_o^2 \varepsilon_o \tag{5.37}$$

Using Eq. (5.36) and (5.37), the grain radius is uniquely defined as

$$r_o = -\frac{3\varepsilon_o}{S_c} \ln\varepsilon_o \tag{5.38}$$

The porosity was obtained from mercury porosimetry measurements. Based on SEM information of a cross-section of the sorbent (Figure 5.12), pores with radius of greater than 1 μm were ignored. These pores were not produced by the space between randomly placed grains and would lead to an erroneously high calculated value for the grain radius.

A useful property which can be calculated with the random grain model for spherical mono-sized grains is the mean pore radius (r_m). Van Eekelen (1973) obtained an

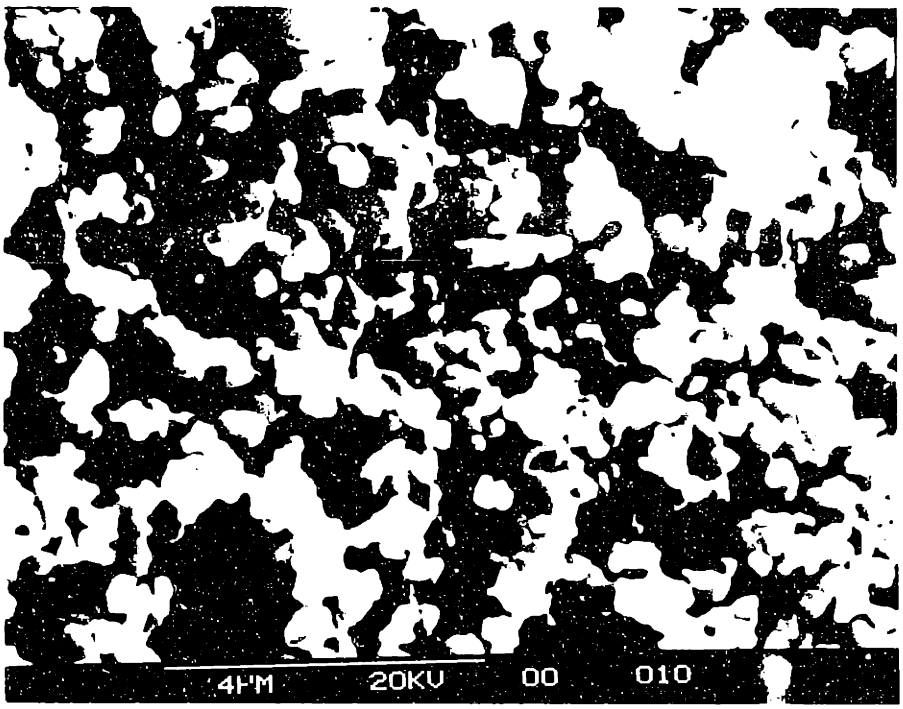

Figure 5.11 SEM micrograph of ZnO calcined at 720°C, 4 h.

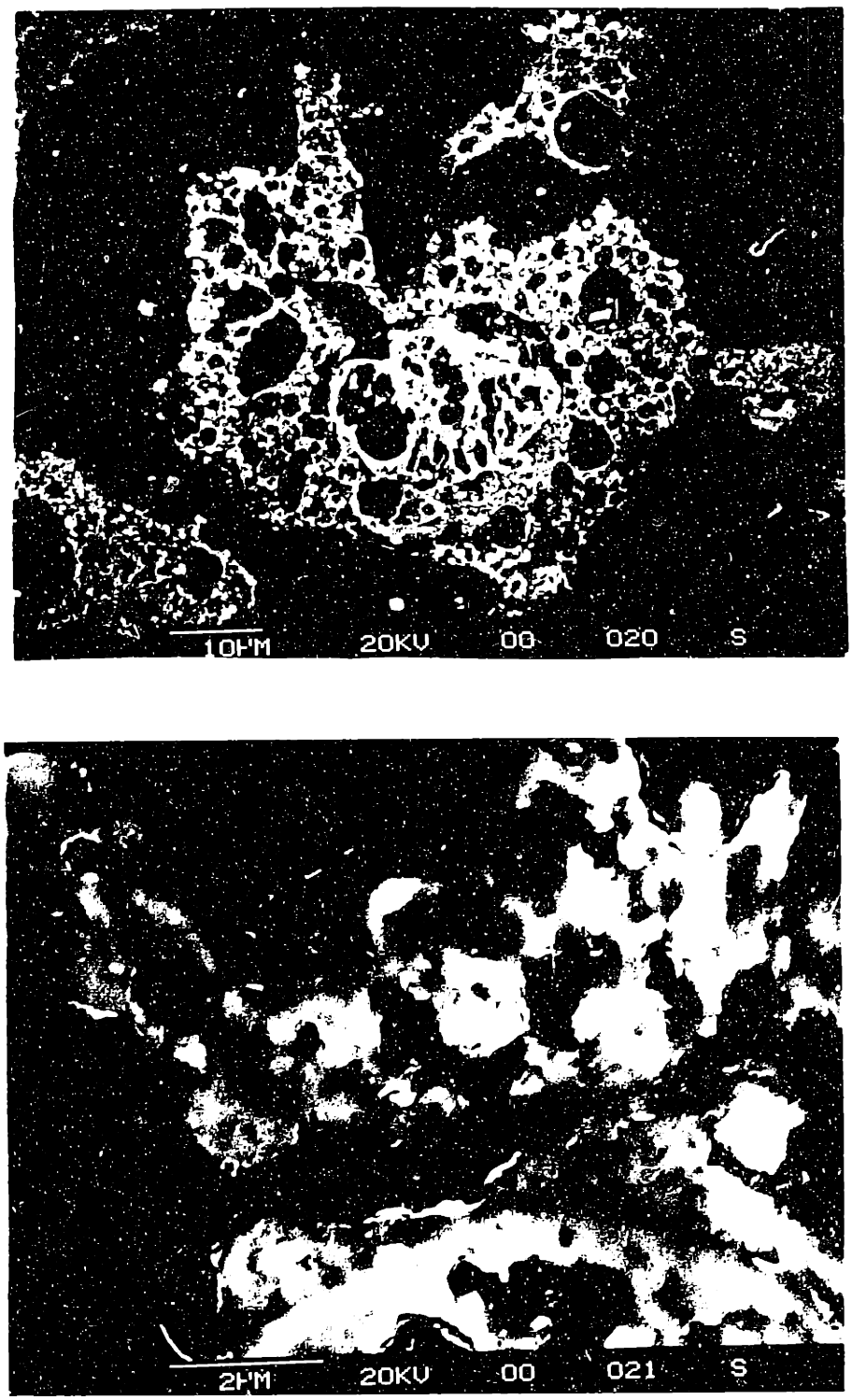

Figure 5.12 SEM micrograph of ZnO cross-sectioned (calcined 720°C, 4 h).

approximate relationship for the mean pore radius which is valid for porosity in the range $0.3 < \varepsilon < 0.8$,

$$r_m = \frac{2\varepsilon_o}{S_o}(1.32-\varepsilon_o) \tag{5.39}$$

The calculated mean pore radius for ZnO using the value of the physical properties values listed in Table 5.3 is 0.16 μm. In comparison, the measured value of the mean pore radius is 0.20 μm.

Modeling of the reaction between ZnO and H_2S was performed with the random grain model (Eq. 5.32-5.35) for spherical grains (Eq. 5.36-5.38). Table 5.3 lists the values of the physical properties for ZnO used in this model. The calculated initial grain radius was 0.16 μm. This was closer to the actual grain size (Figure 5.4a) than the value predicted by the grain model (0.22 μm). A comparison of the predicted reaction profiles with the experimental reaction profiles is shown in Figure 5.13. The values of the effective product layer diffusion coefficients used in the calculation are also listed in Table 5.3.

Unlike the grain model, the random grain model predicted a decreasing surface area with conversion. This was due to overlapping of the product layer. The decrease in surface area was in agreement with the measured value of the surface area after sulfidation at 650°C. Figure 5.14 shows the predicted change in surface area associated with the reaction for both the random grain model and the grain model. In addition, the effective diffusion coefficients calculated for ZnO using the random grain model were slightly smaller than the values found using the grain model. Although the predicted decrease in surface area with conversion in the random grain model would increase the predicted effective diffusion coefficient in comparison to the grain model, the smaller

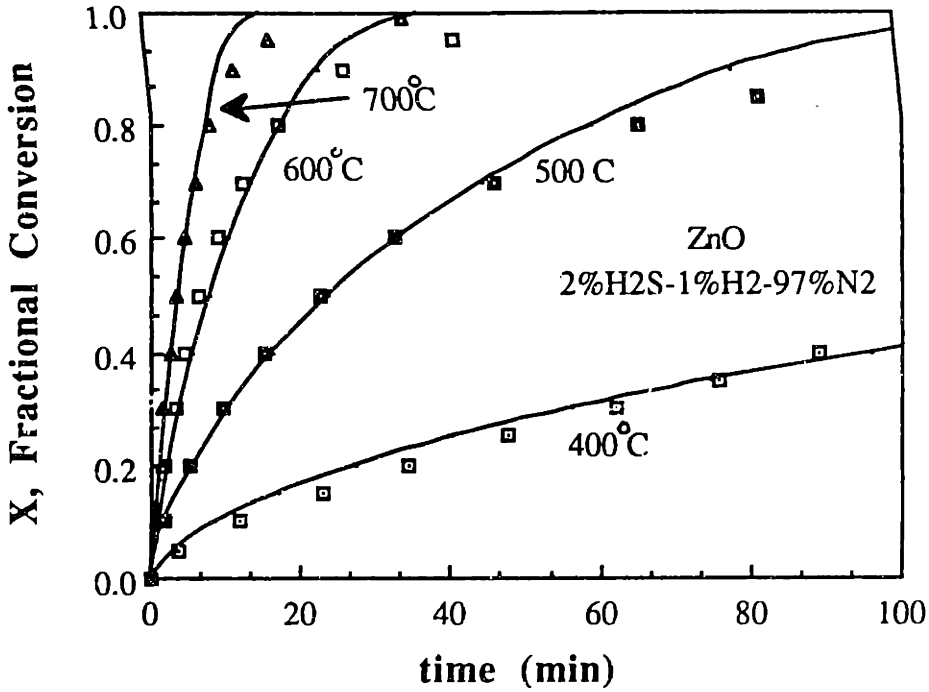

Figure 5.13 Comparison of experimental sulfidation profiles of ZnO at 400-700°C (2%H2S-1%H2-97%N2) with calculated profiles from the random grain model.

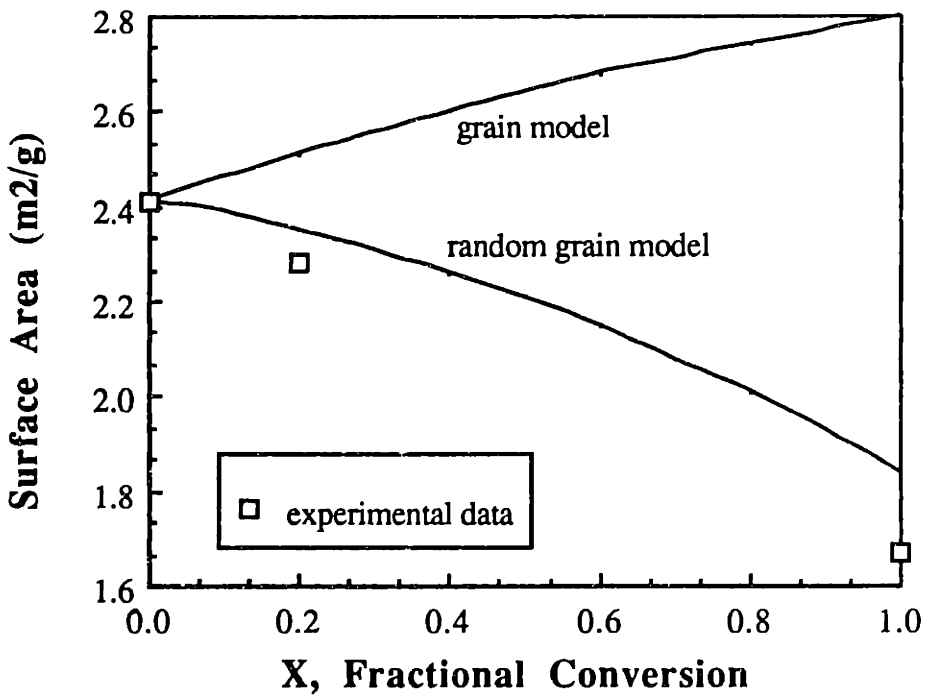

Figure 5.14 Comparison of the surface area variation predicted by the random grain model and the grain model with the experimental results of ZnO sulfidation at 650°C (2%H2S-1%H2-97%N2).

Table 5.3 Parameter values used to calculate ZnO conversion profiles in Figure 5.13

$A_{o,s}$ (surface area, cm^2/cm^3)	$5.54x10^4$
ε_o (porosity)	0.59
ρ_s (density, $mmol/cm^3$)	68.9
k (rate constant, cm/s)	1.3exp[10.3kcal/mol/RT]
Molar Gas Composition	2% H_2S-1% H_2-97% N_2
Z	1.64
F_g	3
b	1
De (cm^2/s) - 400°C	$2.7x10^{-10}$
500°C	$3.0x10^{-9}$
600°C	$2.0x10^{-8}$
700°C	$1.0x10^{-7}$

predicted initial grain radius has the opposite effect and would decrease the diffusion coefficient.

The predicted sulfidation profiles using the value of De calculated from the experiments performed with 2 mol% H_2S-1 mol% H_2-97 mol% N_2 agree very well with the experimental profiles obtained with various H_2S concentrations as shown in Figure 5.15. This indicates that the assumption that the H_2S bulk concentration was equal (or proportional) to the concentration of the species diffusing through the product layer was correct. Eq. 5.11 for the diffusion rate assumes that the driving force is $(C_{Ao}-C_{As})$ where C_{Ao} and C_{As} are the concentrations of H_2S in the bulk gas and at the reaction interface, respectively. However, for solid state diffusion, the driving force should be $(C_{i,o}-C_{i,s})$ where $C_{i,o}$ and $C_{i,s}$ are the concentrations of the diffusing ion at the gas-solid and the reaction interface, respectively. Based on Figure 5.15, the ionic concentration gradient is proportional to H_2S gradient.

5.4.2 Zn-Ti-O Modeling

The random grain model was next applied to sulfidation of Zn-Ti-O solids. From the SEM micrographs, such as Figure 4.21a, Zn-Ti-O solids typically comprise of grains of various sizes. For the modeling, the solid structure was simplified by considering only two discrete grain sizes (discrete bimodal distribution). The sizes of these grains were estimated from the SEM micrographs of the unreacted sorbents. The relative mass fraction of each type of grains was calculated using the surface area and porosity of the solid. The modeling of sorbent Z2T-a and Z2T3 will be discussed. Modeling of the other types of Zn-Ti-O sorbents used a similar approach.

Sorbent Z2T-a consisted of two types of grains, namely small spherical grains of approximately 0.05 μm radius, and flat, plate-like grains, of 0.2 μm (half-thickness). A

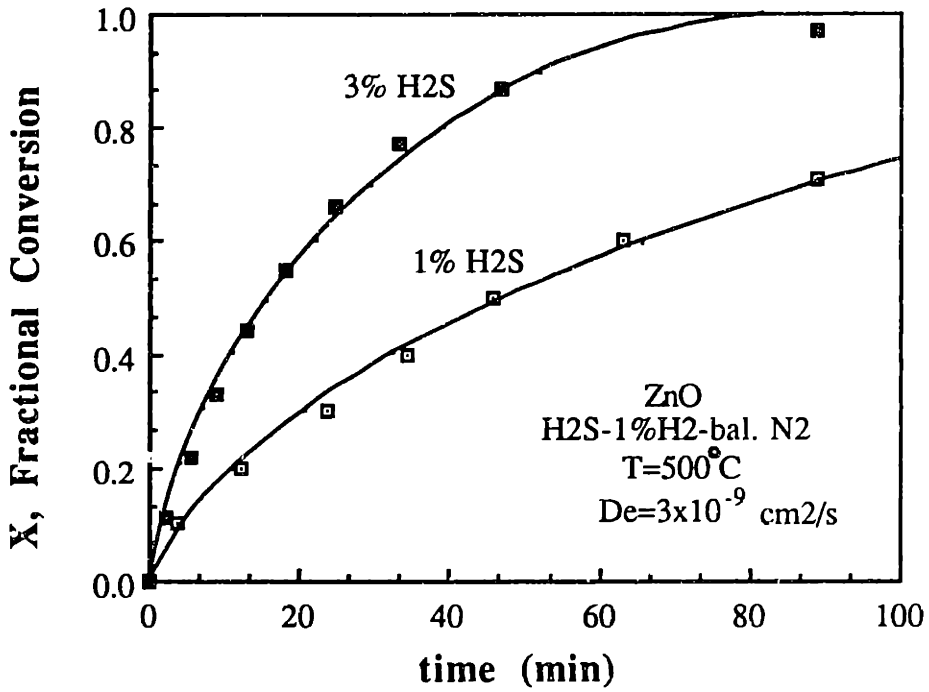

Figure 5.15 Comparison of experimental sulfidation profiles of ZnO reacted at 500°C in 1%H2S and 3%H2S with calculated profiles from the random grain model.

estimate of the relative mass percentage of the two grains types finds approximately a 50-50 distribution from SEM micrographs and porosity and surface area measurements. For the modeling, it was assumed that there was no interaction between the two types of grains (i.e. no overlapping of products originating from the two different grain types).

For the spherical grains, similar reaction and structural equations were used as those for the modeling of ZnO (Section 5.4.1). For reactions of plate-like grains, Eq. 5.36-5.38 become

$$\varepsilon_o = \exp\left[- 2A_{avg} r_o n_o \right] \tag{5.40}$$

$$S_o = n_o 2A_{avg} \varepsilon_o \tag{5.41}$$

$$r_o = - \frac{\varepsilon_o}{S_o} \ln \varepsilon_o \tag{5.42}$$

The inclusion of a discrete bimodal distribution of grain size produced an improvement in the agreement between the experimental reaction profiles and the calculated profiles as can be seen in Figure 5.16 and 5.17. Figure 5.16 shows the reaction profiles at 500°C for the spherical grains and plate-shaped grains. The individual contributions of these two types of grains to the overall conversion profile are also shown in Figure 5.16. The overall predicted conversion profiles at various temperatures are shown in Figure 5.17. The parameter values used to calculate the profiles in Figures 5.16 and 5.17 are listed in Table 5.4. A verification of the improvement obtained by using a discrete bimodal grain size distribution for modeling the sulfidation of sorbent Z2T-a was the agreement between the effective diffusion coefficient predicted from the conversion profiles of both Z2T-a and Z2T-b. Z2T-a and Z2T-b differed only in their

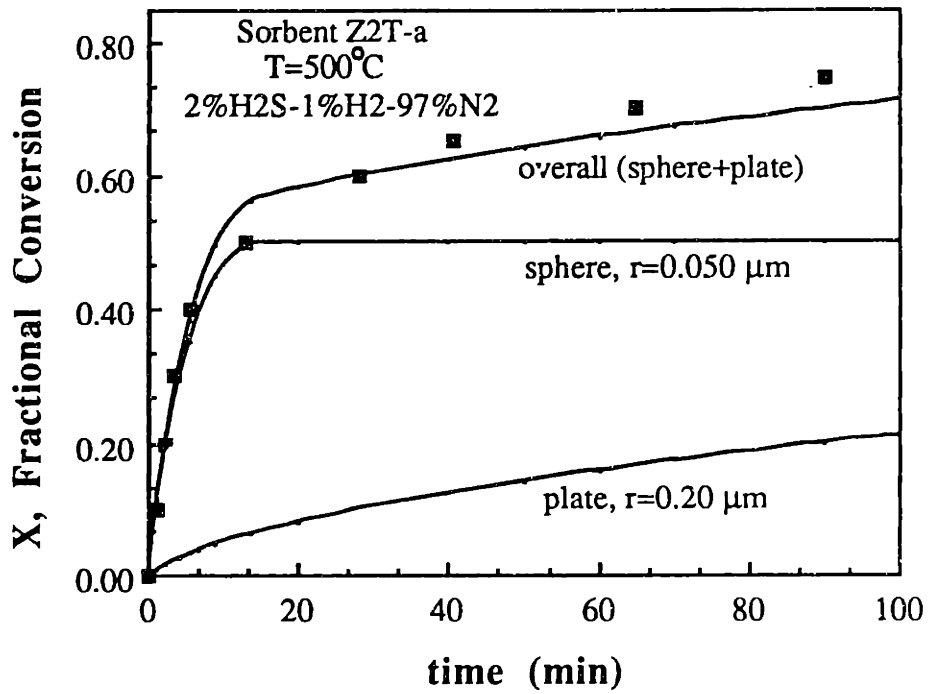

Figure 5.16 Comparison of the experimental sulfidation profile of sorbent Z2T-a at 500°C (2%H2S-1%H2-97%N2) with calculated profile from the random grain model. (Contributions of spherical and plate-like grains are also shown)

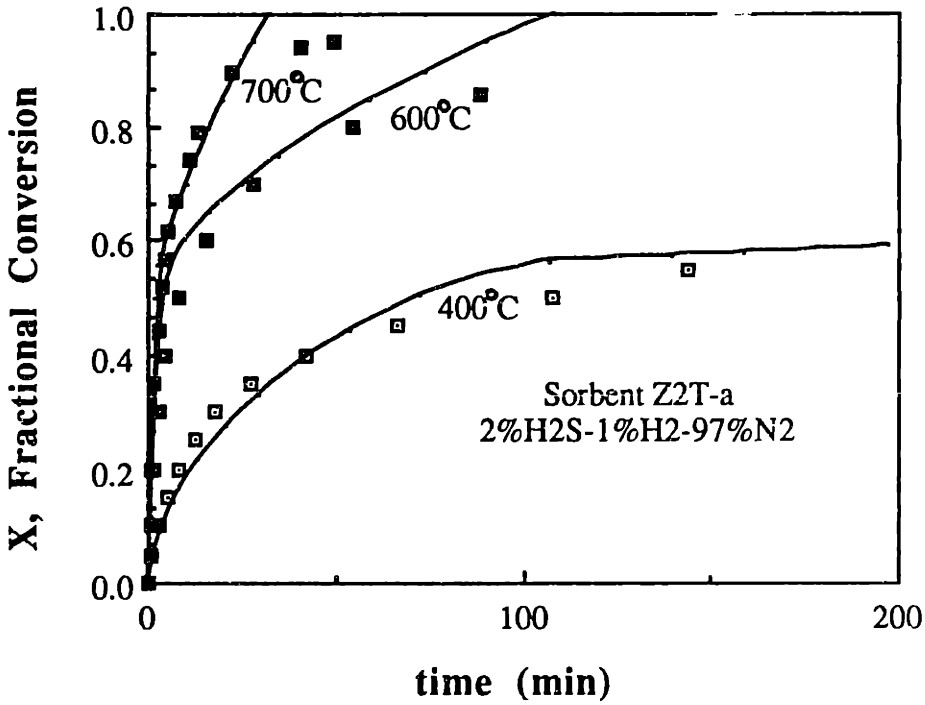

Figure 5.17 Comparison of experimental sulfidation profiles of Z2T-a (2%H2S -1%H2-97%N2) with profiles calculated from the random grain model with a discrete bimodal grain size distribution.

Table 5.4 Parameter values used to calculate Z2T conversion profiles in Figures 5.16 and 5.17

50 wt% sphere-50 wt% plate	
ρ_s (density, mmol/cm^3)	21.8
k (rate constant, cm/s)	0.40exp[9.3kcal/mol/RT]
Molar Gas Composition	2% H_2S-1% H_2-97% N_2
Z	1.45
b	0.5
De (cm^2/s) - 400°C	1.5×10^{-10}
500°C	2.2×10^{-9}
600°C	1.3×10^{-8}
700°C	8.3×10^{-8}
<u>sphere</u>	
ε_o (porosity)	0.42
r_o (grain radius, cm)	5.0×10^{-6}
<u>plate</u>	
ε_o (porosity)	0.72
r_o (grain radius, cm)	2.0×10^{-5}

grain morphology. At 400°C, the calculated effective diffusion coefficient for Z2T-a was $1.8x10^{-10}$ cm^2/s while for Z2T-b, a value of $2.5x10^{-10}$ cm^2/s was calculated. Similar improvement between the predicted and experimental reaction profiles was obtained for sorbent Z2T3 using a bimodal grain size distribution in the random grain model as shown in Figures 5.18 and 5.19. The values used to calculate the profiles in Figures 5.18 and 5.19 are listed in Table 5.5.

5.5 EFFECT OF TiO_2 ON THE PRODUCT LAYER DIFFUSION

The calculated effective diffusion coefficients using the random grain model for the sulfidation of Zn-Ti-O sorbents of various zinc and titanium contents indicated a dependence on the relative amount of titanium in the sorbents. As Figure 5.20 shows, increasing the relative amount of TiO_2 causes a corresponding decrease in the effective product layer diffusion coefficient calculated for sulfidation at 400°C reacting in 2 mol% H_2S-1 mol% H_2-97 mol% N_2. The decrease in De with relative amount of TiO_2 was linear . The best line fit through the points in Figure 5.20 was

$$De\ [cm^2/s] = 2.67x10^{-10} - 3.68x10^{-12}\ y \qquad (5.43)$$

where y is the mol% TiO_2.

The diffusion coefficient can be represented by an Arrhenius expression

$$D = D_o exp(-E/RT) \qquad (5.44)$$

where the pre-exponential factor (D_o) and the activation energy (E) are not temperature dependent. Note, the change in terminology. De is the effective or apparent diffusion coefficient which includes the contributions from several possible diffusion paths. D is the solid diffusion coefficient in general, not necessarily identical to the effective diffusion coefficient. Similar to the Arrhenius equation for chemical reaction, the activation energy for diffusion is associated with the magnitude of energy which must

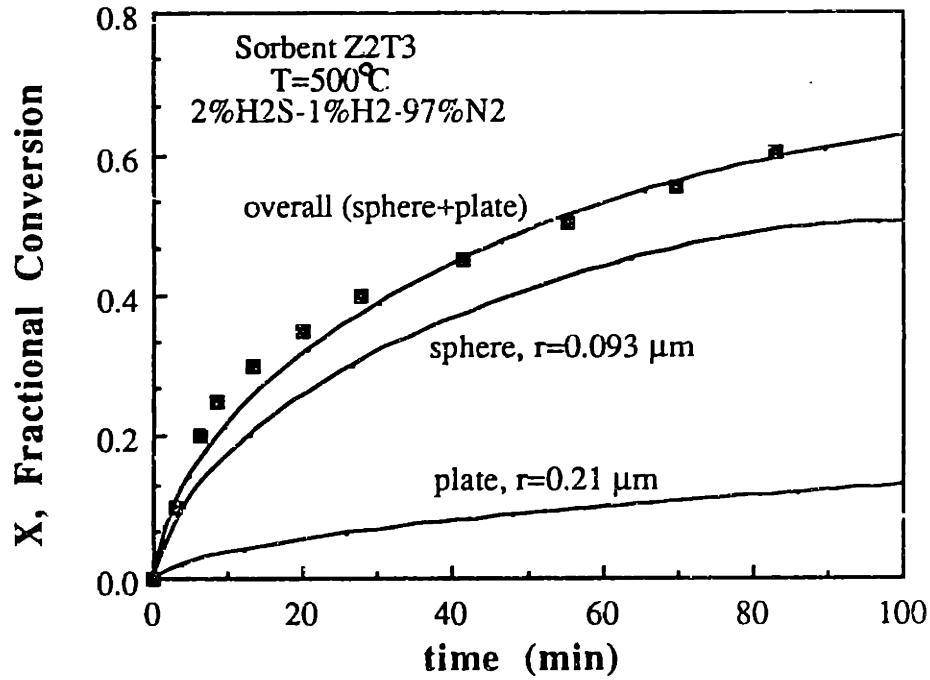

Figure 5.18 Comparison of the experimental sulfidation profile of sorbent Z2T3 at 500°C (2%H2S-1%H2-97%N2) with calculated profile from the random grain model. (Contributions of spherical and plate-like grains are also shown)

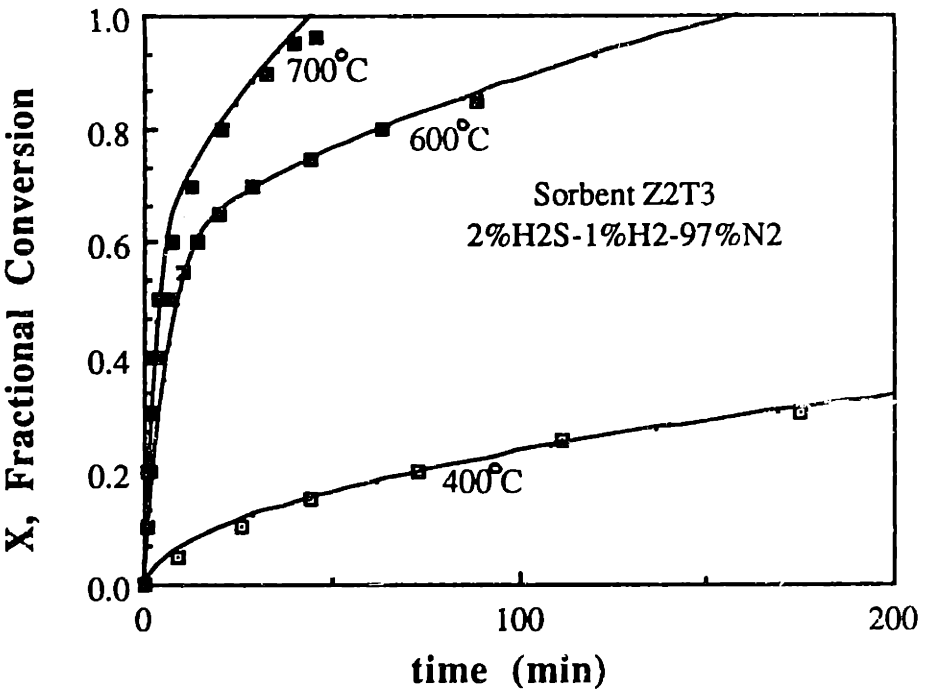

Figure 5.19 Comparison of experimental sulfidation profiles of sorbent Z2T3 (2%H2S-1%H2-97%N2) with calculated profiles from the random grain model with a discrete bimodal grain size distribution.

Table 5.5 Parameter values used to calculate Z2T3 conversion profiles in Figures 5.18 and 5.19.

50 wt% sphere-50 wt% plate	
ρ_s (density, mmol/cm^3)	11.7
k (rate constant, cm/s)	0.40exp[9.3kcal/mol/RT]
Molar Gas Composition	2% H_2S-1% H_2-97% N_2
Z	1.22
b	0.5
De (cm^2/s) - 400°C	3.5×10^{-11}
500°C	4.2×10^{-10}
600°C	3.6×10^{-9}
sphere	
ε_o (porosity)	0.42
r_o (grain radius, cm)	9.3×10^{-6}
plate	
ε_o (porosity)	0.81
r_o (grain radius, cm)	2.0×10^{-5}

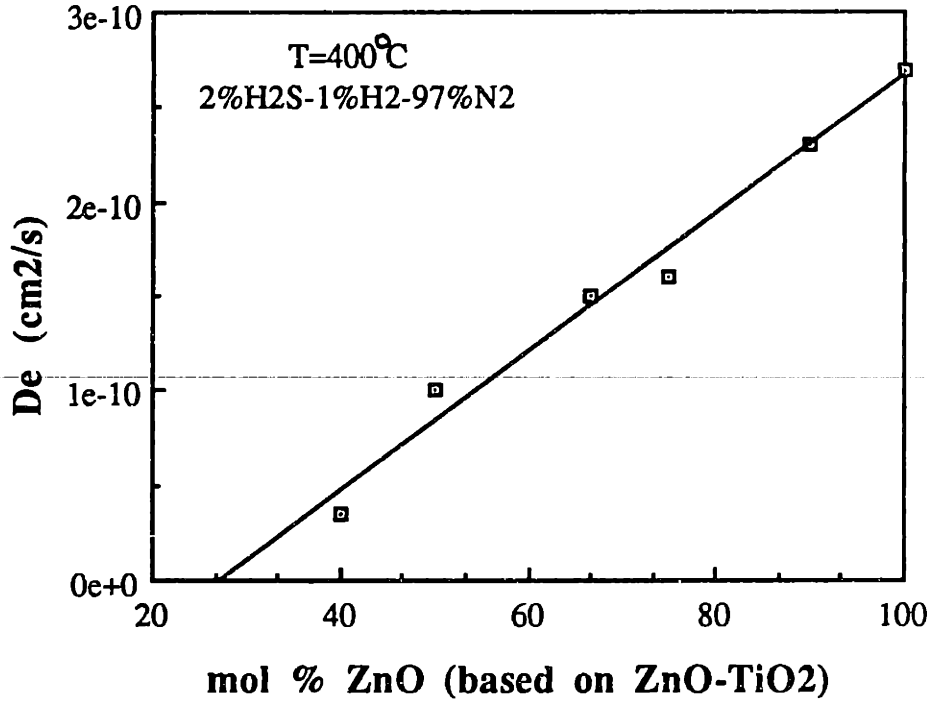

Figure 5.20 Effect of relative amount of TiO2 in the sorbents on the effective product layer diffusion coefficient.

be supplied to overcome the barrier when an atom move from one normal or interstitial site to an adjacent vacant site or interstitial position. The pre-exponential factor, D_o, is directly related to the number of particles involved in the jump or the number of paths over which such jumps can take place. Typically, the value of D_o is in the range of 1-10^{-2} cm^2/s (Bokshtein et al., 1985). By considering diffusion as a special case of reaction rate theory, the diffusion pre-exponential factor for a pure stoichiometric compound may be represented in more fundamental terms (Kingery and Ulmann, 1976) by

$$D_o \text{ (vacancy)} = \gamma\lambda^2 \nu \exp\left[\frac{\Delta S^{\dagger} + \Delta S_s/2}{k}\right] \tag{5.45}$$

$$D_o \text{ (interstitial)} = \gamma\lambda^2 \nu \exp\left[\frac{\Delta S^{\dagger}}{k}\right] \tag{5.46}$$

D_o (vacancy) refers to diffusion via a vacant site mechanism. D_o (intersitial) refers to diffusion along intersitial sites. k is Boltzmann's constant. γ is a geometric factor associated with the number of nearest-neighbor jump sites and the probability that the atoms will jump back to their original position. λ is the jump length or lattice period. ν is the frequency factor which is proportional to the rate of change of the activated complex to the product. $\Delta S^{\dagger}$ is the entropy of the transition state. ΔS_s is the entropy associated with the simultaneous production of both cation and anion vacancies (Schottky disorder).

An Arrhenius plot of the experimentally calculated diffusion coefficients for sorbent ZnO, Z2T, and Z2T3 is shown in Figure 5.21. Table 5.6 lists the calculated Arrhenius constants. The Arrhenius plot of the diffusion coefficient is shown for temperatures up to 600°C. At higher temperatures, values for the diffusion coefficient became less

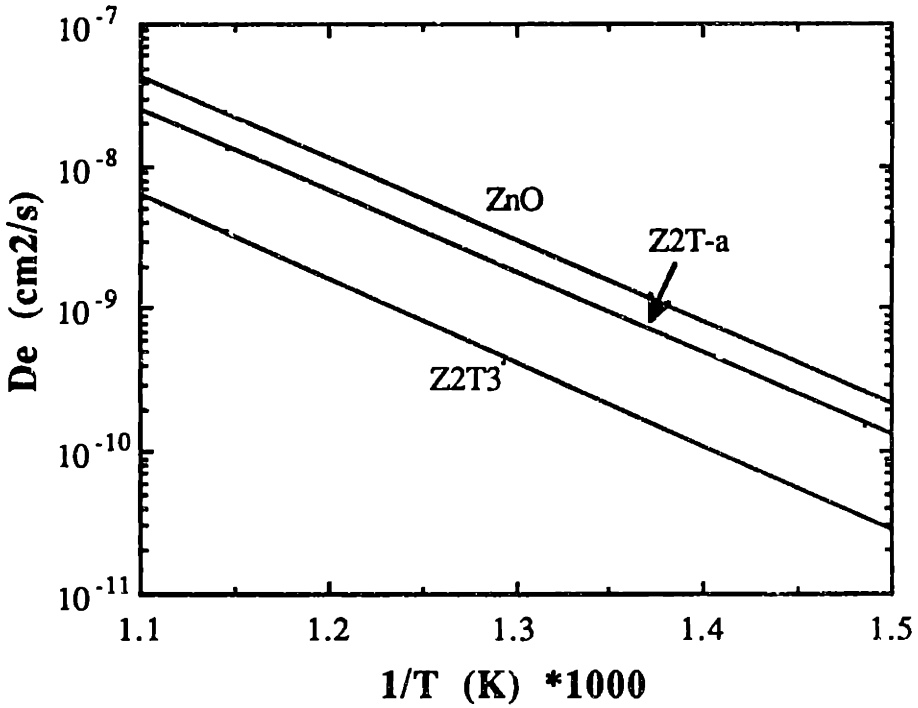

Figure 5.21 Arrhenius plots of the product layer diffusion coefficients for various sorbents. Calculated with the random grain model from experiments with 2%H2S-1%H2-97%N2.

Table 5.6 Arrhenius Constants for the Product Layer Diffusion Coefficient (De).

$$De = D_o \exp[-E/RT]$$ [1]

Sorbent	Temp. Range, (°C)	Arrhenius Constants	
		D_o, cm^2/s	E, kcal/mol
ZnO	400-600	0.098	26.4
Z2T	400-600	0.053	26.3
Z2T3	400-600	0.019	27.0

[1] R is the ideal gas constant and T is the absolute temperature (K)

accurate as the relative resistance of the chemical reaction increased compare to the diffusional resistance. The activation energies for all sorbents were approximately the same (26.6 $\pm$ 0.5 kcal/mol). The major difference was in the pre-exponential factor. The similarity in activation energies suggested that the diffusion mechanisms involved in sulfidation of both ZnO and Zn-Ti-O materials were the same. During sulfidation of ZnO, a product layer of ZnS was formed. Diffusion across this product layer must occur before the reaction can occur. For the Zn-Ti-O sorbents, the product layer consisted of ZnS and TiO_2. From the XRD analyses of the sulfided sorbents, a mixture of α-ZnS, β-ZnS, and TiO_2 (anatase) was formed in sulfided Z2T. In sorbent Z2T3, sulfidation produced the same solid phases but instead of anatase, the rutile phase of TiO_2 was formed. The similarity in activation energies of the product layer diffusion coefficients calculated for the sulfidation of ZnO and Zn-Ti-O sorbents led to the conclusion that for the Zn-Ti-O sorbents diffusion occurred preferentially through ZnS rather than TiO_2. Thus, diffusion through ZnS was faster than through TiO_2. No effect was, therefore, observed with different TiO_2 crystal structures.

The measured activation energy (26.6 $\pm$ 0.5 kcal/mol) for the product layer diffusion coefficient obtained for the sulfidation of ZnO was somewhat higher than the value reported (22.0 kcal/mol) by Ranade and Harrison (1980). However, the pre-exponential factors differed significantly. Ranade and Harrison reported a value of 4.9×10^{-4} cm^2/s, while this study found a value of 0.098 cm^2/s. For example, at 400°C, the De measured in this study was 6.5 times higher than the reported value. The reason for this difference is not clear. However, the solid used in Ranade and Harrison studied was only 94.5% pure. It is not known how the unspecified impurity may have affected the product layer diffusion.

To verify that diffusion through ZnS was faster than through TiO_2, the sulfidation of single crystal ZnO (0001) as well as single crystal ZnO coated with a thin film of TiO_2 (designated as TiO_2/ZnO) was considered. Single crystal ZnO was used in these experiments because of the relative ease of completely coating its surface with a uniform thin, non-porous film compared to coating a porous polycrystalline ZnO because of the microporosity of the latter. The single crystals of ZnO (orientation 0001) was obtained from Atomergic Chemetals Corp. TiO_2/ZnO was prepared by a dip-coating method (Takahashi and Matsuoka, 1988) using the titanium isopropoxide (TTIP)-diethanolamine (DEA)-H_2O-isopropanol (i-PrOH) system. 0.8 M TTIP in i-PrOH was mixed with DEA and H_2O to obtain a solution with a composition TTIP:DEA:H_2O of 1:1:2 molar ratio. The ZnO single crystal was dipped in the solution of TTIP-DEA-H_2O-i-PrOH, slowly pulled out of the solution, dried in air for 24 h (25°C), slowly heated from room temperature to 600°C (heating rate ~5°C/min), and then maintained at 600°C for 30 min. A thin film of approximately 0.3 μm was formed. To ensure that the surface was completely coated with TiO_2, the coating cycle was repeated to produce a film of approximately 0.75 μm thick. During calcination, CO_2 and H_2O were evolved. This can produce cracks in the TiO_2 film. A slow heating rate was used to decrease the formation of cracks. The coating cycle was performed twice so that any crack formed during the first cycle was covered by coating in the second one. From the study performed by Takahashi and Matsuoka (1988), typically a mixture of anatase and rutile forms of TiO_2 is formed at this temperature. Both forms of TiO_2 crystallize in the tetragonal system. The anatase structure has a density of 3.90 g/cm^3 and a lattice period of 9.514 Å along the c-axis and 3.785 Å along the a-axis. The rutile structure is more dense (4.27 g/cm^3) and has a lattice period of 2.959 Å along the c-axis and 4.593 Å along the a-axis. From Eq. (5.45) and (5.46), a larger lattice period would

increase the D_o. Consequently, diffusion through anatase may be somewhat faster than through the rutile.

Sulfidation of the ZnO and TiO_2/ZnO single crystals was performed in 2 mol% H_2S-1 mol% H_2-97 mol% N_2 at 600°C. The properties of the single crystals used in these experiments are shown in Table 5.7. Figure 5.22 shows the conversion profiles for ZnO and TiO_2/ZnO single crystal sulfidation. SEM micrographs of partially sulfided ZnO (~0.3% sulfided) and TiO_2/ZnO (~0.01% sulfided) single crystals are shown in Figures 5.23 and 5.24. As shown in Figure 5.23a, sulfidation of the ZnO single crystal occurred non-uniformly. The more sulfided region (magnified in Figure 5.23b) contained $(S/Zn)_{atomic}$ =0.59 while the less sulfided region (magnified in Figure 5.23c) contained $(S/Zn)_{atomic}$ =0.22. The formation of ZnS layers is evident in Figure 5.23a. Because of the formation ZnS grain boundaries, higher diffusion coefficient may be measured than in diffusion experiments measured in non-reacting system. For example, the diffusion coefficient of Zn in ZnS measured by Secco (1958) was measured with ZnS single crystal where lattice diffusion was dominant.

For TiO_2/ZnO single crystal, the TiO_2 film formed was not completely nonporous as shown in Figure 5.24. Cracks were present. Consequently, the measured diffusion coefficient through TiO_2 may be higher than the true value. However, it is not believed that these cracks exposed the ZnO surface since two coating cycles of TiO_2 were used. EDS analysis at the crack finds $(Ti/Zn)_{atomic}$ =0.2 and $(S/Zn)_{atomic}$ =0.2. In contrast, away from the cracks, the relative concentration are $(Ti/Zn)_{atomic}$ =0.4 and $(S/Zn)_{atomic}$ =0.2. Thus, the cracks did not exposed the ZnO surface.

To calculate the diffusion coefficient, the solid was model as a non-porous plate of infinite length. This is acceptable because the surface area of the material was so low

Table 5.7 Properties of the Single Crystals ZnO and TiO_2/ZnO Used in Sulfidation

ZnO Single Crystal

2x2x1 mm slab
Orientation (0001)
surface area (cm^2/mmol): 0.671
r_o (cm): 0.0216 [1]
ρ_s (mmol/cm^3): 68.9
Z: 1.64
b: 1
k (cm/s): 3.43×10^{-3} (600°C)
De_{ZnS} (cm^2/s): 3×10^{-8} (600°C)

ZnO/TiO_2 Single Crystal

6x6x1 mm slab
Orientation (0001)
h (TiO_2 thickness, cm): 7.5×10^{-5}
surface area (cm^2/mmol): 0.463
r_o (cm): 0.0314 [1]
ρ_s (mmol/cm^3): 68.9
Z: 1.64
b: 1
k (cm/s): 3.43×10^{-3} (600°C)
De_{ZnS} (cm^2/s): 3×10^{-8} (600°C)
De_{TiO2} (cm^2/s): 9×10^{-10} (600°C)

[1] $r_o = V_g/S_g$
where S_g = surface area of the single crystal (cm^2)
V_g = volume of the single crystal (cm^3)
Note: r_o is the half-thickness of a plate for one of infinte length

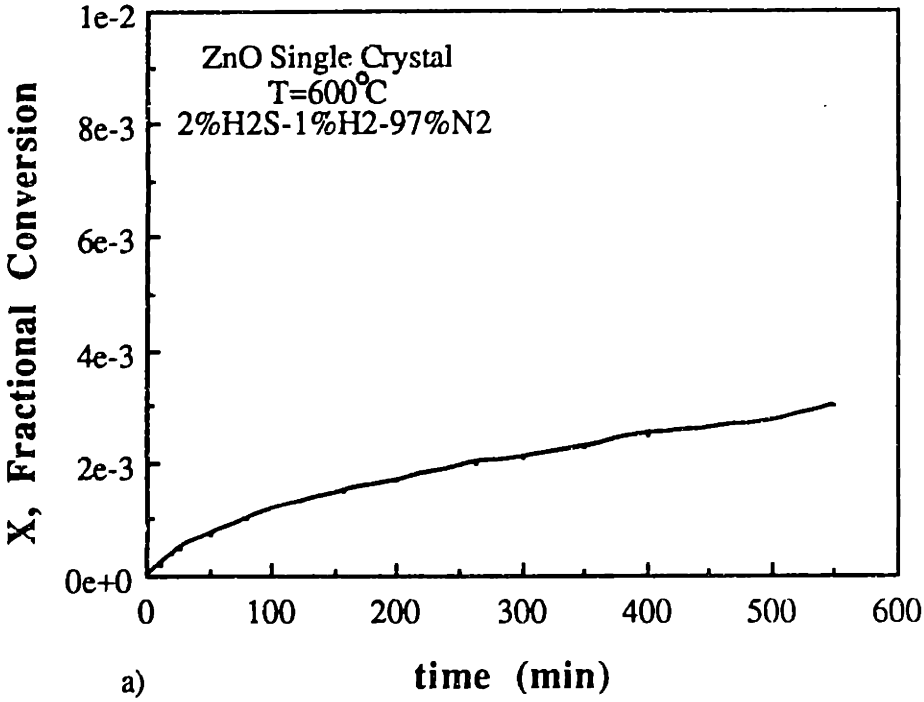

a)

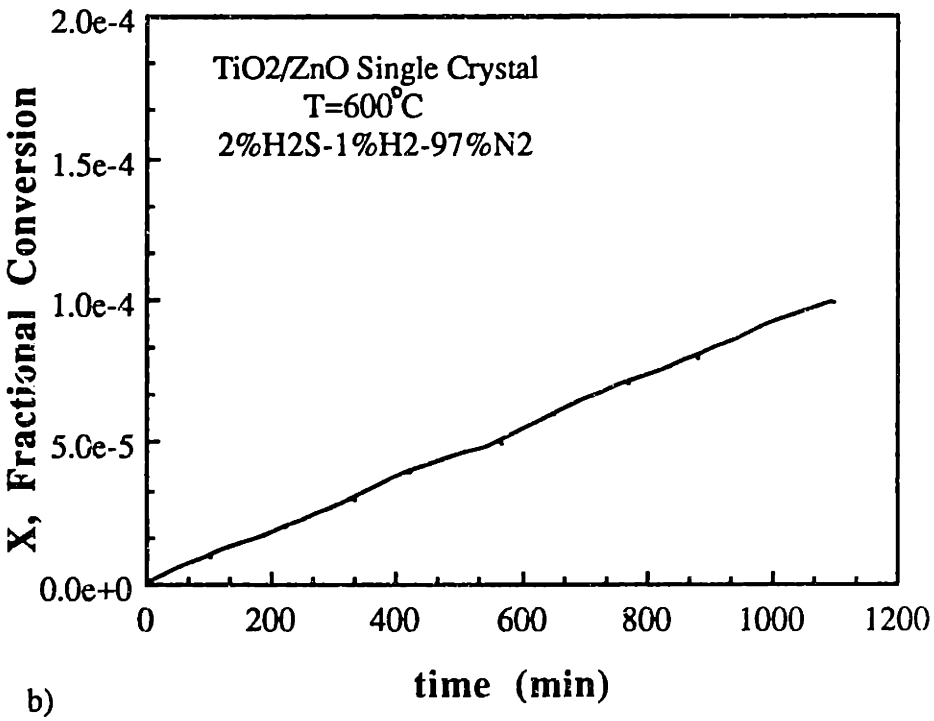

b)

Figure 5.22 Conversion profiles of (a) ZnO (000$\bar{1}$) and (b) TiO2/ZnO single crystals sulfided at 600 C in 2%H2S-1%H2-97%N2.

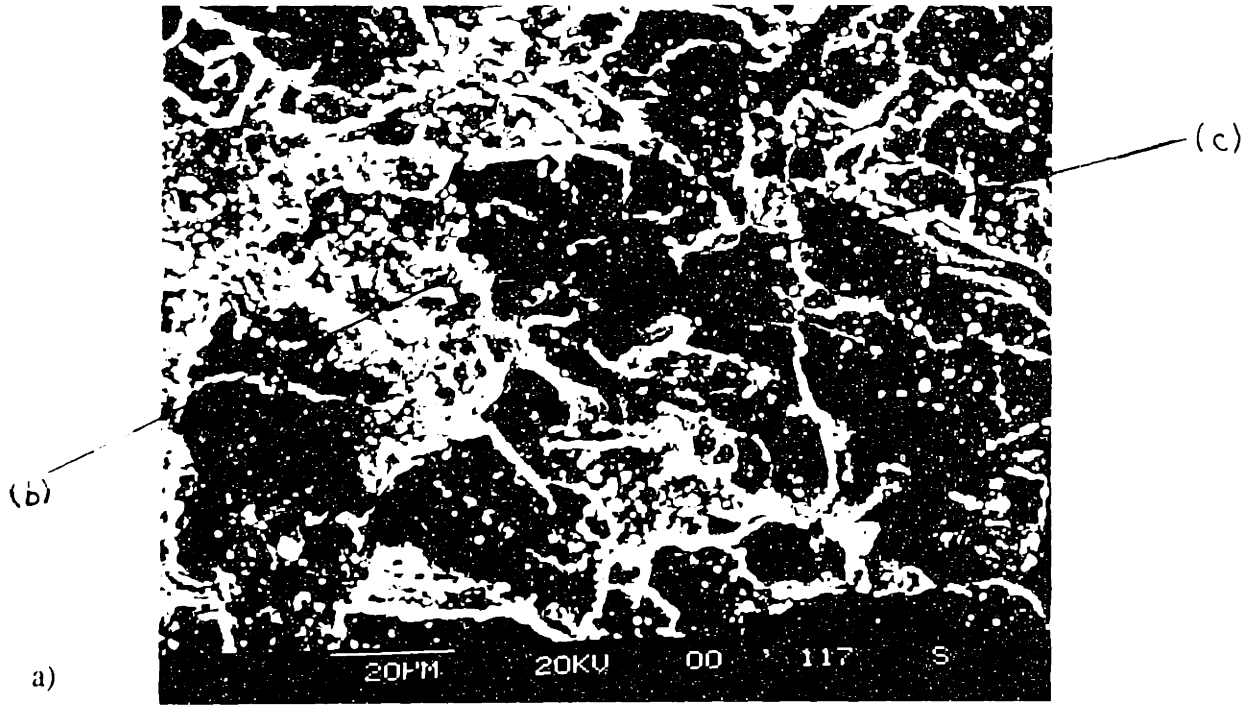

a)

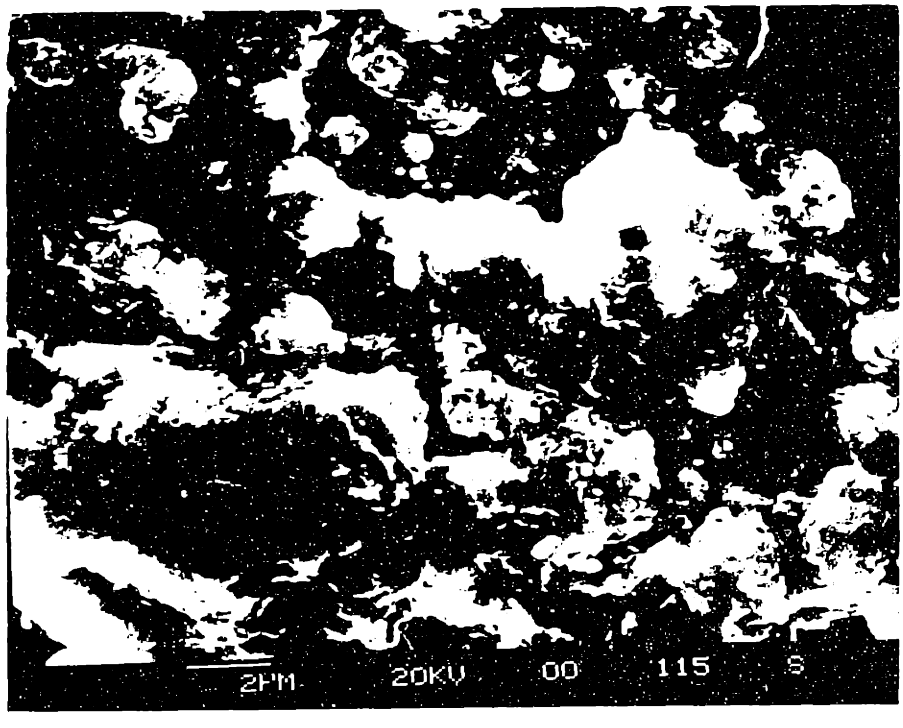

b)

Figure 5.23 SEM micrographs of a) ZnO single crystal partially sulfided (~0.3%) b) magnification of sulfided region $(S/Zn)_{atomic}$ =0.59 and c) less sulfided region $(S/Zn)_{atomic}$ =0.22.

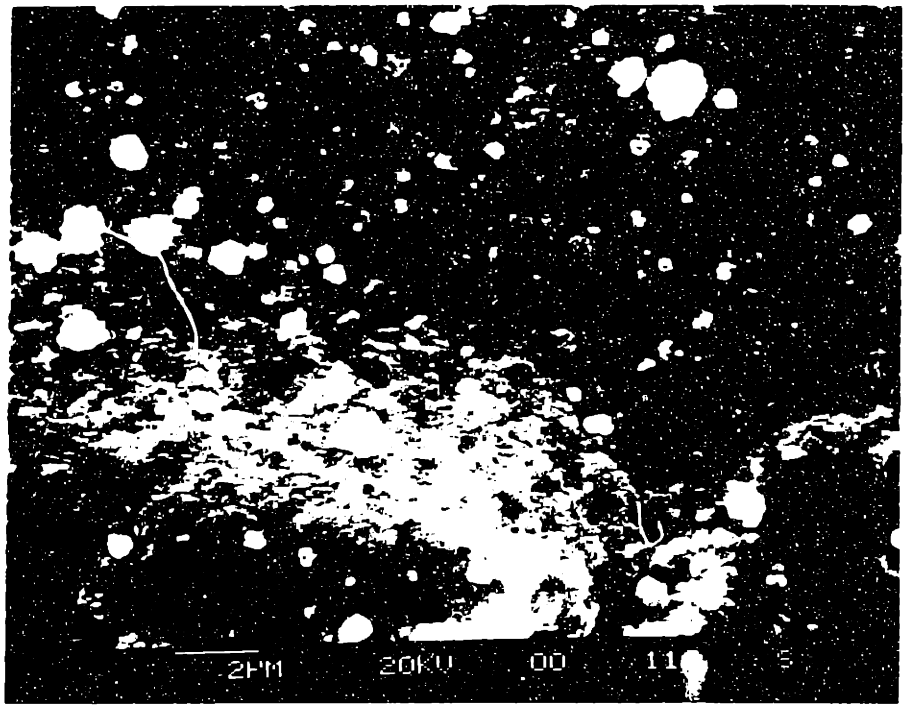

c)

Figure 5.23 (cont'd) SEM micrographs of a) ZnO single crystal partially sulfided (~0.3%) b) magnification of sulfided region $(S/Zn)_{atomic}$ =0.59 and c) less sulfided region $(S/Zn)_{atomic}$ =0.22.

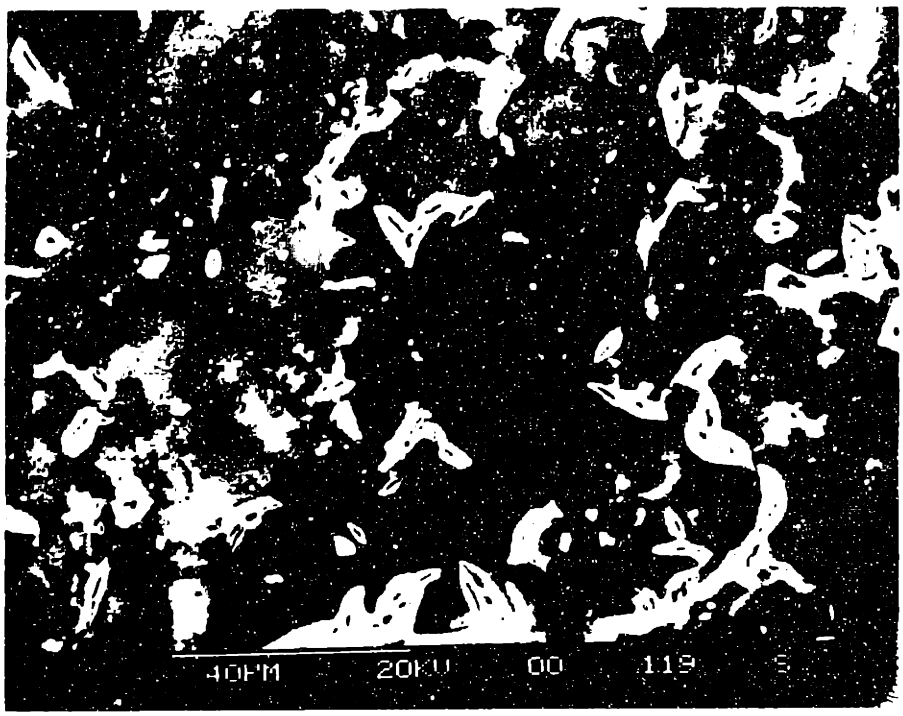

Figure 5.24 SEM micrographs of TiO_2/ZnO single crystal partially sulfided (~0.01%).

(~ 5.46×10^{-4} m^2/g) that only a small amount of sulfidation (~ 0.3 % sulfided) took place. Using Eq. (5.17-5.23) for plate-like grains, the product layer diffusion coefficient was calculated for ZnO sulfidation. The value of the rate constant (k) was obtained from the previous kinetic experiments with polycrystalline ZnO. At 600°C, the diffusion coefficient is equal to 3×10^{-8} cm^2/s. This is somewhat higher than the value calculated for the polycrystalline ZnO (2.5×10^{-8} cm^2/s). Differences in the diffusion coefficient can be ascribed to differences in crystalline structure of the two materials as well as a higher degree of experimental error for the case of the single crystal. Because of its low surface area, the weight change (~0.01 mg after 9 h) was small for the single crystal.

For TiO_2/ZnO sulfidation, diffusion through TiO_2 and ZnS occurred in series. An expression similar to Eq. 5.17 except for an additional term for diffusion through TiO_2 can be derived. The expression for the reaction is

$$t^* = X + \left(\frac{kr_o}{2De_{ZnS}}\right) ZX^2 + \frac{hk}{De_{TiO_2}} X \qquad (5.47)$$

where $t^* = (bk/\rho_s r_o)C_{Ao}t$, k is the rate constant for ZnO sulfidation, C_{Ao} is the bulk H_2S concentration, r_o is the half-thickness of the ZnO plate, De_{ZnS} is the diffusion coefficient through ZnS, h is the thickness of the TiO_2 film, and De_{TiO2} is the diffusion coefficient through TiO_2. The value of De_{ZnS} (3×10^{-8} cm^2/s) was obtained from sulfidation of ZnO single crystal. The calculated diffusion coefficient for TiO_2 (De_{TiO2}) is then 9×10^{-10} cm^2/s.

The ZnO and TiO_2/ZnO experiments verified that diffusion through TiO_2 was significantly slower than diffusion through ZnS. As shown in Figure 5.25, unlike the

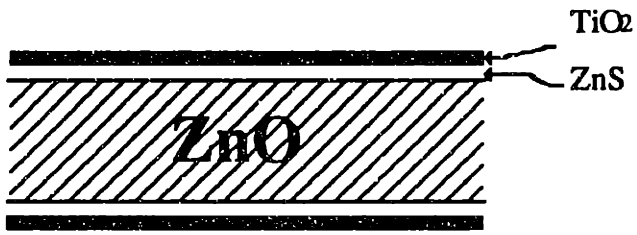

a) TiO_2 /ZnO Single Crystal

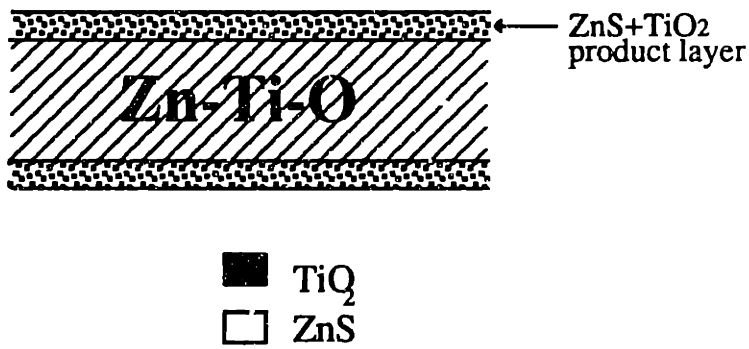

b) Zn-Ti-O bulk sorbent

Figure 5.25 Schematic representation of diffusion layer for partially sulfided a) TiO_2 /ZnO single crystal and b) Zn-Ti-O bulk sorbent

sulfidation of TiO_2/ZnO single crystal where diffusion through TiO_2 and ZnS occurred in series, during the sulfidation of Zn-Ti-O sorbents diffusion through the mixed TiO_2 and ZnS crystals can occur in parallel. Since diffusion through ZnS was much faster than through TiO_2, for the Zn-Ti-O sorbents diffusion through the product layer occurred mainly through ZnS. This explains the similarity in activation energies of the diffusion coefficients for ZnO and Zn-Ti-O sulfidation. The role of TiO_2 is to decrease the volume available for diffusion and increase the tortuosity of the diffusion pathway. The change in the diffusion coefficient can be mathematically expressed by adapting the equation for the "random pore" model proposed by Wakao and Smith (1962) for diffusion in a porous solid having a bimodal pore-size distribution separated into macropores (m) and micropores (μ):

$$De = \varepsilon_m^2 De_m + \left[\frac{\varepsilon_\mu^2(1 + 3\varepsilon_m)}{(1 - \varepsilon_m)}\right] De_\mu \qquad (5.48)$$

where ε_m and ε_μ are the macroporosity and microporosity, respectively. D_m and D_μ are the diffusion coefficients. For this system, a similar expression as equation (5.48) is used with the porosities replaced by the volume fractions (v) of ZnS and TiO_2:

$$De_{ZnS+TiO_2} = v_{ZnS}^2 De_{ZnS} + \left[\frac{v_{TiO_2}^2(1 + 3v_{ZnS})}{(1 - v_{ZnS})}\right] De_{TiO_2} \qquad (5.49)$$

The diffusion flux in the product layer is the sum of that through ZnS, that through TiO_2, and that through ZnS and TiO_2 in series. For $De_{ZnS} >> De_{TiO2}$, this reduces to:

$$De_{ZnS+TiO_2} = v_{ZnS}^2 De_{ZnS} \qquad (5.50)$$

This equation (5.50) is used to predict the product layer diffusion coefficient for various Zn-Ti oxides sulfided at 400 C. As shown in Figure 5.26, the agreement between the experimental and predicted values was good.

The diffusivity was measured using the H_2S concentration for the calculation of the gradient in Eq. (5.11). However, the large value of the activation energy (26.6 kcal/mol) implies ionic diffusion through a solid nonporous product layer. For a pore diffusion mechanism by Knudsen or bulk diffusion, D_e should vary with T^n where n is between 1/2 and 3/2. This would give an apparent activation energy of at most 0.0023 kcal/mol.

In the absence of spectroscopic or other complementary data, it was not possible to unambiguously determine the rate-limiting diffusing species in ZnS. However, from the present work and evidence from previous literature reports, the rate-limiting diffusing species can be inferred. Literature values were obtained by measuring the diffusion of an ionic species through ZnO or ZnS. This is different from the calculation performed in this study. The apparent diffusion coefficient, in this study, was calculated in a reacting system. Because of the volume changes associated with the formation of ZnS from ZnO, the diffusion layer (ZnS) may be formed with many defects and fissure. There was, thus, a greater opportunity for surface and boundary diffusion, both of which are much faster than lattice diffusion, because an atom moving from one site to another is not forced to squeeze between atoms on all sides. Consequently, it is possible to obtain much higher apparent diffusion coefficient and lower activation energy.

The possible rate-limiting diffusing species are Zn and O ions diffusing out to the gas phase and S and H ions diffusing into the unreacted core. In addition, there is the

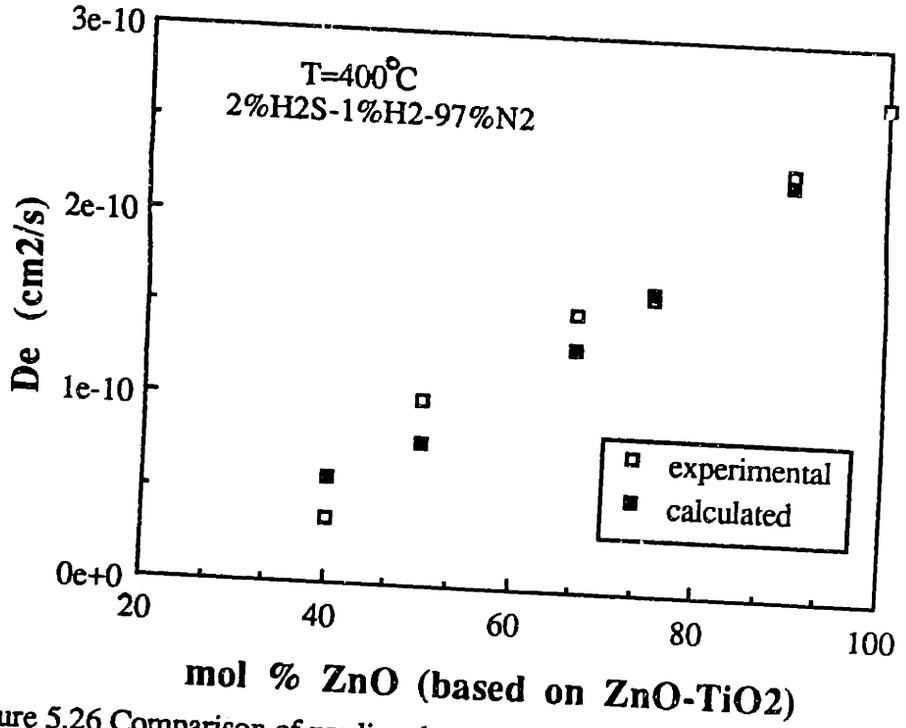

Figure 5.26 Comparison of predicted and experimental product layer diffusion coefficients with various Zn-Ti-O sorbents sulfided at 400°C.

possibility of electron diffusion to maintain the charge balance. The diffusion rate of H^+ has been experimentally found to be very fast in ZnO compare to Zn and O ions. At 600°C, the diffusion coefficient of hydrogen in ZnO is $1.7x10^{-7}$ cm^2/s (Thomas and Lander, 1956). This is much higher than the diffusion coefficient of oxygen or zinc in ZnO. There are some ambiguities in the measurements of the latter, perhaps due to variation in the defect concentration because of non-identical pretreatment conditions and to grain boundary diffusion contribution. However, for zinc ions diffusion through ZnO, the highest value reported for D is $3.0x10^{-14}$ cm^2/s at 600°C (Secco, 1960). An activation energy of 20 kcal/mol and a pre-exponential factor of $3x10^{-9}$ cm^2/s were calculated. For oxygen ions diffusion through ZnO, the highest value reported for D is $2.6x10^{-19}$ cm^2/s (Robin et al., 1973) at 600°C. The last two values of D were extrapolated from results obtained at higher temperatures, 940-1141°C for oxygen diffusion measurement and 905-940°C for zinc diffusion. Since ZnO crystallizes in the hexagonal system, similar to wurzite (α-ZnS), it is expected that the relative order of increasing D for zinc, oxygen, and hydrogen species are the same in α-ZnS. Only values for the diffusion of zinc in α-ZnS were found for temperatures in the range of 927-940°C. Extrapolating to 600°C, D is $5.2x10^{-13}$ cm^2/s (Secco, 1958). Also, the activation energy is 35 kcal/mol and preexponential factor is $3x10^{-4}$ cm^2/s. These values were obtained with wurzite ZnS. Values for sphalerite (β-ZnS) should be approximately the same because the diffusing zinc species experiences the same diffusion paths and interstitial dimension as in the wurzite structure (Secco, 1958). Secco (1958) determined that the diffusion mechanism of zinc is via an interstitial mechanism. From geometrical considerations, he calculated the size of interstitial in ZnS to be larger than in ZnO. The higher value of the diffusion coefficient for zinc ions in ZnS is then due to the larger size of interstices in ZnS than in ZnO. No values of the

S anion diffusion coefficient are available, but it is expected to be smaller since the ionic radii of S^{-2} is 2.45 times larger than Zn^{2+} (Shannon and Prewitt, 1969). Based on these values for the diffusion of zinc and oxygen ions, hydrogen ion cannot be the rate determining species because of its relatively high mobility. Hydrogen ions will rapidly combined with oxygen anions to form OH^- by

$$O^{2-} + H^+ = OH^- \qquad (5.51)$$

Thus, instead of O^{2-} diffusing out, OH^- diffuses out.

It would be expected that the presence of H_2 changes the concentration gradient of Zn ions by the reaction

$$ZnO + H^+ = Zn^{2+} + OH^- \qquad (5.52)$$

Hydrogen ions will rapidly diffuse towards the reactant-product interface. An increase in Zn ions concentration at this interface due to reaction (5.52) will change the zinc ions concentration gradient. Since no observable effect on D_e was found with various amount of H_2 (Chapter 4), it can be concluded that Zn cations are not the diffusion limiting species.

Similar arguments can be made for OH^- anions. At the interface between the solid product and the reactant gas, OH^- ions are consumed by the reaction

$$OH^- + H^+ = H_2O \qquad (5.53)$$

The presence of H_2O in the gas will increase the amount of OH^- ions at the gas-solid interface. This will decrease the diffusion of OH^- out of the solid by decreasing the concentration gradient. The rate of OH^- ions leaving the solid is

$$N_{OH^-} = D_e(C_{OH^-,o} - C_{OH^-,s}) \tag{5.54}$$

where $C_{OH^-,o}$ and $C_{OH^-,s}$ are the concentration of OH^- ions at the gas-solid product and solid product-solid reactant interface, respectively. N_{OH^-} is the transfer rate of OH^- out of the solid. The measured D_e will decrease because a change in the concentration gradient due to the presence of H_2O is not included in the calculation. As discussed in Chapter 4, no noticeable change in the sulfidation profiles was observed when various amounts of H_2O were added to the gas. Consequently, OH^- ions are not the diffusion limiting species.

The most probable diffusion limiting species are S^{2-} ions. The calculation of D_e was based on a gaseous concentration gradient ($C_{H2S,o}$-$C_{H2S,s}$). Since S^{2-} ions are diffusing, an ionic concentration gradient must be used. Thus, the intrinsic reaction rate and product layer diffusion rate are modified to

$$R_s = kC_{S^-,s} \tag{5.55}$$

$$R_s = \frac{D_e(C_{S^-,o} - C_{S^-,s})}{A_r \int_{r_p}^{r_r} \frac{dr}{A_{r,p}}} \tag{5.56}$$

The reaction order of the initial rate of sulfidation of ZnO and Zn-Ti-O sorbents is unity. Also, the reaction order of the product layer diffusion rate in ZnO sulfidation is unity (i.e. product layer diffusion rate α $C_{H_2S,o}$). These observations suggest that the chemisorption of H_2S on the sorbents is a first order process with

$$C_{S^-,o} = K_{H_2S}\, C_{H_2S,o} \tag{5.57}$$

where K_{H_2S} is the adsorption equilibrium constant of H_2S and $C_{H_2S,o}$ is the bulk hydrogen sulfide concentration. Assuming pseudosteady state conditions, the following equation is obtained

$$R_s = \frac{-K_{H_2S} C_{H_2S}}{\frac{1}{k} + \frac{A_r}{De}\int_{r_o}^{r_r} \frac{dr}{A_{r,p}}} \qquad (5.58)$$

With the limitation in scope of this study, it was not possible to determine K_{H2S}. The calculated product layer diffusion in this thesis was based on K_{H2S}=1. Other experimental methods such as radiotracer technique can be used to determine the sulfur ion concentration in the diffusion layer. Thus, comparison with the diffusion coefficient from other studies must keep in mind that differences in values can be attributed to the value used for the driving force of diffusion.

5.6 CONCLUSION

1. The grain model was successful in predicting the sulfidation profiles of ZnO but not the sulfidation of Zn-Ti-O sorbents. The difference is believed to be due to non-uniformity in the grain size of the Zn-Ti-O materials.

2. The grain size predicted by the grain model was larger than observed in SEM micrographs. This was caused by overlapping of the grains which reduced the actual surface area of the sorbent.

3. The random grain model which allowed for randomly overlapping grains, gave a better agreement between the observed and predicted grain size. This model more realistically simulated the grain structure of the ZnO and Zn-Ti-O sorbents.

4. A discrete bimodal grain size distribution with the random grain model successfully predicted the sulfidation profiles of Zn-Ti-O sorbents.

5. Diffusion of S^{2-}, the rate controlling diffusing ion, was faster through ZnS (more than an order of magnitude faster) than through TiO_2. TiO_2 in the product layer reduced the cross-sectional area for diffusion and increased the tortuosity of the diffusion path. Thus, the product layer diffusion coefficient decreased as the TiO_2 content in the product layer increased.

6. Although a drawback of Zn-Ti-O sorbents over ZnO is their lower De, at high temperature and with high sorbent surface area, product layer diffusion is relatively fast compared to the intrinsic sulfidation kinetic. Figure 5.27 shows the regions where kinetic and product layer diffusion are important as a function of particle size and temperature for sorbent Z2T-a.

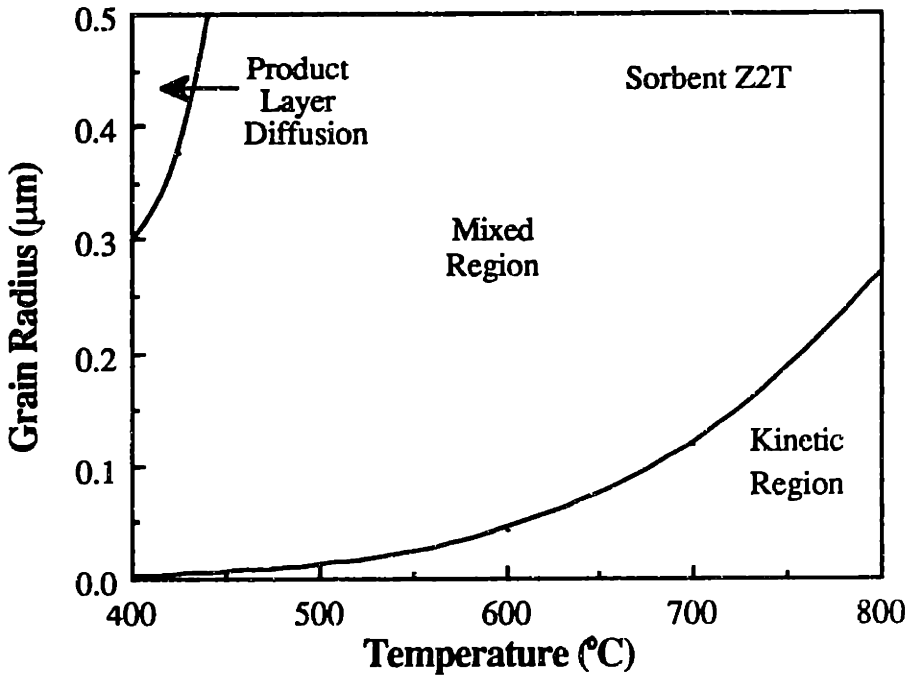

Figure 5.27 Map of regions where kinetic and product layer diffusion are rate limiting

CHAPTER 6

CONCLUSIONS AND RECOMMENDATIONS

6.1 CONCLUSIONS

Mixed oxides of zinc and titanium, Zn-Ti-O, were prepared in the bulk form from pyrolysis of amorphous organic precursors prepared by a complexation method using citric acid. Mixed oxide solids with Zn:Ti atomic ratio ranging from 2:3 to 1:0 were obtained after air calcination at temperatures in the range of 500-1000°C. Substantially higher surface area and pore volume (than for ZnO) characterized the mixed Zn-Ti oxides. For example after calcination at 500°C for 4 h, the surface area of solid Z2T3 (2 Zn : 3 Ti) was ten times higher than ZnO. Three zinc titanate phases were identified in the solids, namely Zn_2TiO_4, $ZnTiO_3$, and $Zn_2Ti_3O_8$. With increasing temperatures, phase change observed was $Zn_2Ti_3O_8$ --> $ZnTiO_3$ --> Zn_2TiO_4. At low temperatures (~500°C), the XRD peaks are very broad. Due to pattern overlapping, the $Zn_2Ti_3O_8$ and

Zn_2TiO_4 phases could not be separated. With increasing Zn/Ti ratio after calcination at 720°C (12 h), the crystalline phase change is TiO_2--> $Zn_2Ti_3O_8$, $ZnTiO_3$ --> Zn_2TiO_4 --> ZnO.

The intrinsic reduction rate of Zn-Ti oxides in hydrogen was compared to the rate for ZnO. Both dry and wet (i.e. the presence of H_2O) reduction gas mixtures were examined. In the absence of H_2O, ZnO reduction took place predominantly on more reactive sites (type A sites). It was proposed that these sites were composed of multiple atoms or an ensemble of Zn-O atoms. Thus, they were easily poisoned by the presence of foreign atoms, such as titanium. Consequently, the reduction rate of ZnO was much higher than for Zn-Ti oxides. At 700°C, the observed reduction rate of ZnO was approximately ten times faster than for a solid with Zn:Ti atomic ratio of approximately 3:1. With this stochiometric composition of Zn-Ti, all type A sites were poisoned and a different type of sites that was not affect by titanium of lower reactivity dominated. No further effect on the intrinsic rate was observed with increasing relative concentration of titanium. In addition, no variation in the reduction rate was observed in the presence of different zinc titanate compounds. Different values for the reduction kinetic constants were obtained for both ZnO and Zn-Ti oxides confirming that reaction occurred on different types of sites. The activation energy observed for ZnO reduction was 23 kcal/mol, and the H_2 reaction order was 0.51 while for Zn-Ti oxides, the values were 35 kcal/mol and 1, respectively.

In the presence of water vapor, reaction sites on ZnO (type A) and on Zn-Ti oxides were poisoned, and the reduction rates for both type of solids decreased. Similar inhibitory effects on reduction were observed with hydrogen sulfide. The same type of reaction sites (type B) were involved in ZnO and Zn-Ti oxides reduction when water

vapor was present. Consequently, similar values for the reduction kinetic constants were obtained for both ZnO and Zn-Ti oxides. The activation energies for both were approximately 41 kcal/mol, and the hydrogen reaction order was 1. Only the pre-exponential factors were different. For example, the pre-exponential factor for Z2T (2 Zn : 1 Ti) was approximately three times smaller than for ZnO. These sites (type B) were believed to be composed of fewer atoms than type A sites. Thus, compare to type A sites, larger relative concentrations of titanium were needed to poison type B sites to the same extent as type A sites. As the sorbent content of titanium was increased from 0 to 60 atomic%, a corresponding decrease in intrinsic rate occurs.

Similar reaction mechanisms appeared to be operative in sulfidation of Zn-Ti oxide and zinc oxide sorbents with hydrogen sulfide. Both the mixed and pure oxides had approximately the same activation energies (~7-9 kcal/mol) and hydrogen sulfide reaction order (~1). However, the sulfidation rates of Zn-Ti oxides were approximately half those of ZnO. Decreasing the Zn:Ti atomic ratio from 3:1 to 2:3 or using different zinc titanate phases did not significantly affect the intrinsic rate. Parametic studies performed with water vapor and hydrogen gas revealed no significant effect of either component on both the intrinsic rate and the overall rate at temperatures up to 700°C. However, water vapor did increase the sintering of the solids. At 800°C, the presence of hydrogen gas led to higher initial sulfidation rate (1.3-1.4 times higher). This was believed to be due to the contribution of the gas-phase reaction of Zn(g) with H_2S. Formation of cracks and fissures were evident at this temperature and with $\geq$ 10 mol% H_2.

Product layer diffusion coefficients were calculated by a random grain model. Based on SEM micrographs, a discrete bimodal grain size distribution was used for the Zn-Ti

oxides, while for ZnO, one grain size was chosen. For ZnO, a product layer of ZnS was formed while for Zn-Ti oxides, the product layer consisted of ZnS and TiO_2. Increasing the relative concentration of titanium in the solid, correspondingly decreased the product layer diffusion coefficient. The similarity in the activation energies (~26.6 kcal/mol) of the product layer diffusion coefficients for the sulfidation of bulk ZnO and Zn-Ti oxides indicated that for Zn-Ti oxides, product layer diffusion was controlled by diffusion in ZnS only. This was in good agreement with the findings that the diffusion coefficient of sulfur ion in ZnS was more than 10 times higher than in TiO_2, based on experiments performed at 600°Cwith ZnO and TiO_2 coated ZnO single crystals. The high value of the activation energy was an indication that diffusion occurs via a solid state mechansim. Although the film of TiO_2 significantly decreased (175 times slower) the reduction rate of ZnO, the sulfidation rate decreased even more (300 times slower). Thus, the diffusion of sulfur ions is much slower than diffusion of zinc or hydroxyl ions in TiO_2.

6.2 RECOMMENDATIONS

Zn-Ti oxides have significantly lower reduction rate (ten times lower at 700°C in 10 mol% H_2 - 90 mol% N_2) than ZnO in the absence of water vapor and hydrogen sulfide. In a packed bed reactor where a significant portion of the sorbent bed can encounter a reducing hydrogen sulfide-free gas, the recommended sorbent composition has Zn:Ti atomic ratio equal to 3:1 (Z3T) in the absence of water vapor. This will give high sulfur loading (0.30 g sulfur/g sorbent), low reduction rate, and initial sulfidation rate only half that of ZnO. A higher relative concentration of titanium will not yield lower reduction rate but will decrease the sulfur loading and product layer diffusivity.

In practice, most coal gas streams are quenched at the gasifier exit and, thus, contain significant amount of water vapor (10-50 mol%). When water vapor is present, the reduction of ZnO is suppressed to the extent that only when the relative concentration of titanium is increased substantially is there also a further substantial decrease in the reduction rate. The recommended sorbent in this case, depends on the tolerable level of sorbent loss due to reduction and the desired sulfur loading. The reduction rate of sorbent Z3T is only half that of ZnO. Sorbent Z2T3 (2 Zn : 3 Ti) has a reduction rate nearly 9 times slower than ZnO (in H_2-H_2O-N_2), and its initial sulfidation rate is only half that of ZnO. However, its sulfur loading is only 0.16 g sulfur/g sorbent (based on complete sulfidation), and its product layer diffusion coefficient in sulfidation is ~7 times slower than ZnO. However, for Z2T3 with a typical surface area of 2 m^2/g, the overall rate is controlled by product layer diffusion only when the temperature is below 520°C. Between 520-1020°C, both chemical kinetic and product layer diffusion control the overall sulfidation rate.

Desulfurization in a fluidized bed reactor may yield lower zinc loss because any zinc vapor formed will react with H_2S. However, although reduction of ZnO might not cause zinc loss, the reduction reaction will cause particle attrition and the formation of fines.

Although Zn-Ti oxides do yield lower reduction rate than ZnO, excessive increase of the amount of TiO_2 in the sorbent will be at the cost of lower sulfur loading. This along with considerations of sorbent structural effects (e.g. cracking and sintering) should be weighed to determine a suitable Zn-Ti-O composition for hot coal gas desulfurization. Further studies of regeneration of sulfided Zn-Ti oxides are also needed to establish their regeneration chemistry and regenerability performance before Zn-Ti oxides can be

conclusively recommended as fully regenerable sorbents for high-temperature gas desulfurization.

CHAPTER 7

REFERENCES

Ayala, R.E.; Kim, B.M. Modeling and Analysis of Mc.ing-Bed Hot-Gas Desulfurization Processes. *Env. Prog.* **1989**, *8*(1), 19-25.

Barin, I.; Knacke, O. *Thermochemical Properties of Inorganic Substances*; Springer-Verlag: New York, 1973.

Barin, I.; Knacke, O.; Kubaschewski, O. *Thermochemical Properties of Inorganic Substances-Supplement*; Springer-Verlag: New York, 1976.

Bartholomew, C.H.; Agrawal, P.K. Sulfur Poisoning of Metals. *Adv. Catal.* **1982**, *31*, 135-242.

Bartlett, R.W.; Krishnan, N.G.; Van Hecke, M.C. Micrograin Models of Reacting Porous Solids with Approximations to Logarithmic Solid Conversion. *Chem. Eng. Sci.* **1973**, *28*, 2179-2186.

Bartram, S.F.; Slepetys, R.A. Compound Formation and Crystal Structure in the System ZnO-TiO_2. *J. Am. Ceram. Soc.* **1961**, *44*(10), 493-499.

Baumbach, H.H.; Wagner, C. Electrical Conductivity of Zinc and Cadmium Oxides. *Z. Phys. Chem.* **1933**, *B22*, 199-211.

Bhatia, S.K.; Perlmutter, D.D. A Random Pore Model for Fluid-Solid Reactions: I. Isothermal, Kinetic Control. *A.I.Ch.E. J.* **1980**, *26*, 379-386.

Bhatia, S.K.; Perlmutter, D.D. Unified Treatment of Structural Effects in Fluid-Solid Reactions. *A.I.Ch.E. J.* **1983**, *29*, 281-289.

Bird, R.B.; Stewart, W.E.; Lightfoot, E.N. *Transport Phenomena*, Wiley: New York, 1960.

Boccuzzi, F.; Borello, E.; Zecchina, A.; Bossi, A.; Camia, M. Infrared Study of ZnO Surface Properties I. Hydrogen and Deuterium Chemisorption at Room Temperature. *J. Catal.* **1978**, *51*, 150-159.

Bodenstein, M. The Mechanism of the Metallurgical Production of Zinc. *Trans. Am. Electrochem. Soc.* **1927**, *51*, 365-376.

Bokshtein, B.S.; Bokshtein, S.Z.; Zhukhovitskii, A.A. *Thermodynamics and Kinetics of Diffusion in Solids*, Amerind Publishing Co. Pvt. Ltd.: New Dehli, 1985.

Bonasewicz, P.; Littbarski, R.; Grunze, M. Adsorption Phenomena. *Current Topics in Material Science*, Kaldis, E., Ed.; North-Holland Publishing Company: New York, 1981; Vol. 7, p 371-409.

Brunauer, S.; Emmet, P.H.; Teller, E. Adsorption of Gases in Multimolecular Layers. *J. Am. Chem. Soc.* **1938**, *60*, 309-318.

Cavelo, A.; Cunningham, R.E. Kinetics of Gas-Solid Reactions. Influence of Surface Area and Effective Diffusivity Profiles. *J. Catal.* **1970**, *17*, 1-9.

Cole, S.S.; Nelson, W.K. The System Zinc Oxide - Titanium Dioxide. Zinc Orthotitanate and Solid Solutions with Titanium Dioxide. *J. Phys. Chem.* **1938**, *42*, 245-251.

Courty, P.; Ajot, H.; Marcilly, C.; Delmon. B. Oxydes Mixtes ou en Solution Solide sous Forme Tres Divisee Obtenus per Decomposition Thermique de Precurseurs Amorphes. *Powder Technol.* **1973**, *7*, 21-38.

Davis, B.L.; Kath, R.; Spilde, M. The Reference Intensity Ratio: Its Measurement and Significance. *Powder Diffraction* **1990**, *5*(2), 76-78.

de Woolf, P.M.; Visser, J.W. Absolute Intensities - Outline of a Recommended Practice. *Powder Diffraction* **1988**, *3*(4), 202-204.

Dent, A.L.; Kokes, R.J. Hydrogenation of Ethylene by Zinc Oxide. I. Role of Slow Hydrogen Chemisorption. *J. Phys. Chem.* **1969**, *73*, 3772-3780.

Dulin, F.H.; Rase, D.E. Phase Equilibria in the System ZnO-TiO_2. *J. Am. Ceram. Soc.* **1960**, *43*(1), 125-131.

Dutta, S.; Wen, C.Y.; Belt, R.J. Reactivity of Coal and Char. 1. In Carbon Dioxide Atmospheres. *Ind. Eng. Chem. Process Des. Dev.* **1977**, *16*, 20-30.

Dutta, S.; Wen, C.Y.; Belt, R.J. Reactivity of Coal and Char. 2. In Oxygen-Nitrogen Atmospheres. *Ind. Eng. Chem. Process Des. Dev.* **1977**, *16*, 31-37.

Eischens, R.P.; Plisken, W.A.; Low, M.J.D. The Infrared Spectrum of Hydrogen Chemisorbed on Zinc Oxide. *J. Catal.* **1962**, *1*, 180-191.

Farha, F.E., Jr.; Gardner, L.E. U.S. Patent 4,313,820, 1982.

Flytzani-Stephanopoulos, M.; Gavalas, G.R.; Tamhankar, S.S.; Sharma, P.K. Novel Sorbents for High-Temperature Regenerative H_2S Removal. Final Report DOE/MC/20417-1898, October 1985.

Flytzani-Stephanopoulos, M.; Gavalas, G.R.; Jothimurugesan, K.; Lew, S.; Sharma, P.K.; Bagajewicz, M.J.; Patrick, V. Detailed Studies of Novel Regenerable Sorbents for High-Temperature Coal-Gas Desulfurization. Final Report DE-FC21-85MC221930, October 1987.

Flytzani-Stephanopoulos, M.; Shao, R.L. Unpublished work, 1988.

Focht, G.D.; Ranade, P.V.; Harrison, D.P. High-Temperature Desulfurization Using Zinc Ferrite: Reduction and Sulfidation Kinetics. *Chem. Eng. Sci.* **1988**, *43*(11), 3005-30013.

Fukuda, K.; Doyika, M.; Kameyama, T.; Kotera, Y. Catalytic Decomposition of Hydrogen Sulfide. *Ind. Eng. Chem. Fund.* **1978**, *17*, 243-248.

Gangwal, S.K.; Stogner, J.M.; Harkins, S.M. Testing of Novel Sorbents for H_2S Removal from Coal Gas. *Env. Prog.* **1989**, *8*(1), 26-34.

Gast, D.; Grunze, M.; Hirschwald, W.; Krebs, S. Struktur - und Fehlordnungsabhangigkeit der Reduktion von Zinkoxid mit Kohlenmonoxid und Wasserstoff. *Zeit. Phys. Chemie Neue Folge* **1976**, *102*, 83-91.

Gavalas, G.R. A Random Capillary Model with Application to Char Gasification at Chemically Controlled Rates. *A.I.Ch.E. J.* **1980**, *26*, 577-585.

Georgakis, C.; Chang, D.W.; Szekely, J. A Changing Grain Size Model for Gas-Solid Reactions. *Chem. Eng. Sci.* **1979**, *34*, 1072-1075.

Gibson, J.B.; Harrison, D.P. The Reaction Between Hydrogen Sulfide and Spherical Pellets Zinc Oxide. *Ind. Eng. Chem. Process Des. Dev.* **1980**, *19*, 231-237.

Giner, Inc., Studies Involving High Temperature Desulfurization/Regeneration Reactions of Metal Oxides for the Fuel Cell Program. Final Report Argonne Natinal Laboratory, Contract 31-109-39-5804, Waltham, MA, 1981.

Gioia, F.; Mura, G.; Viola, A. Experimental Study of the Direct Reduction of Sinterized Zinc Oxide by Hydrogen. *Chem. Eng. Sci.* **1977**, *32*, 1401-1409.

Gluckman, M.J.; Louks, B.M. Second Generation Gasification Combined-Cycle Power Plants for U.S. Utilities - Detailed Performance and Cost Estimates. *Appl. Energy* **1982**, *11*, 85-122.

Grindley, T.; Steinfeld, G. Development and Testing of Regenerable Hot Coal Gas Desulfurization on Sorbents. Final Report DOE/MC/16545-1125, October 1981.

Grunze, M.; Hirschwald, W. Vacuum Microbalance Investigations on Heterogeneous Surface Reaction Mechanisms. *J. Vac. Sci. Technol.*, **1974**, *11*(1), 424-428.

Grunze, M.; Hirschwald, W. Vacuum Microbalance Investigations on the Pressure and Temperature Dependence of Solid/Gas Reactions. *Progress in Vacuum Microbalance*

Techniques, Eyraud, C. and Escoubes, M., Ed.; Eyden: New York, 1975; Vol. 3, p 233-244.

Grunze, M. Reduction and Chlorination of ZnO. *Current Topics in Material Science*, Kaldis, E., Ed.; North-Holland Publishing Company: New York, 1981; Vol. 7, p 432-447.

Guger, C.E.; Manning, F.S. Kinetics of Zinc Oxide Reduction with Carbon Monoxide. *Met. Trans.* **1971**, *2*, 3083-3090.

Gupta, T. Inhibition of Grain Growth in ZnO. *J. Am. Ceram. Soc.* **1971**, *54*(8), 413-414.

Haller, W. Rearrangement Kinetics of the Liquid-Liquid Immiscible Microphases in Alkali Borosilicate Melts. *J. Chem. Phys.* **1965**, *42*, 686-693.

Halow, J.S. An Overview of the U.S. DOE Coal Gasification Program. *21st Intersociety Energy Conversion Engineering Conference* **1986**, *1*, 170-175.

Hartman, M.; Coughlin, R.W. Reactions of Sulfur Dioxide with Limestone and the Grain Model. *A.I.Ch.E. J.* **1976**, *22*, 490-498.

Hegedus, A.J.; Kiss, A.B. Thermogravimetrische Untersuchung der ZnO + H_2 - Reaktion in Stromendem Wasserstoff. *Mikrochim. Acta* **1966**, 4-5, 813-832.

Hindermann, J.P.; Idriss, H.; Kiennemann, A. Adsorbed Species on ZnO in CO-H_2 and CO_2-H_2 Reactions. *Mat. Chem. Phys.* **1988**, *18*, 513-532.

Hirschwald, W.; Stolze, F. Zur Kinetik der Thermischen Dissoziation von Zinkoxid. *Zeit. Phys. Chemie Neue Folge*, **1971**, *77*, 21-42.

Hirschwald, W.; Noack, D. Thermogravimetrische Untersuchung der Reduktionskinetik von Zinkoxid mit Wasserstoff. *Zeit. Phys. Chemie Neue Folge*, **1972**, *77*, 1-20.

Hubbard, C.R.; Snyder, R.L. RIR - Measurement and Use in Quantitative XRD. *Powder Diffraction* **1988**, *3*(2), 74-77.

Jalan, V.; Wu, D. High Temperature Desulfurization of Fuel Gases for Molten Carbonate Fuel Cell Power Plants. Paper presented at the National Fuel Cell Seminar, 1980, San Diego, CA.

Kesavulu, V.; Taylor, H.S. Sites for Hydrogen Chemisorption on Zinc Oxide. *J. Phys. Chem.* **1960**, *64*, 1124-1131.

Kingery, W.D.; Bowen, H.K.; Ulmann, D.K. *Introduction to Ceramic*, 2nd ed.; Wiley: New York, 1976.

Klug, H.P.; Alexander, L.E. *X-Ray Diffraction Procedures for Polycrystalline and Amorphous Materials*, Wiley: New York, 1954.

Kodera, K.; Kusunoki, I.; Shimizu, S. Dissociation Pressures of Various Metallic Oxides. *Bull. Chem. Soc. Japan* **1968**, *41*, 1039-1045.

Krebs, S.; Littbarski, R. Preparation and Crystal Growth. *Current Topics in Material Science*; Kaldis, E., Ed.; North-Holland Publishing: New York, 1981; p. 170-198.

Lee, V.J.; Parravano, G. Sintering Reactions of Zinc Oxide. *J. Appl. Phys.* **1959**, *30*, 1735-1740.

Lercher, J.A.; Vinek, H.; Noller, H. TiO_2/ZnO Mixed Oxide Catalysts, Characterization by X-ray Photoelectron and Infrared-Spectroscopy and Reactions with Propanol and Butanol. *Appl. Catal.* **1984**, *12*, 293-307.

Lew, S. High-Temperature Regenerative H_2S Removal by ZnO-TiO_2 Systems. M.S. Thesis, Massachusetts Institute of Technology, Cambridge, 1987.

Lew, S.; Jothimurugesan, K.; Flytzani-Stephanopoulos, M. High-Temperature H_2S Removal from Fuel Gases by Regenerable Zinc Oxide-Titanium Dioxide Sorbents. *Ind. Eng. Chem. Process Des. Dev.* **1989**, *28*, 535-541.

Lindner, B.; Simonsson, D. Comparison of Structural Models for Gas-Solid Reactions in Porous Solids Undergoing Structural Changes. *Chem. Eng. Sci.* **1981**, *36*, 1519-1527.

Maier, C.G.; Ralston, O.C. The Gaseous Reduction of Zinc. *Trans. Am. Electrochem. Soc.* **1928**, *51*, 339-363.

Marcilly, C.; Courty, P.; Delmon, B. Preparation of Highly Dispersed Mixed Oxides and Oxide Solid Solutions by Pyrolysis of Amorphous Organic Precursors. *J. Am. Ceram. Soc.* **1970**, *53*(1), 56-57.

Marqueen, T.J.; Carbone, D.J.; Ligammari, J. Coal Gasification Combined Cycle Systems - Technical Horizons. *Proc. Am. Pow. Conf.* **1986**, *48*, 235-241.

Matsuda, S.; Kato, A. Titanium Oxide Based Catalyst - A Review. *Appl. Cat.* **1983**, *8*, 149-165.

Mattmann, G.; Oswald, H.R.; Schweizer, F. Untersuchungen zur Physisorption und Chemisorption von Wasser auf Zinkoxid - Oberflachem. *Helvet. Chim. Acta* **1972**, *55*, 1249-1266.

Moore, W.; Williams, E. Decomposition of Zinc Oxide by Zinc Vapor. *J. Phys. Chem.* **1959**, *63*, 1516-1517.

Morgantown Energy Technology Center Hot Gas Cleanup Task Force, Chemistry of Hot Gas Cleanup in Coal Gasification and Combustion. Final Report MERC/SP 78/2, February 1978.

Nicholson, D. Variation of Surface Area During the Thermal Decomposition of Solids. *Trans. Faraday Soc.* **1965**, *61*, 990-998.

Patrick, V. Synthesis, Characterization, and Kinetics of Mixed Copper-Aluminum and Iron-Aluminum Oxides for High-Temperature Desulfurization. Ph.D. Dissertation, California Institute of Technology, Pasedena, CA, 1989.

Patrick, V.; Gavalas, G.R.; Flytzani-Stephanopoulos, M.; Jothimurugesan, K. High-Temperature Sulfidation-Regeneration of $CuO-Al_2O_3$ Sorbents. *Ind. Eng. Chem. Process Des. Dev.* **1989**, *28*, 931-940.

Peterson, E.E. Reaction of Porous Solids. *A.I.Ch.E. J.* **1957**, *3*, 443-448.

Ramachandran, P.A.; Smith, J.M. Effect of Sintering and Porosity Changes on Rates of Gas-Solid Reactions. *Chem. Eng. J.* **1977**, *14*, 137-146.

Ramanchandran, P.A.; Smith, J.M. A Single-Pore Model for Gas-Solid Non-Catalytic Reactions. *A.I.Ch.E. J.* **1977**, *23*, 353-361.

Ranade, P.V.; Harrison, D.P. The Variable Property Grain Model Applied to the Zinc Oxide-Hydrogen Sulfide Reaction. *Chem. Eng. Sci.* **1981**, *36*, 1079-1089.

Reddy, V.B.; Goel, S.P.; Mehrotra, P.N. Investigations on Formation of Zinc Titanates via Thermal Decomposition of Zinc Titanyl Oxalate Hydrate. *Mater. Chem. Phys.* **1984**, *10*, 365-373.

Robin, R.; Cooper, A.R.; Heuer, A.H. Application of a Nondestructive Single-Spectrum Proton Activation Technique to Study Oxygen Diffusion in Zinc Oxide. *J. Appl. Phys.* **1973**, *44*, 3770-3777.

Sa, L.N.; Focht, C.D.; Ranade, P.V.; Harrison, D.P. High-Temperature Desulfurization Using Zinc Ferrite: Solid Structural Property Changes. *Chem. Eng. Sci.* **1989**, *44*(2), 215-224.

Sainamthip, P.; Amarakoon, V.R.W. Role of Zinc Volatilization on the Microstructure Development of Manganese Zinc Ferrites. *J. Am. Ceram. Soc.* **1988**, *71*(8), 644-648.

Secco, E.A. Diffusion and Exchange of Zinc in Crystalline Zinc Sulfide. *J. Appl. Phys.* **1958**, *29*, 406-409.

Secco, E. A. Decomposition of Zinc Oxide. *Can. J. Chem.* **1960**, *38*, 596-601.

Shannon, R.D.; Prewitt, C.T. Effective Ionic Radii in Oxides and Flourides. *Acta Cryst.* **1969**, *B25*, 925-946.

Sheinkman, A.I.; Sheinkman, F.P.; Dobrovol'skii, I.P.; Zvyagina, G.R. Phase Formation Sequence in the Reaction of Zinc Oxide with Titanium Dioxide. *Izv. Akad. Nauk SSSR, Neorg. Mater.* **1977**, *13*(8), 1447-1450.

Smith, B.J. Deactivation in Catalytic Hydrodemetallation. Ph.D. Dissertation, Massachusetts Institute of Technology, Cambridge, 1988.

Smith, J.M. *Chemical Engineering Kinetics*, 2nd ed.; McGraw-Hill: New York, 1970.

Smith, J.M.; Van Ness, H.C. *Introduction to Chemical Engineering Thermodynamics*, McGraw-Hill: New York, 1979, p 110.

Sotirchos, S.V.; Yu, H.C. Overlapping Grain Models for Gas-Solid Reactions with Solid Product. *Ind. Eng. Chem. Res.* **1988**, *27*, 836-845.

Szekely, J.; Propster, M. A Structural Model for Gas-Solid Reaction with a Moving Boundary-VI. *Chem. Eng. Sci.* **1975**, *30*, 1049-1055.

Szekely, J.; Evans, J.W.; Sohn, H.Y. *Gas-Solid Reactions*; Academic Press: New York, 1976.

Takahashi, Y.; Matsuoka, Y. Dip-Coating of TiO_2 Films Using a Sol Derived From $Ti(O\text{-}i\text{-}Pr)_4$-Diethanolamine-$H_2O$-i-PrOH System. *J. Mater. Sci.* **1988**, *23*, 2259-2266.

Tamhankar, S.S.; Hasatani, M.; Wen, C.Y. Kinetic Studies on the Reactions Involved in the Hot Gas Desulfurization Using a Regenerable Iron Oxide Sorbent-I. *Chem. Eng. Sci.*, **1981**, *36*, 1181-1191.

Tamhankar, S.S.; Bagajewicz, M.; Gavalas, G.R.; Sharma, P.K.; Flytzani-Stephanopoulos, M. Mixed-Oxide Sorbents for High-Temperature Removal of Hydrogen Sulfide. *Ind. Eng. Chem. Process Des. Dev.* **1986**, *25*, 429-437.

Thomas, D.G.; Lander, J.J. Hydrogen as a Donor in Zinc Oxide. *J. Chem. Phys.* **1956**, *25*, 1136-1142.

Truesdale, E.C.; Waring, R.K. Relative Rates of Reactions Involved in Reduction of Zinc Ores. *AIME Trans.* **1944**, *159*, 97-109.

Van Eekelen, H.A.M. The Random-Spheres Model for Porous Materials. *J. Catal.* **1973**, *29*, 75-82.

Villa, P.; del Piero, G.; Lietti, L.; Garagiola, F.; Mologni, G.; Tronconi, E.; Pasquon, I. Synthesis of Alcohols from Carbon Oxides and Hydrogen VI. Zn and Ti Oxides: Preparation and Catalytic Activity. *Appl. Catal.* **1987**, *35*, 47-58.

Wakao, N.; Smith, J.M. Diffusion in Catalyst Pellets. *Chem. Eng. Sci.* **1962**, *17*, 825-834.

Weissberg, H.L. Effective Diffusion Coefficient in Porous Media. *J. Appl. Phys.* **1963**, *34*, 2636-2639.

Westmoreland, P.R.; Harrison, D.P. Evaluation of Candidate Solids for High-Temperature Desulfurization of Low Btu Gases. *Environ. Sci. Technol.* **1976**, *10*, 659-660.

Westmoreland, P.R.; Gibson, J.B.; Harrison, D.P. Comparative Kinetics of High-Temperature Reaction Between H_2S and Selected Metal Oxides. *Environ. Sci. Technol.* **1977**, *11*, 488-491.

Weyl, W. Atomistic Interpretation of the Mechanism of Solid State Reactions and of Sintering. *Ceramic Age* **1952**, *60*(5), 28-38.

Yamaguchi, O.; Morimi, M.; Kawabata, H.; Shimizu, K. Formation and Transformation of $ZnTiO_3$. *J. Am. Ceram. Soc.* **1987**, *70*(5), C-97-C-98.

APPENDIX A

Determination of Temperature Difference Across a Gas Film

A simple estimate of the maximum possible temperature difference between the bulk gas and the solid surface using the methods discussed by Smith (1970) was made. The difference between the fluid temperature (T_b) and the temperature at the surface of the solid (T_s) is

$$T_s - T_b = R_o \frac{(-\Delta H)\, Pr^{2/3}}{j_H C_p G} \qquad (A.1)$$

where R_o is the initial reaction rate (mol/cm^2-s), ΔH is the heat of reaction (cal/mol), the Prandtl number is $Pr = c_p\mu/k$, C_p is the heat capacity (cal g^{-1} K^{-1}), μ is the viscosity (g cm^{-1} s^{-1}), k is the thermal conductivity (cal cm^{-1} s^{-1} K^{-1}), j_H is the heat transfer correlation, and G is the mass velocity (g/cm^2-s).

The maximum possible temperature drop based on ZnO reduction at 1300 K in a gas containing 10 mol% H_2-90 mol% N_2 with particles diameter (d_p) of 0.0125 cm and gas flowrate (G) of 1.239×10^{-3} g cm^{-2} s^{-1} was calculated. The following formulae used to calculate fluid property values were obtained from Bird et al. (1960). The viscosity of H_2 and N_2 at 1300 K can be estimated from the Chapman-Enskog theory for gases at low density with the expression:

$$\mu = 2.6693 \times 10^{-5} \frac{\sqrt{MT}}{\sigma^2 \Omega_\mu} \qquad (A.2)$$

where M is the molecular weight of the gas, T [=] K, and values for σ [=] Å and Ω_μ are tabulated in Bird et al. (1960). For N_2 and H_2, the calculated values of the viscosity are 4.758×10^{-4} and 2.327×10^{-4} g/cm-s, respectively. The viscosity of the H_2-N_2 gas mixture is calculated as

$$\mu_{mix} = \sum_{i=1}^{n} \frac{x_i \mu_i}{\sum_{j=1}^{n} x_j \Phi_{ij}} \qquad (A.3)$$

where

$$\Phi_{ij} = \frac{1}{\sqrt{8}} \left(1 + \frac{M_i}{M_j}\right)^{-1/2} \left[1 + \left(\frac{\mu_i}{\mu_j}\right)^{1/2} \left(\frac{M_j}{M_i}\right)^{1/4}\right]^2 \qquad (A.4)$$

For the 10% H_2-90% N_2 gas mixture, the viscosity is 4.746×10^{-4} g/cm-s. This is quite close to the value of the viscosity of N_2. To simplify the calculation, fluid properties will be based on N_2 alone. The heat transfer correlation (j_H) was estimated from a empirical correlation obtained for packed-bed reactor for spherical shape particles. The following correlation was used:

$$j_H = 0.91\ Re^{-0.51} \qquad (A.4)$$

where the Reynolds number $Re = d_p G/\mu$. The Reynolds number for this system is 0.0325. The value of the heat capacity (C_p) for N_2 is 0.259 cal g^{-1} C^{-1} (Smith and Van Ness, 1975). The thermal conductivity (k [=] cal cm^{-1} s^{-1}) of a polyatomic gas at low density can be calculated with the semiempirical method developed by Eucken:

$$k = \left(C_p + \frac{5}{4}\frac{R}{M}\right)\mu \qquad \text{(A.5)}$$

The calculated value for the thermal conductivity of N_2 is 3.544×10^{-3} cal cm^{-1} s^{-1}. The Prandtl number is:

$$Pr = \frac{C_p}{C_p + \frac{5}{4}\frac{R}{M}} \qquad \text{(A.6)}$$

The Prandtl number for this system is 0.745. For ZnO reduction, the heat of reaction at 1300 K is 51396 cal/mol and the initial rate of reaction calculated from Arrhenius parameters measured in this thesis is 6.974×10^{-8} mol cm^{-2} s^{-1} with 10 mol% H_2-90 mol% N_2. From Eq. A-1, the calculated difference in temperature across the gas film is only 1.8 C. Thus, an isothermal assumption is valid for these experiments.